

**Biogenesis of Mitochondrial Signal-anchored  
Proteins - From Early Cytosolic Events to their  
Membranal Integration**

**Dissertation**

der Mathematisch-Naturwissenschaftlichen Fakultät  
der Eberhard Karls Universität Tübingen  
zur Erlangung des Grades eines  
Doktors der Naturwissenschaften  
(Dr. rer. nat.)

vorgelegt von  
Layla Drwesh  
aus Iksal, Israel

Tübingen  
2022





Gedruckt mit Genehmigung der Mathematisch-Naturwissenschaftlichen Fakultät  
der Eberhard Karls Universität Tübingen.

Tag der mündlichen Qualifikation:	04.07.2022
Dekan:	Prof. Dr. Thilo Stehle
1. Berichterstatter:	Prof. Dr. Doron Rapaport
2. Berichterstatter:	Prof. Dr. Ralf-Peter Jansen



## Contents

<b>1</b>	<b>List of abbreviations</b>	<b>1</b>
<b>2</b>	<b>Summary</b>	<b>3</b>
<b>3</b>	<b>Zusammenfassung</b>	<b>5</b>
<b>4</b>	<b>List of publications contained in this thesis</b>	<b>8</b>
	a) Accepted papers	8
	b) Manuscripts in revision	8
<b>5</b>	<b>Personal contribution to the publications contained in this thesis</b>	<b>10</b>
<b>6</b>	<b>Introduction</b>	<b>13</b>
6.1	Structure and function of mitochondria	13
6.2	Mitochondrial outer membrane	13
6.2.1	Topologies of outer membrane proteins	14
6.3	Mitochondrial protein import pathways	16
6.3.1	Import pathways of $\beta$ -barrel proteins	16
6.3.2	Import pathways of single-span $\alpha$ -helical proteins	17
6.3.3	Import pathways of multi-span $\alpha$ -helical proteins	19
6.4	Early cytosolic events in the biogenesis of mitochondrial proteins	19
6.4.1	Classifications of (co)chaperones	19
6.4.2	Involvement of (co)chaperones in mitochondrial protein biogenesis	21
<b>7</b>	<b>Objectives</b>	<b>25</b>
<b>8</b>	<b>Summary of the results</b>	<b>27</b>
8.1	The biogenesis of mitochondrial outer membrane proteins show variable dependence on import factors (Vitali et al. 2020)	27
8.2	A network of cytosolic (co)chaperones promotes the biogenesis of mitochondrial signal-anchored outer membrane proteins (Drwesh et al. 2022, in revision)	28
8.3	Uncovering targeting priority to yeast peroxisomes using an in-cell competition assay (Rosenthal et al. 2020)	33
8.4	Cnm1 mediates nucleus-mitochondria contact site formation in response to phospholipid levels ( Eisenberg-Bord et al. 2021)	34
<b>9</b>	<b>Discussion</b>	<b>38</b>
9.1	The biogenesis of mitochondrial outer membrane proteins show variable dependence on import factors (Vitali et al. 2020)	38

9.2 A network of cytosolic (co)chaperones promotes the biogenesis of mitochondrial signal-anchored outer membrane proteins (Drwesh et al. 2022, in revision). .....	40
<b>10 References .....</b>	<b>44</b>
<b>11 Acknowledgments .....</b>	<b>57</b>
<b>12 Appendix .....</b>	<b>60</b>
a) Accepted papers .....	60
b) Manuscripts in revision.....	132



## 1. List of abbreviations

a.a	amino-acid
BAM	$\beta$ -barrel assembly machinery
CE	carbonate extraction
DHFR	dihydrofolate reductase
ERMES	ER-mitochondria encounter structure
GFP	green fluorescent protein
Hsp	heat shock protein
IM	inner membrane
IMM	inner mitochondrial membrane
IMS	intermembrane space
Mcr1	mitochondrial NADH-cytochrome b5 reductase 1
MIM	mitochondrial import
Msp1	mitochondria sorting protein 1
MTS	mitochondrial targeting sequence
OM	outer membrane
PC	phosphatidylcholine
PTS	peroxisomal targeting signal
SA	signal-anchored
SAM	sorting and assembly machinery
TA	tail-anchored
TAMRA	tetramethylrhodamine
TIM23	translocase of the inner mitochondrial membrane
TMS	transmembrane segment
TOB	topogenesis of the outer membrane $\beta$ -barrel proteins
TOM	translocase of the outer mitochondrial membrane
VDAC	voltage-dependent anion channel
WT	wild type



## 2. Summary

Mitochondria harbour proteins with different topologies in their outer membrane (OM). In this study, I focus on one topological protein category, known as signal-anchored (SA) proteins. This family consists of proteins that span the membrane once via a single helical TMS located at their N-terminus, exposing a large C-terminal domain towards the cytosol. Like all mitochondrial OM proteins, SA proteins are encoded by nuclear DNA, translated by cytosolic ribosomes, and then are targeted to the organelle. Assuring proper and efficient targeting of such proteins is crucial for maintenance of mitochondrial biological function. Despite their importance, our understanding of the import routes that SA proteins follow including the early cytosolic events is scarce.

In this study, I aimed to unravel the biogenesis steps of SA proteins following their synthesis in the cytosol until their recognition at the mitochondrial surface. To this end, I have applied a wide set of *in vivo*, *in organello*, and *in vitro* assays using various mitochondrial SA substrates as model proteins.

I found that the MIM complex is required for the membrane insertion of the SA quality control protein Msp1, while other proteins from this category appear to follow different routes. These findings suggest that proteins from the same category may not necessarily follow the same pathway, but rather rely on different import factors to varying degrees.

To shed light on the early cytosolic events that are essential for maintaining the newly synthesized SA proteins in an import competent conformation, I analysed the involvement of some cytosolic chaperones in their early biogenesis stages. I found that chaperones from distinctive families interact with newly synthesized SA proteins through the hydrophobic segments of the latter. I further could show that such interactions are not only crucial for keeping SA proteins stable in the cytosol, but also for their optimal targeting and import into the organelle.

Next, I investigated the implication of the interplay between cytosolic chaperones and mitochondrial receptors on the biogenesis of SA proteins. My findings suggest a role of the TOM complex receptors in collaboration with the Hsp40 and Hsp70 chaperones in mediating the recognition and the insertion of SA proteins.

Overall, my findings provide new insights into the early cytosolic events in the biogenesis of SA proteins following their synthesis until their recognition at the mitochondrial surface.





### 3. Zusammenfassung

Mitochondrien beherbergen in ihrer äußeren Membran (OM) Proteine verschiedener Topologien. In dieser Arbeit beschäftigte ich mich mit einer Proteinfamilie, die *als signal-anchored* (SA) Proteine bezeichnet werden. Diese Familie besteht aus Proteinen, die die Membran mit ihrer  $\alpha$ -helikalen Transmembrandomäne am N-Terminus einfach durchspannen, während ein großer Teil der C-terminalen Domäne zum Zytosol hin freiliegt. Wie die übrigen mitochondrialen OM-Proteine werden auch SA-Proteine im Zellkern kodiert, von zytosolischen Ribosomen translatiert, anschließend zum Zielorganell geleitet und in die Lipiddoppelschicht eingebettet. Damit die Mitochondrien ihre biologische Funktionen erfüllen können, ist es entscheidend, dass solche Proteine richtig integriert und ausgerichtet werden. Doch wie SA-Proteine in das Zielorganell importiert werden und welche vorherigen Ereignisse im Zytosol dazu benötigt werden, ist nahezu unbekannt.

Zielsetzung dieser Arbeit war, die Schritte der Biogenese von SA-Proteinen, beginnend mit ihrer Synthese im Zytosol, bis hin zu ihrer Erkennung an der mitochondrialen Oberfläche zu entschlüsseln. Zu diesem Zweck habe ich eine Reihe von *in vivo*, *in organello* und *in vitro* Assays durchgeführt, bei denen ich verschiedene mitochondriale SA-Proteine als Modellproteine verwendet habe.

Ich fand heraus, dass der MIM-Komplex für die Insertion des SA-Proteins Msp1 in die OM erforderlich ist, während andere Proteine aus dieser Kategorie über andere Wege inseriert werden. Dies deutete darauf hin, dass Proteine derselben Kategorie nicht unbedingt demselben Importmechanismus folgen, sondern in unterschiedlichem Maße auf verschiedene Importfaktoren angewiesen sind.

Um die früheren zytosolischen Ereignisse aufzuklären, die für die Aufrechterhaltung der neu-synthetisierten Proteine in einer importkompetenten Konformation wesentlich sind, habe ich den Einfluss einiger zytosolischen Chaperone untersucht. Ich fand heraus, dass einige Chaperone aus verschiedenen Familien mit neu-synthetisierten SA-Proteinen über ihre hydrophoben Segmente interagieren. Außerdem konnte ich zeigen, dass solche Wechselwirkungen nicht nur entscheidend für die Stabilität der SA-Proteine im Zytosol sind, sondern auch für deren Import in das Organell und ihre optimale Ausrichtung benötigt werden.

Als nächstes untersuchte ich die Bedeutung des Zusammenspiels zwischen den zytosolischen Chaperonen und den mitochondrialen Rezeptoren für die Biogenese von SA-Proteinen. Meine Ergebnisse deuteten auf eine Rolle der TOM-Komplex-Rezeptoren in Zusammenarbeit mit einigen Hsp70 und Hsp40 Chaperonen bei der Erkennung und dem

Einbau von SA-Proteinen hin. Zusammengefasst bieten meine Ergebnisse neue Einblicke in die früheren zytosolischen Ereignisse bei der Biogenese von SA-Proteinen, von ihrer Synthese bis zu ihrer Erkennung an der mitochondrialen Oberfläche.



## 4. List of publications contained in this thesis

### a) Accepted papers

1. **Drwesh, L.**, & Rapaport, D. (2020). Biogenesis pathways of  $\alpha$ -helical mitochondrial outer membrane proteins. *Biological Chemistry*, 401(6-7), 677–686.
2. Vitali, D. G.\*, **Drwesh, L.\***, Cichocki, B. A., Kolb, A., & Rapaport, D. (2020). The Biogenesis of Mitochondrial Outer Membrane Proteins Show Variable Dependence on Import Factors. *iScience*, 23(1), 100779.  
  
*\*equal contributors*
3. Rosenthal, M., Metzl-Raz, E., Bürgi, J., Yifrach, E., **Drwesh, L.**, Fadel, A., Peleg, Y., Rapaport, D., Wilmanns, M., Barkai, N., Schuldiner, M., & Zalckvar, E. (2020). Uncovering targeting priority to yeast peroxisomes using an in-cell competition assay. *Proceedings of the National Academy of Sciences of the United States of America*, 117(35), 21432–21440.
4. Eisenberg-Bord, M., Zung, N., Collado, J., **Drwesh, L.**, Fenech, E. J., Fadel, A., Dezorella, N., Bykov, Y. S., Rapaport, D., Fernandez-Busnadiego, R., & Schuldiner, M. (2021). Cnm1 mediates nucleus-mitochondria contact site formation in response to phospholipid levels. *The Journal of Cell Biology*, 220(11), e202104100

### b) Manuscripts in revision

5. **Drwesh, L.**, Heim, B., Graf, M., Kher, L., Hansen-Palmus L., Franz-Wachtel M., Macek, B., Kalbacher, H., Buchner, J., and Rapaport, D. (2022). eLife, *in revision*



## 5. Personal contribution

1. **Drwesh, L.**, & Rapaport, D. (2020). Biogenesis pathways of  $\alpha$ -helical mitochondrial outer membrane proteins. *Biological Chemistry*, 401(6-7), 677–686.

I wrote this review and created all figures.

2. Vitali, D. G.\*, **Drwesh, L.\***, Cichocki, B.A., Kolb, A., & Rapaport, D. (2020). The Biogenesis of Mitochondrial Outer Membrane Proteins Show Variable Dependence on Import Factors. *iScience*, 23(1), 100779.

*\*equal contributors*

I isolated mitochondria from *tom20 $\Delta$* , *tom70/71 $\Delta$* , *mim1 $\Delta$* , *mim2 $\Delta$* , *mim1/2 $\Delta$*  and *mas37 $\Delta$*  cells and analysed the steady state levels of their mitochondrial proteins (Fig. 1A-C). Additionally, I conducted *in vitro* import assay of radiolabelled Msp1 protein into mitochondria isolated from *mim1/2 $\Delta$*  cells (Fig. 1D, E). Furthermore, I monitored the subcellular localization of the transmembrane domain of Msp1 (Msp1-TMD-GFP) using either fluorescence microscopy or western blot (Fig. 2A, B). Moreover, I performed the subcellular fractionation shown in Fig. 4 D. I prepared the relevant figures.

3. Rosenthal, M., Metzl-Raz, E., Bürgi, J., Yifrach, E., **Drwesh, L.**, Fadel, A., Peleg, Y., Rapaport, D., Wilmanns, M., Barkai, N., Schuldiner, M., & Zalckvar, E. (2020). Uncovering targeting priority to yeast peroxisomes using an in-cell competition assay. *Proceedings of the National Academy of Sciences of the United States of America*, 117(35), 21432–21440.

I performed subcellular fractionations of cells expressing either high or low levels of mCherry-SKL (peroxisomal targeting sequence fused to mCherry). Each strain also expressed one peroxisomal protein of interest fused to GFP (GFP-Pxp1, GFP-Tes1, GFP-Lys1 and GFP-Pox1). Then, I analysed the steady state levels of the GFP-tagged peroxisomal proteins by SDS-PAGE followed by immunodecoration. Finally, I quantified the levels of selected proteins in the peroxisomal fraction (Fig. 2D-F).

4. Eisenberg-Bord, M., Zung, N., Collado, J., **Drwesh, L.**, Fenech, E. J., Fadel, A., Dezorella, N., Bykov, Y. S., Rapaport, D., Fernandez-Busnadiego, R., & Schuldiner, M. (2021). Cnm1 mediates nucleus-mitochondria contact site formation in response to phospholipid levels. *The Journal of Cell Biology*, 220(11), e202104100.

To characterize the membranal integration of the novel Ybr063c (Cnm1) protein, I isolated mitochondria from a strain over-expressing Ybr063c N-terminally tagged with 3xHA. I analysed the membrane integration of Cnm1 by carbonate extraction (Fig. 3B).

5. **Drwesh, L.** Heim, B., Graf, M., Kher, L., Hansen-Palmus L., Franz-Wachtel M., Macek, B., Kalbacher, H., Buchner, J., and Rapaport, D., (2022). A network of cytosolic (co)chaperones promotes the biogenesis of mitochondrial signal-anchored outer membrane proteins. *eLife*, *In revision*.

To identify cytosolic interaction partners, I performed pull-down experiments with the different SA proteins translated *in vitro* in yeast extract (Fig. 1). I further used the same approach to prove that the hydrophobic transmembrane domain of the SA proteins is sufficient for interactions with the chaperones (Fig. 2). Next, I tested the physiological relevance of some Hsp40 co-chaperones, namely, Ydj1 and Sis1 in the biogenesis of SA proteins by analysing the steady state levels of the mitochondrial SA-proteins in strains depleted of Ydj1 and/or Sis1 chaperones (YS $\downarrow$ ) (Fig. 3). Additionally, I performed *in vitro* import assays of some SA substrates using yeast extract purified from the YS depleted strain to analyse the role of these chaperones in their mitochondrial import (Fig. 4A, B). The same strain was used to analyse the influence of the double depletion on the interaction of other chaperones to SA proteins (Fig. 5A, B). Furthermore, I analysed the involvement of other interacting chaperones by conducting *in vitro* import of SA proteins in the presence of the Hsp70 chaperone inhibitor CBag (Fig. 7A, B). I then analysed the role of mitochondrial receptors in the insertion process of SA proteins by conducting *in vitro* pull-down assays (Fig. 8A and Fig. S1A). Involvement of the mitochondrial receptors was further investigated by conducting additional *in vitro* import assays either in trypsin-treated mitochondria (Fig. 9A, B), or in *tom20 $\Delta$*  mitochondria treated with Tom70 inhibitor, C90 (Fig. 9C, D). Finally, I tested the mitochondrial steady state levels of some OM proteins in *tom20 $\Delta$*  strain (Fig. S1B).



I wrote the first draft of the manuscript, conducted and designed some experiments, and prepared all figures.

## **6. Introduction**

### **6.1 Structure and function of mitochondria**

Mitochondria are organelles that are involved in diverse cellular pathways and perform essential tasks including energy production, signalling and homeostasis of calcium, removal of reactive oxygen species, biogenesis and assembly of iron-sulfur clusters, and regulation of cellular stress responses such as apoptosis and autophagy. These functions are carried out by proteins distributed between four different sub-mitochondrial compartments: the intermembrane space (IMS) and the matrix which are encapsulated by two separate and functionally distinct membranes, the outer membrane (OM) and the inner membrane (IM) (Nunnari and Suomalainen, 2012; Sharma et al., 2021). Mitochondria harbour their own circular genome (mtDNA) that originates from their bacterial ancestor which is believed to be an  $\alpha$ -proteobacterium that was engulfed by a bigger ancestral host cell (Gray, 2012). During this endosymbiosis process, most of the mitochondrial genes were transferred to the host cell's nuclear genome. Consequently, modern day mtDNA encodes only for a small number of mitochondrial proteins, while the rest (including all the OM proteins) are encoded by the nuclear genome and synthesized on cytosolic ribosomes. Following their synthesis, these proteins must be properly targeted to their final destination within the mitochondria by the aid of sophisticated protein import machineries that have evolved in the different mitochondrial compartments (Wiedemann and Pfanner, 2017).

Being involved in many physiological aspects of the cell, including communication with other cellular compartments, mitochondrial malfunction has been implicated in a variety of diseases including neurodegenerative and metabolic disorders (Sharma et al., 2021; Nunnari and Suomalainen, 2012; Lin and Beal, 2006).

### **6.2 Mitochondrial outer membrane**

The outer membrane of the mitochondria acts as a physical barrier, preventing large molecules from freely diffusing into the organelle, while allowing an exchange of small metabolites, ions, and nucleotides from the cytosol through channels formed in the OM by  $\beta$ -barrel proteins called Porin in yeast or Voltage-Dependent Anion Channel (VDAC) in mammals (Ponnalagu and Singh, 2017; Endo and Sakaue, 2019). The rest of the OM proteome consists of distinct proteins assigned for variable functions and pathways, among them mediating the crosstalk

between mitochondria and other cellular compartments. Some of these proteins are physically involved in creating membrane contact sites (MCSs) between the mitochondria and different organelles, namely the nucleus, ER, lysosome, and peroxisome. These contact sites are crucial for facilitating passage of ions and lipids between membranes (Farré et al., 2019; Elbaz-Alon, 2017). Other OM proteins are components of the protein import machineries including receptors, channels, and translocases that ensure efficient and proper transfer of newly synthesized proteins into their correct destination within the different mitochondrial compartments (Straub et al., 2016; Wiedemann and Pfanner, 2017).

Proteins involved in fission and fusion events of mitochondria can also be found in the OM. These proteins are mostly mechano-chemical membrane-remodelling ones that belong to the dynamin protein family. Such opposed processes are highly significant for regulating healthy mitochondrial dynamics and morphology (Meyer et al., 2017; Lee and Yoon, 2016). Furthermore, mitochondrial OM contains proteins involved in quality control and protein turnover which are essential for maintaining membrane proteostasis (Fresenius and Wohlever, 2019).

### **6.2.1 Topologies of outer membrane proteins**

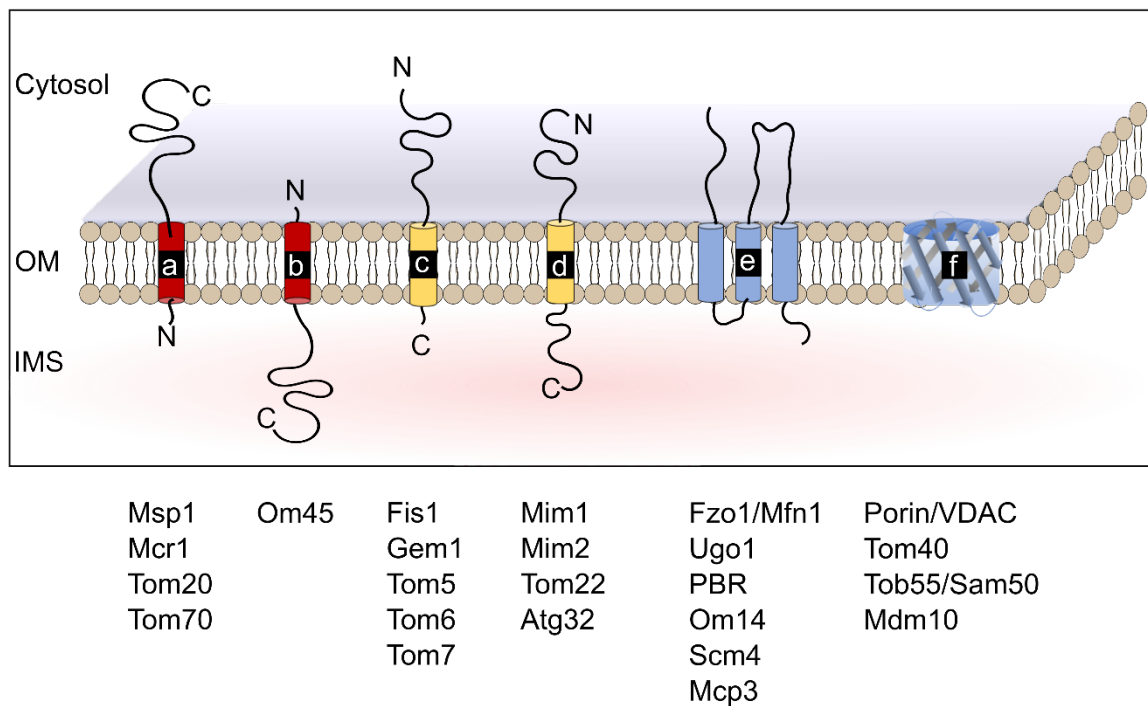
The OM proteome includes integral proteins that are categorized according to their structure into two main families, proteins with  $\alpha$ -helical transmembrane segments and  $\beta$ -barrel proteins that are formed by multiple  $\beta$ -strands (Fig. 1). Whereas the latter family include in yeast only five  $\beta$ -barrel proteins, the former one contains a few dozen membrane-embedded helical proteins (Burri et al., 2006).

$\beta$ -barrel proteins are found in three different membranes, the outer membrane of Gram-negative bacteria, chloroplast, and mitochondria in which they span the membrane by a range of 8-24 anti-parallel  $\beta$ -strands that are connected by loops, forming hydrophilic pore across the membrane. So far, several  $\beta$ -barrel proteins had been identified in yeast mitochondria: the pore forming protein, Porin, and the central component of the TOB complex, Tob55/Sam50, which belongs to an evolutionarily conserved protein family since it has a clear homology with the bacterial Omp85 (BamA) protein. Both Tob55 and BamA are essential for the biogenesis of  $\beta$ -barrel proteins in eukaryotes and bacteria respectively (Paschen et al., 2005). Additional  $\beta$ -barrel proteins are the TOM complex conducting channel Tom40, and the ERMES component Mdm10 which acts as a tether between mitochondria and ER (Böckler and Westermann, 2014; Flinner et al., 2013).

Proteins with  $\alpha$ -helical structures are categorized into distinct groups based on the number and the location of their transmembrane segments. Those who have only one transmembrane segment (TMS) are referred to as single-span  $\alpha$ -helical proteins and based on their topology can be assigned to three subclasses: the first one is the signal-anchored family, members of this family are embedded into the OM through an N-terminal TMS, exposing large C-terminal soluble domain towards either the cytosol or the IMS (Fig. 1). Known proteins of this category are the quality control protein Msp1 which mediates removal of mis-localized proteins from the OM (Wohlever et al., 2017; Matsumoto et al., 2019), the TOM complex receptors Tom20 and Tom70, Om45 with so far, unknown function and finally Mcr1, which is involved in ergosterol biosynthesis (Lamb et al., 1999). The second subclass includes tail-anchored proteins that are characterized by an inverted orientation as compared to the first group, namely, having the TMS at the C-terminus while exposing large soluble N-terminal domain towards the cytosol (Fig. 1). OM tail-anchored proteins include the small TOM complex core components Tom5, Tom6 and Tom7, which are essential for the stability of the complex (Sherman et al., 2005). Additional tail-anchored proteins in the OM are: Fis1 (hFis1 in human), which mediates mitochondrial fission (Bleazard et al., 1999); and Gem1 (Miro1/2 in mammals), which is a GTPase that has been proposed to regulate the ERMES function (Stroud et al., 2011; Kornmann et al., 2011).

In both former subclasses, the region on the opposite side to the soluble domain is very short. In contrast, the third subclass contains proteins with two large soluble domains exposed to both the cytosol and the IMS while having the TMS in the middle (Fig. 1, Walther and Rapaport, 2009). This family includes in yeast cells the MIM component Mim1, which is required for the integration of proteins into the OM (Waizenegger et al., 2005), the TOM complex core subunit Tom22 that acts as a receptor for some precursor proteins (Meisinger et al., 1999), and Atg32 which is involved in mitophagy and degradation of mitochondria (Okamoto et al., 2009; Kanki et al., 2009).

Proteins that cross the OM via multiple  $\alpha$ -helical transmembrane segments are referred to as multi-span proteins (Fig. 1). Several multi-spanning proteins have been identified so far in the mitochondrial OM: Fzo1 that spans the membrane twice and is essential for mitochondrial fusion in yeast (Mfn1/2 in mammals) (Rapaport et al., 1998; Hermann et al., 1998), the fusion mediator Ugo1 (Sesaki and Jensen, 2001), Mcp3, which is probably involved in lipid homeostasis (Sinzel et al., 2017), the quality control adaptor Ubx2 (Mårtensson et al., 2019), Om14, which was suggested to serve as a receptor for cytosolic ribosomes (Lesnik et al., 2014), and the multi-span protein Scm4 with unknown function.



**Figure 1: Topologies of mitochondrial OM proteins.**

From left to right: signal-anchored proteins (a and b), tail-anchored proteins (c), other single-span proteins (d), multi-span proteins (e), and  $\beta$ -barrel proteins (f).

## 6.3 Mitochondrial protein import pathways

### 6.3.1 Import pathways of $\beta$ -barrel proteins

The insertion pathway of mitochondrial  $\beta$ -barrel proteins seems to be conserved during the evolution of mitochondria from endosymbiotic bacterial ancestors. Previous studies have identified the import machineries that are involved in the biogenesis of  $\beta$ -barrel proteins in bacteria and mitochondria as the BAM and TOB complexes, respectively (Selkrig et al., 2014). Similar concept for the biogenesis of  $\beta$ -barrel proteins in chloroplasts was demonstrated (Soll and Schleiff, 2004).

Most of the investigated  $\beta$ -barrel proteins showed post-translational import (Day et al., 2014), and their recognition at the surface of the mitochondria was shown to be mediated by the TOM complex receptors, Tom20 and Tom70 leading to their insertion via the Tom40 channel into the IMS (Jores et al., 2016; Krimmer et al., 2001). In the IMS, these proteins are protected from aggregation and/or misfolding by the assistance of the small TIM chaperones (Tim9/10 and Tim8/13) (Wiedemann et al., 2004). From the IMS side they are then transferred to the

TOB complex that mediates their insertion into the OM by its core component Tob55 (Wiedemann et al., 2004; Waizenegger et al., 2004). The final release of the folded substrates from the TOB complex into the OM was suggested to be mediated by the peripheral subunit of the TOB complex Mas37 (Chan and Lithgow, 2008).

However, different precursor  $\beta$ -barrel proteins showed a distinct dependence on different TOB components, for instance, import of Porin, was less dependent on Tob38 than import of Tom40 and Mdm10 (Waizenegger et al., 2004). Moreover, biogenesis of Tom40 was found to require Mdm10 which interacts with the TOB core complex to facilitate its assembly into the TOM complex (Meisinger et al., 2004). Such an interaction is not relevant to the biogenesis of any other  $\beta$ -barrel protein.

Several studies tried to investigate how TOB complex recognizes  $\beta$ -barrel precursors from the IMS side and facilitate their integration into the outer membrane. One of these studies has suggested that the  $\beta$ -signal formed by the most C-terminus single  $\beta$ -strand serves as intra-mitochondria sorting signal. This signal was suggested as a recognition site by Tob38 creating a ternary complex with Tob38 and Tob55. Forming such a complex leads to an increase in the conductance of Tob55 channel which eventually results in a lateral release of the precursor into the OM (Kutik et al., 2008; Chan and Lithgow, 2008). In contrast, more recently published papers have suggested a partially different mechanism, in which the precursor enters the lumen of Tob55 channel from the IMS side via interaction between the C-terminal part of its  $\beta$  signal and the first  $\beta$  strand of Tob55 ( $\beta$ 1) through an exchange with the last  $\beta$  strand of Tob55 ( $\beta$ 16). This interaction induces opening of the lateral gate of Tob55 allowing the precursor to be laterally released into the OM (Wang et al., 2021; Höhr et al., 2018). This mechanism was previously suggested to be used by the bacterial BAM complex (Noinaj et al., 2014).

### **6.3.2 Import pathways of single-span $\alpha$ -helical proteins**

Recently, several studies have made significant progress in our understanding of how single-span proteins make their way from the cytosol into the mitochondrial OM. Despite sharing the same topology, it seems that these proteins do not follow a unified biogenesis pathway but rather depend to a variable extent on different import factors.

The MIM complex was implicated in the biogenesis of most  $\alpha$ -helical proteins, among them the TOM receptors, Tom20 and Tom70, as well as the small Tom components Tom5, Tom6, and Tom7. The MIM complex consists of two components Mim1 and Mim2. Mim1 was first identified as a protein required for mitochondrial import (Mnaimneh et al., 2004), and its

deletion was later confirmed to affect mitochondrial steady state levels of Tom20, Tom70 and the small Tom components (Ishikawa et al., 2004; Waizenegger et al., 2005; Becker et al., 2008; Popov-Čeleketić et al., 2008; Hulett et al., 2008).

The involvement of the TOM complex in the biogenesis of these proteins was found to be divergent. While TOM complex import channel formed by Tom40 was not required for the initial insertion of Tom20, it was suggested to be involved in late stages of its biogenesis, such as assisting with its appropriate assembly and correct topology formation (Ahting et al., 2005). Nevertheless, the engagement of the TOM complex in the biogenesis of the small Tom components was more significant (Stojanovski et al., 2007). While biogenesis of Tom5 was shown to require mainly the Tom40 channel (Horie et al., 2003), Tom6 and Tom7 biogenesis showed dependency on the TOM complex channel and its receptors Tom20 and Tom70 (Dembowski et al., 2001). Moreover, SAM machinery which was believed to be exclusively dedicated for the biogenesis of  $\beta$ -barrel proteins was found in several studies to be crucial for the insertion and the assembly of the TOM complex components, Tom5, Tom6, Tom7 and the TOM complex receptor Tom22. These findings are based on the observations that mitochondria lacking Sam37 and/or Mdm10 exhibited faulty assembly of the small Tom components and Tom22 into the TOM complex (Stojanovski et al., 2007; Meisinger et al., 2004).

On the other hand, the functions of Sam37 and Mdm10 were not essential for efficient insertion of the other  $\alpha$ -helical proteins, Tom20 and Tom70. Hence, it seems that the MIM complex together with the TOM complex promote the initial integration of the small TOM subunits into the OM in, so far, unknown mechanism, while the TOB complex is required for their final proper assembly into the TOM complex. Such function was recently proposed for Sam37 based on cryo-electron microscopy structures, revealing that Sam37 stabilizes the mature form of Tom40 promoting assembly of the TOM complex (Wang et al., 2021).

Tom22 was shown to follow a different route that includes an initial recognition by the TOM receptors Tom20 and Tom70 (Keil and Pfanner, 1993), and does not require the MIM complex (Becker et al., 2008), but rather depends on the TOB/Mdm10 machinery for its final assembly into the TOM complex (Thornton et al., 2010).

Om45, which is anchored to the OM while its soluble domain is facing the IMS, follows a unique import pathway including recognition by Tom20 and Tom22 receptors before its translocation through the Tom40 channel into the IMS where it is recognized by the presequence translocase of the inner membrane (TIM23 complex) (Wenz et al., 2014; Song et al., 2014). The final insertion steps from the IMS side into the OM was suggested to be facilitated by the MIM complex (Wenz et al., 2014).

Other single-span  $\alpha$ -helical proteins were reported to be independent of any known import factors for their mitochondrial insertion. Accordingly, the import of Mcr1<sub>mom</sub> and Fis1 was unaffected by the deletion of MIM components or the TOM receptors (Kemper et al., 2008; Meineke et al., 2008). Hence, such proteins might integrate into the mitochondrial OM via an unassisted pathway that does not involve any known import components but rather is driven by the unique lipid composition of the mitochondrial OM.

### **6.3.3 Import pathways of multi-span $\alpha$ -helical proteins**

Studies on the biogenesis of multi-span proteins reported an import route involving the TOM and MIM machineries. These findings were based on reduced steady state levels and reduced *in vitro* import efficiency in yeast mitochondria lacking Tom70 (Papić et al., 2011; Mårtensson et al., 2019). Hence, Tom70 is suggested to play a key role in their recognition or by serving as a docking site on mitochondrial surface for chaperones that associate with mitochondrial precursor proteins in the cytosol. Based on the observation that these proteins exhibited a strong dependency on the MIM complex, it was suggested that following their recognition by Tom70, these substrates are transferred to the MIM complex, which facilitates their final integration into the OM (Becker et al., 2011).

Nonetheless, an alternative pathway for one multi-span protein, Mcp3, was reported, which likewise, involves recognition by Tom70 receptor, but then the substrate is translocated across the mitochondrial OM through the Tom40 channel into the IMS side. In the IMS, the substrate interacts with the inner membrane TIM23 machinery and undergoes processing by the inner membrane protease (IMP) followed by integration into the OM, which is most likely facilitated by the MIM complex (Sinzel et al., 2017).

## **6.4 Early cytosolic events in the biogenesis of mitochondrial proteins**

### **6.4.1 Classification of (co)chaperones**

Chaperones, also known as heat shock proteins (Hsp), are unique remodelling proteins that are engaged in a variety of intracellular functions, including protein folding, prevention of misfolding and aggregation events, eliminating aggregated proteins, and assisting in macromolecular structure assembly. Molecular chaperones were initially thought to be mainly required under elevated temperatures which results in conformational changes in the protein's structures. However, several studies have shown that they are not only required in stress



conditions but are also necessary under normal cellular conditions (Solís et al., 2016). Hence, the cell has employed an interconnected network of cytosolic factors and molecular chaperones that work collectively to maintain cellular protein homeostasis. Chaperones' cellular activities in both stress defence and housekeeping tasks are based on their ability to interact with either unfolded proteins or proteins that have not achieved their native conformation.

Molecular chaperones are categorized into distinct classes/families based on their molecular weight and common structural and functional characteristics. Different classes of molecular chaperones appear to target specific non-native protein states. One of the well-studied chaperone family is the GroE chaperone system in bacteria (Hsp60 in yeast, also called chaperonins) that is essential at all temperatures. Members of this family include GroEL and GroES chaperonins (in yeast Hsp60 and Hsp10, respectively). Chaperones from the Hsp60 family hydrolyse ATP and form a large homo-oligomeric protein complex with interior cavity to provide proper environment for the ATP-dependent folding processes of the substrates. Hence, chaperones from this family are mainly involved in protein assembly and in facilitating correct folding of mitochondrial protein monomers (Reading et al., 1989). The second well-studied family is the Hsp70 chaperone system characterized by monomeric 70 kDa proteins and consist of an N-terminal ATPase domain and a C-terminal peptide binding domain. Chaperones from this family can be found in archaea, bacteria, and eukaryotes, and they perform diverse functions ranging from unfolding and refolding, disaggregation and degradation of substrates to promoting protein transport across membranes (Mayer et al., 2000; Nillegoda and Bukau, 2015; Fernández-Fernández et al., 2017). In both cases, Hsp60 and Hsp70 chaperones bind to unfolding intermediates preferentially through exposed hydrophobic patches of the latter, limiting improper intra- and inter-molecular interactions.

The ability of Hsp70 to interact with diverse client proteins is mediated by a wide range of co-chaperones that stimulate the ATPase activity of the Hsp70 chaperone and encapsulate client protein specificity and selectivity (Cyr and Ramos, 2015). Such co-chaperones are mostly members of the DnaJ/Hsp40 family characterized by a highly conserved J domain (75-amino acids) through which they bind to Hsp70s. In humans, more than 40 members constitute this large and diverse family while around 22 Hsp40s were found in yeast. These co-chaperones vary in their substrate selectivity and their structural features (Kampinga and Craig, 2010; Walsh et al., 2004).

Hsp90 is an additional ATP-dependent molecular chaperone family which interact with wide variety of co-chaperones that act as adaptors and modulate its ATPase activity during the processing of client proteins. Despite having independent chaperone activities including folding and remodelling proteins, Hsp90 often collaborate with Hsp70 chaperones in other cellular remodelling reactions (Genest et al., 2019; Morán Luengo et al., 2019). Some of the client proteins are recruited to Hsp90 by a preliminary interaction with chaperones from the Hsp70 family via the co-chaperone Hop/Sti1 (Pratt et al., 2004).

Due to limited chaperone capacity, cells cannot always prevent protein aggregation under severe or protracted stress circumstances, resulting in intracellular and/or extracellular deposits of aggregated proteins that have been linked to a variety of diseases. Due to their high toxicity, the cells can either digest the polypeptide chains that exist in the aggregates by the proteasome system or reactivate them. For the latter alternative, the cell has developed additional ATP-dependent disaggregase chaperone system (Hsp100 machinery). Chaperones from the Hsp100 family, also known as Clp in bacteria, form large homo-oligomeric protein complexes that cooperate with chaperones from the Hsp40 (like Ydj1 and Sis1) and Hsp70 family to resolubilize and reactivate aggregated/denatured substrate proteins (Reidy et al., 2014; Aguado et al., 2015). ClpB and Hsp104 are members of this family in bacteria and yeast, respectively.

Additional conserved chaperone category, which exists in all kingdoms, is the ATP-independent small heat shock proteins (sHsps) that form large dynamic complexes regulated by temperature changes. Chaperones from this family are rich in highly conserved  $\beta$ -structures that perform specific functions essential for cell survival under adverse conditions. Their interaction with the substrates can be either transient when the substrate is unfolded under mild stress condition or demonstrate high-affinity mode when the substrate is heavily aggregated leading to sHSPs-substrate assemblies' formation (Obuchowski and Liberek, 2020). These small chaperones also mediate subsequent transfer of damaged substrates to Hsp70-Hsp100 chaperone system for refolding pathway (Żwirowski et al., 2017).

#### **6.4.2 Involvement of (co)chaperones in mitochondrial protein biogenesis**

To be able to perform their biological function, mitochondrial proteins need to be correctly folded into their three-dimensional structure. Matrix-targeted mitochondrial proteins were found to require members of the mitochondrial Hsp70, Hsp60 and Hsp100 chaperones localized in the matrix (Voos, 2009). The matrix form of Hsp70 (Ssc1 in yeast) is an ATPase that drives

the translocation of mitochondrial polypeptides into the matrix and in collaboration with J-proteins and two partner proteins, Mdj1 and Mge1 facilitates their folding (Strub et al., 2000). However, when preproteins exhibit folding problems, the matrix chaperonin Hsp60 gets engaged and together with its co-chaperone Hsp10, they form a complex with a separate folding cavity for refolding (Walter, 2002). Upon elevated temperatures, the mitochondrial Hsp100 chaperone, Hsp78 (homolog of the bacterial ClpB), has been implicated in protection against thermal damage. Like its cytosolic counterpart, Hsp104, Hsp78 facilitates disaggregating insoluble protein aggregates in collaboration with Hsp70 chaperones (Doyle and Wickner, 2009; Kim et al., 2001).

Despite this detailed knowledge regarding matrix chaperones, the involvement of cytosolic chaperones in the biogenesis of mitochondrial proteins, particularly those proteins residing in the outer membrane, is poorly studied. Since all the mitochondrial OM proteins contain hydrophobic segments, it is believed that cytosolic factors and/or (co)chaperones are recruited to prevent their misfolding/aggregation in the hydrophilic environment of the cytosol prior to their insertion into the OM. The physiological significance and the identity of such factors, however, are largely unknown.

For mitochondrial OM  $\beta$ -barrel proteins, a set of cytosolic chaperones were identified to be essential for their efficient biogenesis. Among the identified factors are the Hsp70 chaperones Ssa1 and Ssa2 and the Hsp40 chaperones Ydj1 and Sis1 (Jores et al., 2018). This involvement was proved to be conserved from yeast to mammals.

The Hsp70 chaperone, Ssa1 and its Hsp40 co-chaperone Ydj1 have been previously reported to be also required for an efficient mitochondrial import of MTS-containing IMM proteins (Deshaies et al., 1988; Endo et al., 1996; Caplan et al., 1992). Additional Hsp40 chaperone, Djp1, which was previously found to mediate peroxisomal protein import (Hettema et al., 1998), was also implicated in the biogenesis of the helical OM protein Mim1, facilitating its mitochondrial targeting through interaction with Tom70 (Papić et al., 2013; Opaliński et al., 2018). Another Hsp40 member, Xdj1 was reported to interact with the cytosolic domain of the Tom22 precursor and facilitate the assembly of the TOM complex (Opaliński et al., 2018). Remarkably, Pex19, a chaperone that was found to stabilize and mediate integration of peroxisomal tail-anchored proteins through cooperation with the membrane receptor Pex3 (Fang et al., 2004), was also reported together with Hsp70 and its co-chaperone Sti1 to mediate mitochondrial import of the tail-anchored proteins, Fis1 and Gem1 (Cichocki et al., 2018; Delille and Schrader, 2008). Of note, both Fis1 and Gem1 are dually localized to mitochondria and peroxisomes which explains the involvement of such chaperones in their biogenesis.

Additional dually localized signal-anchored protein, ATAD1 (human homolog of yeast Msp1) was also found to require pex19 for proper biogenesis (Chen et al., 2014).

Despite the aforementioned progress, it is yet unclear whether the function of the chaperones is limited to keeping newly synthesized proteins in an import competent conformation in the cytosol or is it expanded to mediate their integration into the organelle.



## 7. Objectives

Upon cytosolic synthesis of mitochondrial outer membrane proteins, sorting and assembly of such proteins are critical events required to maintain proper functioning of the organelle and the integrity of the cell. The proper integration of the newly synthesized proteins into the organelle depends on their maintenance in an import-competent state that prevent unwanted events of aggregation and tight folding. Despite the significant progress that has been done to understand the elements involved in the biogenesis of different mitochondrial proteins, there are still various unanswered questions regarding the early cytosolic events and the import process of OM  $\alpha$ -helical proteins. Furthermore, based on multiple studies, it is obvious that cytosolic chaperones are essential for the effective import of certain proteins into different organelles including the mitochondria. However, the identity of such cytosolic factors and their exact mode of action are still elusive. Additionally, it is unclear whether their involvement is limited to a subset of mitochondrial proteins or if it is a general mechanism.

In this study, I aimed to dissect the biogenesis of SA proteins residing in the mitochondrial OM, a process that begins with their synthesis on cytosolic ribosomes and ends with their ultimate insertion into the OM of the mitochondria.

To gain deeper insight into the biogenesis of signal-anchored proteins, I aimed to answer two main questions:

1. Which import machineries facilitate the insertion of SA proteins?

In the article “The Biogenesis of Mitochondrial Outer Membrane Proteins Show Variable Dependence on Import Factors” (Vitali *et al.*, *iScience*, 2020), I investigated the import pathway of signal-anchored proteins using Msp1 as a model protein.

2. Which cytosolic chaperones are involved in the biogenesis of mitochondrial SA proteins?

In the article “A network of cytosolic (co)chaperones promotes the biogenesis of mitochondrial signal-anchored outer membrane proteins” (Drwesh *et al.* 2022, *in revision*), I examined the interaction mode between the newly synthesized SA proteins and cytosolic factors, and then validated their physiological relevance in the proteins’ biogenesis.



## 8. Summary of the results

### 8.1 The biogenesis of mitochondrial outer membrane proteins show variable dependence on import factors (Vitali *et al.* 2020)

Our knowledge regarding the import pathway(s) that  $\alpha$ -helical proteins follow, in particular those that span the membrane once via N-terminal TMS and exposing their C-terminal domain towards the cytosol [defined as signal-anchored (SA) proteins] is limited.

In this study, I investigated the involvement of the known import machineries residing in the mitochondrial OM in the biogenesis of SA proteins using the model protein Msp1. To this end, I monitored the mitochondrial steady state levels of Msp1 in different deletion strains. The investigated strains were lacking the MIM complex components Mim1 and Mim2, the TOM receptors Tom20 and Tom70/Tom71, and the TOB complex subunit Mas37, which facilitates the insertion of  $\beta$ -barrel proteins into the mitochondrial OM.

Notably, the absence of the TOM complex receptor Tom70/Tom71 or of Mas37 did not affect the steady state levels of Msp1, while interestingly, deletion of Tom20 caused almost 60% increase in its levels. In contrast, the absence of each of the two MIM subunits or both resulted in drastically lower levels of Msp1 compared to its levels in the corresponding WT cells (Fig. 1B, C).

To validate the engagement of the MIM complex in the biogenesis of Msp1, I conducted *in vitro* import assay of radiolabelled Msp1 into mitochondria isolated from either WT or *mim1/mim2 $\Delta\Delta$*  double deletion strain. Following the *in vitro* import reaction, mitochondria were subjected to alkaline extraction to verify whether the newly synthesized molecules were indeed integrated into the OM of the isolated organelles. Mitochondria isolated from the double-deletion strain had significantly lower capacity to integrate Msp1 into the OM, supporting a direct involvement of the MIM complex in the import process of the SA protein Msp1. (Fig. 1D, E).

Next, I wanted to determine which part of Msp1 is responsible for the dependency on the MIM complex. Since it was previously published that the hydrophobic transmembrane part of Msp1 facilitates its intracellular targeting (Wohlever *et al.*, 2017), I constructed a fusion protein composed of the TMS (a.a residues 1-32) of Msp1, N-terminally fused to GFP moiety and introduced it into WT cells. Using fluorescence microscopy, I observed a full co-localization of this fusion protein with a mitochondrial marker protein (Fig. 2A). Hence, these results indicate



that the TMS of Msp1 is sufficient for its mitochondrial targeting, likely through recognition by the MIM complex which then facilitates its integration into the OM.

To further verify the dependency of the TMS-containing construct on the MIM complex, I introduced the same construct into cells deleted for *MIM1*, *MIM2*, or both. Next, the steady state levels of the fusion protein in different fractions isolated from the transformed cells were monitored. Isolated fractions corresponding to cytosol, ER, and mitochondria were analysed by SDS-PAGE followed by immunodetection (Fig. 2B). The results of this experiment demonstrated that in the absence of a functional MIM complex, the mitochondrial levels of the fusion protein were highly reduced, corresponding with its detection in the ER fraction.

As expected, the absence of the MIM components caused mis-localization of the known MIM substrates Tom20 and Tom70 to the ER, while the localization of other proteins like Tom40 and the inner membrane protein Pic2 was unaltered.

Overall, these findings suggest that Msp1 is a novel substrate of the MIM complex, and that its TMS mediates this MIM-dependency. Furthermore, the MIM complex appears to be essential for the protein's proper mitochondrial targeting.

## **8.2 A network of cytosolic (co)chaperones promotes the biogenesis of mitochondrial signal-anchored outer membrane proteins (Drwesh *et al.* 2022, *in revision*).**

Despite the well-known function of cytosolic (co)chaperones in keeping proteins stable in the cytosol and preventing undesired events of misfolding and aggregation, their involvement in the biogenesis of mitochondrial proteins is inadequately studied. Particularly, no cytosolic factors have been identified yet to mediate the biogenesis of SA proteins.

Since SA proteins, as many mitochondrial proteins, contain hydrophobic patches that serve as TMS for membranal integration, I searched for potential (co)chaperones and/or other cytosolic factors that might be involved in ensuring the safe passage of such proteins from the moment they emerge from the ribosomes until their recognition by the target organelle.

To study the potential involvement of such factors, I used four model proteins from the SA family: the two receptor subunits of the TOM complex, Tom20 and Tom70, and two additional proteins namely, Msp1 and the OM isoform of Mcr1 (Mcr1<sub>mom</sub>). I employed a combined experimental strategy consisting of assays with yeast cells extract, isolated organelles, and *in vitro* experiments with purified proteins.

To test which of the molecular chaperones interact with those SA proteins, I conducted anti-HA pull-down assay in which I used yeast extract to translate *in vitro* HA-variants of the proteins of interest. Since the yeast extract represents the cytosolic fraction of yeast cells which contains ribosomes for translation and the major repertoire of cytosolic factors, I assume that upon pull down, the chaperones that interact with the newly translated proteins will be co-eluted. To identify such bound proteins, I analyzed the bound fraction by either immunodecoration or mass spectrometry. Molecular chaperones that were identified in the elution fraction of assays with all four model proteins, but not upon usage of the negative control protein DHFR, include: the Hsp70 chaperones Ssa1/2 and the Hsp40 co-chaperones Ydj1, Sis1 and Djp1. Weaker interactions were observed with the Hsp90 chaperones Hsc82/Hsp82 and their co-chaperones Aha1 and Sti1. The eluates contained also Hsp104 chaperone and minor amounts of Hsp42 chaperone, suggesting that a small portion of the newly synthesized proteins got aggregated. The specificity of the assay is demonstrated by the fact that the co-chaperone Hch1 and the cytosolic protein Bmh1 were not co-eluted with any of the tested proteins (Fig. 1A, B). Similar results were observed when mass spectrometry was applied to analyze the eluted fraction (Table S1A).

Next, I asked what part of the SA proteins is responsible for the interaction with the indicated molecular chaperones. Since it was previously suggested that chaperones interact with their substrates mainly through hydrophobic patches of the latter (Li et al., 2009; Saio et al., 2014; Clerico et al., 2015), I wanted to test whether this hypothesis applies also to SA proteins. Hence, I performed the same pull-down assay using two additional HA-tagged constructs for each SA protein: one consists of the cytosolic part of the protein (indicated by protein name-C, Fig. 2) and the second includes the single hydrophobic TMS (indicated by protein name-T, Fig. 2). Similar levels of eluted chaperones were observed in the eluate of the TMS construct and of the full-length variant, while very low, if at all, interaction was observed in the eluate of the cytosolic part of the protein. Taken together, my observations suggest that the interactions between SA proteins and molecular chaperones are mainly mediated by their hydrophobic TMS (Fig. 2A-C).

Subsequently, I focused my research on the Hsp40 chaperones Ydj1 and Sis1, and wanted to test whether the interactions observed with the substrates has a physiological relevance to their biogenesis. Of note, Ydj1 has been found to support the mitochondrial import of presequence-containing proteins (Caplan et al., 1992; Xie et al., 2017). To this end, I have monitored the steady state levels of SA proteins in cells depleted of either Ydj1 or Sis1 or both of them, when grown in the presence of doxycycline (Fig. 3A-D). Mitochondrial levels of SA proteins were

not altered in Ydj1 depleted cells, while levels of Tom20 and Tom70 were moderately reduced in Sis1 depleted cells (Fig. 3A, B). These findings might be explained by the previous observations that the J-domain of Sis1 can compensate for the loss of Ydj1 J-domain but not the other way around (Yan and Craig, 1999).

To eliminate such cross compensation, I monitored the mitochondrial levels of the SA proteins in a strain depleted for both (co)chaperones (Fig. 3C). Interestingly, the levels of Tom20 and Tom70 were gradually reduced over time down to 40-50% of their levels under control conditions while levels of Msp1 and Mcr1 were not altered (Fig. 3C, D). To test whether depletion of Ydj1 and Sis1 has a direct implication on the insertion process of SA proteins, I imported freshly translated Tom20 and Tom70 using yeast extract of cells depleted for both chaperones and monitored the insertion process into WT mitochondria. Surprisingly, only Tom20 had a reduced import efficiency while Tom70 import was not altered (Fig. 4A, B). To further analyze the role of Ydj1 and Sis1 in the biogenesis of SA proteins, I tested whether the interaction pattern between newly synthesized SA proteins and the other chaperones is altered in yeast extract depleted for the Hsp40 (co)chaperones. Interestingly, such down-regulation resulted in increased co-eluted levels of chaperones implicated in disaggregation, like Hsp104 and Hsp26, with newly synthesized SA proteins (Fig. 5A, B). These results suggest that the cytosol of cells with highly reduced levels of Ydj1 and Sis1 offer less stabilization for the newly synthesized substrates and hence these substrates are more prone to aggregation under these conditions.

Overall, these findings suggest that Hsp40 co-chaperones play a variable role in keeping signal-anchored proteins stable in the cytosol.

To gain a better understanding of the dynamics of chaperone-substrate interactions, we next aimed to investigate their binding kinetics. To this end, the group of J. Buchner (Technical University, Munich), performed fluorescence anisotropy measurements using recombinantly expressed purified (co)chaperones, Sis1 and Ssa1 and measured their binding to a TAMRA-labelled peptide corresponding to the TMS of either Tom70 or Mcr1. The fluorescence anisotropy of both peptides increased upon addition of recombinant Ssa1 indicating the formation of a peptide-Ssa1 complex (Fig. 6A, B). To further monitor the binding parameters and compare the binding affinity of the substrate to different (co)chaperones, they implemented titration assay. In this assay, increasing concentrations of Ssa1 (Fig. 6C, D) or Sis1 (Fig. 6E, F) were sequentially added to either Tom70 or Mcr1 peptides. The results of these assays revealed several folds higher affinities of the substrate to the Ssa1 Hsp70 chaperone as compared to the affinity between the substrate and Sis1 co-chaperone. This finding is in line with the

assumption that the co-chaperone is involved in the initial low-affinity association with the substrate before passing it on to the main chaperone, which has a higher affinity for it.

To examine in depth the direct involvement of the Hsp70 chaperone Ssa1 in the biogenesis of SA proteins, I performed *in vitro* import assays. In these experiments, the yeast extract, which is used for protein translation, was supplemented with the Hsp70 inhibitor, CBag (C-terminal Bag domain of human Bag-1M) prior to import of substrate proteins into mitochondria. As a result of the CBag supplementation, the import efficiency of both SA proteins Msp1 and Mcr1 drastically decreased (Fig. 7A, B), suggesting a crucial role for Hsp70 in facilitating proper insertion of SA proteins into the mitochondrial OM.

Demonstrating that both Hsp40 and Hsp70 (co)chaperones cooperate to stabilize the SA proteins in the cytosol, we next aimed to understand the dynamics of the complex formation between the SA substrates, the Hsp40 co-chaperones (Sis1), and the Hsp70 chaperones (Ssa1). To this end, Buchner's group performed additional set of fluorescence anisotropy experiments in which Ssa1, ATP and Sis1 were added, each a few minutes apart and in a different order, to the Mcr1-TAMRA-labeled peptide (Fig. 7C-E). Interestingly, the anisotropy measurements demonstrate the order of events in the cytosol, in which the substrate first forms a complex with the Hsp40 co-chaperone and then the substrate is relayed to Ssa1. Surprisingly, the substrate was able to form a complex with Ssa1 even in the absence of Sis1, yet, with lower affinity and higher sensitivity to ATP, which was reflected in faster release of the substrate from the complex. However, when ATP was added in the presence of Sis1, the substrate-Ssa1 complex became more stable, indicating a role of Sis1 in accelerating ATP hydrolysis which retains Hsp70 chaperone in a conformation that favors substrate binding.

Finally, I wished to investigate later stages in the SA proteins biogenesis in which the proteins are getting recognized at the OM surface prior to their membrane integration. To accomplish this, I conducted pull-down assays using recombinant fusion proteins that consist of the cytosolic domains of the TOM complex receptors, Tom20 or Tom70 N-terminally fused to GST moiety. The GST-fusion proteins were then incubated with HA-tagged variants of Msp1 or Mcr1 that were freshly translated in WT yeast extract. Both substrates displayed variable degrees of interaction with both receptors (Fig. 8A). Since I could show that the TOM complex receptors can interact with a subset of molecular (co)chaperones (Fig. S1A), I assume that facilitating productive delivery of substrates to the receptors at the mitochondrial surface involves cooperation with chaperones followed by subsequent membrane integration. This assumption is consistent with previous studies, which reported that Tom70 has a docking site

for Hsp70 and Hsp90 chaperones (Mills et al., 2009; Fan et al., 2010, 2011; Voos, 2003; Wegele et al., 2006).

The Buchner group could confirm such involvement via fluorescence anisotropy using TAMRA-labelled Mcr1-peptide as a substrate. The change in anisotropy was measured upon addition of GST-Tom70, Ssa1, Sis1, and ATP in different orders (Fig. 8B-E). A complex formation between Mcr1 substrate and Tom70 receptor could be observed regardless of the presence of (co)chaperones (Ssa1 and Sis1) (Fig. 8C). Yet, when chaperones were supplemented first, the substrate formed a complex with them, and when ATP was added, this complex disassociated allowing interaction with higher affinity between the substrate and the Tom70 receptor (Fig. 8B). In support of this proposed order of events, despite adding Ssa1 to the reaction after a complex formation between Mcr1 and Tom70, no further increase in anisotropy was detected (Fig. 8C), indicating that the Tom70-substrate complex remained stable. This observation supports the hypothesis that the substrate has a higher binding affinity for the receptor than to the (co)chaperones. Such enhanced affinity can support substrate transfer from the chaperone to the receptor.

Interestingly, addition of Tom70 after the formation of a Mcr1-Ssa1 complex resulted in a further increase in anisotropy (Fig. 8D), indicating that the Tom70 receptor can bind the substrate while the latter is in a complex with the chaperone. Nonetheless, when the substrate was released from Ssa1 upon ATP addition, higher increase in anisotropy was observed (Fig. 8D), suggesting that Tom70 receptor binds the substrate with enhanced affinity upon its release from the chaperone. To ensure that the receptor can recognize the substrate chaperone complex, Sis1 was co-added to the mixture to stabilize the interaction between Ssa1-Mcr1. Even then, Tom70 still interacted with the substrate (Fig. 8E).

To further examine the role of the TOM receptors in the insertion of SA proteins into the mitochondrial OM, I applied two types of *in vitro* import assays using the two radiolabeled substrates, Msp1 and Mcr1 translated in yeast extract. To avoid cross-compensation of the two receptors, their function was concomitantly abolished by either using trypsin-treated mitochondria prior to import or by using mitochondria lacking the Tom20 receptor (from *tom20Δ* strain) and treated with the C-terminal domain of human Hsp90 (C90). C90 is known to block the chaperone binding site on the mitochondrial import receptor Tom70 (Young et al., 2003; Bhangoo et al., 2007), thus inhibiting its activity. The treatment of isolated mitochondria with trypsin results in the proteolytic removal of the cytosolic domains of both Tom20 and Tom70. This treatment led to a decreased import efficiency of Msp1, however the import efficiency of Mcr1 was surprisingly not affected (Fig. 9B). When WT mitochondria were

treated with C90, which results in non-functional Tom70, import of Msp1 and Mcr1 was reduced (Fig. 9C, D). This seemingly contradicts former study in which mitochondrial steady state levels of Msp1 and Mcr1 were not decreased in Tom70 deleted strain (Vitali et al., 2020). This difference can be explained by the fact that in the previous study, the cells lacking Tom70 could adapt for the loss of Tom70, while the effect of inhibition by C90, on the other hand, is immediate and not reversible. Interestingly, an increased insertion efficiency of Msp1 and Mcr1 into mitochondria lacking Tom20 was observed (Fig. 9C, D), which could be explained by elevated expression of Tom70 in cells lacking Tom20 as a compensation mechanism (Fig. S1B). Supporting this assumption, when the samples lacking Tom20 were treated with C90, the membrane integration of both Msp1 and Mcr1 was reduced.

### **8.3 Uncovering targeting priority to yeast peroxisomes using an in-cell competition assay (Rosenthal *et al.* 2020)**

The vast majority of eukaryotic proteins are encoded by the nuclear genome and synthesized in the cytosol before their final targeting to their destination organelle. Most of these proteins have targeting signals that are recognized by distinctive targeting pathways, which assure their correct delivery to the specific organelle.

Since many proteins have similar targeting signals that might utilize the same targeting pathway, a competition between such proteins may affect their recognition and targeting efficiency. However, the mechanism underlying the targeting priority of proteins was not investigated for any known targeting pathway.

To study targeting priority of proteins to organelles, a systematic tool was developed by the group of Maya Schuldiner. Their approach is based on using the well-studied Pex5-mediated peroxisomal targeting pathway as a model. In this pathway, Pex5 mainly recognizes the PTS1 (peroxisomal targeting signal 1) and targets most matrix proteins into the peroxisomal lumen.

To systematically investigate targeting priority of peroxisomal proteins, a synthetic cargo protein with a PTS1 canonical targeting signal (mCherry-SKL) was overexpressed in yeast cells. This situation induced competition with other peroxisomal proteins over the limited amount of Pex5. The Schuldiner group have examined how the localization of each peroxisomal protein (N-terminally tagged with GFP) is affected by this competition, assuming that only proteins with high targeting priority would still be localized to peroxisomes.

Then, they compared the abundance and localization of each GFP-tagged protein between low- and high-competition conditions by imaging the cells on a high-content screening platform. They found that 14 peroxisomal cargo proteins were accumulated in the cytosol indicating that these proteins were affected by the competition induced by high levels of mCherry-SKL. Limited amounts of Pex5 were next confirmed to be the direct cause of this effect since its overexpression could rescue the targeting of a PTS1 cargo protein. Interestingly, the localization of five cargo proteins was not affected by the induced competition, namely: Cat2, Lys1, Mdh3, Pcs60 and Pox1/Fox1, suggesting that they have a high peroxisomal targeting priority.

To support their findings, I performed subcellular fractionation of cells expressing different peroxisomal cargo proteins fused to GFP. Two of them are “low priority” (Pxp1 and Tes1) and the other two are “high priority” proteins (Lys1 and Pox1). Each cargo protein was expressed under either high or low competition conditions (strain expressed high or low levels of mCherry-SKL). Following the subcellular fractionation, I monitored the levels of the cargo proteins in three different fractions: whole cell lysate, supernatant (representing the cytosol), and pellet fraction (representing peroxisome, but also other organelles). I found that the low-priority proteins are enriched, upon the massive competition, in the soluble fraction (Fig. 2D, F), while the high priority ones remain in the organelle pellet (Fig. 2E, F). These findings support the notion that Pex5 cargoes have different targeting priorities.

The Schuldiner group further dissected the mechanism and the different parameters that determine the priority of these proteins. They found that targeting priority to peroxisome is dependent on metabolic conditions and binding affinity of the targeting signal to the cargo factor.

#### **8.4 Cnm1 mediates nucleus-mitochondria contact site formation in response to phospholipid levels (Eisenberg-Bord *et al.* 2021)**

Mitochondria were shown to interact with different organelles through close proximity or physical contact sites that allow direct crosstalk between the involved organelles and promote their proper functioning. Among these contact sites is the one with the nucleus which facilitates signaling cascades, protein targeting, and transfer of mitochondrial metabolites required for maintenance of the nuclear function. Contact sites are usually formed by the aid of proteins and lipids of two membranes, however, the elements involved in tethering between the

mitochondrial outer membrane and the nuclear envelope remain elusive. Mitochondria have continuous contact sites with the most abundant organelle in the cell, the ER, and these contacts are mediated partially by the ERMES, which is involved in phospholipids metabolism. Therefore, it was challenging to distinguish between the ERMES mediated contacts and other particular contact sites with the nucleus.

To address this task, the Schuldiner group developed a method based on a split Venus approach to visualize the nucleus–mitochondria contact site using fluorescence microscopy. They attached one part of a split Venus molecule to the OM protein Tom70, and the second part to Nsg1, a nuclear periphery protein (Nsg1-VN/Tom70-VC). Only at contact sites, where the two membranes are in proximity, the Venus fragments interact forming a full Venus protein, which enables observation of a clear fluorescent signal. The group later confirmed that this signal indicates nucleus–mitochondria contact which is ERMES-independent suggesting that distinct tethering proteins facilitate this contact site.

Next, they wanted to uncover the tethering elements that mediate such contact sites using a high-content screen with high-throughput microscopy. The screen was done in yeast cells with all proteins overexpressed and tagged with mCherry in addition to the reporter of the nucleus–mitochondria contact site (Nsg1-VN/Tom70-VC). This screen uncovered 48 proteins that partially colocalize with the reporter and 9 proteins that fully colocalize with it (Fig. 2B). To shorten down the long list, they performed a second screen in which they searched for proteins whose overexpression extended the nucleus-mitochondria contact site. This second screen yielded 12 hits as potential tethering molecules (Fig. 2C).

Among the 12 uncovered tether candidates, the protein that mostly appeared to be a direct tether was Ybr063c, an uncharacterized protein with unknown function that was not previously studied or implicated in ER–mitochondria contacts. This protein was predicted by several algorithms to be an integral membrane protein, a feature crucial for providing a tethering capacity. The Schuldiner group verified that this protein is not part of the ERMES, since its overexpression did not extend or colocalize with the ERMES contact site.

The topology of Ybr063c was not apparent, since some prediction algorithms predicted one or two membrane-spanning domains, while others predicted Ybr063c to be a soluble protein. Hence, my aim was to clarify this point and test whether Ybr063c is an integral membrane protein. To this end, I used a strain expressing Ybr063c with a small tag (3HA) on its N-terminus and purified crude mitochondria fraction, which is expected to also contain other organelles which are in contact with mitochondria. Then, I performed carbonate extraction (CE) which dissociates peripheral proteins from membranes but cannot extract membrane-embedded



polypeptides from the bilayer. Following this treatment, 3HA-Ybr063c remained in the membrane fraction, similar to the mitochondrial OM protein Tom20 and in contrast to the soluble mitochondrial matrix protein Hep1 (Fig. 3B). This outcome indicates that this protein is embedded in the lipid bilayer.

Next, the Schuldiner group could show that Ybr063c is embedded in the nuclear envelope, hence they named it contact nucleus mitochondria (Cnm1). Additionally, they suggested that Cnm1, in collaboration with the mitochondrial OM protein Tom70, mediates the tethering of nuclear and mitochondrial membranes.



## 9. Discussion

### 9.1 The biogenesis of mitochondrial outer membrane proteins show variable dependence on import factors (Vitali et al. 2020)

All mitochondrial OM proteins are synthesized in the cytosol, and despite the crowded environment of the cell, must get targeted to their correct destination in the mitochondria. Despite the significant efforts made to better understand the import pathways that mitochondrial proteins from different topological categories follow, we are still trying to decipher which import elements facilitate the biogenesis of single span  $\alpha$ -helical proteins. Additionally, it is still unclear whether proteins from the same topological class follow the same import route.

There are three known import machinery complexes residing in the mitochondrial OM which are involved in protein import into mitochondria namely, TOM, TOB, and MIM complexes. In this study, I aimed to investigate the specific import pathway followed by SA proteins, using Msp1 as a model protein. For this purpose, I have applied *in vitro* and *in vivo* approaches using yeast cells.

Interestingly, I observed that deletion of either *MIM1*, *MIM2*, or both led to highly reduced levels of Msp1 in the mitochondrial fraction isolated from these cells. Additionally, upon *in vitro* import of radiolabelled Msp1 into mitochondria isolated from double deletion of *MIM1/MIM2*, the insertion efficiency of Msp1 was drastically impaired. These findings indicate a direct involvement of the MIM complex in facilitating the membranal insertion of newly synthesized Msp1. On the other hand, the levels of Msp1 were not altered upon deletion of subunits of the TOM or TOB complexes, namely *TOM20*, *TOM70/71* or *MAS37*. Hence, one can assume that such import elements are not critically required for the biogenesis of Msp1.

Involvement of the MIM machinery in Msp1 biogenesis has been described in a recent paper (Doan et al., 2020). Engagement of the MIM complex was previously reported for the biogenesis of other SA proteins, namely the TOM complex receptors Tom20 and Tom70 (Waizenegger et al., 2005; Becker et al., 2008; Popov-Čeleketić et al., 2008). However, it seems that Tom20 do not follow the same import and assembly route as Msp1 since its membranal insertion was shown to require Tom40 with the potential involvement of the membrane-embedded segments of other components of the TOM core complex (Ahting et al., 2005).

Despite sharing similar topology and structural features, the mitochondrial levels of the other SA model protein, Mcr1<sub>mom</sub> was not altered in any of the deletion strains. This observation suggests that Mcr1 can follow a self-insertion mechanism that might be driven by the specific lipid composition of the mitochondrial OM. Such an unassisted insertion pathway was already suggested for the TA protein Fis1 (Kemper et al., 2008).

All precursor proteins of the mitochondrial OM are devoid of a typical N-terminal presequence. The targeting signal of such proteins, particularly the SA ones, consists of the single TMS and positively charged flanking regions (Ellenrieder et al., 2015; Dukanovic and Rapaport, 2011; Waizenegger et al., 2003). Accordingly, and in line with a previous observation (Wohlever et al., 2017), I could show via fluorescence microscopy and western blot that the TMS of Msp1 is sufficient for mitochondrial targeting. Additionally, based on our observations, the TMS of Msp1 appears to mediate protein recognition by the MIM complex, as the absence of Mim1 and Mim2 resulted in decreased mitochondrial levels of the fusion protein GFP-TMS accompanied by its mis-localization to the ER.

To gain a better understanding of the pathways  $\alpha$ -helical proteins follow, additional model proteins were employed in this study, among them the single-span protein Atg32 and the TA protein Gem1. Atg32 was found to largely rely on the presence of MIM complex and Tom20 receptor and partially on Tom70 receptor. Gem1, on the other hand, showed only a mild dependency on the MIM complex, and appeared to require mainly the Tom20 receptor.

Despite sharing structural characteristics,  $\alpha$ -helical proteins appear to follow different insertion routes, as each one showed varying levels of reliance on different import factors. However, the characteristic of the substrate that dictates the distinct requirements is still unknown, and it is speculated to be a combination of parameters, including the specific properties of the TMS and the other soluble domains exposed to the cytosol/IMS.

Altogether, my findings suggest a crucial role of the MIM complex in the biogenesis of some SA proteins and identify Msp1 as a novel substrate. Yet, deletion of MIM components did not fully abolish Msp1 integration into the mitochondria, as a portion of newly synthesized protein was still able to insert into the OM. This finding raises the possibility of an alternative membrane insertion pathway which might involve yet unknown protein/lipid factors.

## **9.2 A network of cytosolic (co)chaperones promotes the biogenesis of mitochondrial signal-anchored outer membrane proteins (Drwesh et al. 2022, *in revision*)**

To gain deeper understanding of the role of cytosolic (co)chaperones in the biogenesis of mitochondrial SA proteins, I have applied pull-down assay to search for cytosolic factors that can interact with such proteins.

I identified several (co)chaperones from distinct families that specifically interacted with SA proteins following their synthesis on cytosolic ribosomes. I could later show that these interactions are mainly governed by the SA proteins' hydrophobic TMS which apparently serve as a signal for the chaperones to bind such proteins and shield them from the hydrophilic environment of the cytosol. Such interactions are hypothesised to be crucial for keeping the newly synthesized proteins in an import competent unfolded conformation and to prevent intermolecular non-native interactions that might cause aggregation.

Among the identified chaperones, were members of the Hsp40 family, including Ydj1, Sis1 and Djp1, in addition to members of Hsp70 family, Ssa1/2 and Hsp90 family including its co-chaperones Aha1 and Sti1. However, being interaction partners does not necessarily indicate a physiological relevance for the (co)chaperones in SA proteins biogenesis. Hence, I decided to investigate their involvement in depth. Mitochondrial levels of SA proteins were not altered when the co-chaperones Djp1 or Aha1 were deleted (data not shown). In contrast, when I analysed the mitochondrial fraction isolated from cells depleted of Ydj1 and Sis1, I detected reduction in the steady state levels of Tom20 and Tom70, while levels of the other SA proteins like Msp1 and Mcr1 were not altered. Similar involvement of Ydj1 and Sis1 was previously reported for the biogenesis of  $\beta$ -barrel proteins (Jores et al., 2018). Nonetheless, depletion of only Ydj1 had no effect on their levels, whereas depletion of Sis1 caused only a mild effect on the levels of Tom20 and Tom70. These findings suggest a compensatory role that Sis1 might play when Ydj1 is absent as suggested in an earlier publication (Yan and Craig, 1999). When analysing the import process of the affected proteins in yeast extract depleted of both co-chaperones, only Tom20 showed impaired insertion efficiency suggesting that various SA proteins rely to a different degree on Hsp40 co-chaperones. The engagement of Ydj1 in the import of mitochondrial proteins, particularly the MTS-containing protein  $F_1\beta$  residing in the IM was reported previously (Caplan et al., 1992), while Sis1 was so far only implicated in the biogenesis of mitochondrial  $\beta$ -barrel proteins (Jores et al., 2018).

Simultaneous depletion of Ydj1 and Sis1, led to some alterations in the interactions pattern between other chaperones and SA proteins. Chaperones that are known to be activated under stress conditions and associate with aggregated proteins namely, Hsp104 and Hsp26 (Zolkiewski et al., 2012; Zhou et al., 2011; Franzmann et al., 2005), were detected in the bound fraction of SA proteins translated in the absence of Ydj1 and Sis1. These observations emphasise the significance of these chaperones in maintaining the unfolded state of newly produced proteins and preventing their aggregation. Such a function was formerly proposed for such chaperones (Cry, 1995; Klaips et al., 2020).

To validate these results, we employed the technique of fluorescence anisotropy in collaboration with the Buchner group in Munich. We used peptides resembling the SA segments of Mcr1 and Tom70 as model proteins and could demonstrate an interaction between the substrates and the two (co)chaperones, Ssa1 and Sis1. Interestingly, the binding affinity of the substrates to the co-chaperone (Sis1) was 10-fold lower than the binding to the Hsp70 chaperone (Ssa1). These observations support the hypothesis that the substrate transfer from the co-chaperone to the main Hsp70 chaperones is driven by increased affinity to the latter. Similar results were previously observed for a peptide representing the mitochondrial targeting element of the  $\beta$ -barrel protein Porin (Jores et al., 2018). Although we detected an interaction between substrate and Hsp70 chaperone also in the absence of Sis1, this association was vulnerable to ATP. In contrast, in the presence of Sis1 the complex was no longer sensitive to ATP, indicating Sis1's regulatory role in Hsp70 ATPase activity. In line with our findings, previous studies have shown that both Sis1 and Ydj1 facilitate binding between substrate and Hsp70 chaperone (Kampinga and Craig, 2010).

The physiological significance of the observed interactions between SA substrates and Hsp70 chaperone was substantiated by our observation that the CBag inhibitor, which disrupts the ATPase function of Hsp70 chaperone, had a significant inhibitory effect on the mitochondrial insertion of SA substrates, Msp1, and Mcr1. Additionally, we could show that Ssa1/2 chaperone can interact with the TOM receptors, particularly Tom70 which has a TPR domain that serves as a docking site for Hsp70 and Hsp90 chaperones. Such interaction was reported in the past to mediate targeting of carrier proteins and  $\beta$ -barrel ones into the mitochondria (Young et al., 2003; Jores et al., 2018).

Based on our observations, we propose a model in which the substrate, after being in a complex with Hsp40/Hsp70 chaperones is released and passed on to Tom70 receptor to which it has a higher affinity. The possible involvement of the TOM complex receptors in the insertion process of SA proteins was verified by showing that newly synthesized SA proteins

can bind these receptors. Furthermore, the insertion of SA proteins was slightly decreased when both receptors Tom20 and Tom70 were deleted, proteolytically removed, or inhibited. Such an effect was barely observed when one of them was absent, suggesting that both receptors can cross compensate for the loss of each other. Alternative explanation, based on an earlier model, suggests that interaction between Tom20 and Tom70 facilitates preprotein release from the chaperones by competition. Hence, a functional interaction between Tom20 and Tom70 may be required at a later step of the Tom70-mediated import, after chaperone docking (Fan et al., 2011).

Overall, we suggest a novel aspect in the biogenesis of SA proteins in which the Hsp40 co-chaperones Ydj1 and Sis1 function together with Hsp70 through their J domain in enabling proper targeting of SA proteins to the mitochondria. We propose that such targeting probably involves the TOM receptors that play an offsetting role in facilitating recognition of substrate/chaperone complex at the cytosolic side of the OM and assist their final insertion into the OM. Beside functioning in concert with Hsp70, some Hsp40 chaperones have evolved functions that mostly do not require their J domains, including prevention of aggregation and modulating the stability of protein complexes. Such a role was previously suggested for the Hsp40 chaperones DNAJB6b and DNAJB8, that were found to be suppressors of aggregation and toxicity of disease-associated polyglutamine proteins (Hageman et al., 2010). However, since Tom20 was the only SA protein whose import efficiency was decreased upon depletion of Ydj1 and Sis1, we assume that additional Hsp40 chaperones may play a role in the biogenesis of the other SA proteins, especially since this family consists of at least 20 other co-chaperones in yeast.





## 10. References

- Aguado, A., Fernández-Higuero, J. A., Moro, F., & Muga, A. (2015). Chaperone-assisted protein aggregate reactivation: Different solutions for the same problem. *Archives of Biochemistry and Biophysics*, *580*, 121–134. <https://doi.org/10.1016/j.abb.2015.07.006>
- Ahting, U., Waizenegger, T., Neupert, W., & Rapaport, D. (2005). Signal-anchored proteins follow a unique insertion pathway into the outer membrane of mitochondria. *The Journal of Biological Chemistry*, *280*(1), 48–53. <https://doi.org/10.1074/jbc.M410905200>
- Sharma, A., Ahmad, S., Ahmad, T., Ali, S., and Syed, M. A. (2021). Mitochondrial dynamics and mitophagy in lung disorders. *Life Sciences*, *284*, 119876.
- Becker, T., Pfanschmidt, S., Guiard, B., Stojanovski, D., Milenkovic, D., Kutik, S., Pfanner, N., Meisinger, C., & Wiedemann, N. (2008). Biogenesis of the mitochondrial TOM complex: Mim1 promotes insertion and assembly of signal-anchored receptors. *The Journal of Biological Chemistry*, *283*(1), 120–127. <https://doi.org/10.1074/jbc.M706997200>
- Becker, T., Wenz, L. S., Krüger, V., Lehmann, W., Müller, J. M., Goroncy, L., Zufall, N., Lithgow, T., Guiard, B., Chacinska, A., Wagner, R., Meisinger, C., & Pfanner, N. (2011). The mitochondrial import protein Mim1 promotes biogenesis of multispanning outer membrane proteins. *The Journal of Cell Biology*, *194*(3), 387–395. <https://doi.org/10.1083/jcb.201102044>
- Bhango, M. K., Tzankov, S., Fan, A. C., Dejgaard, K., Thomas, D. Y., & Young, J. C. (2007). Multiple 40-kDa heat-shock protein chaperones function in Tom70-dependent mitochondrial import. *Molecular Biology of the Cell*, *18*(9), 3414–3428. <https://doi.org/10.1091/mbc.e07-01-0088>
- Bleazard, W., McCaffery, J. M., King, E. J., Bale, S., Mozdy, A., Tieu, Q., Nunnari, J., & Shaw, J. M. (1999). The dynamin-related GTPase Dnm1 regulates mitochondrial fission in yeast. *Nature Cell Biology*, *1*(5), 298–304. <https://doi.org/10.1038/13014>
- Böckler, S., & Westermann, B. (2014). Mitochondrial ER contacts are crucial for mitophagy in yeast. *Developmental Cell*, *28*(4), 450–458. <https://doi.org/10.1016/j.devcel.2014.01.012>
- Burri, L., Vascotto, K., Gentle, I. E., Chan, N. C., Beilharz, T., Stapleton, D. I., Ramage, L., & Lithgow, T. (2006). Integral membrane proteins in the mitochondrial outer membrane of *Saccharomyces cerevisiae*. *The FEBS Journal*, *273*(7), 1507–1515. <https://doi.org/10.1111/j.1742-4658.2006.05171.x>

- Caplan, A. J., Cyr, D. M., & Douglas, M. G. (1992). YDJ1p facilitates polypeptide translocation across different intracellular membranes by a conserved mechanism. *Cell*, *71*(7), 1143–1155. [https://doi.org/10.1016/s0092-8674\(05\)80063-7](https://doi.org/10.1016/s0092-8674(05)80063-7)
- Chan, N. C., & Lithgow, T. (2008). The peripheral membrane subunits of the SAM complex function codependently in mitochondrial outer membrane biogenesis. *Molecular Biology of the Cell*, *19*(1), 126–136. <https://doi.org/10.1091/mbc.e07-08-0796>
- Chen, Y. C., Umanah, G. K., Dephoure, N., Andrabi, S. A., Gygi, S. P., Dawson, T. M., Dawson, V. L., & Rutter, J. (2014). Msp1/ATAD1 maintains mitochondrial function by facilitating the degradation of mislocalized tail-anchored proteins. *The EMBO Journal*, *33*(14), 1548–1564. <https://doi.org/10.15252/embj.201487943>
- Cichocki, B. A., Krumpke, K., Vitali, D. G., & Rapaport, D. (2018). Pex19 is involved in importing dually targeted tail-anchored proteins to both mitochondria and peroxisomes. *Traffic (Copenhagen, Denmark)*, *19*(10), 770–785. <https://doi.org/10.1111/tra.12604>
- Clerico, E. M., Tilitsky, J. M., Meng, W., & Gierasch, L. M. (2015). How hsp70 molecular machines interact with their substrates to mediate diverse physiological functions. *Journal of Molecular Biology*, *427*(7), 1575–1588. <https://doi.org/10.1016/j.jmb.2015.02.004>
- Cyr D. M. (1995). Cooperation of the molecular chaperone Ydj1 with specific Hsp70 homologs to suppress protein aggregation. *FEBS Letters*, *359*(2-3), 129–132. [https://doi.org/10.1016/0014-5793\(95\)00024-4](https://doi.org/10.1016/0014-5793(95)00024-4)
- Cyr, D. M., & Ramos, C. H. (2015). Specification of Hsp70 function by Type I and Type II Hsp40. *Sub-Cellular Biochemistry*, *78*, 91–102. [https://doi.org/10.1007/978-3-319-11731-7\\_4](https://doi.org/10.1007/978-3-319-11731-7_4)
- Day, P. M., Potter, D., & Inoue, K. (2014). Evolution and targeting of Omp85 homologs in the chloroplast outer envelope membrane. *Frontiers in Plant Science*, *5*, 535. <https://doi.org/10.3389/fpls.2014.00535>
- Delille, H. K., & Schrader, M. (2008). Targeting of hFis1 to peroxisomes is mediated by Pex19p. *The Journal of Biological Chemistry*, *283*(45), 31107–31115. <https://doi.org/10.1074/jbc.M803332200>
- Dembowski, M., Kunkele, K. P., Nargang, F. E., Neupert, W., & Rapaport, D. (2001). Assembly of Tom6 and Tom7 into the TOM core complex of *Neurospora crassa*. *The Journal of Biological Chemistry*, *276*(21), 17679–17685. <https://doi.org/10.1074/jbc.M009653200>

- Deshai, R. J., Koch, B. D., Werner-Washburne, M., Craig, E. A., & Schekman, R. (1988). A subfamily of stress proteins facilitates translocation of secretory and mitochondrial precursor polypeptides. *Nature*, *332*(6167), 800–805. <https://doi.org/10.1038/332800a0>
- Doan, K. N., Grevel, A., Mårtensson, C. U., Ellenrieder, L., Thornton, N., Wenz, L. S., Opaliński, Ł., Guiard, B., Pfanner, N., & Becker, T. (2020). The Mitochondrial Import Complex MIM Functions as Main Translocase for  $\alpha$ -Helical Outer Membrane Proteins. *Cell Reports*, *31*(4), 107567. <https://doi.org/10.1016/j.celrep.2020.107567>
- Doyle, S. M., & Wickner, S. (2009). Hsp104 and ClpB: protein disaggregating machines. *Trends in Biochemical Sciences*, *34*(1), 40–48. <https://doi.org/10.1016/j.tibs.2008.09.010>
- Dukanovic, J., & Rapaport, D. (2011). Multiple pathways in the integration of proteins into the mitochondrial outer membrane. *Biochimica et Biophysica Acta*, *1808*(3), 971–980. <https://doi.org/10.1016/j.bbamem.2010.06.021>
- Elbaz-Alon Y. (2017). Mitochondria-organelle contact sites: the plot thickens. *Biochemical Society Transactions*, *45*(2), 477–488. <https://doi.org/10.1042/BST20160130>
- Ellenrieder, L., Mårtensson, C. U., & Becker, T. (2015). Biogenesis of mitochondrial outer membrane proteins, problems and diseases. *Biological Chemistry*, *396*(11), 1199–1213. <https://doi.org/10.1515/hsz-2015-0170>
- Endo, T., Mitsui, S., Nakai, M., & Roise, D. (1996). Binding of mitochondrial presequences to yeast cytosolic heat shock protein 70 depends on the amphiphilicity of the presequence. *The Journal of Biological Chemistry*, *271*(8), 4161–4167. <https://doi.org/10.1074/jbc.271.8.4161>
- Endo, T., & Sakaue, H. (2019). Multifaceted roles of porin in mitochondrial protein and lipid transport. *Biochemical Society Transactions*, *47*(5), 1269–1277. <https://doi.org/10.1042/BST20190153>
- Fan, A. C., Gava, L. M., Ramos, C. H., & Young, J. C. (2010). Human mitochondrial import receptor Tom70 functions as a monomer. *The Biochemical Journal*, *429*(3), 553–563. <https://doi.org/10.1042/BJ20091855>
- Fan, A. C., Kozlov, G., Hoegl, A., Marcellus, R. C., Wong, M. J., Gehring, K., & Young, J. C. (2011). Interaction between the human mitochondrial import receptors Tom20 and Tom70 in vitro suggests a chaperone displacement mechanism. *The Journal of Biological Chemistry*, *286*(37), 32208–32219. <https://doi.org/10.1074/jbc.M111.280446>

- Fang, Y., Morrell, J. C., Jones, J. M., & Gould, S. J. (2004). PEX3 functions as a PEX19 docking factor in the import of class I peroxisomal membrane proteins. *The Journal of Cell Biology*, *164*(6), 863–875. <https://doi.org/10.1083/jcb.200311131>
- Farré, J. C., Mahalingam, S. S., Proietto, M., & Subramani, S. (2019). Peroxisome biogenesis, membrane contact sites, and quality control. *EMBO Reports*, *20*(1), e46864. <https://doi.org/10.15252/embr.201846864>
- Fernández-Fernández, M. R., Gragera, M., Ochoa-Ibarrola, L., Quintana-Gallardo, L., & Valpuesta, J. M. (2017). Hsp70 - a master regulator in protein degradation. *FEBS Letters*, *591*(17), 2648–2660. <https://doi.org/10.1002/1873-3468.12751>
- Flinner, N., Ellenrieder, L., Stiller, S. B., Becker, T., Schleiff, E., & Mirus, O. (2013). Mdm10 is an ancient eukaryotic porin co-occurring with the ERMES complex. *Biochimica et biophysica Acta*, *1833*(12), 3314–3325. <https://doi.org/10.1016/j.bbamcr.2013.10.006>
- Franzmann, T. M., Wühr, M., Richter, K., Walter, S., & Buchner, J. (2005). The activation mechanism of Hsp26 does not require dissociation of the oligomer. *Journal of Molecular Biology*, *350*(5), 1083–1093. <https://doi.org/10.1016/j.jmb.2005.05.034>
- Fresenius, H. L., & Wohlever, M. L. (2019). Sorting out how Msp1 maintains mitochondrial membrane proteostasis. *Mitochondrion*, *49*, 128–134. <https://doi.org/10.1016/j.mito.2019.07.011>
- Genest, O., Wickner, S., & Doyle, S. M. (2019). Hsp90 and Hsp70 chaperones: Collaborators in protein remodeling. *The Journal of Biological Chemistry*, *294*(6), 2109–2120. <https://doi.org/10.1074/jbc.REV118.002806>
- Gray M. W. (2012). Mitochondrial evolution. *Cold Spring Harbor Perspectives in Biology*, *4*(9), a011403. <https://doi.org/10.1101/cshperspect.a011403>
- Hageman, J., Rujano, M. A., van Waarde, M. A., Kakkar, V., Dirks, R. P., Govorukhina, N., Oosterveld-Hut, H. M., Lubsen, N. H., & Kampinga, H. H. (2010). A DNAJB chaperone subfamily with HDAC-dependent activities suppresses toxic protein aggregation. *Molecular Cell*, *37*(3), 355–369. <https://doi.org/10.1016/j.molcel.2010.01.001>
- Hermann, G. J., Thatcher, J. W., Mills, J. P., Hales, K. G., Fuller, M. T., Nunnari, J., & Shaw, J. M. (1998). Mitochondrial fusion in yeast requires the transmembrane GTPase Fzo1p. *The Journal of Cell Biology*, *143*(2), 359–373. <https://doi.org/10.1083/jcb.143.2.359>

- Hettema, E. H., Ruigrok, C. C., Koerkamp, M. G., van den Berg, M., Tabak, H. F., Distel, B., & Braakman, I. (1998). The cytosolic DnaJ-like protein djp1p is involved specifically in peroxisomal protein import. *The Journal of Cell Biology*, *142*(2), 421–434. <https://doi.org/10.1083/jcb.142.2.421>
- Höhr, A., Lindau, C., Wirth, C., Qiu, J., Stroud, D. A., Kutik, S., Guiard, B., Hunte, C., Becker, T., Pfanner, N., & Wiedemann, N. (2018). Membrane protein insertion through a mitochondrial  $\beta$ -barrel gate. *Science (New York, N.Y.)*, *359*(6373), eaah6834. <https://doi.org/10.1126/science.aah6834>
- Horie, C., Suzuki, H., Sakaguchi, M., & Mihara, K. (2003). Targeting and assembly of mitochondrial tail-anchored protein Tom5 to the TOM complex depend on a signal distinct from that of tail-anchored proteins dispersed in the membrane. *The Journal of Biological Chemistry*, *278*(42), 41462–41471. <https://doi.org/10.1074/jbc.M307047200>
- Hulett, J. M., Lueder, F., Chan, N. C., Perry, A. J., Wolyneć, P., Likić, V. A., Gooley, P. R., & Lithgow, T. (2008). The transmembrane segment of Tom20 is recognized by Mim1 for docking to the mitochondrial TOM complex. *Journal of Molecular Biology*, *376*(3), 694–704. <https://doi.org/10.1016/j.jmb.2007.12.021>
- Ishikawa, D., Yamamoto, H., Tamura, Y., Moritoh, K., & Endo, T. (2004). Two novel proteins in the mitochondrial outer membrane mediate beta-barrel protein assembly. *The Journal of Cell Biology*, *166*(5), 621–627. <https://doi.org/10.1083/jcb.200405138>
- Jores, T., Klinger, A., Groß, L. E., Kawano, S., Flinner, N., Duchardt-Ferner, E., Wöhnert, J., Kalbacher, H., Endo, T., Schleiff, E., & Rapaport, D. (2016). Characterization of the targeting signal in mitochondrial  $\beta$ -barrel proteins. *Nature Communications*, *7*, 12036. <https://doi.org/10.1038/ncomms12036>
- Jores, T., Lawatscheck, J., Beke, V., Franz-Wachtel, M., Yunoki, K., Fitzgerald, J. C., Macek, B., Endo, T., Kalbacher, H., Buchner, J., & Rapaport, D. (2018). Cytosolic Hsp70 and Hsp40 chaperones enable the biogenesis of mitochondrial  $\beta$ -barrel proteins. *The Journal of Cell Biology*, *217*(9), 3091–3108. <https://doi.org/10.1083/jcb.201712029>
- Kampinga, H. H., & Craig, E. A. (2010). The HSP70 chaperone machinery: J proteins as drivers of functional specificity. *Nature Reviews. Molecular cell biology*, *11*(8), 579–592. <https://doi.org/10.1038/nrm2941>
- Kanki, T., Wang, K., Cao, Y., Baba, M., & Klionsky, D. J. (2009). Atg32 is a mitochondrial protein that confers selectivity during mitophagy. *Developmental cell*, *17*(1), 98–109. <https://doi.org/10.1016/j.devcel.2009.06.014>

- Keil, P., & Pfanner, N. (1993). Insertion of MOM22 into the mitochondrial outer membrane strictly depends on surface receptors. *FEBS Letters*, *321*(2-3), 197–200. [https://doi.org/10.1016/0014-5793\(93\)80107-6](https://doi.org/10.1016/0014-5793(93)80107-6)
- Kemper, C., Habib, S. J., Engl, G., Heckmeyer, P., Dimmer, K. S., & Rapaport, D. (2008). Integration of tail-anchored proteins into the mitochondrial outer membrane does not require any known import components. *Journal of Cell Science*, *121*(Pt 12), 1990–1998. <https://doi.org/10.1242/jcs.024034>
- Kim, Y. I., Levchenko, I., Fraczkowska, K., Woodruff, R. V., Sauer, R. T., & Baker, T. A. (2001). Molecular determinants of complex formation between Clp/Hsp100 ATPases and the ClpP peptidase. *Nature Structural Biology*, *8*(3), 230–233. <https://doi.org/10.1038/84967>
- Klaips, C. L., Gropp, M., Hipp, M. S., & Hartl, F. U. (2020). Sis1 potentiates the stress response to protein aggregation and elevated temperature. *Nature Communications*, *11*(1), 6271. <https://doi.org/10.1038/s41467-020-20000-x>
- Kornmann, B., Osman, C., & Walter, P. (2011). The conserved GTPase Gem1 regulates endoplasmic reticulum-mitochondria connections. *Proceedings of the National Academy of Sciences of the United States of America*, *108*(34), 14151–14156. <https://doi.org/10.1073/pnas.1111314108>
- Krimmer, T., Rapaport, D., Ryan, M. T., Meisinger, C., Kassenbrock, C. K., Blachly-Dyson, E., Forte, M., Douglas, M. G., Neupert, W., Nargang, F. E., & Pfanner, N. (2001). Biogenesis of porin of the outer mitochondrial membrane involves an import pathway via receptors and the general import pore of the TOM complex. *The Journal of Cell Biology*, *152*(2), 289–300. <https://doi.org/10.1083/jcb.152.2.289>
- Kutik, S., Stojanovski, D., Becker, L., Becker, T., Meinecke, M., Krüger, V., Prinz, C., Meisinger, C., Guiard, B., Wagner, R., Pfanner, N., & Wiedemann, N. (2008). Dissecting membrane insertion of mitochondrial beta-barrel proteins. *Cell*, *132*(6), 1011–1024. <https://doi.org/10.1016/j.cell.2008.01.028>
- Lamb, D. C., Kelly, D. E., Manning, N. J., Kaderbhai, M. A., & Kelly, S. L. (1999). Biodiversity of the P450 catalytic cycle: yeast cytochrome b5/NADH cytochrome b5 reductase complex efficiently drives the entire sterol 14-demethylation (CYP51) reaction. *FEBS Letters*, *462*(3), 283–288. [https://doi.org/10.1016/s0014-5793\(99\)01548-3](https://doi.org/10.1016/s0014-5793(99)01548-3)
- Lee, H., & Yoon, Y. (2016). Mitochondrial fission and fusion. *Biochemical Society Transactions*, *44*(6), 1725–1735. <https://doi.org/10.1042/BST20160129>

- Lesnik, C., Cohen, Y., Atir-Lande, A., Schuldiner, M., & Arava, Y. (2014). OM14 is a mitochondrial receptor for cytosolic ribosomes that supports co-translational import into mitochondria. *Nature Communications*, *5*, 5711. <https://doi.org/10.1038/ncomms6711>
- Lin, M. T., & Beal, M. F. (2006). Mitochondrial dysfunction and oxidative stress in neurodegenerative diseases. *Nature*, *443*(7113), 787–795. <https://doi.org/10.1038/nature05292>
- Li, Y., Gao, X., & Chen, L. (2009). GroEL Recognizes an Amphipathic Helix and Binds to the Hydrophobic Side. *The Journal of Biological Chemistry*, *284*(7), 4324–4331. <https://doi.org/10.1074/jbc.M804818200>
- Mårtensson, C. U., Priesnitz, C., Song, J., Ellenrieder, L., Doan, K. N., Boos, F., Floerchinger, A., Zufall, N., Oeljeklaus, S., Warscheid, B., & Becker, T. (2019). Mitochondrial protein translocation-associated degradation. *Nature*, *569*(7758), 679–683. <https://doi.org/10.1038/s41586-019-1227-y>
- Matsumoto, S., Nakatsukasa, K., Kakuta, C., Tamura, Y., Esaki, M., & Endo, T. (2019). Msp1 Clears Mistargeted Proteins by Facilitating Their Transfer from Mitochondria to the ER. *Molecular Cell*, *76*(1), 191–205.e10. <https://doi.org/10.1016/j.molcel.2019.07.006>
- Mayer, M., Kies, U., Kammermeier, R., & Buchner, J. (2000). BiP and PDI cooperate in the oxidative folding of antibodies in vitro. *The Journal of Biological Chemistry*, *275*(38), 29421–29425. <https://doi.org/10.1074/jbc.M002655200>
- Mayer, M. P., Schröder, H., Rüdiger, S., Paal, K., Laufen, T., & Bukau, B. (2000). Multistep mechanism of substrate binding determines chaperone activity of Hsp70. *Nature Structural Biology*, *7*(7), 586–593. <https://doi.org/10.1038/76819>
- Meineke, B., Engl, G., Kemper, C., Vasiljev-Neumeyer, A., Paulitschke, H., & Rapaport, D. (2008). The outer membrane form of the mitochondrial protein Mcr1 follows a TOM-independent membrane insertion pathway. *FEBS Letters*, *582*(6), 855–860. <https://doi.org/10.1016/j.febslet.2008.02.009>
- Meisinger, C., Brix, J., Model, K., Pfanner, N., & Ryan, M. T. (1999). The preprotein translocase of the outer mitochondrial membrane: receptors and a general import pore. *Cellular and Molecular Life Sciences: CMLS*, *56*(9-10), 817–824. <https://doi.org/10.1007/s000180050028>
- Meisinger, C., Rissler, M., Chacinska, A., Szklarz, L. K., Milenkovic, D., Kozjak, V., Schönfisch, B., Lohaus, C., Meyer, H. E., Yaffe, M. P., Guiard, B., Wiedemann, N., & Pfanner, N. (2004). The mitochondrial morphology protein Mdm10 functions in assembly

- of the preprotein translocase of the outer membrane. *Developmental Cell*, 7(1), 61–71. <https://doi.org/10.1016/j.devcel.2004.06.003>
- Meyer, J. N., Leuthner, T. C., & Luz, A. L. (2017). Mitochondrial fusion, fission, and mitochondrial toxicity. *Toxicology*, 391, 42–53. <https://doi.org/10.1016/j.tox.2017.07.019>
- Mills, R. D., Trehwella, J., Qiu, T. W., Welte, T., Ryan, T. M., Hanley, T., Knott, R. B., Lithgow, T., & Mulhern, T. D. (2009). Domain organization of the monomeric form of the Tom70 mitochondrial import receptor. *Journal of Molecular Biology*, 388(5), 1043–1058. <https://doi.org/10.1016/j.jmb.2009.03.070>
- Mnaimneh, S., Davierwala, A. P., Haynes, J., Moffat, J., Peng, W. T., Zhang, W., Yang, X., Pootoolal, J., Chua, G., Lopez, A., Trochesset, M., Morse, D., Krogan, N. J., Hiley, S. L., Li, Z., Morris, Q., Grigull, J., Mitsakakis, N., Roberts, C. J., Greenblatt, J. F., ... Hughes, T. R. (2004). Exploration of essential gene functions via titratable promoter alleles. *Cell*, 118(1), 31–44. <https://doi.org/10.1016/j.cell.2004.06.013>
- Morán Luengo, T., Mayer, M. P., & Rüdiger, S. (2019). The Hsp70-Hsp90 Chaperone Cascade in Protein Folding. *Trends in Cell Biology*, 29(2), 164–177. <https://doi.org/10.1016/j.tcb.2018.10.004>
- Nillegoda, N. B., & Bukau, B. (2015). Metazoan Hsp70-based protein disaggregases: emergence and mechanisms. *Frontiers in Molecular Biosciences*, 2, 57. <https://doi.org/10.3389/fmolb.2015.00057>
- Noinaj, N., Kuszak, A. J., Balusek, C., Gumbart, J. C., & Buchanan, S. K. (2014). Lateral opening and exit pore formation are required for BamA function. *Structure (London, England : 1993)*, 22(7), 1055–1062. <https://doi.org/10.1016/j.str.2014.05.008>
- Nunnari, J., & Suomalainen, A. (2012). Mitochondria: in sickness and in health. *Cell*, 148(6), 1145–1159. <https://doi.org/10.1016/j.cell.2012.02.035>
- Obuchowski, I., & Liberek, K. (2020). Small but mighty: a functional look at bacterial sHSPs. *Cell Stress & Chaperones*, 25(4), 593–600. <https://doi.org/10.1007/s12192-020-01094-0>
- Okamoto, K., Kondo-Okamoto, N., & Ohsumi, Y. (2009). Mitochondria-anchored receptor Atg32 mediates degradation of mitochondria via selective autophagy. *Developmental Cell*, 17(1), 87–97. <https://doi.org/10.1016/j.devcel.2009.06.013>
- Opaliński, Ł., Song, J., Priesnitz, C., Wenz, L. S., Oeljeklaus, S., Warscheid, B., Pfanner, N., & Becker, T. (2018). Recruitment of Cytosolic J-Proteins by TOM Receptors Promotes Mitochondrial Protein Biogenesis. *Cell Reports*, 25(8), 2036–2043.e5. <https://doi.org/10.1016/j.celrep.2018.10.083>



- Papić, D., Elbaz-Alon, Y., Koerdt, S. N., Leopold, K., Worm, D., Jung, M., Schuldiner, M., & Rapaport, D. (2013). The role of Djp1 in import of the mitochondrial protein Mim1 demonstrates specificity between a cochaperone and its substrate protein. *Molecular and Cellular Biology*, *33*(20), 4083–4094. <https://doi.org/10.1128/MCB.00227-13>
- Papic, D., Krumpe, K., Dukanovic, J., Dimmer, K. S., & Rapaport, D. (2011). Multispan mitochondrial outer membrane protein Ugo1 follows a unique Mim1-dependent import pathway. *The Journal of Cell Biology*, *194*(3), 397–405. <https://doi.org/10.1083/jcb.201102041>
- Paschen, S. A., Neupert, W., & Rapaport, D. (2005). Biogenesis of beta-barrel membrane proteins of mitochondria. *Trends in Biochemical Sciences*, *30*(10), 575–582. <https://doi.org/10.1016/j.tibs.2005.08.009>
- Ponnalagu, D., & Singh, H. (2017). Anion Channels of Mitochondria. *Handbook of Experimental Pharmacology*, *240*, 71–101. [https://doi.org/10.1007/164\\_2016\\_39](https://doi.org/10.1007/164_2016_39)
- Popov-Celeketić, J., Waizenegger, T., & Rapaport, D. (2008). Mim1 functions in an oligomeric form to facilitate the integration of Tom20 into the mitochondrial outer membrane. *Journal of Molecular Biology*, *376*(3), 671–680. <https://doi.org/10.1016/j.jmb.2007.12.006>
- Pratt, W. B., Galigniana, M. D., Morishima, Y., & Murphy, P. J. (2004). Role of molecular chaperones in steroid receptor action. *Essays in Biochemistry*, *40*, 41–58. <https://doi.org/10.1042/bse0400041>
- Rapaport, D., Brunner, M., Neupert, W., & Westermann, B. (1998). Fzo1p is a mitochondrial outer membrane protein essential for the biogenesis of functional mitochondria in *Saccharomyces cerevisiae*. *The Journal of Biological Chemistry*, *273*(32), 20150–20155. <https://doi.org/10.1074/jbc.273.32.20150>
- Reading, D. S., Hallberg, R. L., & Myers, A. M. (1989). Characterization of the yeast HSP60 gene coding for a mitochondrial assembly factor. *Nature*, *337*(6208), 655–659. <https://doi.org/10.1038/337655a0>
- Reidy, M., Sharma, R., Shastry, S., Roberts, B. L., Albino-Flores, I., Wickner, S., & Masison, D. C. (2014). Hsp40s specify functions of Hsp104 and Hsp90 protein chaperone machines. *PLoS Genetics*, *10*(10), e1004720. <https://doi.org/10.1371/journal.pgen.1004720>
- Saio, T., Guan, X., Rossi, P., Economou, A., & Kalodimos, C. G. (2014). Structural basis for protein antiaggregation activity of the trigger factor chaperone. *Science (New York, N.Y.)*, *344*(6184), 1250494. <https://doi.org/10.1126/science.1250494>

- Selkrig, J., Leyton, D. L., Webb, C. T., & Lithgow, T. (2014). Assembly of  $\beta$ -barrel proteins into bacterial outer membranes. *Biochimica et Biophysica Acta*, 1843(8), 1542–1550. <https://doi.org/10.1016/j.bbamcr.2013.10.009>
- Sesaki, H., & Jensen, R. E. (2001). UGO1 encodes an outer membrane protein required for mitochondrial fusion. *The Journal of Cell Biology*, 152(6), 1123–1134. <https://doi.org/10.1083/jcb.152.6.1123>
- Sherman, E. L., Go, N. E., & Nargang, F. E. (2005). Functions of the small proteins in the TOM complex of *Neurospora crassa*. *Molecular Biology of the Cell*, 16(9), 4172–4182. <https://doi.org/10.1091/mbc.e05-03-0187>
- Sinzel, M., Tan, T., Wendling, P., Kalbacher, H., Özbalci, C., Chelius, X., Westermann, B., Brügger, B., Rapaport, D., & Dimmer, K. S. (2017). Mcp3 is a novel mitochondrial outer membrane protein that follows a unique IMP-dependent biogenesis pathway. *EMBO Reports*, 18(10), 1869. <https://doi.org/10.15252/embr.201745020>
- Solís, E. J., Pandey, J. P., Zheng, X., Jin, D. X., Gupta, P. B., Airoidi, E. M., Pincus, D., & Denic, V. (2016). Defining the Essential Function of Yeast Hsf1 Reveals a Compact Transcriptional Program for Maintaining Eukaryotic Proteostasis. *Molecular Cell*, 63(1), 60–71. <https://doi.org/10.1016/j.molcel.2016.05.014>
- Soll, J., & Schleiff, E. (2004). Protein import into chloroplasts. *Nature Reviews. Molecular Cell Biology*, 5(3), 198–208. <https://doi.org/10.1038/nrm1333>
- Song, J., Tamura, Y., Yoshihisa, T., & Endo, T. (2014). A novel import route for an N-anchor mitochondrial outer membrane protein aided by the TIM23 complex. *EMBO Reports*, 15(6), 670–677. <https://doi.org/10.1002/embr.201338142>
- Stojanovski, D., Guiard, B., Kozjak-Pavlovic, V., Pfanner, N., & Meisinger, C. (2007). Alternative function for the mitochondrial SAM complex in biogenesis of alpha-helical TOM proteins. *The Journal of Cell Biology*, 179(5), 881–893. <https://doi.org/10.1083/jcb.200706043>
- Straub, S. P., Stiller, S. B., Wiedemann, N., & Pfanner, N. (2016). Dynamic organization of the mitochondrial protein import machinery. *Biological Chemistry*, 397(11), 1097–1114. <https://doi.org/10.1515/hsz-2016-0145>
- Stroud, D. A., Oeljeklaus, S., Wiese, S., Bohnert, M., Lewandrowski, U., Sickmann, A., Guiard, B., van der Laan, M., Warscheid, B., & Wiedemann, N. (2011). Composition and topology of the endoplasmic reticulum-mitochondria encounter structure. *Journal of Molecular Biology*, 413(4), 743–750. <https://doi.org/10.1016/j.jmb.2011.09.012>

- Strub, A., Lim, J. H., Pfanner, N., & Voos, W. (2000). The mitochondrial protein import motor. *Biological Chemistry*, *381*(9-10), 943–949. <https://doi.org/10.1515/BC.2000.115>
- Thornton, N., Stroud, D. A., Milenkovic, D., Guiard, B., Pfanner, N., & Becker, T. (2010). Two modular forms of the mitochondrial sorting and assembly machinery are involved in biogenesis of alpha-helical outer membrane proteins. *Journal of Molecular Biology*, *396*(3), 540–549. <https://doi.org/10.1016/j.jmb.2009.12.026>
- Vitali, D. G., Drwesh, L., Cichocki, B. A., Kolb, A., & Rapaport, D. (2020). The Biogenesis of Mitochondrial Outer Membrane Proteins Show Variable Dependence on Import Factors. *iScience*, *23*(1), 100779. <https://doi.org/10.1016/j.isci.2019.100779>
- Voos W. (2003). A new connection: chaperones meet a mitochondrial receptor. *Molecular Cell*, *11*(1), 1–3. [https://doi.org/10.1016/s1097-2765\(03\)00002-9](https://doi.org/10.1016/s1097-2765(03)00002-9)
- Voos W. (2009). Mitochondrial protein homeostasis: the cooperative roles of chaperones and proteases. *Research in Microbiology*, *160*(9), 718–725. <https://doi.org/10.1016/j.resmic.2009.08.003>
- Waizenegger, T., Habib, S. J., Lech, M., Mokranjac, D., Paschen, S. A., Hell, K., Neupert, W., & Rapaport, D. (2004). Tob38, a novel essential component in the biogenesis of beta-barrel proteins of mitochondria. *EMBO Reports*, *5*(7), 704–709. <https://doi.org/10.1038/sj.embor.7400183>
- Waizenegger, T., Schmitt, S., Zivkovic, J., Neupert, W., & Rapaport, D. (2005). Mim1, a protein required for the assembly of the TOM complex of mitochondria. *EMBO Reports*, *6*(1), 57–62. <https://doi.org/10.1038/sj.embor.7400318>
- Waizenegger, T., Stan, T., Neupert, W., & Rapaport, D. (2003). Signal-anchor domains of proteins of the outer membrane of mitochondria: structural and functional characteristics. *The Journal of Biological Chemistry*, *278*(43), 42064–42071. <https://doi.org/10.1074/jbc.M305736200>
- Walsh, P., Bursać, D., Law, Y. C., Cyr, D., & Lithgow, T. (2004). The J-protein family: modulating protein assembly, disassembly and translocation. *EMBO Reports*, *5*(6), 567–571. <https://doi.org/10.1038/sj.embor.7400172>
- Walter S. (2002). Structure and function of the GroE chaperone. *Cellular and Molecular Life Sciences: CMLS*, *59*(10), 1589–1597. <https://doi.org/10.1007/pl00012485>
- Walther, D. M., & Rapaport, D. (2009). Biogenesis of mitochondrial outer membrane proteins. *Biochimica et Biophysica Acta*, *1793*(1), 42–51. <https://doi.org/10.1016/j.bbamcr.2008.04.013>

- Wang, Q., Guan, Z., Qi, L., Zhuang, J., Wang, C., Hong, S., Yan, L., Wu, Y., Cao, X., Cao, J., Yan, J., Zou, T., Liu, Z., Zhang, D., Yan, C., & Yin, P. (2021). Structural insight into the SAM-mediated assembly of the mitochondrial TOM core complex. *Science (New York, N.Y.)*, *373*(6561), 1377–1381. <https://doi.org/10.1126/science.abh0704>
- Wegele, H., Wandinger, S. K., Schmid, A. B., Reinstein, J., & Buchner, J. (2006). Substrate transfer from the chaperone Hsp70 to Hsp90. *Journal of Molecular Biology*, *356*(3), 802–811. <https://doi.org/10.1016/j.jmb.2005.12.008>
- Wenz, L. S., Opaliński, L., Schuler, M. H., Ellenrieder, L., Ieva, R., Böttinger, L., Qiu, J., van der Laan, M., Wiedemann, N., Guiard, B., Pfanner, N., & Becker, T. (2014). The presequence pathway is involved in protein sorting to the mitochondrial outer membrane. *EMBO Reports*, *15*(6), 678–685. <https://doi.org/10.1002/embr.201338144>
- Wiedemann, N., & Pfanner, N. (2017). Mitochondrial Machineries for Protein Import and Assembly. *Annual Review of Biochemistry*, *86*, 685–714. <https://doi.org/10.1146/annurev-biochem-060815-014352>
- Wiedemann, N., Truscott, K. N., Pfannschmidt, S., Guiard, B., Meisinger, C., & Pfanner, N. (2004). Biogenesis of the protein import channel Tom40 of the mitochondrial outer membrane: intermembrane space components are involved in an early stage of the assembly pathway. *The Journal of Biological Chemistry*, *279*(18), 18188–18194. <https://doi.org/10.1074/jbc.M400050200>
- Wohlever, M. L., Mateja, A., McGilvray, P. T., Day, K. J., & Keenan, R. J. (2017). Msp1 Is a Membrane Protein Dislocase for Tail-Anchored Proteins. *Molecular Cell*, *67*(2), 194–202.e6. <https://doi.org/10.1016/j.molcel.2017.06.019>
- Xie, J. L., Bohovych, I., Wong, E., Lambert, J. P., Gingras, A. C., Khalimonchuk, O., Cowen, L. E., & Leach, M. D. (2017). Ydj1 governs fungal morphogenesis and stress response, and facilitates mitochondrial protein import via Mas1 and Mas2. *Microbial cell (Graz, Austria)*, *4*(10), 342–361. <https://doi.org/10.15698/mic2017.10.594>
- Yan, W., & Craig, E. A. (1999). The glycine-phenylalanine-rich region determines the specificity of the yeast Hsp40 Sis1. *Molecular and Cellular Biology*, *19*(11), 7751–7758. <https://doi.org/10.1128/MCB.19.11.7751>
- Young, J. C., Hoogenraad, N. J., & Hartl, F. U. (2003). Molecular chaperones Hsp90 and Hsp70 deliver preproteins to the mitochondrial import receptor Tom70. *Cell*, *112*(1), 41–50. [https://doi.org/10.1016/s0092-8674\(02\)01250-3](https://doi.org/10.1016/s0092-8674(02)01250-3)

- Zhou, C., Slaughter, B. D., Unruh, J. R., Eldakak, A., Rubinstein, B., & Li, R. (2011). Motility and segregation of Hsp104-associated protein aggregates in budding yeast. *Cell*, 147(5), 1186–1196. <https://doi.org/10.1016/j.cell.2011.11.002>
- Zolkiewski, M., Zhang, T., & Nagy, M. (2012). Aggregate reactivation mediated by the Hsp100 chaperones. *Archives of Biochemistry and Biophysics*, 520(1), 1–6. <https://doi.org/10.1016/j.abb.2012.01.012>
- Żwirowski, S., Kłosowska, A., Obuchowski, I., Nillegoda, N. B., Piróg, A., Ziętkiewicz, S., Bukau, B., Mogk, A., & Liberek, K. (2017). Hsp70 displaces small heat shock proteins from aggregates to initiate protein refolding. *The EMBO Journal*, 36(6), 783–796. <https://doi.org/10.15252/emj.201593378>

## 11. Acknowledgments

First and foremost, I am extremely grateful to my supervisor, Prof. Dr. Doron Rapaport for giving me the opportunity to join his lab, and for placing his faith in me. I am thankful for his continuous support, essential guidance, and patience throughout my PhD study.

My gratitude extends to the prestigious grant Minerva-Stiftung for their generous funding opportunity to undertake my studies. Additionally, I would like to express gratitude to my thesis advisory committee, Prof. Dr. Ralf Jansen and Prof. Dr. Tassula Proikas-Cezanne for all the scientific discussions and the useful input and suggestions. I also thank Prof. Dr. Gabriele Dodt and Prof. Dr. Johannes Hermann for kindly being part of my thesis examining committee.

Special thanks go to Prof. Dr. Maya Schuldiner for the wonderful and fruitful scientific collaboration we had together and for expanding my scientific horizon beyond my main project. Thanks go to my collaboration partners in Tübingen and Munich, for their immense contribution to my project.

I'd like to convey my gratefulness to my lab colleagues for a cherished time spent together in the lab and for the social activities we had together “in 😊”, and outside the lab. For creating a bright atmosphere in the dark depths of the lab when things go wrong, hence maintaining me in PhD-competent condition 😊. To Tobias Jores and Diana Sofia-Antunes, for introducing me to the lab and sharing materials and protocols. To my previous lab mates, Janani Natarajan, Bogdan Chichocki, Daniela Vitali, and Monika Sinzel for the lovely time we had together. To our amazing technical assistant Elena Kracker, for maintaining the lab and to Dr. Kai Stefan Dimmer for his immense scientific assistance. Jialin Zhou for being my PhD batch buddy and for all the delicious cakes and the “matcha motchi 🍰”. Fenja Vaas for keeping the lab clean and intact and for being our DEUTSCH translator tool. Anasuya Moitra for serving as the lab FBI agent, reliable secretary, birthdays reminder, and for her efficient proofreading activity. Klaudia Maruszczak for sharing her controversial opinions with me and for being the revolutionary of the lab. Nitya Aravindan for the nice trips, after-work visits and the animal obsession 🐾. Vitasta Tiku for promoting the guilt-free snack consumption “YOLO”. To all the new ambitious lab members, Roza Dimogkioka, Zacharias Fakihi and Jiaxin Qian for keeping our lab legacy on. Big thanks to the students: Max, Linda and Lea who worked tirelessly to get my project done.

Lastly, I would like to express my great appreciation to my family: my partner for life, Adam for always supporting me in this long journey, for constantly listening to me vent and

talk things out, for cracking jokes when things become too serious and for keeping me mentally stable amid the ups and downs. To my parents for their everlasting love, trust and support.





## 12. Appendix

### a) Accepted papers

1. **Drwesh, L.**, & Rapaport, D. (2020). Biogenesis pathways of  $\alpha$ -helical mitochondrial outer membrane proteins. *Biological Chemistry*, 401(6-7), 677–686.
2. Vitali, D. G.\*, **Drwesh, L.\***, Cichocki, B. A., Kolb, A., & Rapaport, D. (2020). The Biogenesis of Mitochondrial Outer Membrane Proteins Show Variable Dependence on Import Factors. *iScience*, 23(1), 100779.  
*\*equal contributors*
3. Rosenthal, M., Metzl-Raz, E., Bürgi, J., Yifrach, E., **Drwesh, L.**, Fadel, A., Peleg, Y., Rapaport, D., Wilmanns, M., Barkai, N., Schuldiner, M., & Zalckvar, E. (2020). Uncovering targeting priority to yeast peroxisomes using an in-cell competition assay. *Proceedings of the National Academy of Sciences of the United States of America*, 117(35), 21432–21440.
4. Eisenberg-Bord, M., Zung, N., Collado, J., **Drwesh, L.**, Fenech, E. J., Fadel, A., Dezorella, N., Bykov, Y. S., Rapaport, D., Fernandez-Busnadiego, R., & Schuldiner, M. (2021). Cnm1 mediates nucleus-mitochondria contact site formation in response to phospholipid levels. *The Journal of Cell Biology*, 220(11), e202104100

## Review

Layla Drwesh and Doron Rapaport\*

# Biogenesis pathways of $\alpha$ -helical mitochondrial outer membrane proteins

<https://doi.org/10.1515/hsz-2019-0440>

Received December 19, 2019; accepted January 21, 2020

**Abstract:** Mitochondria harbor in their outer membrane (OM) proteins of different topologies. These proteins are encoded by the nuclear DNA, translated on cytosolic ribosomes and inserted into their target organelle by sophisticated protein import machineries. Recently, considerable insights have been accumulated on the insertion pathways of proteins into the mitochondrial OM. In contrast, little is known regarding the early cytosolic stages of their biogenesis. It is generally presumed that chaperones associate with these proteins following their synthesis in the cytosol, thereby keeping them in an import-competent conformation and preventing their aggregation and/or mis-folding and degradation. In this review, we outline the current knowledge about the biogenesis of different mitochondrial OM proteins with various topologies, and highlight the recent findings regarding their import pathways starting from early cytosolic events until their recognition on the mitochondrial surface that lead to their final insertion into the mitochondrial OM.

**Keywords:** chaperones; MIM complex; signal-anchored proteins; single-span proteins; tail-anchored proteins; TOM complex.

## Introduction

Mitochondria are involved in various cellular pathways and they fulfill well-characterized vital functions, among them, energy production, signaling and homeostasis of calcium, removal of reactive oxygen species, biogenesis and assembly of iron-sulfur proteins, and apoptosis

regulation. These functions are carried out by proteins distributed between four different sub-mitochondrial compartments; outer membrane (OM), inner membrane (IM), intermembrane space (IMS) and the matrix (Harbauer et al., 2014). Even though the mitochondria have their own genome, most mitochondrial proteins (including all the OM proteins) are encoded by the nuclear genome and synthesized on cytosolic ribosomes. Then, these newly synthesized proteins are targeted to the organelle and translocated into mitochondria by different routes. The early stages of these pathways are mediated by cytosolic factors and chaperones whereas the later ones are facilitated by sophisticated protein import machineries that have evolved in the different mitochondrial compartments (Paschen and Neupert, 2001).

The mitochondrial OM, which is rich in pore-forming proteins, provides a physical barrier that prevents free diffusion of large molecules into the organelle and allows small molecules (<5 kDa) to pass. The OM proteome includes integral proteins that are categorized according to their structure into two main families, proteins with  $\alpha$ -helical transmembrane segments and  $\beta$ -barrel proteins that are formed by multiple  $\beta$ -strands (Burri et al., 2006). Whereas the latter family include in yeast only five  $\beta$ -barrel proteins, the former one contains a few dozen membrane-embedded helical proteins in fungi (Burri et al., 2006; Schmitt et al., 2006; Zahedi et al., 2006). Part of the OM proteins function as channels and transporters that mediate the cross-talk between the cytosol and the mitochondria by enabling exchange of ions, metabolites and nucleotides (Hoogenboom et al., 2007). Others are components of the protein import machineries including receptors and channels. The OM also contains proteins involved in fission and fusion of the organelle as well as a set of enzymes that mediate diverse functions. Furthermore, proteins that are part of the contact sites between the mitochondria and other organelles [like the endoplasmic reticulum (ER) or lysosomes] also reside in the OM (Elbaz-Alon, 2017).

In this review, we will deal with the biogenesis pathways of the different topological groups of mitochondrial helical OM proteins.

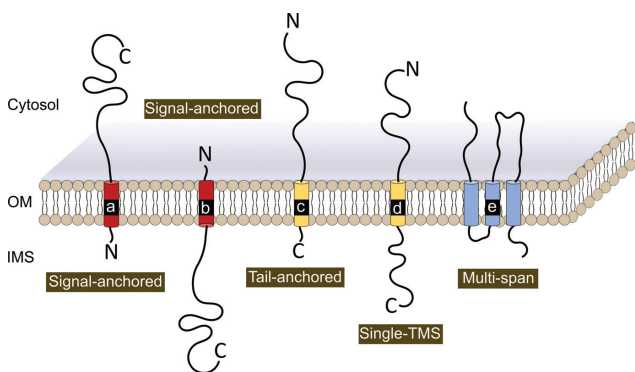
\*Corresponding author: Doron Rapaport, Interfaculty Institute of Biochemistry, University of Tübingen, Hoppe-Seyler-Str. 4, 72076 Tübingen, Germany, e-mail: [doron.rapaport@uni-tuebingen.de](mailto:doron.rapaport@uni-tuebingen.de).  
<https://orcid.org/0000-0003-3136-1207>

Layla Drwesh: Interfaculty Institute of Biochemistry, University of Tübingen, Hoppe-Seyler-Str. 4, 72076 Tübingen, Germany

## Single-span mitochondrial OM proteins

Mitochondrial OM single-span proteins cross the membrane once by a single membrane-spanning  $\alpha$ -helix structure, and, based on their topology, can be divided into three subclasses. The first group are signal-anchored proteins, which are embedded into the mitochondrial OM through N-terminal transmembrane segment (TMS) exposing a large soluble domain towards either the cytosol or the IMS (Figure 1a, b). The second subclass are tail-anchored proteins, which are characterized by an inverted orientation as compared to the first group. These proteins cross the membrane through the C-terminal TMS and expose a large soluble domain toward the cytosol whereas only the very short N-terminal region is facing the IMS (Figure 1c). The third group contains proteins with two large soluble domains exposed to both the cytosol and the IMS (Figure 1d) (reviewed in Walther and Rapaport, 2009).

Like all mitochondrial OM proteins, single-span proteins are encoded by the nuclear genome, synthesized on cytosolic ribosomes, and then they are imported into the OM of the mitochondria. Of note, none of these proteins has a canonical cleavable N-terminal presequence, which directs most of the matrix and some inner membrane proteins to the organelle. The mitochondrial targeting signal of OM proteins can be found either at their termini or as internal structural elements. As will be described in detail in the following sections, such single-span proteins do not share a common import pathway but rather show a variable dependency on different import elements depending on their orientation and internal features.



**Figure 1:** Topologies of mitochondrial OM proteins with helical transmembrane segments.

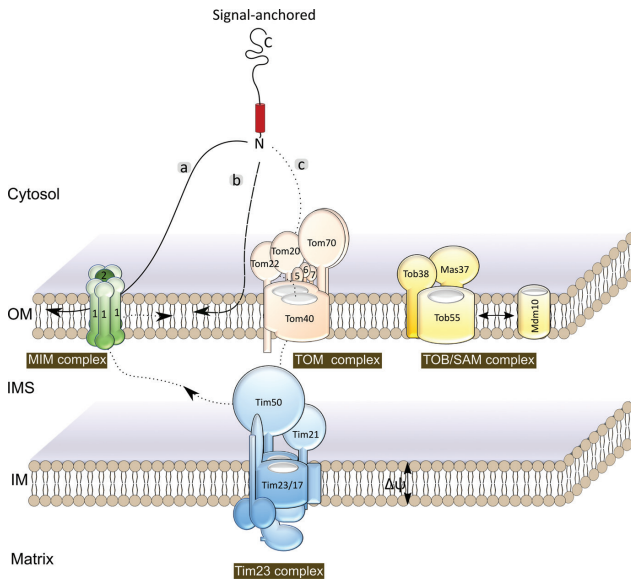
From left to right: signal anchored proteins (a and b), tail-anchored proteins (c), other single-span proteins (d), and multi-span proteins (e).

## Biogenesis of signal-anchored proteins

Several signal-anchored proteins have been identified so far in the yeast mitochondrial OM. Among them are the TOM complex receptors Tom20 and Tom70 (as well as a paralog of the latter in yeast, Tom71) that recognize the majority of newly synthesized precursor proteins on the mitochondrial surface (Lithgow et al., 1994; Yamamoto et al., 2009). Other signal-anchored proteins in yeast mitochondria are: (i) the quality control protein Msp1 that mediates removal of mislocalized tail-anchored proteins from the mitochondrial OM (Chen et al., 2014a; Okreglak and Walter, 2014); (ii) Om45, which exposes its bulk C-terminal domain towards the IMS and was found to interact with Porin and Om14 (Lauffer et al., 2012). The biological function of Om45 is still unknown; and (iii) the mitochondrial OM isoform of Mcr1 (Mcr1<sub>mom</sub>) (mitochondrial NADH-cytochrome b5 reductase), which is involved in ergosterol biosynthesis (Lamb et al., 1999).

Although these proteins share similar topology, they do not seem to follow the same import pathway. Early studies demonstrated that insertion and assembly of Tom20 and Tom70 requires the MIM complex, an insertase of the mitochondrial OM which is composed of Mim1 and Mim2 (Figure 2A) (Becker et al., 2008; Hulett et al., 2008; Popov-Čeleketić et al., 2008). Further details of the biogenesis of Tom20 and Tom70 were described in detail in a previous review (Dukanovic and Rapaport, 2011). Recently, two additional signal-anchored proteins, Mcy1 and Pth2, were found to interact initially with Tom70 and then to be inserted into the OM by the MIM complex (Doan, Pfanner and Becker, personal communication). Of note, the MIM complex is not directly involved in the biogenesis of all signal anchored proteins, as the import of Mcr1<sub>mom</sub> was found to be affected neither by the depletion of Mim1 and/or Mim2 (Vitali et al., 2020), nor by depletion of the TOM complex receptors (Meineke et al., 2008). Hence, Mcr1<sub>mom</sub> might integrate into the mitochondrial OM via a pathway that does not involve any known import components (Figure 2B).

Om45, in contrast, follows another unique import pathway where it is initially recognized by the Tom20 and Tom22 receptors before it then crosses the mitochondrial OM through the Tom40 channel into the IMS where it is recognized by the presequence translocase of the inner membrane (TIM23 complex) (Song et al., 2014; Wenz et al., 2014). It has been suggested that the final insertion step from the IMS side involves the MIM complex (Figure 2C) (Wenz et al., 2014). Recently, we identified an additional signal-anchored protein, Msp1 to be a substrate of the



**Figure 2:** Import pathways of signal-anchored proteins. Three main import pathways have been identified for signal-anchored proteins. The first, which is probably followed by Tom20, Tom70 or Msp1 involves only the MIM complex (pathway a), the second, which is followed by Mcr1<sub>mom</sub>, is an unassisted pathway that probably depends on the unique lipid composition of the OM (pathway b). The last one was described for Om45 and involves TOM-mediated transfer into the IMS where the precursor is recognized by the TIM23 machinery and then inserted into the OM from the IMS side, most likely by the MIM complex (pathway c).

MIM complex but not to require the receptors or channel of the TOM complex for its membrane integration (Vitali et al., 2020).

Collectively, it is evident that signal-anchored proteins do not follow a common pathway but rather, each one of them seems to use a unique import route. It appears that the specific route is dictated by, yet unknown, elements that are present in the particular protein. The spectrum of dependency on different import factors varies between not being dependent on any of the known import components, through exhibiting dependency solely on the MIM complex, to reliance on three complexes namely, TOM, TIM23 and MIM.

## Biogenesis of tail-anchored proteins

The subclass of tail-anchored proteins includes the small TOM complex core components Tom5, Tom6 and Tom7 in yeast and mammals. Tom5 was proposed to maintain the stability of the TOM complex and to mediate the transfer

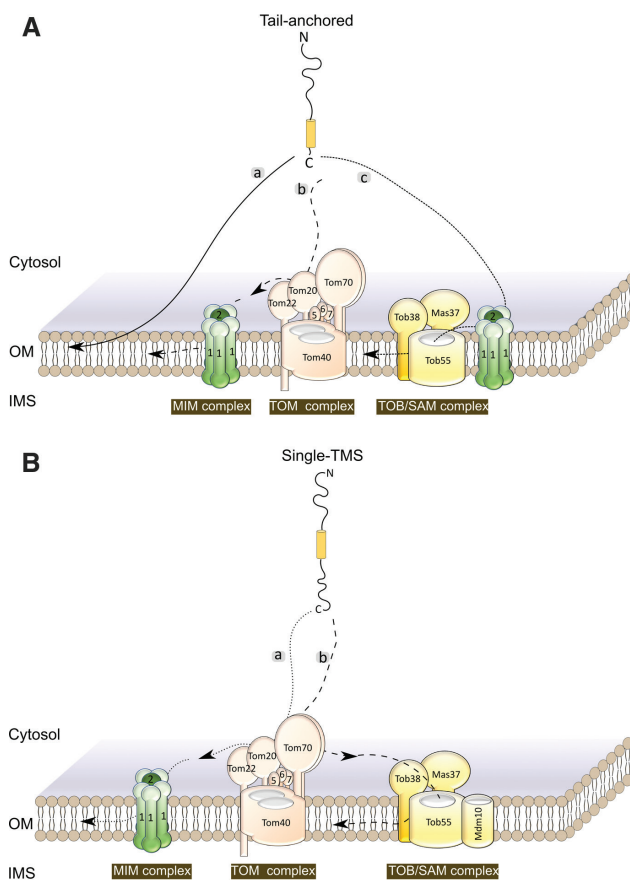
of preproteins from the receptors to the pore (Dietmeier et al., 1997; Schmitt et al., 2005), whereas Tom6 and Tom7 were found to modulate the assembly and stability of the TOM complex (Sherman et al., 2005; Becker et al., 2011a). Additional tail-anchored proteins in the OM are: Fis1 (hFis1 in human), which mediates mitochondrial fission (Mozdy et al., 2000); and Gem1 (Miro1/2 in mammals), which is a GTPase that has been proposed to regulate the ERMES function (Kornmann et al., 2011; Stroud et al., 2011). In addition, mammalian OM contains tail-anchored proteins without homologues in yeast. Among those are VAMP-1B (splice-isoform of vesicle-associated membrane protein-1), a protein involved in the targeting and/or fusion of transport vesicles to their target membrane (Isenmann et al., 1998); anti- and proapoptotic proteins of the Bcl-2 family like Bcl2, Bak or Bax; mitochondrial fission factor (MFF), the fission factor ganglioside-induced differentiation associated protein 1 (GDAP1); the adaptor protein outer membrane protein 25 (OMP25); and the monoamine oxidase-A (MAOA) (Costello et al., 2017).

An additional group of single-span proteins are the non-canonical tail-anchored proteins that expose soluble domains towards both sides of the OM namely, the IMS and the cytosol. This family includes in yeast cells the MIM component Mim1, which is required for the integration of proteins into the OM (Waizenegger et al., 2005; Dimmer et al., 2012), the TOM complex core subunit Tom22 that acts as a receptor for some precursor proteins (Meisinger et al., 1999), and Atg32 which is involved in the mitophagy and degradation of mitochondria (Kanki et al., 2009; Okamoto et al., 2009). Although, the biogenesis of proteins from this group is not fully understood, it seems that they do not share a common pathway.

Fis1 was found to be inserted into the MOM without the assistance of any of the known import components (Figure 3A, pathway a), suggesting that the unique lipid composition of the mitochondrial OM contributes to the selectivity of the process (Kemper et al., 2008). In contrast, none of the other tail-anchored proteins appears to follow this unassisted pathway. Rather they show variable dependency on different import elements. For example, Gem1 steady state levels were recently found to be moderately affected by the absence of the MIM complex and more so by the deletion of *TOM20*. These observations suggest that it is recognized first by the Tom20 receptor and inserted into the OM by the MIM complex (Figure 3A, pathway b).

Contrary to previous assumptions that the TOB/SAM complex (topogenesis of the mitochondrial outer membrane  $\beta$ -barrel proteins/sorting and assembly





**Figure 3:** Biogenesis routes of tail-anchored and single-span proteins.

(A) Tail-anchored proteins can follow various routes. One option, which is followed by Fis1, is an unassisted membrane integration (route a). The second route, which is taken by Gem1, is mediated by the TOM complex receptors and then the precursor is inserted into the OM by the MIM complex (route b), while the third route, that is taken probably by the small TOM components, was reported to require the MIM complex and subsequently the TOB complex (route c). (B) Single-span proteins exposing soluble domains towards both the cytosol and the IMS were found to follow one of two pathways. The first, which is followed by Atg32, involves precursor recognition by the TOM receptors and then MIM-mediated membrane insertion (route a). The second, which is used by Tom22, involves recognition by Tom70 and then insertion into the OM by the TOB-Mdm10 module (route b).

machinery) is dedicated only to the biogenesis of  $\beta$ -barrel proteins, several studies suggested that this complex is also essential for the biogenesis of some tail-anchored proteins, like the small TOM components (Tom5, Tom6, Tom7) and Tom22. While the MIM complex was found to promote the membrane integration of the precursors of Tom5, Tom6 and Tom7 (Becker et al., 2008), the TOB complex was required for their assembly into the TOM complex (Figure 3A, pathway c) (Stojanovski et al.,

2007). Tom22 follows a different route that includes an initial recognition by the TOM receptors Tom20 and Tom70 (Keil and Pfanner, 1993), and does not require the MIM complex (Becker et al., 2008). Surprisingly, Tom22 requires for its integration into the OM and final assembly into the TOM complex a TOB complex form that also contains Mdm10 (Figure 3B, pathway b) (Stojanovski et al., 2007; Thornton et al., 2010). Of note, the function of this TOB-Mdm10 species is not required for the biogenesis of other tail-anchored proteins. Interestingly, gradual depletion of the central component of the TOB complex, Tob55 resulted in dramatic reduction of Mim1 levels (Papić et al., 2013). However, it is not clear whether this effect is direct or indirect. The steady-state levels of the third non-canonical TA protein, Atg32 were recently shown to be heavily reduced upon deletion of MIM components and moderately compromised in the absence of the import receptors Tom20 or Tom70 suggesting that Atg32 is first recognized by the TOM receptors followed by an insertion into the OM, which is facilitated by the MIM complex (Figure 3B, pathway a) (Vitali et al., 2020).

The biogenesis of an additional TA protein namely, mammalian Bcl-2 was intensively investigated, however, with contradicting results. On the one hand, its import into the mitochondrial OM was not hampered by protease treatment of the mitochondria arguing against potential involvement of receptor elements (Janiak et al., 1994). On the other hand, upon its expression in yeast cells, Bcl-2 was shown to interact with the import receptor Tom20, but not with other TOM components, suggesting that it does not use the Tom40 pore for membrane integration but rather, directly inserts into the lipid bilayer after initial recognition by Tom20 (Motz et al., 2002). Yet, another report suggested that mammalian TA proteins (including Bcl-2) follow a common import pathway which is TOM-independent (Setoguchi et al., 2006). Thus, it seems that further experiments are required to shed light on the potential involvement of the TOM complex in the biogenesis of this protein.

Recently, a quality control pathway to remove mislocalized tail-anchored proteins from the mitochondrial OM was characterized (Chen et al., 2014a,b; Okreglak and Walter, 2014). An AAA-ATPase anchored to the OM, Msp1 was reported to extract such mislocalized proteins from the OM and together with additional factors to facilitate their degradation by the ubiquitin-proteasome system (Chen et al., 2014a,b; Okreglak and Walter, 2014; Wohlever et al., 2017; Matsumoto et al., 2019). It should be noted that, so far, Msp1 was found to mediate the removal of mistargeted proteins that usually reside in the ER or

peroxisome and its relevance for the biogenesis of *bona fide* mitochondrial OM proteins is still unclear.

## Mitochondrial OM multi-span proteins

Multi-spanning proteins are embedded into the lipid bilayer of the OM through multiple  $\alpha$ -helical transmembrane segments (Figure 1e). Several multi-spanning proteins have been identified so far in the mitochondrial OM: Fzo1 which spans the membrane twice, and is essential for mitochondria fusion in yeast (Mfn1/2 in mammalian) with the N- and C-terminal domains exposed toward the cytosol (Hermann et al., 1998; Rapaport et al., 1998); the fusion mediator Ugo1 (Sesaki and Jensen, 2001), Mcp3, which is probably involved in lipid homeostasis (Sinzel et al., 2016), the quality control adaptor Ubx2 (Mårtensson et al. 2019), and Om14, which was suggested to serve as a receptor for cytosolic ribosomes (Lesnik et al., 2014). Additional multi-span proteins are Scm4, a protein with unknown function, mammalian peripheral benzodiazepine receptor (PBR) (Joseph-Liauzun et al., 1998), and mammalian mitochondrial ubiquitin ligase (MITOL) (Nakamura et al., 2006).

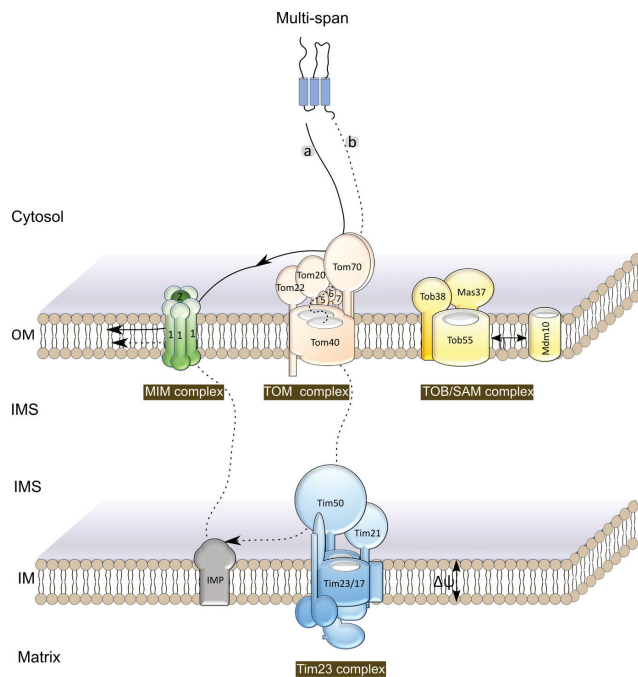
## Biogenesis of multi-span proteins

Most of the multi-span OM proteins share the same import route involving the TOM and the MIM machineries. Earlier research suggested that Fzo1 requires import receptor(s) for its insertion into the mitochondria OM (Rapaport et al., 1998). Later studies with mammalian multi-span proteins refined this observation and suggested a strong dependency on the Tom70 receptor but not on the other receptors; namely Tom20 and Tom22 nor on the TOM complex channel Tom40 (Otera et al., 2007). These findings are further supported by studies with yeast cells, which reported that steady state levels and the *in vitro* import of Ugo1, Om14, Ubx2 and Scm4 were reduced in yeast mitochondria lacking Tom70 (Papic et al., 2011; Becker et al., 2011b; Mårtensson et al., 2019). Importantly, a strong dependency of the membrane integration of these proteins on the MIM complex was observed. Altogether, these studies emphasize the importance of Tom70 in the biogenesis of multi-span OM proteins either by acting as a receptor that recognizes these substrates or by serving as an

anchor for the chaperones that associate with them in the cytosol. After the initial recognition, Tom70 relays the substrate proteins to the MIM complex that facilitates their integration into the OM.

The only multi-span protein that has been reported, so far, to follow an alternative pathway is Mcp3, which is recognized by the Tom70 receptor followed by translocation across the OM via the Tom40 channel into the IMS side. In the IMS, it was found to interact with the TIM23 complex; as in the case of the signal-anchored protein Om45, however, in case of Mcp3, it was shown to undergo an additional step of processing by the inner membrane protease (IMP). Finally, Mcp3 is integrated into the OM in a process that might be facilitated by the MIM complex (Figure 4B) (Sinzel et al., 2016).

To provide an overview on the various pathways that helical OM proteins follow, we summarize in Table 1 the known information. Of note, for clarity, only proteins with clear indications for transmembrane helical segments are included in this table.



**Figure 4:** Import pathways of multi-span proteins.

Most of the precursors of multi-span proteins follow an insertion route which starts with recognition by the Tom70 and then MIM-dependent insertion into the OM (route a). A special route is followed by Mcp3. This precursor protein crosses the OM via the TOM complex, interacts with the TIM23 complex at the IMS and then get processed by IMP. Finally, the processed form is inserted into the OM in a process that is probably mediated by the MIM complex (route b).

**Table 1:** Import pathways of yeast helical OM proteins.

Name	Other names	ORF	Import pathway
Atg32	Ecm37	YIL146C	Tom20, Tom70, MIM
Fis1	Mdv2	YIL065C	Unassisted, MIM(?)
Fzo1		YBR179C	Tom70→MIM
Gem1	Gon1	YAL048C	Tom20→MIM
Mcp1		YOR228C	Unknown
Mcp3	Fun14	YAL008W	TOM→TIM23→IMP→MIM(?)
Mcr1		YKL150W	Unassisted, MIM(?)
Mcy1		YGR012W	Tom70→MIM
Mim1	Tom13	YOL026C	Djp1→Tom70→MIM
Mim2		YLR099W-A	Unknown
Msp1	Yta4	YGR028W	MIM
OM14		YBR230C	Tom70→MIM
OM45		YIL136W	TOM→TIM23→MIM(?)
Pth2		YBL057C	Tom70→MIM
Scm4		YGR049W	Tom70→MIM
Tom20	Mas20, Mom19	YGR082W	MIM
Tom22	Mas17, Mas22	YNL131W	Xdj1, Tom20(?), Tom70(?), TOB/SAM-Mdm10
Tom5	Mom8A	YPR133W-A	MIM, TOB/SAM
Tom6	Isp6, Mom8B	YOR045W	MIM, TOB/SAM
Tom7	Mom7	YNL070W	MIM, TOB/SAM
Tom70	Mas70, Mom72	YNL121C	Tom40
Tom71	Tom72	YHR117W	Unknown
Ubp16		YPL072W	MIM
Ubx2	Sel1	YML013W	Tom70→MIM
Ugo1		YDR470C	Tom70→MIM

## Mitochondrial targeting signal of OM helical proteins

Mitochondrial targeting of newly synthesized helical OM proteins is mediated by elements that are part of the mature form of the protein. In both signal- and tail-anchored proteins as well as other single-span ones, the TMS and its flanking regions are necessary and sufficient for mitochondrial targeting. The examination of structural elements that can serve as a targeting signal in both signal- and tail-anchored proteins in yeast and mammals suggested that moderate hydrophobicity and appropriate length (19–20 residues) of the TMS appear to be key characteristics. In addition, the net positive charge of the flanking regions of the TMS were found to enhance mitochondrial targeting (Isenmann et al., 1998; Kanaji et al., 2000; Dembowski et al., 2001; Allen et al., 2002; Horie et al., 2002; Habib et al., 2003; Waizenegger et al., 2003). However, some proteins exhibit additional features that might help in targeting and/or membrane integration. For example, Tom5, Tom6, Tom7 and Tom22 contain in their TMS a conserved proline residue, which contributes to their correct targeting and assembly (Allen et al., 2002). Additional relevant segments were reported for Tom22,

in which small parts in the cytosolic and IMS domains were found to interact with import elements, suggesting that Tom22 might be inserted as a hairpin structure (Rodriguez-Cousiño et al., 1998; Nakamura et al., 2004).

## Early cytosolic stages in the biogenesis of mitochondrial OM proteins

The biogenesis of newly synthesized proteins, a process that starts on cytosolic ribosomes, involves a repertoire of cytosolic factors that contribute to the reduction of misfolding, aggregation and mislocalization of such precursor proteins. These factors are required already at the early stages during or directly after protein synthesis. Accordingly, three systems that assist in the early stages of proteins biogenesis have been identified in yeast. The first is the heterodimeric ribosome-associated complex (RAC) formed by chaperones of the Hsp70 and Hsp40 (Ssz1) and (Zuo1), respectively, and it promotes the co-translational folding of nascent polypeptide chains (Gautschi et al., 2001). The second system is the heterodimeric nascent

polypeptide-associated complex (NAC) consisting of  $\alpha$ - and  $\beta$ -NAC. This NAC dimer is highly conserved from yeast to humans and was found as the initial factor to interact with nascent polypeptides as they emerge from the ribosomal exit tunnel thereby protecting them from aggregation and degradation. NAC function was mainly found to regulate the protein transport from the cytosol to ER (in cooperation with SRP) (Zhang et al., 2012), yet, NAC-deleted yeast cells showed mitochondrial protein import defect causing mitochondria stress response (George et al., 1998; Gamerdinger et al., 2015). The third system is the ribosome quality control complex (RQC), which recognizes stalled ribosomes, and degrades the faulty mRNAs and the nascent polypeptide chains to avoid creating defective proteins during the translation process. Then, the RQC recycles the ribosomal subunits for the next round of translation (Nüenberg and Tampé, 2013; Gamerdinger, 2016).

Considering that all the mitochondrial OM proteins, including some that are highly hydrophobic, are synthesized in the cytosol prior to their import into the organelle, it is assumed that these precursors require cytosolic factors and/or chaperones to keep them in an import competent conformation (Neupert et al., 1993; Hartl and Hayer-Hartl, 2002). Yet, it is mostly unknown whether these chaperones are required for the biogenesis fidelity of all the OM proteins. Furthermore, the identity and the physiological relevance of these factors for the biogenesis of helical OM proteins are still largely uncertain.

One of the (co)chaperone with a reported function in the biogenesis of helical OM proteins is Djp1, a Hsp40 cochaperone, which was previously found to be involved in peroxisomal protein import (Hetteema et al., 1998). Djp1 supports the import of the single-span protein Mim1 enabling its targeting to the OM through Tom70 (Papić et al., 2013). Moreover, a direct interaction between Djp1 and Tom70 was demonstrated, raising the possibility that this association facilitates the transfer of newly synthesized Mim1 molecules to the organelle (Opaliński et al., 2018). In addition, the deletion of *DJP1* caused a massive mislocalization of Mim1 to the ER (Papić et al., 2013), suggesting that Djp1 contributes to its specific targeting to the mitochondria. A possible mechanism for the contribution of Djp1 to the targeting of Mim1 could be by removal of mis-targeted molecules from the ER, a function that was proposed recently for Djp1 (Hansen et al., 2018). Of note, the levels of the other known single-span proteins like Tom22 and Atg32 were not altered by the absence of Djp1 (Papić et al., 2013). Another cytosolic Hsp40 co-chaperone Xdj1 was found to bind to the cytosolic domain of Tom22 and support the biogenesis of the TOM complex. It seems

that Xdj1 binds to the precursor of Tom22 and maintains the levels of this protein (Opaliński et al., 2018).

Surprisingly, the peroxisomal targeting chaperone Pex19 is an additional chaperone that was found to be involved in the biogenesis of both peroxisome and mitochondria. This protein was initially reported to stabilize peroxisomal tail-anchored proteins in the cytosol and mediate their integration into the peroxisome by guiding them to the membrane receptor Pex3 (Fang et al., 2004; Chen et al., 2014b). Recently, Pex19, as well as the Hsp70 chaperone Ssa1 and its co-chaperone Sti1, were observed to mediate mitochondrial import of the tail-anchored proteins Fis1 and Gem1. Of note, the single-span protein Tom22 did not show any binding to Pex19 (Cichocki et al., 2018). Importantly, Fis1 and Gem1 are both dually targeted to the mitochondrial OM and peroxisomes, and this may explain why such dually targeted proteins are dependent on the same cytosolic factor. In line with these data, the involvement of Pex19 in the biogenesis of human Fis1 was previously described (Delille and Schrader, 2008).

Although a study using mammalian cells proposed that tail-anchored proteins do not need cytosolic factors for their insertion into the membrane (Setoguchi et al., 2006), yet these proteins may still need chaperone activity for keeping their hydrophobic segments in an import competent state. Nevertheless, as several lines of evidence suggest that Fis1 is inserted in an unassisted manner into the OM, it remains unclear whether Pex19 is only required for stabilizing the precursor in the cytosol or if it is also needed for Fis1 integration into the mitochondria via a so far, unknown receptor. Involvement of Pex19 in targeting to peroxisomes was also shown for the signal-anchored protein ATAD1, (the human homolog of yeast Msp1), which is also dually localized to both peroxisome and mitochondria (Chen et al., 2014a; Okreglak and Walter, 2014). An involvement of chaperones or cytosolic factors in the biogenesis of the other known members of the single-span protein family has not been reported yet.

## Concluding remarks

Despite the high physiological importance and the functional diversity of proteins residing in the mitochondrial OM, our knowledge on cytosolic factors and membrane components that affect and regulate their targeting to the organelle and membrane insertion is very limited. Recently, several studies led to considerable progress in our understanding of how these proteins pave their way from the cytosol into the mitochondrial OM. It became



clear that Hsp40 co-chaperones and Pex19 are involved in maintaining the newly synthesized proteins in import competent conformation whereas TOM receptors and the MIM complex are involved in their recognition at the organelle surface and membrane integration. Future studies will help to determine whether the cytosolic chaperones are also involved in active targeting of precursor proteins to mitochondria and which structural characteristics determine the pathway that the various helical OM proteins follow.

**Acknowledgments:** This review is dedicated to Walter Neupert who founded the field of mitochondrial biogenesis and pioneered our research on this topic. We thank K.S. Dimmer for helpful discussions. This work was supported by the Deutsche Forschungsgemeinschaft (RA 1028/7-2 and 10-1 to D.R., Funder Id: <http://dx.doi.org/10.13039/501100001659>). L.D. is supported by a long-term fellowship from the Minerva Foundation, Funder Id: <http://dx.doi.org/10.13039/501100001658>.

## References

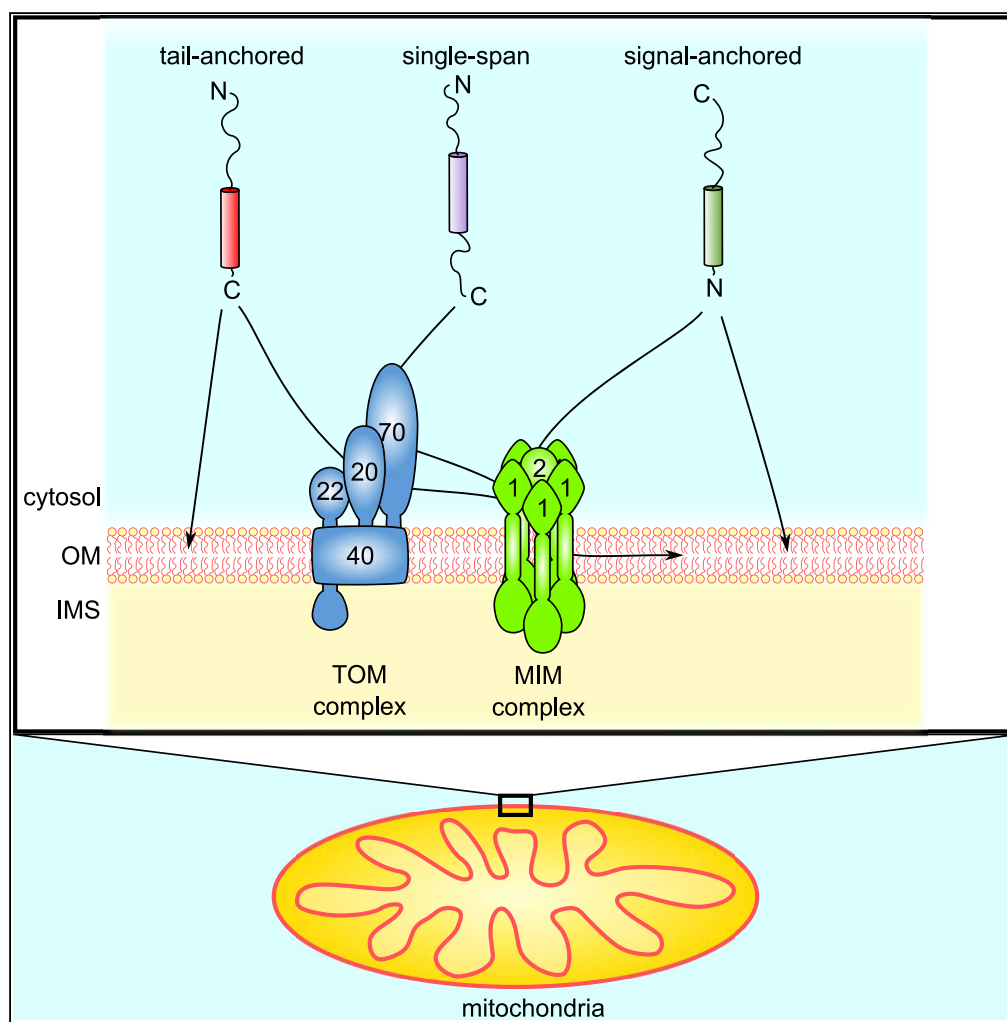
- Allen, R., Egan, B., Gabriel, K., Beilharz, T., and Lithgow, T. (2002). A conserved proline residue is present in the transmembrane-spanning domain of Tom7 and other tail-anchored protein subunits of the TOM translocase. *FEBS Lett.* *514*, 347–350.
- Becker, T., Pfanschmidt, S., Guiard, B., Stojanovski, D., Milenkovic, D., Kutik, S., Pfanner, N., Meisinger, C., and Wiedemann, N. (2008). Biogenesis of the mitochondrial TOM complex: Mim1 promotes insertion and assembly of signal-anchored receptors. *J. Biol. Chem.* *283*, 120–127.
- Becker, T., Wenz, L.S., Thornton, N., Stroud, D., Meisinger, C., Wiedemann, N., and Pfanner, N. (2011a). Biogenesis of mitochondria: Dual role of Tom7 in modulating assembly of the preprotein translocase of the outer membrane. *J. Mol. Biol.* *405*, 113–124.
- Becker, T., Wenz, L.-S., Krüger, V., Lehmann, W., Müller, J.M., Goroncy, L., Zufall, N., Lithgow, T., Guiard, B., Chacinska, A., et al. (2011b). The mitochondrial import protein Mim1 promotes biogenesis of multispanning outer membrane proteins. *J. Cell Biol.* *194*, 387–395.
- Burri, L., Vascotto, K., Gentle, I.E., Chan, N.C., Beilharz, T., Stapleton, D.I., Ramage, L., and Lithgow, T. (2006). Integral membrane proteins in the mitochondrial outer membrane of *Saccharomyces cerevisiae*. *FEBS J.* *273*, 1507–1515.
- Chen, Y.-C., Umanah, G.K.E., Dephoure, N., Andrabi, S.A., Gygi, S.P., Dawson, T.M., Dawson, V.L., and Rutter, J. (2014a). Msp1/ATAD1 maintains mitochondrial function by facilitating the degradation of mislocalized tail-anchored proteins. *EMBO J.* *33*, 1548–1564.
- Chen, Y., Pieuchot, L., Loh, R.A., Yang, J., Kari, T.M.A., Wong, J.Y., and Jedd, G. (2014b). Hydrophobic handoff for direct delivery of peroxisome tail-anchored proteins. *Nat. Commun.* *5*, 5790.
- Cichocki, B.A., Krumpe, K., Vitali, D.G., and Rapaport, D. (2018). Pex19 is involved in importing dually targeted tail-anchored proteins to both mitochondria and peroxisomes. *Traffic* *19*, 770–785.
- Costello, J.L., Castro, I.G., Camões, F., Schrader, T.A., McNeall, D., Yang, J., Giannopoulou, E.A., Gomes, S., Pogenberg, V., Bonekamp, N.A., et al. (2017). Predicting the targeting of tail-anchored proteins to subcellular compartments in mammalian cells. *J. Cell Sci.* *130*, 1675–1687.
- Delille, H.K. and Schrader, M. (2008). Targeting of hFis1 to peroxisomes is mediated by Pex19p. *J. Biol. Chem.* *283*, 31107–31115.
- Dembowski, M., Kunkle, K.P., Nargang, F.E., Neupert, W., and Rapaport, D. (2001). Assembly of Tom6 and Tom7 into the TOM core complex of *Neurospora crassa*. *J. Biol. Chem.* *276*, 17679–17685.
- Dietmeier, K., Hönlinger, A., Bömer, U., Dekker, P.J.T., Eckerskorn, C., Lottspeich, F., Kübrich, M., and Pfanner, N. (1997). Tom5 functionally links mitochondrial preprotein receptors to the general import pore. *Nature* *388*, 195–200.
- Dimmer, K.S., Papic, D., Schumann, B., Sperl, D., Krumpe, K., Walther, D.M., and Rapaport, D. (2012). A crucial role for Mim2 in the biogenesis of mitochondrial outer membrane proteins. *J. Cell Sci.* *125*, 3464–3473.
- Dukanovic, J. and Rapaport, D. (2011). Multiple pathways in the integration of proteins into the mitochondrial outer membrane. *Biochim. Biophys. Acta Biomembr.* *1808*, 971–980.
- Elbaz-Alon, Y. (2017). Mitochondria-organelle contact sites: the plot thickens. *Biochem. Soc. Trans.* *45*, 477–488.
- Fang, Y., Morrell, J.C., Jones, J.M., and Gould, S.J. (2004). PEX3 functions as a PEX19 docking factor in the import of class I peroxisomal membrane proteins. *J. Cell Biol.* *164*, 863–875.
- Gamerding, M. (2016). Protein quality control at the ribosome: focus on RAC, NAC and RQC. *Essays Biochem.* *60*, 203–212.
- Gamerding, M., Hanebuth, M.A., Frickey, T., and Deuring, E. (2015). The principle of antagonism ensures protein targeting specificity at the endoplasmic reticulum. *Science*. *348*, 201–207.
- Gautschi, M., Lillie, H., Fünfschilling, U., Mun, A., Ross, S., Lithgow, T., Rücknagel, P., and Rospert, S. (2001). RAC, a stable ribosome-associated complex in yeast formed by the DnaK-DnaJ homologs Ssz1p and zutin. *Proc. Natl. Acad. Sci. U.S.A.* *98*, 3762–3767.
- George, R., Beddoe, T., Landl, K., and Lithgow, T. (1998). The yeast nascent polypeptide-associated complex initiates protein targeting to mitochondria *in vivo*. *Proc. Natl. Acad. Sci. U.S.A.* *95*, 2296–2301.
- Habib, S.J., Vasiljev, A., Neupert, W., and Rapaport, D. (2003). Multiple functions of tail-anchor domains of mitochondrial outer membrane proteins. *FEBS Lett.* *555*, 511–515.
- Hansen, K.G., Aviram, N., Laborenz, J., Bibi, C., Meyer, M., Spang, A., Schuldiner, M., and Herrmann, J.M. (2018). An ER surface retrieval pathway safeguards the import of mitochondrial membrane proteins in yeast. *Science* *361*, 1118–1122.
- Harbauer, A.B., Zahedi, R.P., Sickmann, A., Pfanner, N., and Meisinger, C. (2014). The protein import machinery of mitochondria – a regulatory hub in metabolism, stress, and disease. *Cell Metab.* *19*, 357–372.
- Hartl, F.U. and Hayer-Hartl, M. (2002). Protein folding. Molecular chaperones in the cytosol: from nascent chain to folded protein. *Science* *295*, 1852–1858.

- Hermann, G.J., Thatcher, J.W., Mills, J.P., Hales, K.G., Fuller, M.T., Nunnari, J., and Shaw, J.M. (1998). Mitochondrial fusion in yeast requires the transmembrane GTPase Fzo1p. *J. Cell Biol.* *143*, 359–373.
- Hettema, E.H., Ruigrok, C.C.M., Koerkamp, M.G., Van Den Berg, M., Tabak, H.F., Distel, B., and Braakman, I. (1998). The cytosolic DnaJ-like protein Djp1p is involved specifically in peroxisomal protein import. *J. Cell Biol.* *142*, 421–434.
- Hoogenboom, B.W., Suda, K., Engel, A., and Fotiadis, D. (2007). The supramolecular assemblies of voltage-dependent anion channels in the native membrane. *J. Mol. Biol.* *370*, 246–255.
- Horie, C., Suzuki, H., Sakaguchi, M., and Mihara, K. (2002). Characterization of signal that directs C-tail-anchored proteins to mammalian mitochondrial outer membrane. *Mol. Biol. Cell* *13*, 1615–1625.
- Hulett, J.M., Lueder, F., Chan, N.C., Perry, A.J., Wolyneć, P., Likić, V.A., Gooley, P.R., and Lithgow, T. (2008). The transmembrane segment of Tom20 is recognized by Mim1 for docking to the mitochondrial TOM complex. *J. Mol. Biol.* *376*, 694–704.
- Iseñmann, S., Khew-Goodall, Y., Gamble, J., Vadas, M., and Wattenberg, B.W. (1998). A splice-isoform of vesicle-associated membrane protein-1 (VAMP-1) contains a mitochondrial targeting signal. *Mol. Biol. Cell* *9*, 1649–1660.
- Janiak, F., Leber, B., and Andrews, D.W. (1994). Assembly of Bcl-2 into microsomal and outer mitochondrial membranes. *J. Biol. Chem.* *269*, 9842–9849.
- Joseph-Liauzun, E., Delmas, P., Shire, D., and Ferrara, P. (1998). Topological analysis of the peripheral benzodiazepine receptor in yeast mitochondrial membranes supports a five-transmembrane structure. *J. Biol. Chem.* *273*, 2146–2152.
- Kanaji, S., Iwahashi, J., Kida, Y., Sakaguchi, M., and Mihara, K. (2000). Characterization of the signal that directs Tom20 to the mitochondrial outer membrane. *J. Cell Biol.* *151*, 277–288.
- Kanki, T., Wang, K., Cao, Y., Baba, M., and Klionsky, D.J. (2009). Atg32 is a mitochondrial protein that confers selectivity during mitophagy. *Dev. Cell* *17*, 98–109.
- Keil, P. and Pfanner, N. (1993). Insertion of MOM22 into the mitochondrial outer membrane strictly depends on surface receptors. *FEBS Lett.* *321*, 197–200.
- Kemper, C., Habib, S.J., Engl, G., Heckmeyer, P., Dimmer, K.S., and Rapaport, D. (2008). Integration of tail-anchored proteins into the mitochondrial outer membrane does not require any known import components. *J. Cell Sci.* *121*, 1990–1998.
- Kornmann, B., Osman, C., and Walter, P. (2011). The conserved GTPase Gem1 regulates endoplasmic reticulum-mitochondria connections. *Proc. Natl. Acad. Sci. U.S.A.* *108*, 14151–14156.
- Lamb, D.C., Kelly, D.E., Manning, N.J., Kaderbhai, M.A., and Kelly, S.L. (1999). Biodiversity of the P450 catalytic cycle: yeast cytochrome b5/NADH cytochrome b5 reductase complex efficiently drives the entire sterol 14-demethylation (CYP51) reaction. *FEBS Lett.* *462*, 283–288.
- Lauffer, S., Mäbert, K., Czupalla, C., Pursche, T., Hoflack, B., Rödel, G., and Krause-Buchholz, U. (2012). *Saccharomyces cerevisiae* porin pore forms complexes with mitochondrial outer membrane proteins Om14p and Om45p. *J. Biol. Chem.* *287*, 17447–17458.
- Lesnik, C., Cohen, Y., Atir-Lande, A., Schuldiner, M., and Arava, Y. (2014). OM14 is a mitochondrial receptor for cytosolic ribosomes that supports co-translational import into mitochondria. *Nat. Commun.* *5*, 5711.
- Lithgow, T., Junne, T., Wachter, C., and Schatz, G. (1994). Yeast mitochondria lacking the two import receptors Mas20p and Mas70p can efficiently and specifically import precursor proteins. *J. Biol. Chem.* *269*, 15325–15330.
- Mårtensson, C.U., Priesnitz, C., Song, J., Ellenrieder, L., Doan, K.N., Boos, F., Floerchinger, A., Zufall, N., Oeljeklaus, S., Warscheid, B., et al. (2019). Mitochondrial protein translocation-associated degradation. *Nature* *569*, 679–683.
- Matsumoto, S., Nakatsukasa, K., Kakuta, C., Tamura, Y., Esaki, M., and Endo, T. (2019). Msp1 clears mistargeted proteins by facilitating their transfer from mitochondria to the ER. *Mol. Cell* *76*, 191–205.e10.
- Meineke, B., Engl, G., Kemper, C., Vasiljev-Neumeyer, A., Paulitschke, H., and Rapaport, D. (2008). The outer membrane form of the mitochondrial protein Mcr1 follows a TOM-independent membrane insertion pathway. *FEBS Lett.* *582*, 855–860.
- Meisinger, C., Brix, J., Model, K., Pfanner, N., and Ryan, M.T. (1999). The preprotein translocase of the outer mitochondrial membrane: receptors and a general import pore. *Cell. Mol. Life Sci.* *56*, 817–824.
- Motz, C., Martin, H., Krimmer, T., and Rassow, J. (2002). Bcl-2 and porin follow different pathways of TOM-dependent insertion into the mitochondrial outer membrane. *J. Mol. Biol.* *323*, 729–738.
- Mozdy, A.D., McCaffery, J.M., and Shaw, J.M. (2000). Dnm1p GTPase-mediated mitochondrial fission is a multi-step process requiring the novel integral membrane component Fis1p. *J. Cell Biol.* *151*, 367–379.
- Nakamura, Y., Suzuki, H., Sakaguchi, M., and Mihara, K. (2004). Targeting and assembly of rat mitochondrial translocase of outer membrane 22 (TOM22) into the TOM complex. *J. Biol. Chem.* *279*, 21223–21232.
- Nakamura, N., Kimura, Y., Tokuda, M., Honda, S., and Hirose, S. (2006). MARCH-V is a novel mitofusin 2- and Drp1-binding protein able to change mitochondrial morphology. *EMBO Rep.* *7*, 1019–1022.
- Neupert, W., Pfanner, N., Welch, W.J., Baker, A., Gething, M.-J., and Jaenicke, R. (1993). Roles of molecular chaperones in protein targeting to mitochondria. *Philos. Trans. R. Soc. Lond. B: Biol. Sci.* *339*, 355–362.
- Nürnberg, E. and Tampé, R. (2013). Tying up loose ends: Ribosome recycling in eukaryotes and archaea. *Trends Biochem. Sci.* *38*, 64–74.
- Okamoto, K., Kondo-Okamoto, N., and Ohsumi, Y. (2009). Mitochondria-anchored receptor Atg32 mediates degradation of mitochondria via selective autophagy. *Dev. Cell* *17*, 87–97.
- Okreglak, V. and Walter, P. (2014). The conserved AAA-ATPase Msp1 confers organelle specificity to tail-anchored proteins. *Proc. Natl. Acad. Sci. U.S.A.* *111*, 8019–8024.
- Opaliński, Ł., Song, J., Priesnitz, C., Wenz, L.-S., Oeljeklaus, S., Warscheid, B., Pfanner, N., and Becker, T. (2018). Recruitment of cytosolic J-proteins by TOM receptors promotes mitochondrial protein biogenesis. *Cell Rep.* *25*, 2036–2043.e5.
- Otera, H., Taira, Y., Horie, C., Suzuki, Y., Suzuki, H., Setoguchi, K., Kato, H., Oka, T., and Mihara, K. (2007). A novel insertion pathway of mitochondrial outer membrane proteins with multiple transmembrane segments. *J. Cell Biol.* *179*, 1355–1363.
- Papic, D., Krumpke, K., Dukanovic, J., Dimmer, K.S., and Rapaport, D. (2011). Multispan mitochondrial outer membrane protein Ugo1 follows a unique Mim1-dependent import pathway. *J. Cell Biol.* *194*, 397–405.
- Papić, D., Elbaz-Alon, Y., Koerdt, S.N., Leopold, K., Worm, D., Jung, M., Schuldiner, M., and Rapaport, D. (2013). The role of Djp1 in import of the mitochondrial protein Mim1 demonstrates

- specificity between a cochaperone and its substrate protein. *Mol. Cell. Biol.* 33, 4083–4094.
- Paschen, S.A. and Neupert, W. (2001). Protein import into mitochondria. *IUBMB Life* 52, 101–112.
- Popov-Čeleketić, J., Waizenegger, T., and Rapaport, D. (2008). Mim1 functions in an oligomeric form to facilitate the integration of Tom20 into the mitochondrial outer membrane. *J. Mol. Biol.* 376, 671–680.
- Rapaport, D., Brunner, M., Neupert, W., and Westermann, B. (1998). Fzo1p is a mitochondrial outer membrane protein essential for the biogenesis of functional mitochondria in *Saccharomyces cerevisiae*. *J. Biol. Chem.* 273, 20150–20155.
- Rodriguez-Cousiño, N., Nargang, F.E., Baardman, R., Neupert, W., Lill, R., and Court, D.A. (1998). An import signal in the cytosolic domain of the *Neurospora* mitochondrial outer membrane protein TOM22. *J. Biol. Chem.* 273, 11527–11532.
- Schmitt, S., Ahting, U., Eichacker, L., Granvogel, B., Go, N.E., Nargang, F.E., Neupert, W., and Nussberger, S. (2005). Role of Tom5 in maintaining the structural stability of the TOM complex of mitochondria. *J. Biol. Chem.* 280, 14499–14506.
- Schmitt, S., Prokisch, H., Schlunck, T., Camp II, D.G., Ahting, U., Waizenegger, T., Scharfe, C., Meitinger, T., Imhof, A., Neupert, W., et al. (2006). Proteome analysis of mitochondrial outer membrane from *Neurospora crassa*. *Proteomics* 6, 72–80.
- Sesaki, H. and Jensen, R.E. (2001). UGO1 encodes an outer membrane protein required for mitochondrial fusion. *J. Cell Biol.* 152, 1123–1134.
- Setoguchi, K., Otera, H., and Mihara, K. (2006). Cytosolic factor- and TOM-independent import of C-tail-anchored mitochondrial outer membrane proteins. *EMBO J.* 25, 5635–5647.
- Sherman, E.L., Go, N.E., and Nargang, F.E. (2005). Functions of the small proteins in the TOM complex of *Neurospora crassa*. *Mol. Biol. Cell* 16, 4172–4182.
- Sinzel, M., Tan, T., Wendling, P., Kalbacher, H., Özbalci, C., Chelius, X., Westermann, B., Brügger, B., Rapaport, D., and Dimmer, K.S. (2016). Mcp3 is a novel mitochondrial outer membrane protein that follows a unique IMP-dependent biogenesis pathway. *EMBO Rep.* 17, 965–981.
- Song, J., Tamura, Y., Yoshihisa, T., and Endo, T. (2014). A novel import route for an N-anchor mitochondrial outer membrane protein aided by the TIM23 complex. *EMBO Rep.* 15, 670–677.
- Stojanovski, D., Guiard, B., Kozjak-Pavlovic, V., Pfanner, N., and Meisinger, C. (2007). Alternative function for the mitochondrial SAM complex in biogenesis of alpha-helical TOM proteins. *J. Cell Biol.* 179, 881–893.
- Stroud, D.A., Oeljeklaus, S., Wiese, S., Bohnert, M., Lewandrowski, U., Sickmann, A., Guiard, B., Van Der Laan, M., Warscheid, B., and Wiedemann, N. (2011). Composition and topology of the endoplasmic reticulum-mitochondria encounter structure. *J. Mol. Biol.* 413, 743–750.
- Thornton, N., Stroud, D.A., Milenkovic, D., Guiard, B., Pfanner, N., and Becker, T. (2010). Two modular forms of the mitochondrial sorting and assembly machinery are involved in biogenesis of  $\alpha$ -helical outer membrane proteins. *J. Mol. Biol.* 396, 540–549.
- Vitali, D.G., Drwesh, L., Cichocki, B.A., Kolb, A., and Rapaport, D. (2020). The biogenesis of mitochondrial outer membrane proteins show variable dependence on import factors. *iScience* 23, 100779.
- Waizenegger, T., Stan, T., Neupert, W., and Rapaport, D. (2003). Signal-anchor domains of proteins of the outer membrane of mitochondria. *J. Biol. Chem.* 278, 42064–42071.
- Waizenegger, T., Schmitt, S., Zivkovic, J., Neupert, W., and Rapaport, D. (2005). Mim1, a protein required for the assembly of the TOM complex of mitochondria. *EMBO Rep.* 6, 57–62.
- Walther, D.M. and Rapaport, D. (2009). Biogenesis of mitochondrial outer membrane proteins. *Biochim. Biophys. Acta Mol. Cell Res.* 1793, 42–51.
- Wenz, L.-S., Opaliński, L., Schuler, M.-H., Ellenrieder, L., Ieva, R., Bottinger, L., Qiu, J., van der Laan, M., Wiedemann, N., Guiard, B., et al. (2014). The presequence pathway is involved in protein sorting to the mitochondrial outer membrane. *EMBO Rep.* 15, 678–685.
- Wohlever, M.L., Mateja, A., McGilvray, P.T., Day, K.J., and Keenan, R.J. (2017). Msp1 is a membrane protein dislocase for tail-anchored proteins. *Mol. Cell* 67, 194–202.e6.
- Yamamoto, H., Fukui, K., Takahashi, H., Kitamura, S., Shiota, T., Terao, K., Uchida, M., Esaki, M., Nishikawa, S.I., Yoshihisa, T., et al. (2009). Roles of Tom70 in import of presequence-containing mitochondrial proteins. *J. Biol. Chem.* 284, 31635–31646.
- Zahedi, R.P., Sickmann, A., Boehm, A.M., Winkler, C., Zufall, N., Schönfisch, B., Guiard, B., Pfanner, N., and Meisinger, C. (2006). Proteomic analysis of the yeast mitochondrial outer membrane reveals accumulation of a subclass of preproteins. *Mol. Biol. Cell* 17, 1436–1450.
- Zhang, Y., Berndt, U., Götz, H., Tais, A., Oellerer, S., Wölfle, T., Fitzke, E., and Rospert, S. (2012). NAC functions as a modulator of SRP during the early steps of protein targeting to the endoplasmic reticulum. *Mol. Biol. Cell* 23, 3027–3040.

## Article

# The Biogenesis of Mitochondrial Outer Membrane Proteins Show Variable Dependence on Import Factors



Daniela G. Vitali,  
Layla Drwesh,  
Bogdan A.  
Cichocki, Antonia  
Kolb, Doron  
Rapaport

doron.rapaport@  
uni-tuebingen.de

### HIGHLIGHTS

The single-span proteins Atg32 and Msp1 are new substrates of the MIM complex

Different domains of Atg32 mediate dependency on either Tom20 or MIM components

The MIM complex facilitates the membrane insertion of the tail-anchored protein Gem1

The membrane integration of Mcr1 and Fis1 is mainly MIM independent

Vitali et al., iScience 23,  
100779  
January 24, 2020 © 2019 The  
Author(s).  
[https://doi.org/10.1016/  
j.isci.2019.100779](https://doi.org/10.1016/j.isci.2019.100779)

## Article

# The Biogenesis of Mitochondrial Outer Membrane Proteins Show Variable Dependence on Import Factors

Daniela G. Vitali,<sup>1,2</sup> Layla Drwesh,<sup>1,2</sup> Bogdan A. Cichocki,<sup>1,3</sup> Antonia Kolb,<sup>1</sup> and Doron Rapaport<sup>1,4,\*</sup>

## SUMMARY

**Biogenesis of mitochondrial outer membrane proteins involves their integration into the lipid bilayer. Among these proteins are those that form a single-span topology, but our understanding of their biogenesis is scarce. In this study, we found that the MIM complex is required for the membrane insertion of some single-span proteins. However, other such proteins integrate into the membrane in a MIM-independent manner. Moreover, the biogenesis of the studied proteins was dependent to a variable degree on the TOM receptors Tom20 and Tom70. We found that Atg32 C-terminal domain mediates dependency on Tom20, whereas the cytosolic domains of Atg32 and Gem1 facilitate MIM involvement. Collectively, our findings (1) enlarge the repertoire of MIM substrates to include also tail-anchored proteins, (2) provide new mechanistic insights to the functions of the MIM complex and TOM import receptors, and (3) demonstrate that the biogenesis of MOM single-span proteins shows variable dependence on import factors.**

## INTRODUCTION

Mitochondria harbor between 800 (in budding yeast) to 1,500 (in mammals) different proteins, and their outer membrane is estimated to harbor several dozens of those proteins. Such mitochondrial outer membrane (MOM) proteins include enzymes, components of protein import complexes, metabolites transporters, and factors that mediate mitochondrial fusion, fission, and motility. The biogenesis of the MOM requires targeting of newly synthesized proteins to the organelle and their integration into the lipid bilayer. An important group among MOM proteins are those that span the membrane once with a single  $\alpha$ -helical segment. Like all other MOM proteins, these single-span proteins are nuclear encoded and synthesized on cytosolic ribosomes (Dukanovic and Rapaport, 2011; Endo and Yamano, 2009; Wiedemann and Pfanner, 2017). Therefore, they must bear appropriate signals that ensure both their correct targeting to the organelle and their membrane integration by mitochondrial import components. None of these proteins contains a canonical cleavable N-terminal presequence, and instead, they carry internal targeting and sorting signals. Despite their well-recognized importance, the diverse molecular mechanisms by which such MOM proteins are specifically targeted to the organelle and inserted into their target membrane remain incompletely defined.

Depending on their orientation, single-span MOM proteins can be classified into three groups: the first two are signal- and tail-anchored proteins, which face the intermembrane space (IMS) with either the amino- or carboxyl-terminus, respectively. These proteins typically expose the bulk of the protein to the cytosol and only a very short segment faces the IMS. A third subclass of single-span proteins exposes soluble domains toward both the IMS and the cytosol, with the N terminus facing the cytosol.

Mitochondrial signal-anchored proteins in fungi include, according to current knowledge, the TOM receptor components, Tom20 and Tom70, and three additional proteins: OM45, Msp1, and the MOM isoform of Mcr1 (Mcr1<sub>MOM</sub>). The targeting signal of these proteins consists of the transmembrane segment (TMS) and positively charged flanking regions (Dukanovic and Rapaport, 2011; Ellenrieder et al., 2015). Despite the common structural characteristics, it appears as if signal-anchored proteins do not share a common pathway of targeting and membrane integration. Mcr1<sub>MOM</sub> and Msp1 follow a still uncharacterized membrane integration pathway that seems for Mcr1<sub>MOM</sub> to be recapitulated with pure lipid vesicles (Meineke et al., 2008), whereas the TOM receptors use a pathway where preexisting TOM complexes play an undefined role (Ahting et al., 2005). Furthermore, the MOM proteins, Mim1 and Mim2, that form together the MIM complex promote both insertion of Tom20 and Tom70 into the MOM and their final assembly into the TOM core complex (Becker et al., 2008; Dimmer et al., 2012; Hulett et al., 2008; Ishikawa et al., 2004; Waizenegger et al., 2005). OM45, which exposes its

<sup>1</sup>Interfaculty Institute of Biochemistry, University of Tübingen, Hoppe-Seyler-Str. 4, 72076 Tübingen, Germany

<sup>2</sup>These authors contributed equally

<sup>3</sup>Present address: Institut de Biologie Moléculaire et Cellulaire, 67084 Strasbourg, France

<sup>4</sup>Lead Contact

\*Correspondence: [doron.rapaport@uni-tuebingen.de](mailto:doron.rapaport@uni-tuebingen.de)

<https://doi.org/10.1016/j.isci.2019.100779>





soluble domain to the IMS, follows a unique membrane assembly pathway that involves crossing the outer membrane via the TOM complex and then insertion into the MOM from the IMS side with a possible contribution of the MIM complex (Song et al., 2014; Wenz et al., 2014).

In comparison with such detailed analysis of the insertion pathway of some signal-anchored proteins, much less is known about the mechanisms by which tail-anchored (TA) proteins are targeted to and integrated into the MOM. As for the signal-anchored proteins, it seems that these proteins do not follow a unified biogenesis pathway. On the one hand, the steady-state levels of yeast mitochondrial TA proteins such as the small TOM complex subunits, Tom5, Tom6, and Tom7, were reduced upon deletion of Mim1, Mas37/Sam37, and TOM receptors (Becker et al., 2008; Horie et al., 2002; Setoguchi et al., 2006; Stojanovski et al., 2007; Thornton et al., 2010). On the other hand, in mammalian cells import of other TA proteins like Omp25, Bak, and Bcl-X<sub>L</sub> was completely independent of the TOM subunits and of any protease accessible protein on the surface of the organelle (Horie et al., 2003; Setoguchi et al., 2006). Likewise, the biogenesis of Fis1 in yeast cells remained unchanged upon deletion of subunits of the import complexes TOM or TOB/SAM and by digestion of any protease-accessible protein on the mitochondrial surface. Furthermore, *in vitro* import assays demonstrated that Fis1 can insert into pure lipid vesicles in an unassisted manner (Kemper et al., 2008). We previously proposed that the specificity of such an insertion could be mediated by the low ergosterol levels of the MOM. In line with this proposal, reduction of ergosterol levels in ER membranes resulted in mislocalization of Fis1 to the ER (Krumpe et al., 2012). Although these previous results raise doubts about the necessity of import factors for the membrane integration of Fis1, they do not address the biogenesis pathway of other TA proteins like Gem1.

The biogenesis of single-span proteins exposing domains toward both sides of the membrane is even less understood. Proteins belonging to this group in yeast MOM are Mim1, Mim2, Atg32, and Tom22. The only protein from this group whose membrane integration process was studied is Tom22, which was reported to require TOM import receptors for its own import as well as the TOB complex and the MOM protein Mdm10 (Court et al., 1996; Thornton et al., 2010). However, since Tom22 is a core component of the TOM complex, its biogenesis mechanism probably reflects a specific case and does not provide a general model for other proteins from this group.

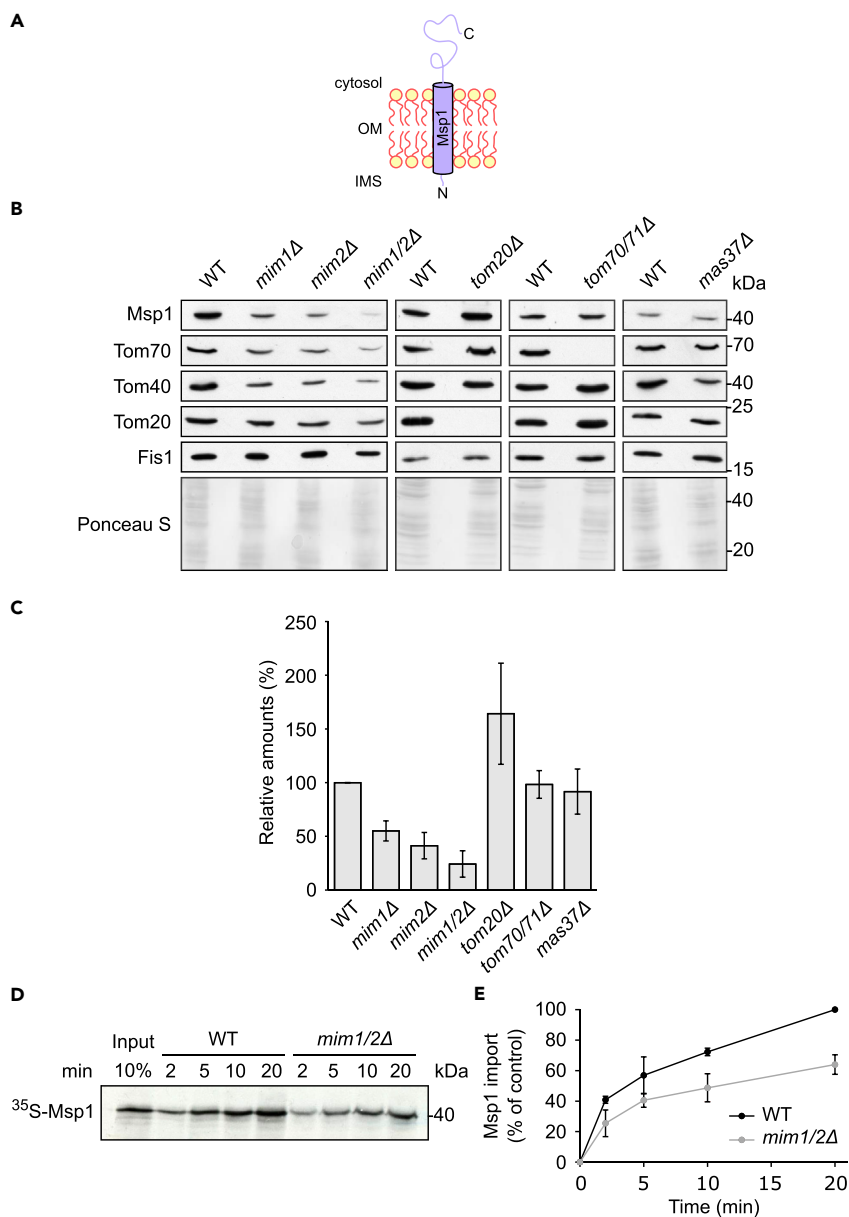
In the current study, we addressed some of the open questions regarding the biogenesis of single-span MOM proteins. We observed that the biogenesis of these proteins is variably dependent on import factors like the MIM complex or the TOM receptors. Furthermore, by constructing hybrid proteins composed of defined domains of these proteins, we could dissect the determinants that cause a variable dependency.

## RESULTS

### The Membrane Integration of Signal-Anchored Proteins Variably Depends on MIM Components

To better characterize the pathways that culminate in the integration of signal-anchored proteins into the MOM, we chose two model proteins that in contrast to the previously established MIM substrates Tom20 and Tom70 are not subunits of the TOM complex. The first is the MOM isoform of Mcr1 (Mcr1<sub>mom</sub>, Figure S1A). We monitored the levels of Mcr1<sub>mom</sub> in the crude mitochondrial fraction from the deletion strains of MIM1, MIM2, or the TOM receptors TOM20 and TOM70/TOM71. As we observed before (Meineke et al., 2008), the absence of the TOM receptors did not cause a reduction in the levels of Mcr1<sub>mom</sub>. Actually, its relative levels were even enhanced in the absence of Tom20 (Figures S1B and S1C). Similarly, the relative amounts of Mcr1<sub>mom</sub> in cells lacking either Mim1 or Mim2 were higher than in control organelles (Figures S1B and S1C). We suggest that this apparent increase results from loading a fixed amount of mitochondrial proteins in each lane. Accordingly, reduction in the relative amounts of certain proteins in these altered organelles leads to an apparent increase in the relative levels of other proteins. To substantiate our results, we isolated mitochondria from either wild-type (WT) or cells lacking both Mim1 and Mim2 and monitored the levels of Mcr1<sub>mom</sub> in these organelles. The levels of Mcr1<sub>mom</sub> were unaltered in the cells lacking the MIM complex (Figures S1D and S1E). These findings demonstrate that the MOM isoform of Mcr1 can integrate into its target membrane in a process that is independent of the MIM complex or import receptors.

Next, we turned to monitor the mitochondrial steady-state levels of the other model protein, namely, the ATPase Msp1 (Figure 1A). Of note, the absence of the TOM receptors or of Mas37, a subunit of the TOB complex, which mediates membrane integration of  $\beta$ -barrel proteins, did not cause major alterations in



### Figure 1. The MIM Complex Is Required for the Biogenesis of Msp1

(A) Schematic depiction of Msp1 topology.

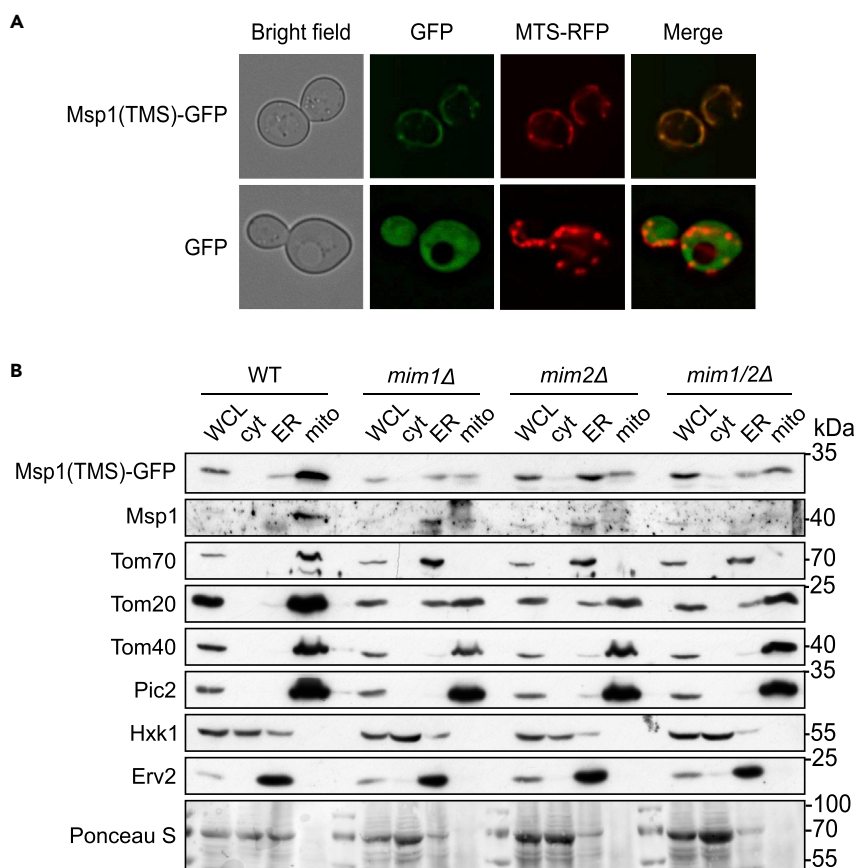
(B) Mitochondria isolated from either the indicated deletion or their respective WT cells were analyzed by SDS-PAGE and immunodecoration with antibodies against the indicated proteins. Staining with Ponceau S is shown as a loading control.

(C) Msp1 levels were quantified and normalized to the intensities of the Ponceau S staining. The values in the corresponding WT cells were set to 100%. The bar diagram shows the average  $\pm$  SD of at least three independent experiments.

(D) Radiolabeled Msp1 was imported *in vitro* for the indicated time periods into mitochondria isolated from either WT or *mim1/2Δ* cells. After import, mitochondria were subjected to alkaline extraction and the pellet was analyzed by SDS-PAGE and autoradiography.

(E) Quantification of the band corresponding to Msp1 in experiments as in (D). Import into mitochondria from WT cells after 20 min was set to 100%. The graph represents the mean values  $\pm$  SD of three independent experiments. See also Figure S1.

the steady-state levels of Msp1, and interestingly, its relative levels were even increased in the absence of Tom20 (Figures 1B and 1C). In contrast, Msp1 levels in the mitochondria isolated from cells deleted for *MIM1*, *MIM2*, or both genes were highly reduced as compared with control samples. We further confirmed



### Figure 2. The TMS of Msp1 Is Sufficient for Recognition by the MIM Complex

(A) Yeast WT cells harboring mitochondrial targeted RFP (MTS-RFP) and expressing either Msp1(TMS)-GFP or GFP alone as a control were visualized by fluorescence microscopy.

(B) Whole-cell lysate (WCL) and fractions corresponding to cytosol (cyt), microsomes (ER), and mitochondria (mito) from the indicated strains expressing Msp1(TMS)-GFP were analyzed by SDS-PAGE and immunodecoration. The fusion protein was detected by an anti-GFP antibody, whereas the endogenous Msp1 protein by anti-Msp1 antibody. Tom20 and Tom70 are known MIM substrate proteins. Hexokinase (Hxk1) is a cytosolic marker, whereas Erv2 is an ER protein. Ponceau S staining of the membrane is shown as a loading control.

the dependency on the MIM complex by importing *in vitro* radiolabeled Msp1 molecules into organelles isolated from either wild-type or *mim1/2Δ* double deletion strain. The proper insertion of the newly synthesized Msp1 molecules into the MOM was verified by their resistance to alkaline extraction. This assay demonstrated that mitochondria isolated from the mutated cells had significantly lower capacity to integrate Msp1 into their membrane (Figures 1D and 1E).

Since it was shown that the TMS of Msp1 mediates the intracellular targeting of the protein (Wohlever et al., 2017), we wondered whether this part of Msp1 is responsible for the dependency on the MIM complex. To address this point, we constructed a fusion protein composed of the TMS (a.a. residues 1–32) of Msp1 fused N terminally to a GFP moiety (Msp1(TMS)-GFP) and introduced it into WT cells. First, we monitored the subcellular localization of this fusion protein by fluorescence microscopy and noted its complete co-localization with a mitochondrial marker protein (MTS-RFP, Figure 2A). Thus, it seems that the TMS of Msp1 is sufficient for mitochondrial targeting.

Next, we transformed this construct into cells deleted for the single MIM components or for both genes and obtained from the transformed cells fractions corresponding to cytosol, ER, and mitochondria. Analysis of these fractions by SDS-PAGE followed by immunodetection revealed that the deletion of the MIM components caused a reduction in the levels of the fusion protein in the mitochondrial fraction of the mutated cells concomitantly with appearance of Msp1(TMS)-GFP in the ER fraction (Figure 2B). Of note, the absence of a



functional MIM complex resulted in the mislocalization of the known MIM substrates Tom20 and Tom70 to the ER, whereas the  $\beta$ -barrel MOM protein Tom40 or the inner membrane protein Pic2 was detected only in the mitochondrial fraction (Figure 2B). These findings indicate that Msp1 is a new substrate of the MIM complex and its TMS is sufficient for this reliance. Moreover, the MIM complex seems to be required for the correct mitochondrial location of the protein.

### Atg32 Is a New Substrate of the MIM Complex

Atg32 is a receptor for mitophagy factors that exposes domains to both sides of the MOM (Figure 3A). To study the requirements for its membrane integration, we employed a functional version where an HA-tag was placed within the cytosolic domain (Okamoto et al., 2009). We introduced this construct into WT and various mutated strains and monitored its steady-state levels in the crude mitochondrial fractions of these cells. We noticed that the levels of Atg32 were dramatically compromised upon the deletion of Mim1, Mim2, and Tom20 and moderately reduced by the absence of Tom70 (Figures 3B and 3C). Atg32 has a similar topology to the TOM component Tom22, which was reported to require the TOB/SAM complex for its proper biogenesis (Thornton et al., 2010). To test whether Atg32 shares such TOB dependency, we monitored its steady-state levels in a strain lacking Mas37, a non-essential component of the TOB complex. As reported, the levels of Tom22 were highly reduced in crude mitochondria isolated from this strain, but the amounts of Atg32 were unaffected, even when the cells were grown at 37°C (Figure 3D). Thus, we concluded that Atg32 does not require the TOB complex for proper membrane integration.

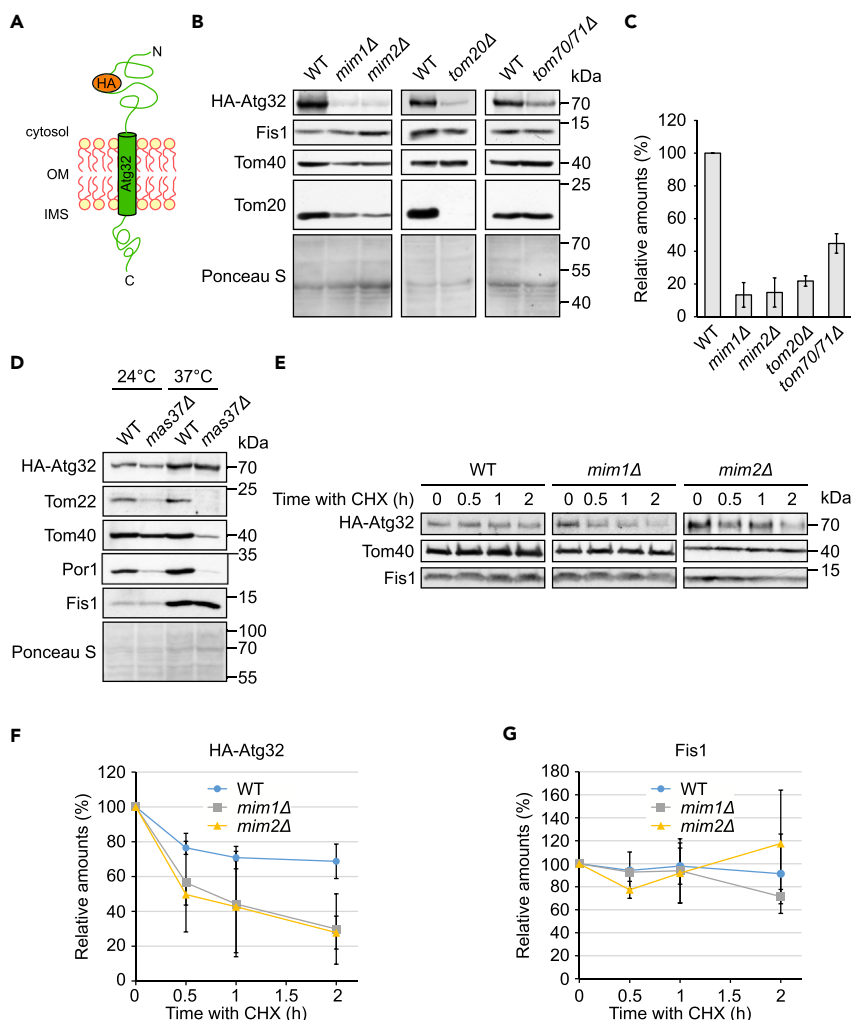
Since the steady-state levels of proteins reflect the combined outcome of biogenesis and degradation, we wondered whether the absence of the Mim proteins affects also the life span of Atg32. To this end, we add to WT or *mim* single deletion strains cycloheximide (CHX), which is known to stop new synthesis of proteins, and monitored the levels of Atg32 after different time intervals. The results of this assay revealed that the absence of either Mim1 or Mim2 shortened significantly the life span of Atg32, whereas it did not affect the stability of the control TA protein Fis1 (Figures 3E–3G). We propose that the absence of the MIM complex slows down the integration of newly synthesized Atg32 molecules into the MOM. This interference in the import process causes then accumulation of the non-imported molecules in the cytosol and subsequently their elimination. Taken together, these findings establish Atg32 as a novel substrate of the MIM pathway.

Since Atg32 showed a dependency on both the MIM complex and Tom70/71, we wondered whether these factors are involved in the same import pathway or in two parallel ones. To address this question, we over-expressed Mim1 in cells lacking both Tom70 and its paralog Tom71. We observed that these elevated amounts of Mim1 could not enhance the reduced levels of Atg32 in *tom70/71* $\Delta$  cells (Figure S2). These results might suggest that Tom70 is involved in the same pathway as the MIM complex, as already shown for the insertion of multi-span proteins (Becker et al., 2011; Papic et al., 2011), and reduced recognition by Tom70 cannot be compensated by more efficient MIM-mediated membrane insertion. However, this option should be taken with caution since it is not clear whether, in the absence of elevated levels of Mim2, the excess amounts of Mim1 molecules assemble into functional complexes.

### The MIM Complex Contributes to the Membrane Integration of the Tail-Anchored Protein Gem1

Previous results suggested that Fis1 can assemble into the MOM in an unassisted manner (Kemper et al., 2008). We next aimed to test its dependency on the MIM complex and to compare its behavior with another TA protein, Gem1 (Figure 4A). To that goal, we monitored the steady-state levels of Fis1 and an N-terminally HA-tagged version of Gem1 in crude mitochondrial fractions of various mutated cells. Of note, the HA-tagged version of Gem1 is functional as we confirmed its ability to complement the growth defect resulting from the absence of chromosomally encoded Gem1 (Figure S3A). The relative levels of Fis1 were actually higher in the MIM mutant cells or unaffected in cells lacking the TOM receptors, whereas those of Gem1 were moderately reduced in cells lacking Mim1 or Mim2 and even more hampered in *tom20* $\Delta$  cells (Figures 4B and 4C). To verify that the difference in behavior of both proteins does not result from the presence of the N terminal HA-tag on one of them, we monitored the behavior of HA-tagged Fis1 and noticed that, like the native protein, it showed independency of the examined import factors (Figures S3B and S3C).

Despite the higher relative levels of Fis1 in the crude mitochondrial fractions of cells deleted for MIM components (Figures 4B and 4C), when we performed subcellular fractionations of these cells, we actually observed a minor population of the Fis1 molecules in the ER (Figure 4D). Of note, this mistargeting involves



### Figure 3. Atg32 Biogenesis Requires the MIM Complex and the TOM Receptors

(A) Schematic representation of the topology of HA-Atg32.

(B) Crude mitochondrial fractions were obtained from *mim1Δ*, *mim2Δ*, *tom20Δ*, *tom70/71Δ*, and their respective WT strains containing a plasmid encoding HA-Atg32. Samples were analyzed by SDS-PAGE and immunodecoration with anti-HA and the other indicated antibodies.

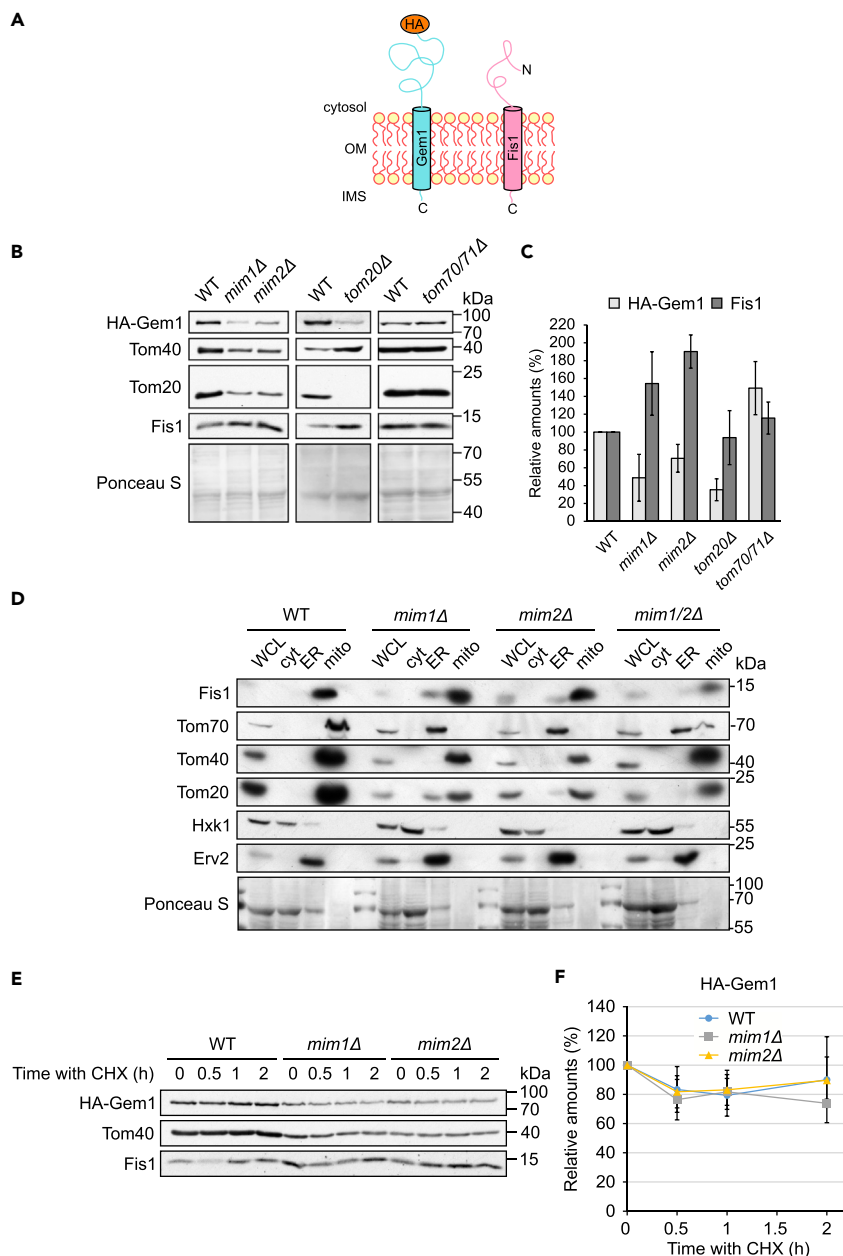
(C) Quantification of the relative amounts of HA-Atg32 from at least three independent experiments as in (B). The levels were normalized to the intensities of the Ponceau S staining and presented as percentage of the levels in the corresponding WT samples. The graph represents average  $\pm$  SD.

(D) Crude mitochondrial fractions were obtained from *mas37Δ* and its respective WT strains after growth at either 24°C or 37°C. Both cell types contained a plasmid encoding HA-Atg32. Samples were analyzed by SDS-PAGE and immunodecoration with anti-HA and the other indicated antibodies.

(E) WT, *mim1Δ*, and *mim2Δ* cells expressing HA-Atg32 were grown to logarithmic phase, treated at time = 0 with cycloheximide (CHX), and then collected after the indicated time intervals. Crude mitochondria were isolated and analyzed by SDS-PAGE and immunodecoration with antibodies against the HA-tag and the indicated proteins.

(F and G) Quantifications of the levels of HA-Atg32 (F) and Fis1 (G) from three independent experiments as in (E) using Tom40 as loading control. The values at time = 0 in each strain were set to 100%. Error bars correspond to  $\pm$  SD. See also Figures S2 and S4.

only a tiny fraction of the Fis1 molecules and is in clear contrast to the massive ER mislocalization of the canonical MIM substrate Tom70 in these mutated cells (Figure 4D). Taken together, these results suggest that Gem1 does not absolutely depend on the MIM pathway for correct biogenesis but might use it when it is available. In contrast, the membrane integration of Fis1 into the MOM seems to be basically MIM independent, although the Mim proteins might slightly contribute to the fidelity of the correct targeting.



**Figure 4. The Biogenesis of Gem1 Depends on the MIM Complex and on Tom20**

(A) Schematic representation of the topologies of HA-Gem1 and Fis1.

(B) Crude mitochondria were isolated from the indicated deletion and their respective WT strains containing a plasmid encoding HA-Gem1. Samples were analyzed by SDS-PAGE and immunodecoration with anti-HA and the indicated antibodies.

(C) Quantification of the relative amounts of HA-Gem1 and Fis1. The intensity of the bands from at least three independent experiments as the one presented in (B) were quantified and normalized to the Ponceau S signal. The levels in the corresponding WT cells were set to 100%. Error bars represent  $\pm$ SD.

(D) Whole-cell lysate (WCL) and fractions corresponding to cytosol (cyt), microsomes (ER), and mitochondria (mito) from the indicated cells were analyzed by SDS-PAGE and immunodecoration. Tom20 and Tom70 are known MIM substrate proteins. Tom40 is a mitochondrial  $\beta$ -barrel protein, Hexokinase (Hxk1) is a cytosolic marker, whereas Erv2 is an ER protein. Ponceau S staining is shown as a loading control.

(E) WT, *mim1Δ*, and *mim2Δ* cells expressing HA-Gem1 were grown to logarithmic phase, treated at time = 0 with CHX, and then collected after the indicated time intervals. Crude mitochondria were isolated and then analyzed by SDS-PAGE and immunodecoration with anti-HA and the indicated antibodies.

**Figure 4. Continued**

(F) Quantifications of the levels of HA-Gem1 from three independent experiments as in (E) using Tom40 as loading control. The values at time = 0 in each strain were set to 100%. Error bars correspond to  $\pm$ SD. See also Figures S3 and S4.

Next, we examined the life span of Gem1 in the *mim* single deletion strains by addition of CHX. In agreement with the aforementioned experiments, the initial levels of Gem1 in the mutated cells were lower than those in the control cells. However, the turnover of the protein was similar in all tested cells (Figures 4E and 4F). Thus, it seems that the absence of a functional MIM complex has no effect on the stability of the TA proteins Fis1 and Gem1 (Figures 3G and 4F).

**pATOM36 Can Replace the MIM Complex in Mediating the Import of MOM Proteins**

We previously found that the *Trypanosoma brucei* protein pATOM36 can functionally compensate the absence of the MIM complex (Vitali et al., 2018). Hence, we next aimed to test whether this protein can also replace the MIM function in facilitating the membrane integration of the two new substrates that we identified, Atg32 and Gem1. To that end, we compared the steady-state levels of Atg32 and Gem1 in the crude mitochondrial fraction of WT and single *mim* deletion strains that were transformed with an empty vector with those transformed with a vector encoding pATOM36. The results depicted in Figure S4 illustrate that pATOM36 can indeed reverse the reduction in the steady-state levels of these MIM substrates. These results further support the identification of pATOM36 as the functional equivalent of the MIM complex.

**Different Domains of Atg32 Mediate Dependency on either Tom20 or MIM Components**

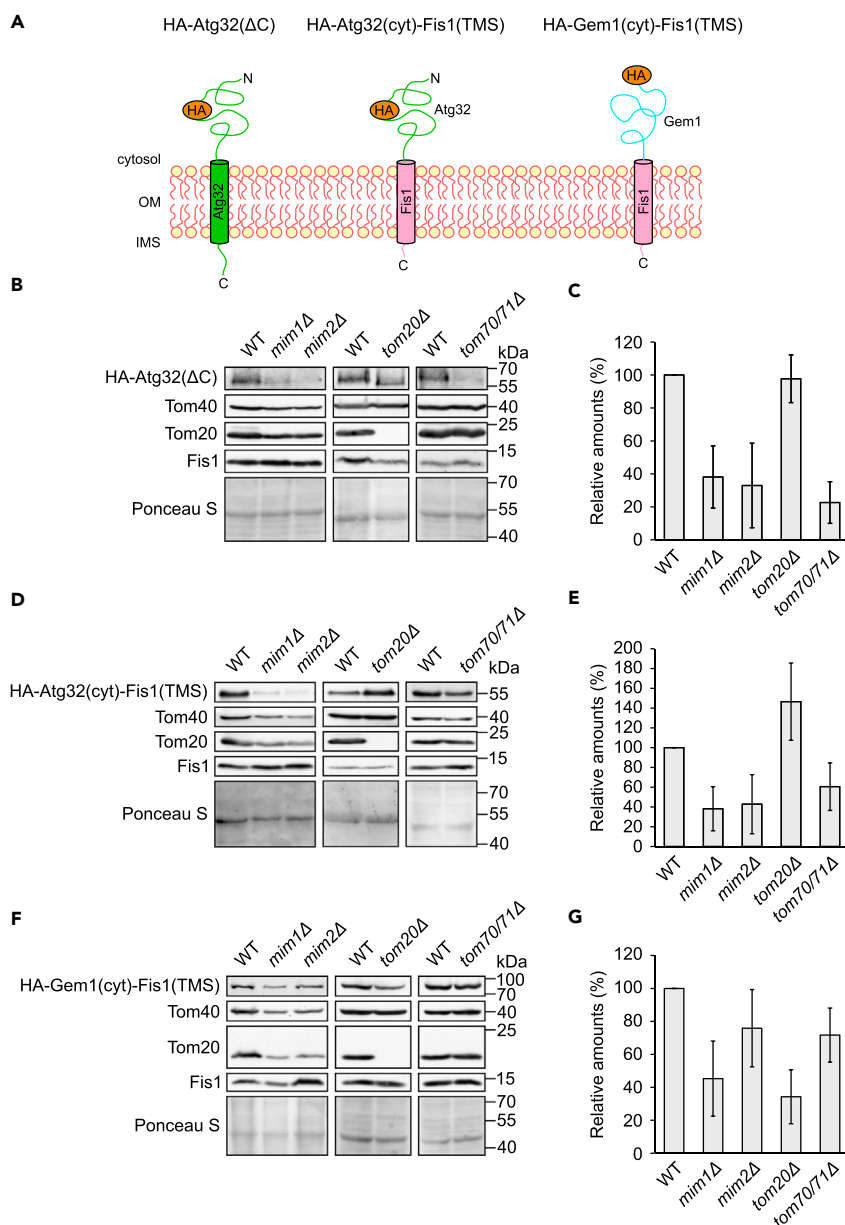
Our results so far indicate that different single-span proteins depend to a variable extent on the MIM complex. To better understand the reason for this variability, we constructed a C-terminally truncated version of Atg32 (HA-Atg32( $\Delta$ C)) and two fusion proteins that are composed of the tail-anchor segment of Fis1 fused to the cytosolic domain of either Atg32 or Gem1 [HA-Atg32(cyt)-Fis1(TMS) or HA-Gem1(cyt)-Fis1(TMS), respectively] (Figure 5A). Of note, the latter construct has probably native-like topology as it can rescue the growth phenotype of cells lacking native Gem1 (Figure S3A). Next, we monitored the steady-state levels of these proteins in the crude mitochondrial fraction of control cells or cells deleted for selected import components. We observed that removal of the C-terminal domain of Atg32 eliminated the dependency of the protein on Tom20, whereas the reduced levels in the absence of MIM components or Tom70 remained (compare Figures 5B and 5C with Figures 3B and 3C). These findings suggest that the dependency on Tom20 is mediated by the IMS part of Atg32, whereas that on the MIM complex by the other parts of the protein.

To narrow down these parts, we analyzed the fusion protein that is composed of the TMS of Fis1 and the cytosolic domain of Atg32. Remarkably, this construct presented similar dependency on Mim1/2 and Tom70 as the truncated version of Atg32 (Figures 5D and 5E). As the membrane integration of the TMS segment of Fis1 appears to be independent of the MIM complex, these findings suggest the surprising possibility that actually the cytosolic domain of Atg32 is responsible for the dependency on these proteins.

To better understand which parts of the single-span proteins facilitate reliance on the import factors, we examined also the construct where the Fis1 TMS was fused to the cytosolic domain of Gem1. Notably, this construct behaved similar to Gem1 and did not resemble the MIM independency of Fis1 (compare Figures 5F and 5G with Figures 4B and 4C). Thus, these results also support the assumption that the cytosolic domain of some single-span proteins dictate largely the insertion pathway that these proteins follow.

Since we suspected that the IMS domain of Atg32 mediates Tom20-dependency, we wished to study this possibility in more detail. To that aim, we constructed a fusion protein where the IMS domain of Atg32 is fused C terminally to Fis1 (HA-Fis1-Atg32(IMS)), Figure 6A. Analysis of the steady-state levels of this fusion protein indicated that, like Fis1, it was Tom70- and MIM-independent, but similarly to Atg32 it showed dependency on Tom20 (Figures 6B and 6C). Hence, these findings indicate that the IMS domain of Atg32 mediates the requirement for Tom20.

To further substantiate these conclusions, we fused the cytosolic domain of Fis1 to the TMS and IMS domains of Atg32 (HA-Fis1(cyt)-Atg32(TMS + IMSD)), Figure 6A. Importantly, this construct showed strong



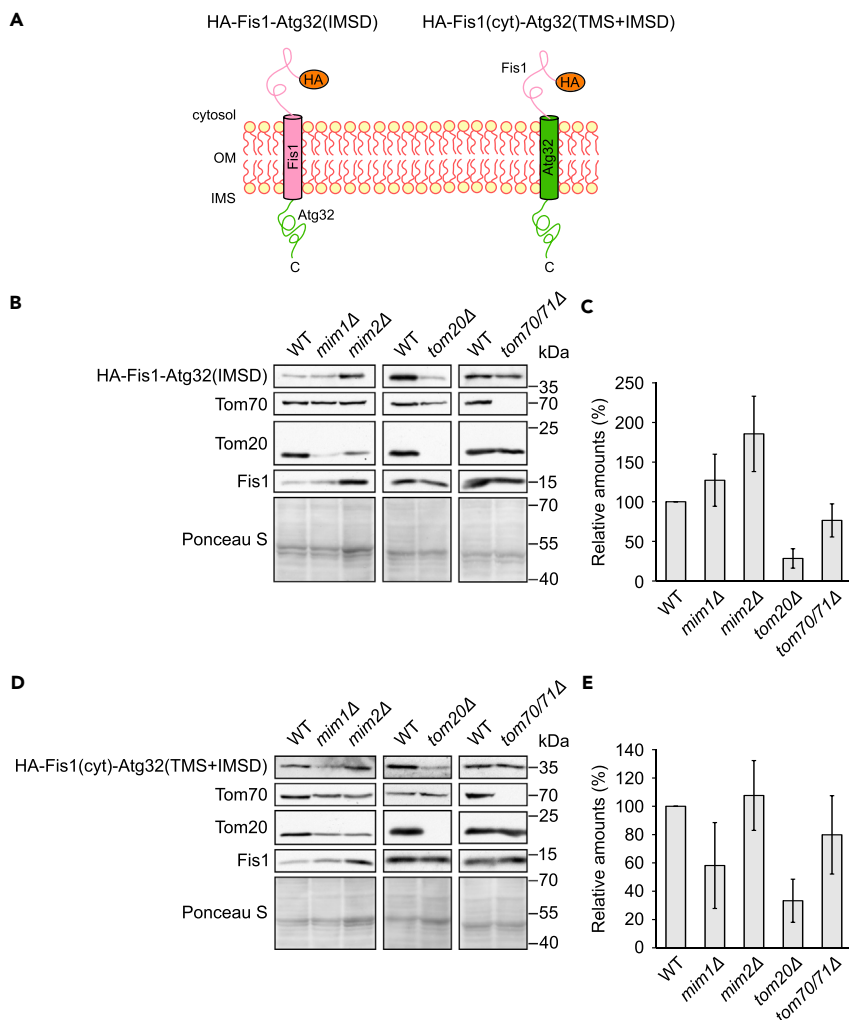
**Figure 5. The Cytosolic Domain of Atg32 and Gem1 Dictates the Dependency on the MIM Complex**

(A) Schematic representation of the topology of HA-Atg32(ΔC), HA-Atg32(cyt)-Fis1(TMS), and HA-Gem1(cyt)-Fis1(TMS).

(B, D, and F) Crude mitochondria were extracted from the indicated strains containing a plasmid expressing HA-Atg32(ΔC) (B), HA-Atg32(cyt)-Fis1(TMS) (D), or HA-Gem1(cyt)-Fis1(TMS) (F). Samples were analyzed by SDS-PAGE and immunodecoration with anti-HA and the indicated antibodies.

(C, E, and G) The intensities of the bands corresponding to the HA signal from at least three independent experiments as in (B), (D), or (F) were quantified and normalized with the signal of the Ponceau S staining. The relative intensity, as compared with the corresponding WT strain, of HA-Atg32(ΔC) (C), HA-Atg32(cyt)-Fis1(TMS) (E), and HA-Gem1(cyt)-Fis1(TMS) (G) are depicted. Error bars represent ±SD.

dependency on Tom20 and only moderate requirement for Mim1. No significant dependency on Mim2 or Tom70 was observed (Figures 6D and 6E). Collectively, these results support the findings that the C-terminal domain of Atg32 mediates dependency on Tom20, whereas the cytosolic domains of Atg32, and to a lesser extent that of Gem1, have a major contribution to the requirement of the Mim proteins.



**Figure 6. Tom20 Is Required for the Biogenesis of Hybrid Proteins Containing the IMS Domain of Atg32**

(A) Schematic representation of the topology of HA-Fis1-Atg32(IMSD) and HA-Fis1(cyt)-Atg32(TMS + IMSD).

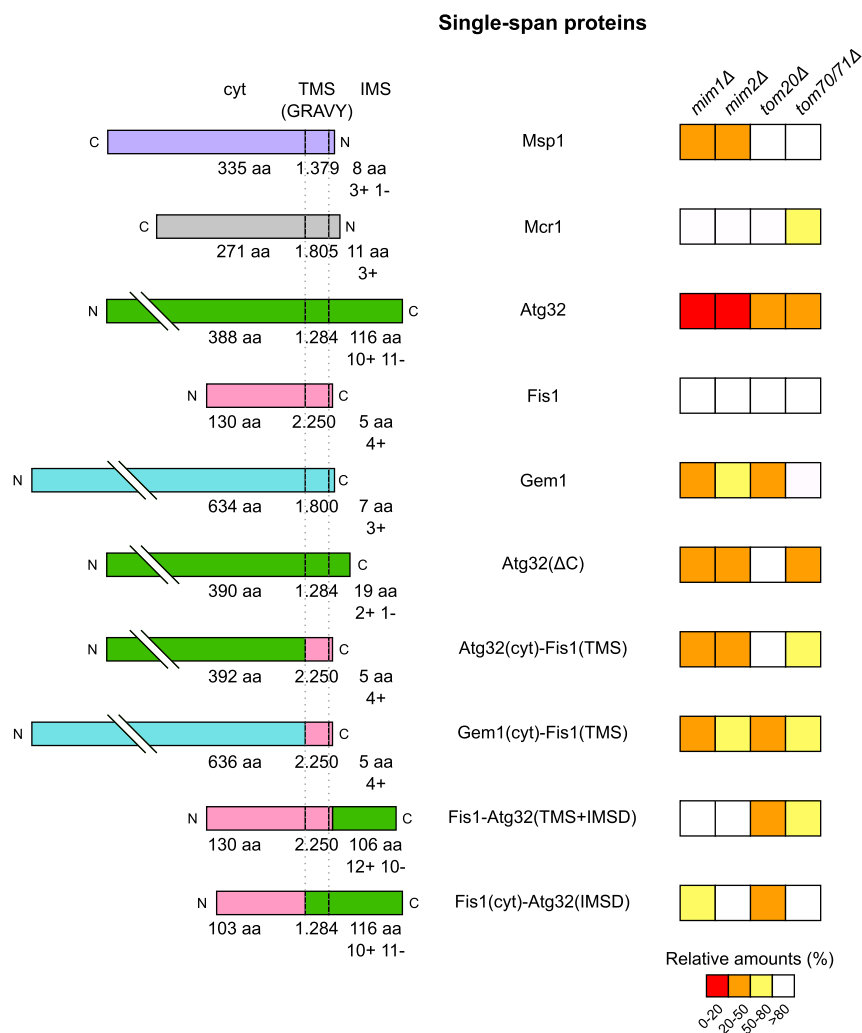
(B and D) Crude mitochondrial fractions isolated from the indicated strains containing a plasmid expressing either HA-Fis1-Atg32(IMSD) (B) or HA-Fis1(cyt)-Atg32(TMS + IMSD) (D) were analyzed by SDS-PAGE and immunodecoration with anti-HA and the indicated antibodies.

(C and E) The intensity of the bands corresponding to HA-Fis1-Atg32(IMSD) (C) or HA-Fis1(cyt)-Atg32(TMS + IMSD) (E) from at least three independent experiments as in (B) or (D), respectively, were quantified and normalized to the intensity of the Ponceau S. The levels are presented as percentage of the corresponding WT samples and error bars represent  $\pm$ SD.

## DISCUSSION

The biogenesis of newly synthesized MOM proteins involves their synthesis on cytosolic ribosomes, possible association with cytosolic factors to maintain them in import competent conformation, targeting to the surface of the organelle, and finally integration into the membrane. In the current study, we investigated which proteins on the surface of mitochondria are involved in the targeting and membrane assembly of single-span proteins. Remarkably, we observed that, although these proteins share some structural features, each one of them depends to a different extent on the presence of import receptors and an insertase complex.

Some proteins like the MOM isoform of Mcr1 or Fis1 hardly, if at all, require the assistance of import factors. In contrast, the signal-anchored proteins Msp1 and the single-span protein Atg32 rely heavily on the presence of the MIM subunits and the latter protein depends also on Tom20 and Tom70. Yet, other proteins like



**Figure 7. The Biogenesis of the Tested Proteins Depends on Their Domain Composition**

Left: Schematic representation of the analyzed proteins. The topology of the proteins is depicted (cyt, cytosolic domain; TMS, transmembrane segment; IMS, intermembrane space domain). In addition, the grand average of hydrophobicity (GRAVY) value of the corresponding TMS, the length of the soluble domains, and the charges of the IMS segment are indicated.

Right: The average values of the steady-state levels measured for each protein in the indicated deletion strains is depicted with a color-coded system, which is explained at the bottom.

Gem1 are only moderately dependent on the presence of the MIM complex and appear to require Tom20. Thus, it seems that yet undefined determinants of the substrate proteins govern their distinct requirements for support. Such determinants can be length and/or average hydrophobicity of the TMS, net charge of its flanking regions, the tendency of the TMS to form helical structure, the presence of a soluble domain in the IMS, or various parameters of the cytosolic domain. Inspection of the hydrophobicity and the flanking charges did not reveal a clear correlation between these parameters and the behavior of the proteins (Figure 7). Most likely, rather than a single parameter a combination of several of the aforementioned determinants dictate the behavior of a certain protein.

A link that we could identify is a Tom20 requirement that is mediated by the IMS domain of Atg32. All fusion proteins harboring this domain showed dependency on Tom20, and Atg32 variant lacking it lost this requirement. Tom20 can recognize directly this domain and/or the IMS domain is associated in the cytosol with a chaperone and Tom20 serves as the receptor for this chaperone-substrate complex. Regardless of the correct possibility, the biogenesis pathway of Atg32 and Gem1 provides a unique example where

targeting to the organelle is facilitated by Tom20, whereas the membrane integration is mediated by the MIM complex. So far, known substrates of the MIM pathway, like multi-span helical proteins, were reported to interact with Tom70 prior to their engagement by the MIM complex (Becker et al., 2011; Papic et al., 2011); however, Atg32 is only moderately dependent on Tom70. Hence, this study indicates a novel cooperation between Tom20 and the MIM complex.

Another surprising finding of our study is the contribution of the cytosolic domains of the substrate proteins Atg32 and Gem1 to the dependency on the MIM complex. Since these domains remain in the cytosol and do not have to cross the MOM, their effect might be via their influence on the availability of the TMS for recognition and insertion by the MIM complex. Alternatively, the MIM complex may help in obtaining the correct conformation of the cytosolic domain by interacting with hydrophobic segments, which in the final conformation will be buried within this domain. A third possibility is that, as discussed above for the involvement of Tom20, the cytosolic domain of Atg32 or Gem1 is stabilized by cytosolic factor(s) and the MIM complex functions as a receptor for such factors. Actually, a study by Vögtle et al. support the latter option as it suggested that, at least for the multi-span protein Ugo1, the MIM complex functions more as a receptor than as an insertase (Vogtle et al., 2015).

The results of the current study substantiate that the membrane integration of the MOM proteins Fis1 and Mcr1 is basically MIM independent. Of note, although the MIM complex does not appear to affect the mitochondrial levels of Fis1, it seems that in its absence more Fis1 molecules are mis-targeted to the ER. One explanation for this observation is a potential involvement of the MIM complex in a quality control process that re-targets mitochondrial proteins, which were wrongly associated with the ER, to the mitochondria. It might be that the MIM complex is not required for the direct insertion of newly synthesized Fis1 molecules from the cytosol, but, due to unclear reason, it does facilitate the re-targeting of those molecules that were initially associated with the ER. Such an ER surface retrieval pathway was described recently for several mitochondrial proteins (Hansen et al., 2018).

Our findings also establish Atg32, Msp1, and Gem1 as novel substrates of the MIM pathway. However, also for these clear substrates, MIM deletion reduces the extent of membrane integration but still allows a considerable portion of these newly synthesized proteins to associate with the MOM. Thus, it is quite obvious that an alternative membrane insertion pathway must exist. Such an alternative route might involve a yet unknown protein factor or the lipid core of the membrane as it was reported that the optimal integration of helical proteins into the MOM requires low ergosterol content and the presence of cardiolipin and phosphatidic acid (Kemper et al., 2008; Sauerwald et al., 2015; Vogtle et al., 2015). A similar multi pathway scenario is also discussed for the membrane integration of TA proteins into the ER membrane where at least four, partially overlapping, potential pathways are postulated (Borgese et al., 2019).

Collectively, our results could be explained by a variable dependency on the MIM complex that is dictated by yet undefined combination of determinants. At one edge of the spectrum are proteins like Fis1 and Mcr1 that can be inserted into the MOM in an unassisted manner. On the other side are those proteins like Msp1 and Atg32 that heavily rely on the help of the MIM insertase, and in between these poles are substrates like Gem1 that are not absolutely dependent on the MIM machinery but probably can utilize it when it is present. Moreover, the import of single-span MOM proteins is further influenced by cytosolic factors and the lipid composition of the membrane. This collection of, partially unknown, parameters makes any attempt to predict which pathway a certain protein will follow a very demanding task.

### Limitations of the Study

This study used Baker's yeast as a model organism. Higher eukaryotes do not have a MIM complex but rather, yet unidentified, equivalent factors. Hence, it is unclear whether the various import requirements that were identified for the different utilized substrate proteins are valid also in higher eukaryotes.

### METHODS

All methods can be found in the accompanying [Transparent Methods supplemental file](#).

### SUPPLEMENTAL INFORMATION

Supplemental Information can be found online at <https://doi.org/10.1016/j.isci.2019.100779>.



## ACKNOWLEDGMENTS

We thank E. Kracker for excellent technical assistance, K.S. Dimmer for helpful discussions, K. Okamoto for constructs and antibodies, and T. Endo for antibodies. This work was supported by the Deutsche Forschungsgemeinschaft (RA 1028/7-2 and 10-1 to D.R.) and the ITN TAMPTing to D.G.V., B.C., and D.R. (funded by the People Programme [Marie Curie Actions] of the European Union's Seventh Framework Programme [FP7/2007–2013/] under the Research Executive Agency [grant number 607072]). L.D. is supported by a long-term fellowship from the Minerva Foundation.

## AUTHOR CONTRIBUTIONS

D.G.V., L.D., and B.A.C. designed and conducted experiments. A.K. conducted experiments. D.R. designed experiments and analyzed data. D.G.V. and D.R. wrote the manuscript.

## DECLARATION OF INTERESTS

The authors declare no competing interests.

Received: August 30, 2019

Revised: November 12, 2019

Accepted: December 12, 2019

Published: January 24, 2020

## REFERENCES

- Ahting, U., Waizenegger, T., Neupert, W., and Rapaport, D. (2005). Signal-anchored proteins follow a unique insertion pathway into the outer membrane of mitochondria. *J. Biol. Chem.* 280, 48–53.
- Becker, T., Pfanschmidt, S., Guiard, B., Stojanovski, D., Milenkovic, D., Kutik, S., Pfanner, N., Meisinger, C., and Wiedemann, N. (2008). Biogenesis of the mitochondrial TOM complex: Mim1 promotes insertion and assembly of signal-anchored receptors. *J. Biol. Chem.* 283, 120–127.
- Becker, T., Wenz, L.S., Kruger, V., Lehmann, W., Muller, J.M., Goroncy, L., Zufall, N., Lithgow, T., Guiard, B., Chacinska, A., et al. (2011). The mitochondrial import protein Mim1 promotes biogenesis of multispanning outer membrane proteins. *J. Cell Biol.* 194, 387–395.
- Borgese, N., Coy-Vergara, J., Colombo, S.F., and Schwappach, B. (2019). The ways of tails: the GET pathway and more. *Protein J.* 38, 289–305.
- Court, D.A., Nargang, F.E., Steiner, H., Hodges, R.S., Neupert, W., and Lill, R. (1996). Role of the intermembrane space domain of the preprotein receptor Tom22 in protein import into mitochondria. *Mol. Cell. Biol.* 16, 4035–4042.
- Dimmer, K.S., Papic, D., Schumann, B., Sperl, D., Krumpe, K., Walther, D.M., and Rapaport, D. (2012). A crucial role for Mim2 in the biogenesis of mitochondrial outer membrane proteins. *J. Cell Sci.* 125, 3464–3473.
- Dukanovic, J., and Rapaport, D. (2011). Multiple pathways in the integration of proteins into the mitochondrial outer membrane. *Biochim. Biophys. Acta* 1808, 971–980.
- Ellenrieder, L., Martensson, C.U., and Becker, T. (2015). Biogenesis of mitochondrial outer membrane proteins, problems and diseases. *Biol. Chem.* 396, 1199–1213.
- Endo, T., and Yamano, K. (2009). Multiple pathways for mitochondrial protein traffic. *Biol. Chem.* 390, 723–730.
- Hansen, K.G., Aviram, N., Laborenz, J., Bibi, C., Meyer, M., Spang, A., Schuldiner, M., and Herrmann, J.M. (2018). An ER surface retrieval pathway safeguards the import of mitochondrial membrane proteins in yeast. *Science* 361, 1118–1122.
- Horie, C., Suzuki, H., Sakaguchi, M., and Mihara, K. (2002). Characterization of signal that directs C-tail-anchored proteins to mammalian mitochondrial outer membrane. *Mol. Biol. Cell* 13, 1615–1625.
- Horie, C., Suzuki, H., Sakaguchi, M., and Mihara, K. (2003). Targeting and assembly of mitochondrial tail-anchored protein Tom5 to the TOM complex depend on a signal distinct from that of tail-anchored proteins dispersed in the membrane. *J. Biol. Chem.* 278, 41462–41471.
- Hulett, J.M., Lueder, F., Chan, N.C., Perry, A.J., Wolyne, P., Likic, V.A., Gooley, P.R., and Lithgow, T. (2008). The transmembrane segment of Tom20 is recognized by Mim1 for docking to the mitochondrial TOM complex. *J. Mol. Biol.* 376, 694–704.
- Ishikawa, D., Yamamoto, H., Tamura, Y., Moritoh, K., and Endo, T. (2004). Two novel proteins in the mitochondrial outer membrane mediate  $\beta$ -barrel protein assembly. *J. Cell Biol.* 166, 621–627.
- Kemper, C., Habib, S.J., Engl, G., Heckmeyer, P., Dimmer, K.S., and Rapaport, D. (2008). Integration of tail-anchored proteins into the mitochondrial outer membrane does not require any known import components. *J. Cell Sci.* 121, 1990–1998.
- Krumpe, K., Frumkin, I., Herzig, Y., Rimon, N., Özbacı, C., Brügger, B., Rapaport, D., and Schuldiner, M. (2012). Ergosterol content specifies targeting of tail-anchored proteins to mitochondrial outer membranes. *Mol. Biol. Cell* 23, 3927–3935.
- Meineke, B., Engl, G., Kemper, C., Vasiljev-Neumeyer, A., Paulitschke, H., and Rapaport, D. (2008). The outer membrane form of the mitochondrial protein Mcr1 follows a TOM-independent membrane insertion pathway. *FEBS Lett.* 582, 855–860.
- Okamoto, K., Kondo-Okamoto, N., and Ohsumi, Y. (2009). Mitochondria-anchored receptor Atg32 mediates degradation of mitochondria via selective autophagy. *Dev. Cell* 17, 87–97.
- Papic, D., Krumpe, K., Dukanovic, J., Dimmer, K.S., and Rapaport, D. (2011). Multispanning mitochondrial outer membrane protein Ugo1 follows a unique Mim1-dependent import pathway. *J. Cell Biol.* 194, 397–405.
- Sauerwald, J., Jores, T., Eisenberg-Bord, M., Chuartzman, S.G., Schuldiner, M., and Rapaport, D. (2015). Genome-wide screens in *Saccharomyces cerevisiae* highlight a role for cardiolipin in biogenesis of mitochondrial outer membrane multispan proteins. *Mol. Cell. Biol.* 35, 3200–3211.
- Setoguchi, K., Otera, H., and Mihara, K. (2006). Cytosolic factor- and TOM-independent import of C-tail-anchored mitochondrial outer membrane proteins. *EMBO J.* 25, 5635–5647.
- Song, J., Tamura, Y., Yoshihisa, T., and Endo, T. (2014). A novel import route for an N-anchor mitochondrial outer membrane protein aided by the TIM23 complex. *EMBO Rep.* 15, 670–677.
- Stojanovski, D., Guiard, B., Kozjak-Pavlovic, V., Pfanner, N., and Meisinger, C. (2007). Alternative function for the mitochondrial SAM complex in biogenesis of  $\alpha$ -helical TOM proteins. *J. Cell Biol.* 179, 881–893.
- Thornton, N., Stroud, D.A., Milenkovic, D., Guiard, B., Pfanner, N., and Becker, T. (2010). Two

modular forms of the mitochondrial sorting and assembly machinery are involved in biogenesis of  $\alpha$ -helical outer membrane proteins. *J. Mol. Biol.* 396, 540–549.

Vitali, D.G., Kaser, S., Kolb, A., Dimmer, K.S., Schneider, A., and Rapaport, D. (2018). Independent evolution of functionally exchangeable mitochondrial outer membrane import complexes. *Elife* 7, e34488.

Vogtle, F.N., Keller, M., Taskin, A.A., Horvath, S.E., Guan, X.L., Prinz, C., Opalinska, M., Zorzini,

C., van der Laan, M., Wenk, M.R., et al. (2015). The fusogenic lipid phosphatidic acid promotes the biogenesis of mitochondrial outer membrane protein Ugo1. *J. Cell Biol.* 210, 951–960.

Waizenegger, T., Schmitt, S., Zivkovic, J., Neupert, W., and Rapaport, D. (2005). Mim1, a protein required for the assembly of the TOM complex of mitochondria. *EMBO Rep.* 6, 57–62.

Wenz, L.S., Opalinski, L., Schuler, M.H., Ellenrieder, L., Ieva, R., Bottinger, L., Qiu, J., van der Laan, M., Wiedemann, N., Guiard, B., et al.

(2014). The presequence pathway is involved in protein sorting to the mitochondrial outer membrane. *EMBO Rep.* 15, 678–685.

Wiedemann, N., and Pfanner, N. (2017). Mitochondrial machineries for protein import and assembly. *Annu. Rev. Biochem.* 86, 685–714.

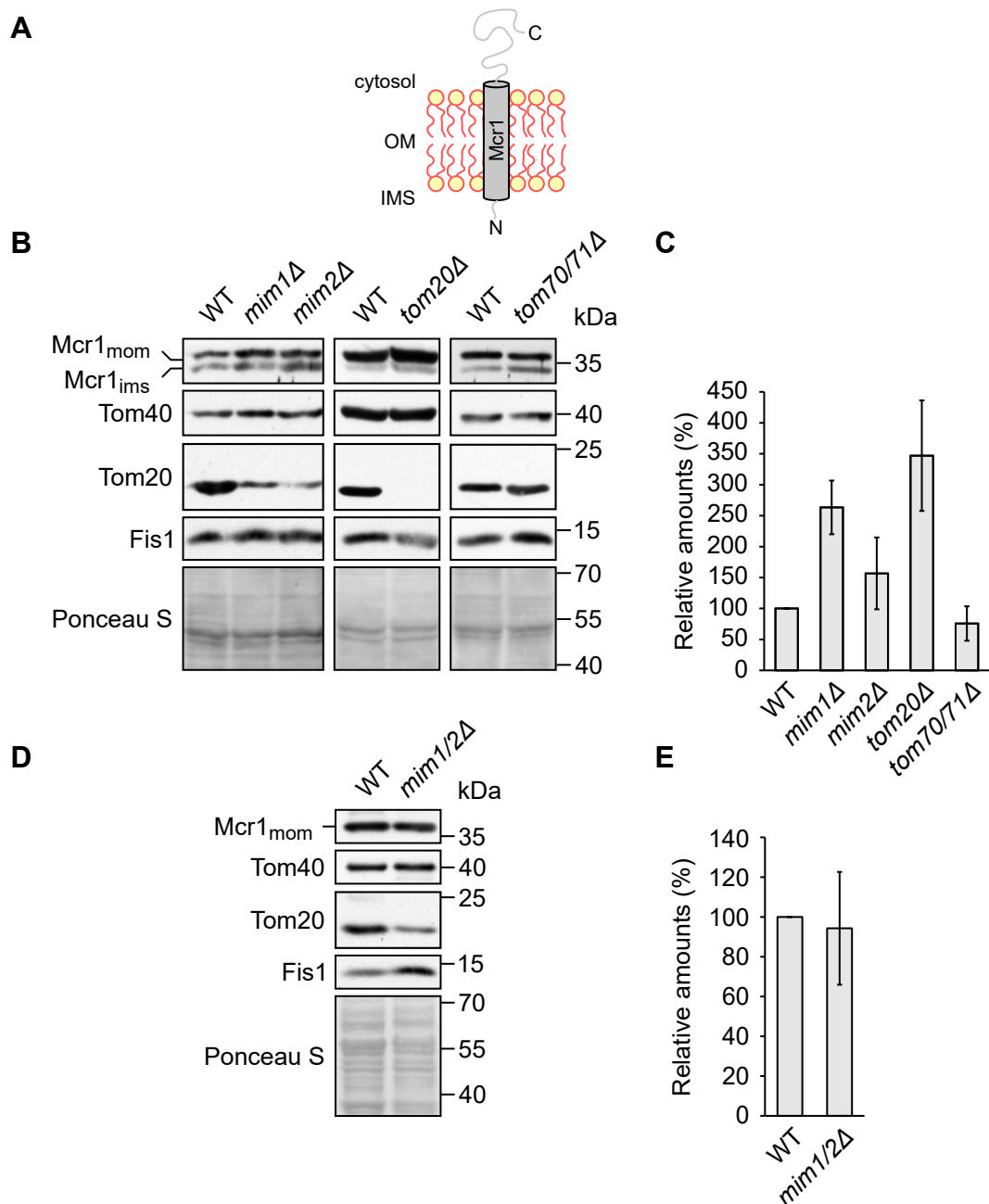
Wohlever, M.L., Mateja, A., McGilvray, P.T., Day, K.J., and Keenan, R.J. (2017). Msp1 is a membrane protein dislocase for tail-anchored proteins. *Mol. Cell* 67, 194–202.

**iScience, Volume 23**

**Supplemental Information**

**The Biogenesis of Mitochondrial Outer  
Membrane Proteins Show Variable  
Dependence on Import Factors**

**Daniela G. Vitali, Layla Drwesh, Bogdan A. Cichocki, Antonia Kolb, and Doron Rapaport**



**Figure S1. Related to Figure 1. Mcr1 levels are not affected by deletions of MOM import factors.**

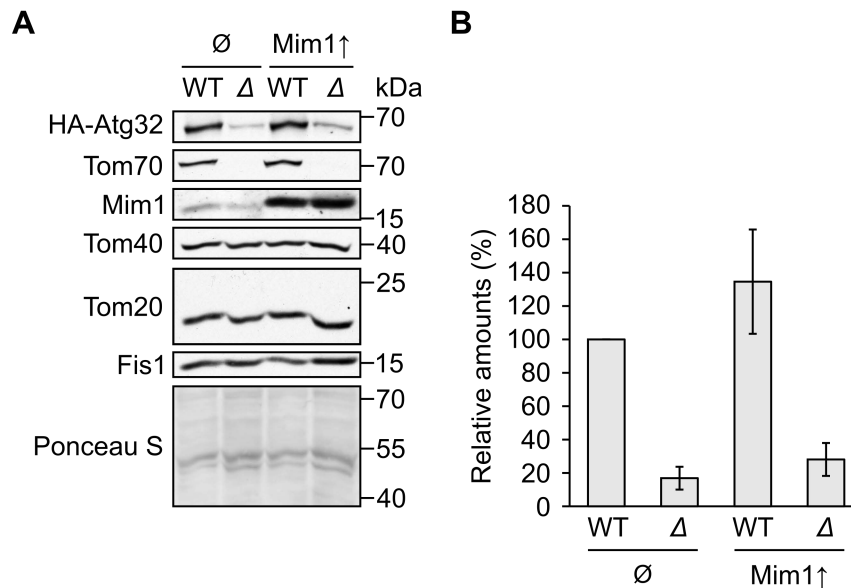
(A) Schematic representation of the topology of Mcr1<sub>mom</sub>. IMS: intermembrane space.

(B) Crude mitochondrial fractions of *mim1*Δ, *mim2*Δ, *tom20*Δ, *tom70/71*Δ, and their respective WT strains were analysed by SDS-PAGE and immunodecoration with the indicated antibodies. The outer membrane (Mcr1<sub>mom</sub>) and IMS (Mcr1<sub>ims</sub>) isoforms of Mcr1 are indicated.

(C) Quantification of the band corresponding to Mcr1<sub>mom</sub> in experiments as in (B). The levels were normalized with the Ponceau S signal and presented as percentage of the amounts in the corresponding WT samples. The graph represents the average of at least three independent experiments ± standard deviation (SD).

(D) Isolated mitochondria were obtained from WT and *mim1/2*Δ strains and analysed by SDS-PAGE and immunodecoration with the indicated antibodies.

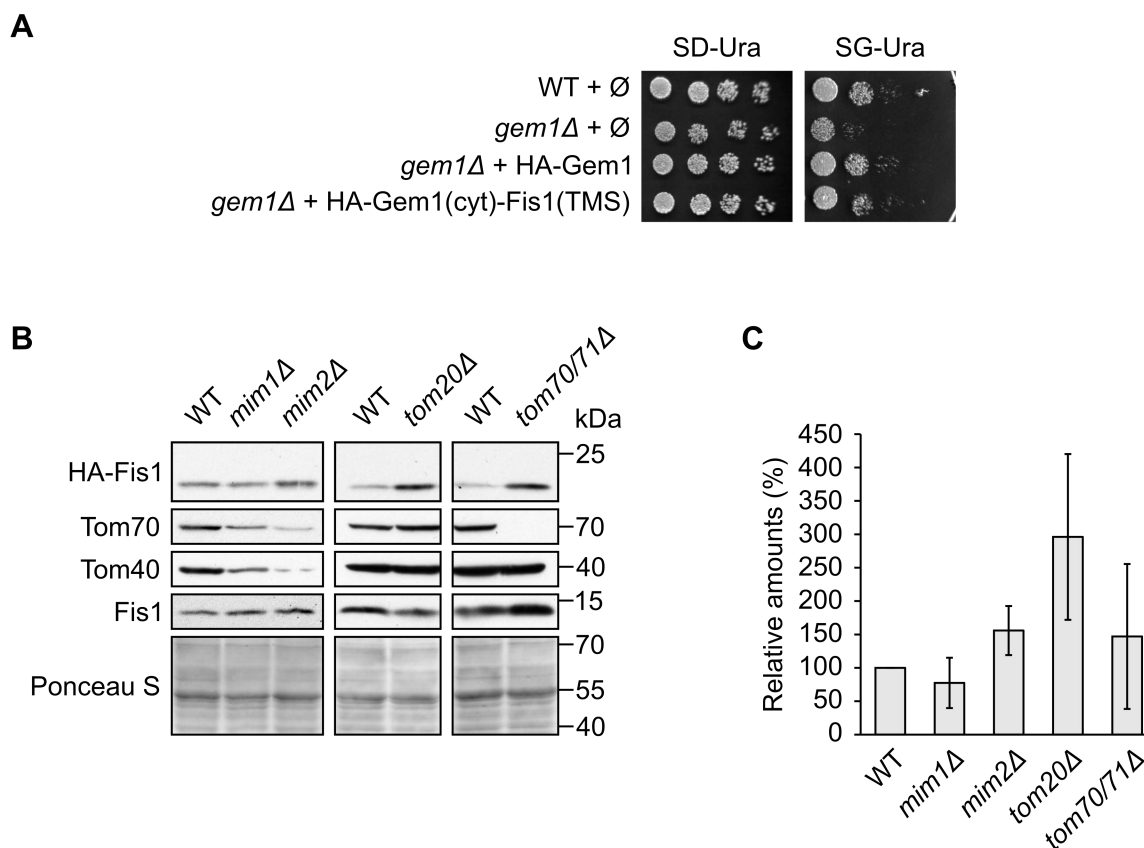
(E) Mcr1<sub>mom</sub> levels from three independent experiment as in (D) were quantified and normalized to the intensities of the Ponceau S staining. The values are presented as percentage of the amounts in WT cells. Error bars represent ± SD.



**Figure S2. Related to Figure 3. Overexpression of Mim1 does not rescue the reduced levels of HA-Atg32 in cells lacking Tom70/71.**

(A) Crude mitochondria fractions were isolated from either WT or *tom70/71Δ* ( $\Delta$ ) strains transformed with a plasmid expressing HA-Atg32 and either an empty plasmid ( $\emptyset$ ) or a plasmid overexpressing MIM1 (Mim1 $\uparrow$ ). Proteins were analysed by SDS-PAGE and immunodecoration with anti-HA and the indicated antibodies.

(B) Quantification of the band corresponding to HA-Atg32 in three independent experiments as the one shown in (A). The levels were normalized to the intensity of the Ponceau S signal and are shown as percentage of the WT transformed with the empty vector. Error bars correspond to  $\pm$ SD.

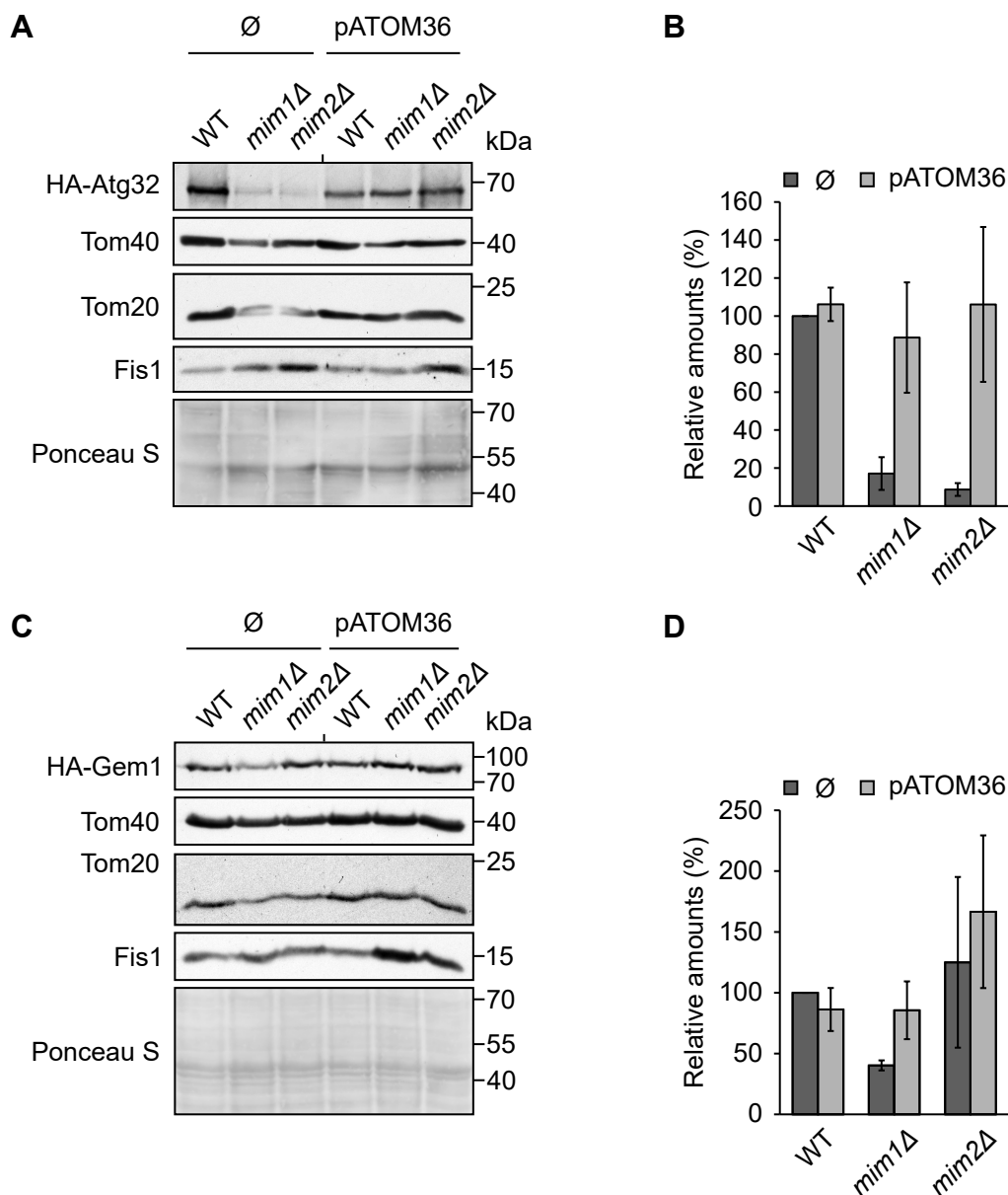


**Figure S3. Related to Figure 4. N-terminally HA-tagged Fis1 and Gem1 behave as the native proteins.**

(A) The indicated strains transformed with an empty plasmid ( $\emptyset$ ), or a plasmid expressing either HA-Gem1 or HA-Gem1(cyt)-Fis1(TMS) were tested by drop dilutions at 30°C on synthetic glucose-containing (SD-Ura) or glycerol-containing (SG-Ura) media.

(B) Crude mitochondria fractions were isolated from the indicated strains expressing HA-Fis1. Proteins were analysed by SDS-PAGE and immunodecorated with anti-HA and the indicated antibodies.

(C) Quantification of the band corresponding to HA-Fis1 in three independent experiments as the one shown in (B). The levels were normalized to the intensity of the Ponceau S signal and are shown as percentage of the corresponding WT. The graph represents the average of at least three independent experiments. Error bars correspond to  $\pm$ SD.



**Figure S4. Related to Figures 3 and 4. The reduced levels of HA-Atg32 and HA-Gem1 in the absence of the MIM complex can be complemented by pATOM36.**

(A and C) Crude mitochondrial fractions were obtained from WT, *mim1Δ*, and *mim2Δ* cells transformed with a plasmid encoding HA-Atg32 (A) or HA-Gem1 (C) and with either an empty plasmid (∅) or a plasmid overexpressing pATOM36. Samples were analysed by SDS-PAGE and immunodecoration with anti-HA and the indicated antibodies.

(B and D) The intensity of the bands corresponding to HA-Atg32 (B) or HA-Gem1 (D) from at least three independent experiments as in (A) or (C), respectively, were quantified and normalized to the Ponceau S signal. The levels are presented as percentage of the levels in WT cells transformed with the empty plasmid. Error bars represent  $\pm$  SD.

## Transparent Methods

### Yeast strains and growth conditions

Yeast strains used in the study were isogenic to *Saccharomyces cerevisiae* strain W303a, W303 $\alpha$ , YPH499, or JSY7452. All strains used in this study are listed in Table S1. Standard genetic techniques were used for growth and manipulation of yeast strains. Yeast cells were grown in either rich medium YP (2% [w/v] bacto peptone, 1% [w/v] yeast extract) or synthetic medium S (0.67% [w/v] bacto-yeast nitrogen base without amino acids). Glucose (2% [w/v]), galactose (2% [w/v]), sucrose (2% [w/v]), or lactate (2% [w/v]) were used as carbon source. Transformation of yeast cells was performed by the lithium acetate method. For drop-dilution assay, cells were grown in a synthetic medium to logarithmic phase and diluted in fivefold increments followed by spotting five  $\mu$ l of the diluted cells on solid media.

### Recombinant DNA techniques

The *MSP1* open reading frame (ORF) was amplified by PCR from yeast genomic DNA with specific primers containing BamHI and HindIII restriction sites. The yeast Kozak sequence was introduced directly upstream of the start codon via a primer. The PCR product was cloned into the plasmid pGEM4 to obtain pGEM4-yk-Msp1. The pYX142-Msp1(TMS)-GFP plasmid was obtained by PCR amplification of the DNA sequence encoding amino acid residues 1-32 of Msp1 using pYX142-Msp1-3HA as a template. Primers containing EcoRI and KpnI restriction sites were used and the PCR product was inserted upstream and in-frame with the eGFP coding region of pGEM4-eGFP plasmid. Next, the sequence encoding Msp1(TMS)-GFP was sub-cloned, using EcoRI and BamHI restriction sites, from the pGEM4 plasmid to the yeast expression pYX142 plasmid.

To insert the *FISI* promoter (pr) and terminator (ter) into the pRS316 plasmid, DNA segments of around 500 bp upstream and downstream of the *FISI* ORF were amplified by PCR from genomic DNA. The promoter region was cloned between SpeI and XmaI restriction sites, while the terminator sequence was inserted between HindIII and Sall sites. To obtain the pRS316-*FISI*pr-Fis1(cyt)-*FISI*ter, the sequence encoding for the cytosolic domain of Fis1 (amino acid residues 1-103) was amplified by PCR from genomic DNA and inserted with XmaI and NheI restriction sites between the *FISI* promoter and terminator segments. The plasmid pRS316-3HA-Gem1 was obtained upon amplifying by PCR the *GEM1* ORF from pYX132-GFP-Gem1 (Cichocki et al., 2018) with primers containing the XmaI and HindIII restriction



sites. The obtained DNA fragment was inserted into the pRS316-*FIS1pr-FIS1ter* plasmid. The 3xHA tag was amplified by PCR from pYX142-3HA-YadA (Müller et al., 2011) and inserted in-frame at the N-terminus of Gem1, between two XmaI restriction sites.

The pRS316-*FIS1pr*-3HA-Fis1(cyt)-*FIS1ter* plasmid was obtained by amplifying the 3xHA tag by PCR from pYX142-3HA-YadA (Müller et al., 2011) with primers containing XmaI and EcoRI restriction sites and inserting it into the pRS316-*FIS1pr*-Fis1cyt-*FIS1ter* plasmid. To obtain the plasmid pRS316-3HA-Fis1, the *FIS1* ORF was amplified by PCR from genomic DNA with primers containing EcoRI and HindIII restriction sites and inserted into the pRS316-*FIS1pr*-3HA-*FIS1ter* plasmid. The pRS316-3HA-Gem1(cyt) plasmid, encoding the cytosolic domain of Gem1 (amino acid residues 1-634), was obtained by digesting pRS316-HA-Gem1 with Sall and XhoI, employing the SallI restriction site present in the *GEM1* ORF upstream the sequence coding for the TMS of the protein. To construct the plasmid pRS316-3HA-Gem1(cyt)-Fis1(TMS), the sequence coding for Fis1 TMS (amino acid residues 129-155) followed by *FIS1* terminator was amplified by PCR from pRS316-3HA-Fis1 with primers containing Sall and XhoI restriction sites and inserted in-frame into pRS316-3HA-Gem1(cyt).

The pRS316-3HA-Fis1-Atg32(IMS) plasmid was obtained upon PCR amplification of the *FIS1* ORF without the stop codon, using pRS316-3HA-Fis1 plasmid as a template, and inserting it into the pRS316-*FIS1pr*-3HA-*FIS1ter* between EcoRI and NheI restriction sites. Subsequently, the sequence coding for the IMS domain of Atg32 (amino acid residues 431-529 aa) was amplified by PCR from the pRS316-3HAN-Atg32 plasmid (Okamoto et al., 2009) with primers containing the NheI and HindIII restriction sites and inserted in-frame downstream the *FIS1* ORF. pRS316-3HA-Fis1(cyt)-Atg32(TMS+IMS) was constructed by PCR amplification of the sequence coding for Atg32 TMS and IMS domain (amino acid residues 389-529), employing pRS316-3HAN-Atg32 (Okamoto et al., 2009) as template. The PCR product was inserted into pRS316-*FIS1pr*-3HA-Fis1(cyt)-*FIS1ter* between NheI and HindIII restriction sites. pRS316-3HAN-Atg32( $\Delta$ C) and pRS316-3HAN-Atg32(cyt)-Fis1(TMS) were constructed as follows, a point mutation was introduced in the pRS316-3HAN-Atg32(1-388)-TM<sup>pexo</sup>- plasmid (Kondo-Okamoto et al., 2012) to insert the NheI restriction site directly downstream the sequence encoding for the TMS of Pex15. Afterwards, this latter sequence, which was located between two NheI sites, was excised and then the sequences coding for the TMS of either Atg32 (a.a. residues 389-430) or of Fis1 (amino acid residues 129-155), amplified from pRS316-3HAN-Atg32 and pRS316-HA-Fis1 respectively, were inserted between the two NheI restriction sites. All constructs were confirmed by DNA sequencing. Tables S2 and S3 include a full list of plasmids and primers, respectively, used in this study.

## **Biochemical methods**

Protein samples for immunodecoration were analysed on 12.5% SDS-PAGE and subsequently transferred onto nitrocellulose membranes by semi-dry Western blotting. Before loading on the gels, the samples were heated for 10 min at either 50°C, for samples containing variants of Atg32, or at 95°C, for all other samples. Proteins were detected by incubating the membranes first with primary antibodies and then with horseradish peroxidase-conjugates of either goat anti-rabbit or goat anti-rat secondary antibodies. Band intensities were quantified with AIDA software (Raytest). See Table S4 for a list of primary antibodies used in this study.

Subcellular fractionation was performed as described before (Walther et al., 2009). Isolation of mitochondria from yeast cells was performed by differential centrifugation, as previously described (Daum et al., 1982). To obtain highly pure mitochondria, isolated organelles were layered on top of a Percoll gradient and isolated according to a published procedure (Graham, 2001).

To obtain fractions of crude mitochondria, cells were ruptured with glass beads ( $\emptyset$  0.25-0.5 mm) using FastPrep-24 5G (MP Biomedicals) for 40 sec, 6.0 m/sec. The samples were then centrifuged (20000g, 10 min, 4°C) and the pellet was resuspended in a 2xLämmli solution.

## **Protein stability assay**

For the protein stability assay, cells were grown to logarithmic phase and then treated with cycloheximide (CHX) at final concentration of 0.1 mg/ml. Samples were collected at different time points, crude mitochondria were obtained as described above and samples were analysed by SDS-PAGE and immunoblotting.

## ***In vitro* synthesis and mitochondrial import of radiolabelled proteins**

Cell-free transcription was performed with SP6 polymerase from pGEM4 plasmid encoding *MSP1*. The protein was then translated *in vitro* from the acquired mRNA in rabbit reticulocyte lysate (Promega) in the presence of <sup>35</sup>S-methionine. Protein import was performed by adding 50  $\mu$ l of the reticulocyte lysate (containing the translated protein) to 30  $\mu$ g of isolated mitochondria diluted to a final concentration of 1  $\mu$ g/ $\mu$ l in import buffer (250 mM sucrose, 0.25 mg/ml BSA, 80 mM KCl, 10 mM MOPS-KOH, 5 mM MgCl<sub>2</sub>, 8 mM ATP and 4 mM NADH, pH 7.2). Import of Msp1 was performed at 10°C for 2, 5, 10, or 20 minutes. The import reactions were terminated by diluting the reaction with 400  $\mu$ l SEM-K<sup>80</sup> buffer (250 mM sucrose, 80 mM KCl, 10 mM MOPS, 1 mM EDTA, pH 7.2) and pelleting the mitochondria (13200g, 10 min, 2°C). The pellet fraction was subjected to alkaline extraction by resuspending

it in 100  $\mu$ l of 0.1 M Na<sub>2</sub>CO<sub>3</sub> solution and incubation for 30 min on ice. Then, the membrane fraction was isolated by centrifugation (180000g, 30 min, 2°C). The pellet was resuspended with 40  $\mu$ l of 2xLaemmli buffer, heated for 10 min at 95°C, and analysed by SDS-PAGE followed by autoradiography.

### Fluorescence microscopy

Microscopy images of strains expressing Msp1(TMS)-eGFP, eGFP, and mtRFP were acquired with an Axioskop 20 fluorescence microscope equipped with an AxioCam MRm camera using the 43 Cy3 filter set and the AxioVision software (Carl Zeiss).

**Table S1. Yeast strains used in this study**

Name	Mating type	Genetic background	Source or reference
W303a	MATa	<i>ade2-1 can1-100 his3-11 leu2 3_112 trp1<math>\Delta</math>2 ura3-52</i>	Lab stock
W303 $\alpha$	MAT $\alpha$	<i>ade2-1 can1-100 his3-11 leu2 3_112 trp1<math>\Delta</math>2 ura3-52</i>	Lab stock
YPH499	MATa	<i>ura3-52 lys2-801_amber ade2-101 ochre trp1-<math>\Delta</math>63 his3-<math>\Delta</math>200 leu2-<math>\Delta</math>1</i>	Lab stock
JSY7452	MAT $\alpha$	<i>ade2-1 can1-100 his3-11,15 leu2-3 trp1-1 ura3-1</i>	(Kondo-Okamoto et al., 2006)
<i>mim1<math>\Delta</math></i>	MATa	W303a; <i>mim1<math>\Delta</math>::KanMX</i>	(Dimmer et al., 2012)
<i>mim2<math>\Delta</math></i>	MATa	W303a; <i>mim2<math>\Delta</math>::HIS3</i>	(Dimmer et al., 2012)
<i>mim1/2<math>\Delta</math></i>	MATa	W303a; <i>mim1<math>\Delta</math>::KanMX mim2<math>\Delta</math>::HIS3</i>	(Dimmer et al., 2012)
<i>tom20<math>\Delta</math></i>	MAT $\alpha$	W303 $\alpha$ ; <i>tom20<math>\Delta</math>::HIS3</i>	(Müller et al., 2011)
<i>tom70/71<math>\Delta</math></i>	MATa	JSY7452; <i>tom70<math>\Delta</math>::TRP1 tom71<math>\Delta</math>::HIS3</i>	(Kondo-Okamoto et al., 2008)
<i>mas37<math>\Delta</math></i>	MATa	YPH499; <i>mas37<math>\Delta</math>::HIS3</i>	(Habib et al., 2005)

**Table S2. Plasmids used in this study**

Plasmid	Promoter	Coding sequence (aa)	Markers	Source
pGEM4-yk-Msp1	SP6	Msp1 full length	Amp <sup>R</sup>	This study
PYX142-Msp1-3HA	TPI	Msp1 full length	LEU2, Amp <sup>R</sup>	This study
pGEM4-eGFP	SP6	GFP	Amp <sup>R</sup>	Lab stock
PRS416-MTS-RFP	TPI	MTS-RFP	URA3 Amp <sup>R</sup>	Lab stock
pYX142-Msp1(TMS)-eGFP	TPI	Msp1(1-32)	LEU2, Amp <sup>R</sup>	This study
pRS316-3HAn-Atg32	Atg32Pr (580 bp 5'-UTR / 744 bp 3'-UTR from <i>ATG32</i> )	Atg32 full length	URA3, Amp <sup>R</sup>	(Okamoto et al., 2009)
pRS316-3HA-Gem1	Fis1Pr (496 bp 5'-UTR / 408 bp 3'-UTR from <i>FIS1</i> )	Gem1 full length	URA3, Amp <sup>R</sup>	This study
pYX142	TPI		LEU2, Amp <sup>R</sup>	Lab stock
pYX142-pATOM36	TPI	pATOM36 full length	LEU2, Amp <sup>R</sup>	(Vitali et al., 2018)
pRS316-3HAn-Atg32( $\Delta$ C)	Atg32Pr (580 bp 5'-UTR / 744 bp 3'-UTR from <i>ATG32</i> )	Atg32(1-430)	URA3, Amp <sup>R</sup>	This study
pRS316-3HAn-Atg32(cyt)-Fis1(TMS)	Atg32Pr (580 bp 5'-UTR / 744 bp 3'-UTR from <i>ATG32</i> )	Atg32(1-388) + Fis1(129-155)	URA3, Amp <sup>R</sup>	This study
pRS316-3HA-Gem1(cyt)-Fis1(TMS)	Fis1Pr (496 bp 5'-UTR / 408 bp 3'-UTR from <i>FIS1</i> )	Gem1(1-634) + Fis1(129-155)	URA3, Amp <sup>R</sup>	This study
pRS316-3HA-Fis1-Atg32(IMSD)	Fis1Pr (496 bp 5'-UTR / 408 bp 3'-UTR from <i>FIS1</i> )	Fis1(1-155) + Atg32(431-529)	URA3, Amp <sup>R</sup>	This study
pRS316-3HA-Fis1(cyt)-Atg32(TMD+IMSD)	Fis1Pr (496 bp 5'-UTR / 408 bp 3'-UTR from <i>FIS1</i> )	Fis1(1-103) + Atg32(389-529)	URA3, Amp <sup>R</sup>	This study
pRS316-3HA-Fis1	Fis1Pr (496 bp 5'-UTR / 408 bp 3'-UTR from <i>FIS1</i> )	Fis1 full length	URA3, Amp <sup>R</sup>	This study
pYX142-Mim1	TPI	Mim1 full length	LEU2, Amp <sup>R</sup>	(Dimmer et al., 2012)

**Table S3. Primers used in this study**

Primer name	Sequence (5'-3')	Note
BamHIMsp1F	GGGGGATCCAAAAAATGTCTCGCA AATTTGATTAAAAACGATTACTGA TCTTT	Amplification of <i>MSP1</i> , BamHI restriction site at 5'
HindIIIMsp1R	GGGAAGCTTTTAATCAAGAGGTTGA GATGACAAC	Amplification of <i>MSP1</i> , HindIII restriction site at 5'
EcoRIMsp1F	GGGGAATTCATGTCTCGCAAATTTGATT TAAAAACGATTACTG	Amplification of the sequence encoding the TMS of Msp1 (a.a. 1- 32), <i>EcoRI</i> restriction site at 5'
KpnIMsp1R	GGGGGTACCGCCGGCCGTTGAGTAG CCGACTGACCAGGTAG	Amplification of the sequence encoding the TMS of Msp1 (a.a. 1- 32), <i>KpnI</i> restriction site at 5'
XmaIGem1F	GGGCCCGGGACTAAAGAAACGATT CGGGTAG	Amplification of <i>GEM1</i> , XmaI restriction site at 5'
HindIIIGem1R	CCCAAGCTTTTATTTGAGAATTTTG ATGATTTGAATAATTTTCAT	Amplification of <i>GEM1</i> , HindIII restriction site at 5'
XmaIHAF	CCCCCGGGATGTACCCATACGATG TTCCTG	Amplification of HA coding sequence, XmaI restriction site at 5'
XmaIHAR	GGGCCCGGGAGCGTAATCTGGAAC GTCAT	Amplification of HA coding sequence, XmaI restriction site at 5'
XmaIFis1CytF	GGGCCCGGGATGACCAAAGTAGATT TTTGGCC	Amplification of sequence encoding the cytosolic domain of Fis1, XmaI restriction site at 5'
NheIHindIIIFis1CytR	CCCAAGCTTGCTAGCTAAAGTGTCT ACATATCTCTTCGCC	Amplification of sequence encoding the cytosolic domain of Fis1, NheI and HindIII restriction site at 5'
mutKOB131F	CTAGCGAGTATAGCTAGCTAACCTT	Insertion of point mutation to include NheI restriction site in pRS316- atg32(1-388)-TM <sup>pexo</sup> -3HAn
mutKOB131R	AAGGTTAGCTAGCTATACTCGCTAG	Insertion of point mutation to include NheI restriction site in pRS316- atg32(1-388)-TM <sup>pexo</sup> -3HAn
NheIAtg32TMDF	CCCGTAGCAGCTGGTTCACTTGGG GCATTC	Amplification of sequence encoding the TMS of Atg32, NheI restriction site at 5'
NheIAtg32TMD+R	GGGGCTAGCCAATATGGAGGGCCG CAAACCTAAAG	Amplification of sequence encoding the TMS of Atg32, NheI restriction site at 5'
NheIFis1TMDF	CCCGTAGCCTCAAGGGTGTGTCG TCG	Amplification of sequence encoding the TMS of Fis1, NheI restriction site at 5'
NheIFis1TMDR	GGGGCTAGCTTACCTTCTCTTGTTTC TTAAGAAGAAAC	Amplification of sequence encoding the TMS of Fis1, NheI restriction site at 5'
SallIFis1TMDF	GGGGTCTGACTACAGACAAACGGCTC TCAAGGGTGTGTCGTCGC	Amplification of sequence encoding the TMS of Fis1, Sall restriction site at 5'
XhoIFis1TerR	CCCCTCGAGATCTCACAATACAGTA TTACGATTTAACAATAGACTATTG	Amplification of sequence encoding the TMS of Fis1, XhoI restriction site at 5'
EcoRIFis1HACytF	GGGGAATTCATGACCAAAGTAGATT TTTGGCC	Amplification of <i>FIS1</i> without stop codon, <i>EcoRI</i> restriction site at 5'
NheIFis1NOSTOPR	CCCGTAGCCCTTCTCTTGTTCCTTA AGAAGAAAC	Amplification of <i>FIS1</i> without stop codon, NheI restriction site at 5'
NheIAtg32IMSDF	GGGGCTAGCGCTCTTTACTTTCCCTT AGATTCCTCTAG	Amplification of sequence encoding the IMS domain of Atg32, NheI restriction site at 5'

HindIIIAtg32R	CCCAAGCTTTTACAATAGAATATAA CCCAGTGCCAAAATC	Amplification of sequence encoding the IMS domain of Atg32, HindIII restriction site at 5'
5-Fis1Pr-SpeI	AAAAGTAGTTCAAATAACATGTGTC CATTACC	Amplification of Fis1Pr, SpeI restriction site at 5'
3-Fis1pr-SmaI	AAACCCGGGGTTGTATGGCTGTG	Amplification of Fis1Pr, SmaI restriction site at 5'
5-Fis1THindIII	CCCAAGCTTATAAAAAATCAGCACA TACGTACATAC	Amplification of Fis1Term, HindIII restriction site at 5'
3-Fis1TSalI	CCCGTCGACATCTCACAAATACAGTA TTACG	Amplification of Fis1Term, SalI restriction site at 5'

**Table S4. Antibodies used in this study**


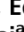

Antibodies	Dilution	Source
polyclonal rat anti-HA	1 : 1000	11867423001 (Roche)
polyclonal rabbit anti-GFP	1: 2000	TP401 (Torrey Pines)
polyclonal rabbit anti-Mcr1	1 : 2000	Lab stocks
polyclonal rabbit anti-Tom40	1 : 4000	Lab stocks
polyclonal rabbit anti-Tom20	1 : 5000	Lab stocks
polyclonal rabbit anti-Fis1	1 : 1000	Lab stocks
polyclonal rabbit anti-Tom70	1 : 5000	Lab stocks
polyclonal rabbit anti-Mim1	1 : 500	Lab stocks
polyclonal rabbit anti-Msp1	1 : 1000	Lab of Toshiya Endo
polyclonal rabbit anti-Pic2	1 : 2000	Lab stocks
polyclonal rabbit anti-Bmh1	1 : 1500	Lab stocks
polyclonal rabbit anti-Erv2	1 : 2000	Lab of Roland Lill

## References

- Cichocki, B.A., Krumpe, K., Vitali, D.G., and Rapaport, D. (2018). Pex19 is involved in importing dually targeted tail-anchored proteins to both mitochondria and peroxisomes. *Traffic* *19*, 770-785.
- Daum, G., Böhni, P.C., and Schatz, G. (1982). Import of proteins into mitochondria: cytochrome b2 and cytochrome c peroxidase are located in the intermembrane space of yeast mitochondria. *J Biol Chem* *257*, 13028-13033.
- Dimmer, K.S., Papic, D., Schumann, B., Sperl, D., Krumpe, K., Walther, D.M., and Rapaport, D. (2012). A crucial role for Mim2 in the biogenesis of mitochondrial outer membrane proteins. *J Cell Sci* *125*, 3464-3473.
- Graham, J.M. (2001). Isolation of mitochondria from tissues and cells by differential centrifugation. *Current protocols in cell biology Chapter 3*, Unit 3 3.
- Habib, S.J., Waizenegger, T., Lech, M., Neupert, W., and Rapaport, D. (2005). Assembly of the TOB complex of mitochondria. *J Biol Chem* *280*, 6434-6440.
- Kondo-Okamoto, N., Noda, N.N., Suzuki, S.W., Nakatogawa, H., Takahashi, I., Matsunami, M., Hashimoto, A., Inagaki, F., Ohsumi, Y., and Okamoto, K. (2012). Autophagy-related protein 32 acts as autophagic degron and directly initiates mitophagy. *J Biol Chem* *287*, 10631-10638.
- Kondo-Okamoto, N., Ohkuni, K., Kitagawa, K., McCaffery, J.M., Shaw, J.M., and Okamoto, K. (2006). The novel F-box protein Mfb1p regulates mitochondrial connectivity and exhibits asymmetric localization in yeast. *Mol Biol Cell* *17*, 3756-3767.
- Kondo-Okamoto, N., Shaw, J.M., and Okamoto, K. (2008). Tetratricopeptide repeat proteins Tom70 and Tom71 mediate yeast mitochondrial morphogenesis. *EMBO Rep* *9*, 63-69.
- Müller, J.E., Papic, D., Ulrich, T., Grin, I., Schütz, M., Oberhettinger, P., Tommassen, J., Linke, D., Dimmer, K.S., Autenrieth, I.B., *et al.* (2011). Mitochondria can recognize and assemble fragments of a beta-barrel structure. *Mol Biol Cell* *22*, 1638-1647.
- Okamoto, K., Kondo-Okamoto, N., and Ohsumi, Y. (2009). Mitochondria-anchored receptor Atg32 mediates degradation of mitochondria via selective autophagy. *Dev Cell* *17*, 87-97.
- Vitali, D.G., Käser, S., Kolb, A., Dimmer, K.S., Schneider, A., and Rapaport, D. (2018). Independent evolution of functionally exchangeable mitochondrial outer membrane import complexes. *Elife* *7*.
- Walther, D.M., Papic, D., Bos, M.P., Tommassen, J., and Rapaport, D. (2009). Signals in bacterial b-barrel proteins are functional in eukaryotic cells for targeting to and assembly in mitochondria. *Proc Natl Acad Sci USA* *106*, 2531-2536.



# Uncovering targeting priority to yeast peroxisomes using an in-cell competition assay

Mira Rosenthal<sup>a,1</sup>, Eyal Metzl-Raz<sup>a,1</sup> , Jérôme Bürgi<sup>b</sup>, Eden Yifrach<sup>a</sup> , Layla Drwesh<sup>c</sup>, Amir Fadel<sup>a</sup>, Yoav Peleg<sup>d</sup>, Doron Rapaport<sup>c</sup>, Matthias Wilmanns<sup>b,e</sup>, Naama Barkai<sup>a</sup>, Maya Schuldiner<sup>a,2</sup> , and Einat Zalckvar<sup>a,2</sup>

<sup>a</sup>Department of Molecular Genetics, Weizmann Institute of Science, 7610001 Rehovot, Israel; <sup>b</sup>Hamburg Unit c/o DESY, European Molecular Biology Laboratory, 22607 Hamburg, Germany; <sup>c</sup>Interfaculty Institute of Biochemistry, University of Tübingen, 72074 Tübingen, Germany; <sup>d</sup>Structural Proteomics Unit, Department of Life Sciences Core Facilities, Weizmann Institute of Science, 7610001 Rehovot, Israel; and <sup>e</sup>University Medical Center Hamburg-Eppendorf, 20246 Hamburg, Germany

Edited by William A. Prinz, National Institutes of Health, Bethesda, MD, and accepted by Editorial Board Member Tony Hunter July 17, 2020 (received for review November 16, 2019)

**Approximately half of eukaryotic proteins reside in organelles. To reach their correct destination, such proteins harbor targeting signals recognized by dedicated targeting pathways. It has been shown that differences in targeting signals alter the efficiency in which proteins are recognized and targeted. Since multiple proteins compete for any single pathway, such differences can affect the priority for which a protein is catered. However, to date the entire repertoire of proteins with targeting priority, and the mechanisms underlying it, have not been explored for any pathway. Here we developed a systematic tool to study targeting priority and used the Pex5-mediated targeting to yeast peroxisomes as a model. We titrated Pex5 out by expressing high levels of a Pex5-cargo protein and examined how the localization of each peroxisomal protein is affected. We found that while most known Pex5 cargo proteins were outcompeted, several cargo proteins were not affected, implying that they have high targeting priority. This priority group was dependent on metabolic conditions. We dissected the mechanism of priority for these proteins and suggest that targeting priority is governed by different parameters, including binding affinity of the targeting signal to the cargo factor, the number of binding interfaces to the cargo factor, and more. This approach can be modified to study targeting priority in various organelles, cell types, and organisms.**

yeast | peroxisomes | protein targeting | systems cell biology

In eukaryotic cells, most proteins are encoded in the nuclear genome and are synthesized on cytosolic ribosomes. Approximately half of these proteins require targeting to specific organelles to execute their function (1). Organellar proteins are recognized and targeted to their correct cellular destination by various targeting pathways (2–4). Defects in protein targeting can lead to diseases that can be caused either by loss of protein function at its destination organelle, mistargeting to another organelle, or by accumulation of proteins in the cytosol, where they can misfunction or aggregate (5, 6).

Most organelle proteins have a targeting signal that is recognized by one or more cytosolic targeting factors. The complex of cargo protein with its targeting factor is directionally recruited to the correct organelle by binding receptor proteins on the destination membrane (4, 7, 8). Many cargo proteins carry the same type of targeting signal. For example, tens of proteins carry a peroxisomal targeting signal type I (PTS1), and hundreds of proteins carry a signal peptide to travel to the endoplasmic reticulum or a mitochondrial targeting sequence to travel to the inner mitochondrial compartments. Often proteins with a similar targeting signal also utilize the same targeting pathway (3). As many proteins are targeted via the same pathway, and the abundance of the cargo factor may become limiting, it has been shown that certain cargo proteins have evolved to have stronger targeting signals than others (9). Moreover, it is clear that some cargo can utilize multiple pathways to ensure optimal targeting, whereas others are restricted to a single pathway (4, 10, 11). Despite these anecdotal demonstrations, it is not yet clear for

any pathway what all of the proteins that have evolved to be optimally targeted by it are, what the various mechanisms by which they do so are, and how this is rewired under the changing metabolic conditions of the cell.

To study targeting priority for entire pathways and in living cells, we developed a systematic tool that is based on high content imaging in the yeast *Saccharomyces cerevisiae* (hereafter called yeast). As a proof-of-concept, we used the well-described Pex5-mediated pathway that recognizes the PTS1 and targets most matrix (lumen) peroxisomal proteins (12–14). We expressed to very high levels a synthetic cargo protein with a PTS1 targeting signal and systematically examined how the competition over Pex5 affects the localization of each of the known peroxisomal proteins. We found that, as expected, the vast majority of PTS1-containing proteins were affected by the competition over Pex5. However, a few PTS1 proteins had targeting priority in a manner dependent on the carbon source consumed. By following up on priority cargoes, we suggest that they use various strategies to gain their priority, such as additional binding interface on Pex5 or targeting signals with strong affinity.

## Significance

**Half of eukaryotic proteins reside in organelles to which they are directed by dedicated targeting pathways, each recognizing unique targeting signals. Multiple proteins compete for any targeting pathway and might have different priority of reaching an organelle. However, the proteins with targeting priority, and the mechanisms underlying it, have not been explored. We developed a systematic tool to study targeting priority. We expressed a competitor protein and examined how it affects the localization of all other proteins targeted by the same pathway. We found several proteins with high targeting priority, dissected the mechanism of priority, and suggest that priority is governed by different parameters. This approach can be modified to study targeting priority in various organelles, cell types, and organisms.**

Author contributions: D.R., M.W., N.B., M.S., and E.Z. designed research; M.R., E.M.-R., J.B., E.Y., L.D., A.F., and Y.P. performed research; E.M.-R. analyzed data; and M.R., M.S., and E.Z. wrote the paper.

The authors declare no competing interest.

This article is a PNAS Direct Submission. W.A.P. is a guest editor invited by the Editorial Board.

This open access article is distributed under [Creative Commons Attribution-NonCommercial-NoDerivatives License 4.0 \(CC BY-NC-ND\)](https://creativecommons.org/licenses/by-nc-nd/4.0/).

<sup>1</sup>M.R. and E.M.-R. contributed equally to this work.

<sup>2</sup>To whom correspondence may be addressed. Email: maya.schuldiner@weizmann.ac.il or einat.zalckvar@weizmann.ac.il.

This article contains supporting information online at <https://www.pnas.org/lookup/suppl/doi:10.1073/pnas.1920078117/-DCSupplemental>.

First published August 17, 2020.



## Results

**Developing a Tool to Study Targeting Priority.** As a test case for our method of dissecting targeting priority of proteins to organelles, we used the Pex5-mediated targeting machinery of peroxisomal proteins in yeast. Pex5 mediates the targeting of most peroxisomal matrix proteins, mainly through binding to a PTS1 targeting signal (12, 14). This pathway is a good model as it is well characterized and has a well-known cargo repertoire. To induce conditions in which cargo proteins compete over a limited amount of Pex5, we expressed different levels of the mCherry protein tagged on its carboxy (C') terminus with a well-studied PTS1 targeting signal (15) composed of the last three amino acids serine-lysine-leucine (mCherry-SKL) that are considered as a canonical targeting signal. Our rationale was that when the mCherry-SKL is expressed in low amounts, it will not affect targeting of peroxisomal matrix proteins since it will be one of many other cargoes requiring this pathway. However, when mCherry-SKL is expressed in high levels, it will compete with other Pex5 cargo proteins. Hence, only proteins that have high targeting priority would still be localized to peroxisomes (Fig. 1A).

To express high levels of the mCherry-SKL protein, we integrated into the yeast genome multiple copies of the mCherry-SKL-encoding gene driven by a strong promoter (15). This has the advantage of reaching very high expression levels that are not reachable using increasing strengths of promoters alone (16). Yeast colonies that highly expressed the competitor protein became intensely red; therefore, we were able to select colonies based on the intensity of their color and establish a collection of strains, each expressing different levels of mCherry-SKL (Fig. 1B).

To ensure that we indeed created a competition situation, we verified that when mCherry-SKL is expressed in low amounts, it is localized predominantly to peroxisomes, while when it is expressed at high amounts it is also localized to the cytosol (Fig. 1C). While cytosolic accumulation could also result from a feedback loop causing decreased degradation, the most likely explanation for this is that under these conditions the Pex5-targeting machinery becomes saturated. Indeed, we found that Pex5 was not up-regulated in the presence of elevated amounts of the mCherry-SKL competitor (Fig. 1D), supporting the hypothesis that Pex5 amounts are limiting. Taking these data together, we established an *in vivo* system that can be applied to study targeting priority.

### Systematically Investigating Peroxisomal Proteins during Competition Uncovers a Subgroup of Cargo Proteins with High Targeting Priority.

We chose two strains that had either low or high levels of the competitor (mCherry-SKL) that we verified had a homogenous level of expression. Using an automated procedure we used these to create two collections of strains: One expressing low (no competition) and one expressing high (competition) levels of mCherry-SKL, and each expressing all known peroxisomal proteins tagged with GFP at their amino (N') terminus and expressed under a generic *NOP1* promoter (17–19) (Fig. 2A). The N' tagging ensured that the C' PTS1 sequences were not obstructed. The strains were imaged on a high-content screening platform (20) and the abundance and localization of each GFP-tagged protein was compared between the low- and high-competition conditions. While abundance was evaluated computationally, localization was manually annotated using a binary measure: Unaffected (no visible difference in the GFP signal between low or high levels of mCherry-SKL) or affected (less/weaker GFP puncta and a stronger cytosolic GFP signal in the presence of high mCherry-SKL) (Dataset S1). We first verified that while the expression of the mCherry-SKL was increased in the high mCherry-SKL strains, it did not affect the expression level of the GFP-tagged peroxisomal proteins (SI Appendix, Fig. S1, glucose). Focusing on localization, we found that peroxisomal membrane proteins and matrix proteins that contain a PTS2 signal (these rely on Pex7 for targeting)

(21) were not affected by the mCherry-SKL competitor (SI Appendix, Fig. S2). This gave us an indication that high levels of mCherry-SKL do not unspecifically alter peroxisomal physiology nor block the import machinery of matrix proteins. Unexpectedly, Pex18, a coreceptor of Pex7 (22), had reduced localization to peroxisomes when high levels of the competitor were expressed (Dataset S1). This hints that, in addition to the contribution of Pex18 to Pex7-mediated targeting, Pex18 may also have some interplay with the Pex5 targeting machinery in a way that should be further studied. Conversely, the localization to peroxisomes of the recently identified PTS1 targeting factor, Pex9 (9, 10), and one of its cargoes Gto1 (glutathione transferase omega-like 1 protein 1) was enhanced during competitive conditions rather than being reduced (Dataset S1), suggesting that it may function as a back-up pathway under these conditions.

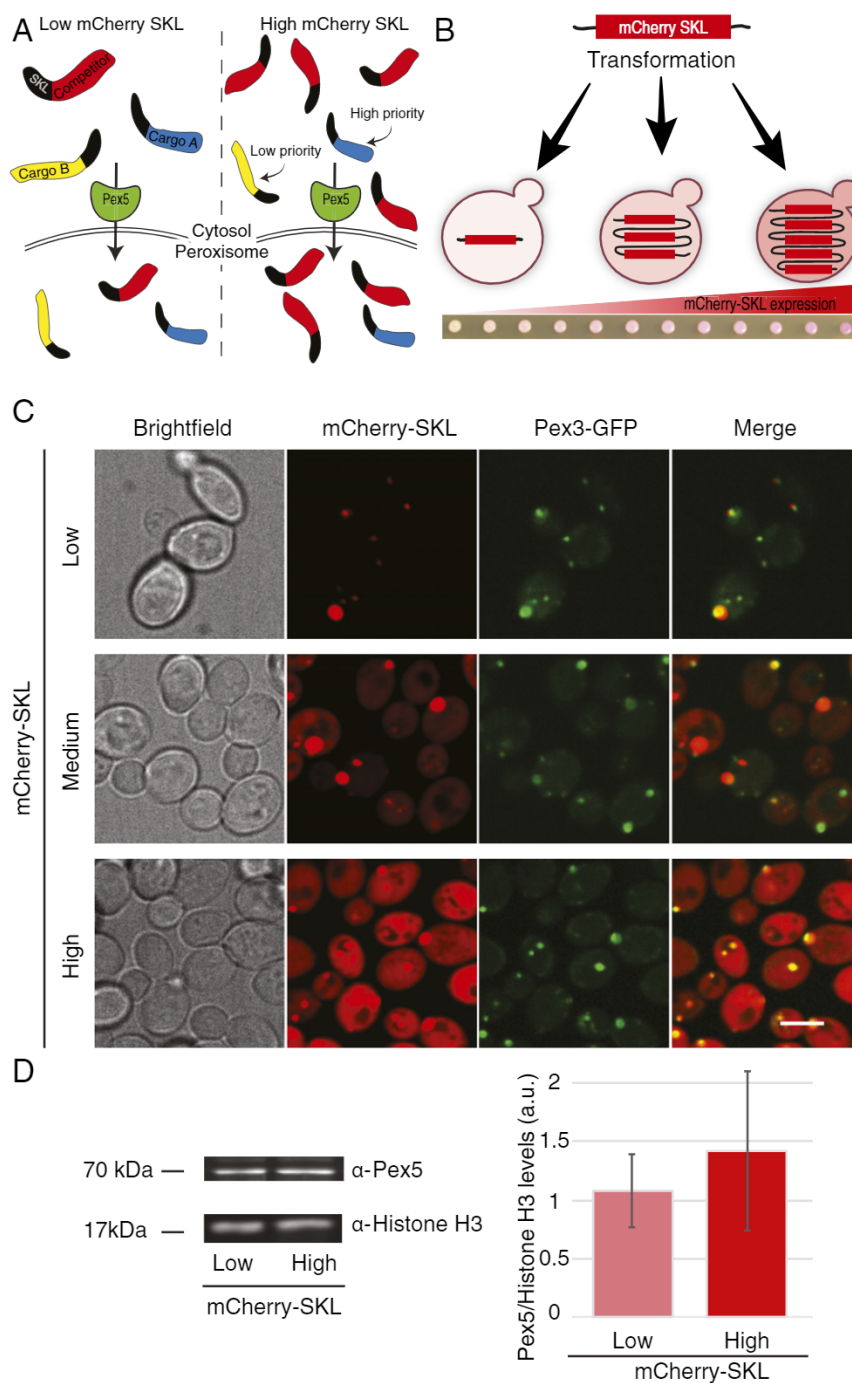
Focusing on the Pex5 cargo proteins [19 were correctly localized to peroxisomes in our collection (18, 23)], we observed that the localization of most (14 cargo proteins) was affected by the competition and that they accumulated in the cytosol (Dataset S1; examples shown in Fig. 2B). In support of the effect on Pex5 cargo being a direct result of saturating Pex5 amounts, we found that overexpressing Pex5 could rescue the targeting of such a PTS1 cargo, Pxp1 (SI Appendix, Fig. S3).

Interestingly, the localization of five Pex5 cargo proteins (carnitine acetyl-CoA transferase, Cat2; saccharopine dehydrogenase, Lys1; malate dehydrogenase 3, Mdh3; oxalyl-CoA synthetase, Pcs60; and fatty-acyl CoA oxidase, Pox1/Fox1) was not affected by the high levels of mCherry-SKL (Fig. 2C). Since targeting of these proteins seems completely unaffected by competition, we dub these proteins as having a high targeting priority. We verified the targeting priority observed by microscopy by performing subcellular fractionation experiments. Indeed, tracking two “low-priority” (Pxp1 and Tes1) and two “high-priority” (Lys1 and Pox1) proteins during low- and high-competition states uncovered that the low-priority proteins become mainly soluble (Fig. 2D and F), while the high priority ones remain in the organelle pellet (Fig. 2E and F). In summary, by systematically imaging all peroxisomal proteins in the presence of competition, we found that Pex5 cargoes have different targeting priorities.

### Targeting Priority to Peroxisomes Is Dependent on Metabolic Conditions.

To examine if targeting priority of Pex5 cargo proteins is affected by the metabolic state of the cells, we repeated the high-content screen using the fatty acid oleate as a carbon source instead of glucose (Fig. 2A and Dataset S1). In *S. cerevisiae* the peroxisome is the sole organelle in which  $\beta$ -oxidation of fatty acids occurs, and hence peroxisomes are essential when cells rely on oleate (24). We observed that all proteins that had high-targeting priority in glucose maintained it in oleate (SI Appendix, Fig. S4A). Interestingly, three Pex5 cargo proteins [Cta1, peroxisomal catalase A; Faa2, fatty acyl-CoA synthetase; and Fox2, 3-hydroxyacyl-CoA dehydrogenase and enoyl-CoA hydratase (25–27)], which did not have priority in glucose (Fig. 3A), gained priority in oleate (Fig. 3B). As we saw in glucose, the localization of Pex9 and one of its cargo proteins Mls2 (malate synthase 2) was enhanced in oleate during competitive conditions (Dataset S1), suggesting that Pex9 may function as a back-up pathway under these conditions as well.

Since all GFP-tagged proteins were expressed under a generic promoter, this reduced the possibility that oleate-specific targeting priority is determined by an increased level of transcription in our experimental setting. However, to verify this, we compared protein intensity of all peroxisomal proteins between the two conditions (using GFP levels as a proxy) (SI Appendix, Fig. S4B) and by specifically measuring protein levels of cargo proteins that had priority in oleate but not in glucose (SI Appendix, Fig. S4C). We found that, indeed, the protein levels were not elevated, ruling out elevation by posttranscriptional or translational regulation. Since mCherry levels were more variable in oleate than in glucose (SI Appendix, Fig. S1),

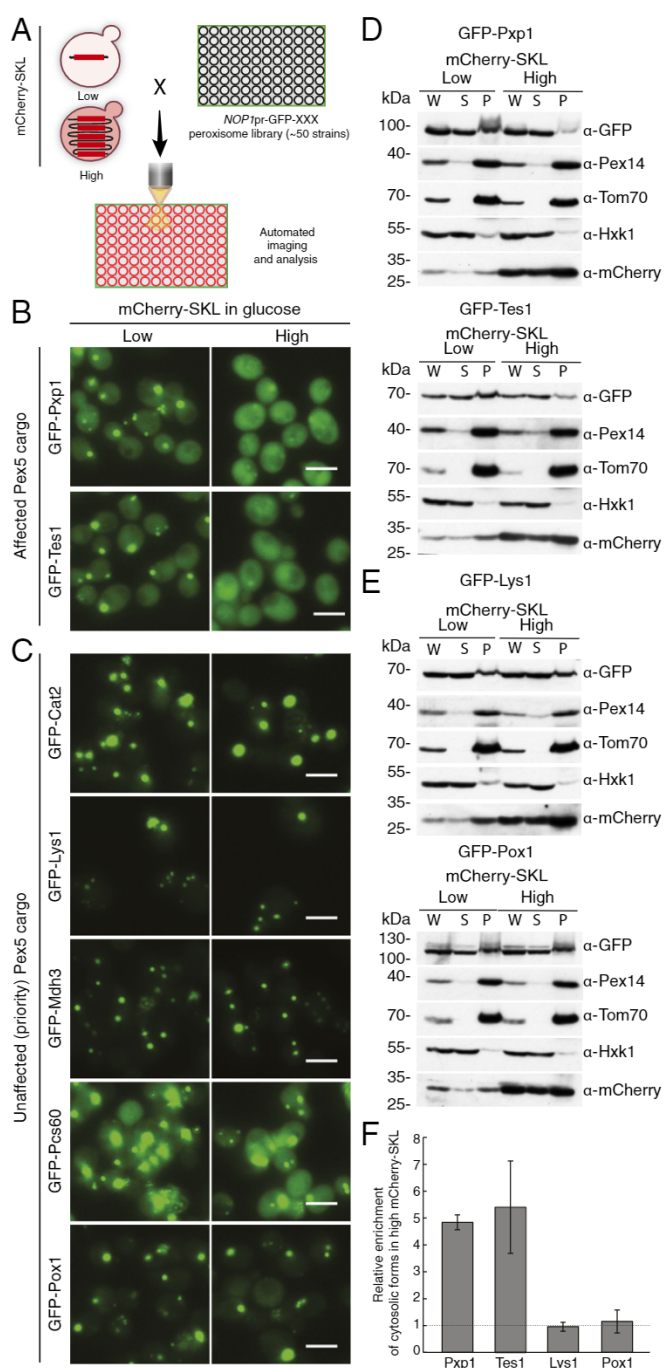


**Fig. 1.** An in vivo tool to systematically study protein targeting priority. (A) Schematic representation of targeting competition created by the increasing levels of mCherry-SKL, indicated as “competitor” (red). (Left) When low levels of mCherry-SKL are expressed, peroxisomal matrix proteins are imported into the organelle. (Right) High levels of mCherry-SKL saturate the import machinery and create a competition for the limiting Pex5 targeting factor. Hence, proteins with low targeting priority (“cargo B,” yellow) will not be targeted to peroxisomes while proteins with high priority (“cargo A,” blue) will retain their capacity to target efficiently. (B) Schematic representation of a methodology to create targeting competition. An inert, peroxisome-destined, substrate with a peroxisomal targeting signal (mCherry-SKL) is integrated into the yeast genome in multiple copies, creating strains with increasing levels of mCherry-SKL. The increased mCherry expression is detected by the color of the colony and later verified by flow cytometry. (C) mCherry-SKL is localized to peroxisomes (colocalization with the peroxisomal membrane protein Pex3-GFP in diploid cells). When mCherry-SKL was expressed in high levels the mCherry signal was also detected in the cytosol implying that the targeting machinery is saturated. (Scale bar, 5  $\mu$ m.) (D) Measurement of Pex5 levels in low and high mCherry-SKL strains grown in glucose. (Left) Western blot analysis with anti-Pex5 antibody. (Right) Quantification of Pex5 levels in the two different mCherry-expressing strains. Protein levels were normalized to the loading control, Histone H3. Values represent the mean  $\pm$  SD of two biological repeats and four technical repeats.

we ensured that our results were not simply due to lower levels of competition by checking that the mCherry levels in the strains that had oleate-specific priority are not the lowest in the distribution. Ruling out these potential sources of false positives, we suggest that

targeting priority can be modulated depending on the metabolic requirements of the cell. This could occur through posttranslational modifications of the targeting factor Pex5 or of the specific cargo, such that binding to certain cargo is enhanced.





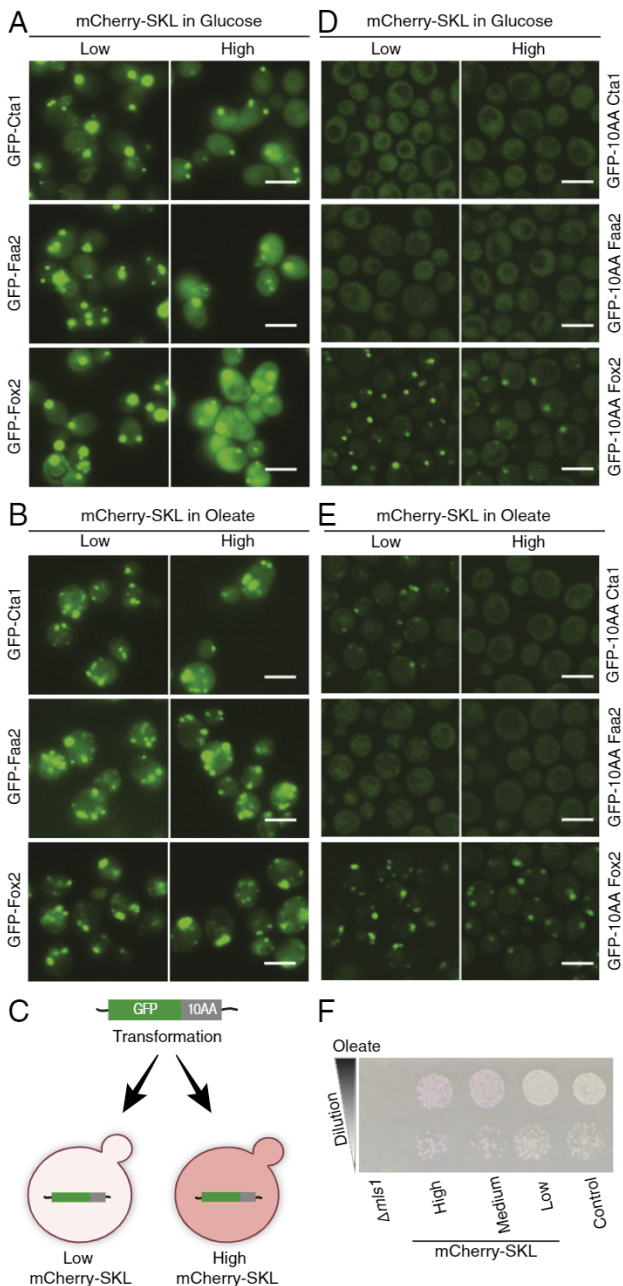
**Fig. 2.** A high-content screen reveals a subgroup of Pex5 cargo proteins that have targeting priority. (A) A schematic representation of the high-content microscopy screen. Yeast strains with low or high levels of mCherry-SKL were mated with a collection of strains each expressing one peroxisomal protein tagged with GFP at the N' terminus under the regulation of a constitutive *NOP1* promoter. The mating was followed by sporulation and selection for haploids containing both the mCherry-SKL protein and a GFP-peroxisomal protein. Cells were imaged using a fluorescent microscope in glucose-containing media and the localization of each GFP peroxisomal protein was annotated in the presence of low or high mCherry levels. (B) Representative images of two Pex5 cargo proteins on the background of either low or high levels of mCherry-SKL. The GFP-tagged proteins were mainly localized to peroxisomes when low levels of mCherry-SKL were expressed but were mostly observed in the cytosol when high levels of mCherry-SKL were expressed. We dub such substrates as having low targeting priority. (Scale bars, 5  $\mu$ m.) (C) Representative images of five Pex5 cargo proteins whose cellular localization was not affected by the mCherry-

To examine if the PTS1 is sufficient to enable oleate-specific targeting priority, we fused the last 10 aa of Cta1, Faa2, or Fox2 to the C' of GFP and integrated the different GFP fusions into the yeast genome of strains expressing low or high levels of mCherry-SKL (Fig. 3C). We then grew the cells in glucose or in oleate and examined if the last 10 aa were sufficient to bestow targeting priority to the GFP fusions in glucose or in oleate. The GFPs with the last 10 aa of Cta1 or Faa2 did not have high targeting priority, neither in glucose nor in oleate (Fig. 3D and E), suggesting that for these proteins the oleate-specific targeting priority information was encoded elsewhere. In contrast, the GFP last 10 aa of Fox2 behaved exactly like full-length Fox2; it was affected by the competition in glucose (Fig. 3D) but was not affected by the competitor when grown in oleate (Fig. 3E). This demonstrates that in the case of Fox2, the last 10 aa are sufficient to enable oleate-specific targeting priority. While it is not clear how the same 10 aa provide condition-specific priority, we hypothesize that they may become posttranslationally modified in oleate. In support of this, while protein levels were not altered for GFP-Fox2, we detected a difference in the pattern in which GFP-Fox2 (full protein) ran in an SDS gel in oleate compared to glucose (*SI Appendix, Fig. S4C*).

A central function of peroxisomes is the breakdown of fatty acids by  $\beta$ -oxidation. We noticed that the proteins that gained priority in oleate are enzymes involved in  $\beta$ -oxidation and in removal of  $H_2O_2$ , a product of  $\beta$ -oxidation. This suggests that part of the reason to employ targeting priority is to ensure that sufficient amounts of the peroxisomal proteins required for growth in oleate are localized to peroxisomes, even under suboptimal growth conditions (simulated in our experiment by high mCherry-SKL levels). Indeed, the cells expressing high levels of mCherry-SKL did not have a severe growth defect when grown on oleate, despite the fact that many peroxisomal proteins were not targeted correctly (Fig. 3F). These results indicate that protein targeting to peroxisomes can be adjusted upon environmental changes and cellular requirements.

**Strong Binding Affinity of the PTS1 to Pex5 Provides One Way of Obtaining Targeting Priority.** We decided to focus on the five Pex5 cargo proteins (Cat2, Lys1, Mdh3, Pcs60, and Pox1) that had targeting priority in both glucose and oleate to identify the molecular mechanisms by which their targeting priority is gained. It was previously shown that Pox1 does not contain a PTS1 signal and that it binds to Pex5 by a unique mechanism (28). Hence, we suggest that the way by which Pox1 gains priority is by avoiding competition on the same binding site. It is not yet clear if Pex5 can bind two cargo proteins simultaneously (a PTS1 and a non-PTS1

SKL protein expressed at very high levels. These proteins seem to have high targeting priority compared to mCherry-SKL. (Scale bars, 5  $\mu$ m.) (D) Subcellular fractionation of cells expressing the indicated peroxisomal protein fused to GFP in the presence of low or high levels of mCherry-SKL. Fractions corresponding to whole-cell lysate (W), supernatant (S) that represents the cytosol, and pellet (P) that contains most organelles including peroxisomes, were obtained by differential centrifugation. The fractions were analyzed by SDS/PAGE and Western blot with antibodies against GFP, the peroxisomal protein Pex14, the mitochondrial protein Tom70, the cytosolic protein Hexokinase1 (Hxk1), and mCherry. Representative blots of GFP-Pxp1 and GFP-Tes1 indicate that the organellar localization of Pxp1 and Tes1 is reduced in the presence of high levels of mCherry-SKL. (E) Representative blots showing that the localization of Lys1 and Pox1 is not altered when high levels of mCherry-SKL are expressed. (F) The intensities of bands representing the GFP-tagged Pxp1, Tes1, Lys1, and Pox1, were quantified from three independent experiments and adjusted to the intensity of the Ponceau staining in the corresponding lane. The supernatant/pellet ratio was calculated for each GFP-tagged protein. To examine if there is a difference in the supernatant/pellet ratio when different amounts of mCherry-SKL were expressed, we divided the ratio obtained in the presence of high mCherry-SKL by the ratio obtained in the presence of low mCherry-SKL. The graph represents the average of three independent experiments  $\pm$ SD.



**Fig. 3.** Targeting priority to peroxisomes is dependent on the metabolic conditions. (A) The localization of GFP-Cta1 (peroxisome catalase), GFP-Faa2 (fatty acyl-CoA synthetase), and GFP-Fox2 (fatty acid oxidase) all under regulation of the *NOP1* promoter, was affected by the high mCherry-SKL levels when cells were grown in glucose. (B) The localization was not affected in oleate making Cta1, Faa2, and Fox2 condition-specific priority cargo. (C) Schematic showing how GFP was fused at its C' to the last 10 aa (10AA) of different cargo proteins and expressed from a genomic copy in the presence of low or high levels of mCherry-SKL, allowing examination of whether targeting priority is encoded in the PTS1 of proteins. (D) GFP was fused at its C' to the last 10 aa of Cta1, Faa2, or Fox2. The GFP fusions had low targeting priority in glucose. (E) GFP fused to the last 10 aa of Fox2 had a targeting priority in oleate, suggesting that in the case of Fox2 the oleate-specific targeting priority is embedded in the last 10 aa. (Scale bars in A, B, D, and E, 5  $\mu$ m.) (F) Dilution assay of strains expressing three levels of mCherry-SKL on oleate. No significant growth defect was observed in the presence of high levels of mCherry-SKL. A strain lacking *MIs1* (malate synthetase 1), which is essential for growth on oleate, was used as a control for the oleate media, and a control yMS721, strain was used for growth baseline.

cargo, for example) or simply that the alternate binding interface provides stronger affinity.

We further focused on the remaining four PTS1 proteins (Cat2, Lys1, Mdh3, and Pcs60) and examined if their priority is determined by their PTS1 signal. To test this, we fused the last 10 aa of these four PTS1 proteins as well as low-priority controls, to the C' of GFP and integrated the different GFP fusions into the yeast genome of strains expressing low or high levels of mCherry-SKL (Fig. 3C). For two of the proteins, Mdh3 and Pcs60, targeting priority information was not encoded in the PTS1 since GFP fused to their last 10 aa could not provide priority in the face of high competition (Fig. 4A). When GFP was fused to the last 10 aa of Cat2 or Lys1, it was targeted efficiently even when high levels of mCherry-SKL were expressed (Fig. 4B); hence, for these two proteins targeting priority is encoded in the last 10 aa.

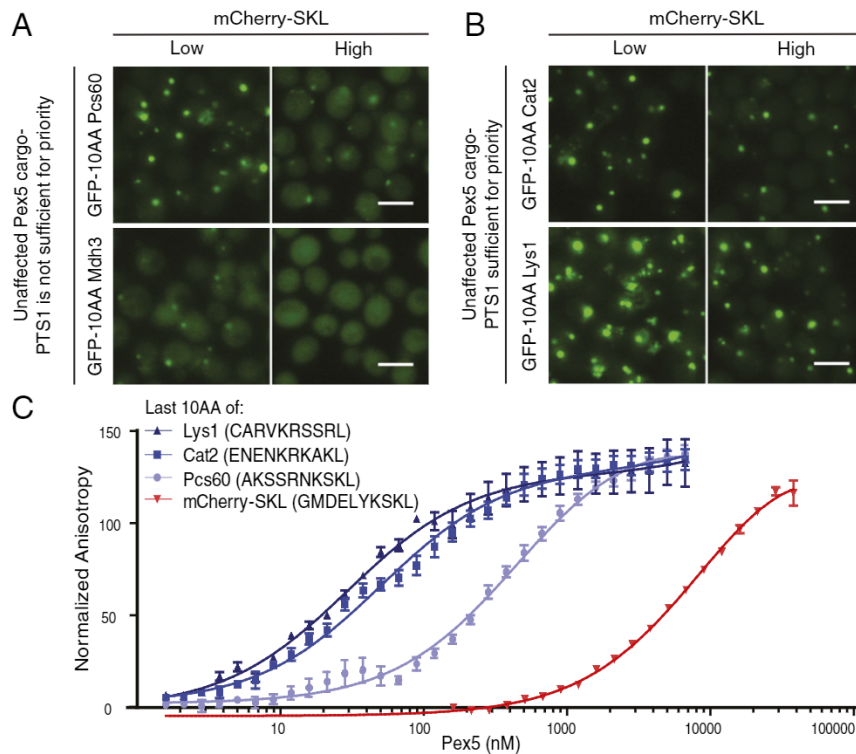
To verify that the PTS1 of Cat2 and Lys1 indeed confers priority through higher association with Pex5, we directly measured binding affinity to Pex5 by fluorescence anisotropy (29). In vitro binding of the full-length yeast Pex5 to fluorescent peptides containing the last 10 aa of Cat2, Lys1, and Pcs60, as well as to mCherry-SKL, showed that the binding affinity of Pex5 to the last 10 aa of Cat2 and Lys1 is  $\sim$ 10-fold higher than the binding of Pex5 to the last 10 aa of Pcs60. This strongly supports the theory that high-affinity interaction with Pex5 is sufficient to confer priority and that both Cat2 and Lys1 employ this strategy to secure targeting (Fig. 4C). Surprisingly, both the mCherry competitor and Pcs60 end with SKL, which is considered to be the strongest PTS1 signal, but still they have a different binding affinity to Pex5. This supports the notion that the PTS1 strength is not simply determined by the last 3 aa but rather by a wider context (13, 30).

#### Targeting Priority Is Governed by Various Molecular Mechanisms.

While high affinity explains the priority targeting of Cat2 and Lys1, and we hypothesize that binding to an alternate interface of Pex5 explains the targeting priority of Pox1, the priority mechanism for Pcs60 and Mdh3 remained unclear. The ability of a cargo protein to bind to its targeting factor is a combination of both affinity and abundance; therefore, we hypothesized that another possibility to gain targeting priority is simply by having very high protein amounts. Hence, we examined the protein abundance, previously measured by mass spectrometry (MS) (31) of all native PTS1 proteins and plotted them against the GFP intensity measured in our strains. While Pcs60, Lys1, and Mdh3 are indeed very highly expressed, in both the MS data and the GFP intensity data (such as Aat2), did not have a targeting priority in our assay (Fig. 5). Hence, high concentrations may support targeting for Pcs60 and Mdh3, but this precludes the option that high concentrations of the protein in the cytosol are enough to confer targeting priority. Additionally, it was previously suggested that Cat2, Pcs60, and Mdh3 bind to Pex5 not only through the PTS1 motif but also through other motifs (25, 32, 33). Having multiple binding sites of a single protein to the targeting factor might therefore also increase binding affinity and determine targeting priority. One additional option for obtaining priority lies in the unique feature of the peroxisomal translocon that allows translocation of entire complexes (34). For example, malate dehydrogenases form homo-complexes (35) that may be imported in an assembled state forming a complex that contains several targeting signals, creating avidity.

In summary, herein we established a tool to systematically study targeting priority of proteins to organelles. To test our setup, we chose to use the well-characterized Pex5-mediated targeting of peroxisomal proteins. Using systematic imaging, we identified a subgroup of Pex5 cargo proteins that has targeting priority in both glucose and oleate and others that are oleate-specific. The discovery that targeting priority is dependent on the metabolic state of the cell suggests that priority could be regulated by posttranslational modifications (36).



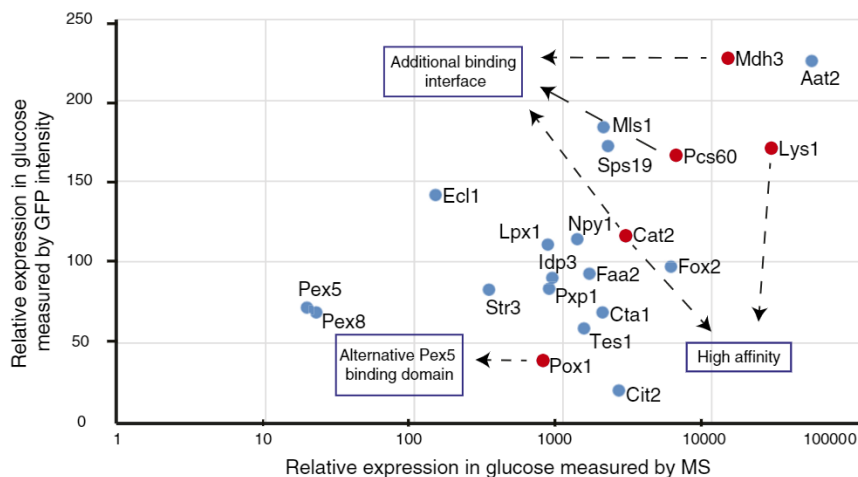


**Fig. 4.** Strong binding affinity of the PTS1 to Pex5 provides one way of obtaining targeting priority. (A) GFP was fused to the last 10 aa of the priority targets Mdh3 or Pcs60 and localization was measured under low or high competition in glucose. Priority was not encoded in the PTS1 context of these two proteins. (Scale bars, 5  $\mu$ m.) (B) GFP was fused to the last 10 aa of the priority targets Cat2 or Lys1 and localization was measured under low or high competition in glucose. For these two constructs, the last 10 aa were enough to endow priority supporting the notion that the information that governs priority is embedded in the last 10 aa of these cargo proteins. (Scale bars, 5  $\mu$ m.) (C) Binding affinity of various PTS1 peptides was quantified using fluorescence anisotropy. Both Cat2 and Lys1 have strong binding affinities for Pex5, which explain their targeting priority. Interestingly, Pcs60 PTS1 is a weaker binder to Pex5, which correlates with its inability to confer priority when coupled to GFP. The last 10 aa of the mCherry-SKL competitor has a lower affinity, despite ending with an SKL. Calculated  $K_d$ s from the anisotropy experiment are: Lys1 peptide  $29.3 \pm 3.65$  nM, Cat2 peptide  $49.94 \pm 4.1$  nM, Pcs60 peptide  $454.7 \pm 43.81$  nM, mCherry-SKL peptide  $9,844 \pm 1,177$  nM.

We suggest that targeting priority can be obtained by different mechanisms, including harboring nonstandard targeting signals, encoding a strong binding affinity to the targeting factor, or maintaining multiple binding sites.

The tool that we developed here enabled us to supply a holistic overview on targeting priority to organelles and demonstrate

some of the parameters that can govern targeting priority, as well as their physiological significance. The competition tool that we developed can be easily modified to unravel targeting priority to other organelles and is not limited to yeast. Understanding the rules that govern targeting of proteins to different cellular compartments will not only shed light on how the basic unit of



**Fig. 5.** Different parameters govern targeting priority. Relative expression of native Pex5 and its cargo proteins measured by MS in cells grown in glucose (taken from ref. 36) plotted versus the GFP intensity measured in the *NOP1 N'* tagged strains, which correlates to the protein levels. Cargo proteins with high targeting priority are marked in red. The graph implies that targeting priority is guided by different parameters and is not simply governed by protein abundance.

life—a cell—functions, but also has great potential for therapeutic and biotechnological uses.

## Materials and Methods

**Yeast Media.** SD media used in this study contains 6.7 g/L yeast nitrogen base and 2% glucose, with complete amino acid mix, unless written otherwise; 1 g/L of monosodium glutamic acid replaces ammonium sulfate in the SD if antibiotics are used. When mentioned, 300 mg/L Hygromycin B (CAS#: 31282-04-9, Roche) was used. S oleate media was made with synthetic media, 0.2% oleate (Sigma) +0.1% Tween 80 and a complete amino acids mix.

**Yeast Strains, Plasmids, and Primers.** *S. cerevisiae* strains used in this study are described in [Dataset S2](#), excluding strains that were included in the yeast libraries and were frozen as a library and not as single strains. Strains yMS5243 to yMS5252 are shown in Fig. 3 *D* and *E* and the strains yMS4346, yMS4347, yMS4350, yMS4351, yMS4353, yMS4355, yMS4356, yMS4357, yMS4359, and yMS4360 are shown in Fig. 4.

Primers are described in [Dataset S3](#) and plasmids are described in [Dataset S4](#).

Cells were genetically manipulated using a transformation method that includes the usage of lithium-acetate, polyethylene glycol, and single-stranded DNA (37). Primers for manipulations and validation were designed using Primers4-Yeast (38).

Plasmid pMS934 (p69\_TDH3) (39) was modified using a restriction-free method (40) with the primers described in [Dataset S3](#) creating plasmid pMS816 (mCherry-SKL).

The pYM-based pMS555 plasmid that was originally used for N-terminal GFP tagging (17) was modified to contain the last 10 aa of Cat2, Cta1, Faa2, Fox2, Lys1, Mdh3, and Pcs60 at the C' of the GFP sequence. Using these plasmids, GFP-PTS1 was genomically integrated into the HO locus in strains expressing low and high levels of mCherry-SKL (Figs. 3 *D* and *E* and 4 *A* and *B*).

The mCherry-SKL strains were based on the yMS721 (41). pMS816 plasmid was integrated into the yeast genome after linearization by a unique Mun1 restriction enzyme (ThermoFisher Scientific) in the TDH3 promoter (39). After Hygromycin B (300 mg/L) antibiotics selection, single colonies were hand-picked to create several hundred candidates. The candidates grew overnight in synthetic media [SD<sub>(MSG)</sub>] with Hygromycin B selection, and then their mCherry fluorescence levels were measured by flow cytometry to determine the expression level of the mCherry-SKL protein.

Flow cytometer measurements and analysis were done using an LSRII system (BD Biosciences). Flow cytometry was conducted with excitation at 488 nm and emission at 525 ± 25 nm for GFP samples. For mCherry, excitation was conducted at 594 nm and emission at 610 ± 10 nm. The average number of cells analyzed was 30,000.

**Yeast Library Preparation.** To create collections of haploid strains containing both the mCherry-SKL and the peroxisomal proteins tagged with a GFP, automated mating, sporulation, and haploid selection steps were taken (42). Strains expressing low or high levels of mCherry-SKL were crossed with a collection of ~90 strains of controls and known peroxisomal proteins tagged with GFP at their N' terminus and expressed under the constitutive *NOP1* promoter (17–19). A RoToR bench-top colony arrayer (Singer Instruments) was used to handle libraries (42, 43). In brief, mating was performed on rich medium plates. Diploid cell selection was performed on SD<sub>(MSG)</sub>-URA-Hygromycin B. The cells were then transferred for 7 d to nitrogen starvation plates to induce sporulation. Selection of haploid cells with the desired mutations was performed by transferring cells to SD<sub>(MSG)</sub>-URA-LYS-ARG+Hygromycin B plates. Spores with  $\alpha$ -mating type were selected in the absence of leucine. To select against remaining diploid cells the plates contained the toxic amino acid derivatives Canavanine and Thialysine (Sigma-Aldrich).

**Yeast Culturing for High-Content Screening.** To visualize the strains containing low/high levels of mCherry-SKL and a GFP-tagged peroxisomal protein, we used an automated microscopy set-up. In short, for growth in liquid media we used a RoToR arrayer to transfer the cells from agar plates into 384-well polystyrene plates (Greiner Bio-One). We then grew the liquid cultures overnight at 30 °C in SD<sub>(MSG)</sub>-URA+Hygromycin B media in a LiCONiC incubator. We used a JANUS liquid handler (PerkinElmer) connected to the incubator to dilute the strains to an OD<sub>600</sub> of ~0.2 into plates containing SD medium. Plates were incubated at 30 °C for 4 h in SD medium. For the screen performed in oleate, cells were transferred with OD<sub>600</sub> of ~0.2 into plates containing S oleate medium. Plates were incubated at 30 °C for 20 h. The cultures were then transferred by the liquid handler into glass-bottom 384-well microscope plates (Matrical Bioscience) coated with Con A (Sigma-Aldrich). After 20 min,

wells were washed four times and then left with SD-Riboflavin complete medium in case of the glucose screen or DDW in case of oleate screen, to obtain a cell monolayer and remove nonadherent cells. We then transferred the plates to a ScanR automated inverted fluorescence microscope system (Olympus) using a robotic swap arm (Hamilton). Images were recorded using a 60× air lens (NA 0.9) and with an ORCA-ER charge-coupled device camera (Hamamatsu) at room temperature. We acquired the images in a GFP channel (excitation filter 490/20 nm, emission filter 535/50 nm) and an mCherry channel (excitation filter 572/35 nm, emission filter 632/60 nm). We manually reviewed the images using the ImageJ analysis program (<https://imagej.net/Downloads>).

**Manual Microscopy.** Manual microscopy was performed (Figs. 1 *C*, 3 *D* and *E*, and 4 *A* and *B*) using the VisiScope Confocal Cell Explorer system. The system is composed of a Yokogawa spinning disk scanning unit (CSU-W1) coupled with an inverted Olympus IX83 microscope. We acquired the images using a 60× oil lens and a connected PCO-Edge sCMOS camera, controlled by VisView software, with a wavelength of 561 nm (mCherry) and 488 nm (GFP). For slight linear adjustments to brightness and contrast, we transferred the images to ImageJ. For image visualization of the yeast cells we used the brightfield channel to segment the cells. All images taken are of haploid cells, except Fig. 1 *C*, which shows images of diploids.

**Protein Extraction and Western Blot Analysis.** Proteins from cells expressing low or high levels of mCherry-SKL were extracted by Urea protein extraction. In short, 10 mL of 0.5 OD<sub>600</sub> yeast cells were harvested by centrifugation. Next, 200  $\mu$ L of lysis buffer containing 8 M Urea, 50 mM Tris, protease inhibitor (Merck) pH = 7 were added to the pellet and the cell wall was broken down by vortexing at high speed with ready-to-use glass beads (Scientific Industries) at 4 °C for 10 min; 25  $\mu$ L of 20% SDS were added and the extracts were incubated at 95 °C for 5 min. Protein extracts were transferred into new tubes and stored at –20 °C. Samples in Fig. 1 *D* were analyzed by SDS/PAGE and Western blotting using an anti-Pex5 antibody 1:10,000 (44) (kindly provided by Ralf Erdmann, Ruhr-Universität Bochum, Bochum, Germany), and anti-Histone H3 (Abcam, # ab1791; 1:10,000) was used as the loading control. The anti-Histone H3 antibody was diluted in a mix of 3% BSA, 0.01% sodium azide and Phenol red in PBS (Biological Industries) solution. IRDye 680LT goat anti-rabbit IgG secondary antibody (LI-COR Biosciences) was used at 1:10,000 dilution, followed by scanning using the Odyssey Imaging System (LI-COR Biosciences).

**Subcellular Fractionation.** Cells were grown in 100 mL of synthetic medium containing 2% glucose (SD) for 5 to 6 h until OD<sub>600</sub> of 1 to 2. Cells were then harvested by centrifugation (4,000 × g, 5 min, room temperature) and the pellet was resuspended with 25 mL water. Next, cells were pelleted again as above and kept at –20 °C till further processing.

For subcellular fractionation, the cells pellet was thawed on ice, washed with 1 mL water, centrifuged as above, and the pellet was weighed. Then, cells were resuspended in 400  $\mu$ L of resuspension buffer (100 mM Tris, 10 mM DTT, pH 7.2) per 0.2-g pellet and incubated for 10 min at 30 °C while shaking at 450 rpm. Cells were harvested as above and resuspended in 1 mL spheroblast buffer (1.2 M sorbitol, 20 mM KPI, pH 7.2) followed by pelleting of the cells as above. The pellet was resuspended with 1 mL spheroblast buffer supplemented with Zymolyase (6-mg/g pellet) and incubated for 1 h at 30 °C while shaking at 450 rpm. The efficiency of spheroblast was tested by measuring the OD<sub>600</sub> of spheroblasts diluted 1:100 in either water or 1.2 M sorbitol and, from this step on, cells were kept at 4 °C.

After spheroblast was completed, cells were harvested (3,000 × g, 5 min, 4 °C). The pellet was resuspended with 3 mL homogenization buffer (0.6 M sorbitol, 10 mM Tris, 1 mM EDTA, 2 mM Phenylmethanesulfonyl fluoride [PMSF], pH 7.2), and cell lysate was obtained by douncing 20 times in an ice bath. Protein concentration was determined by Bradford assay and proteins from 200  $\mu$ L of the lysate suspension were taken as whole-cell lysate fraction and proteins were precipitated by methanol-chloroform (see below). The rest of the lysate was centrifuged (600 × g 5 min, 4 °C) to remove unruptured cells and cell debris and the supernatant was centrifuged at high speed (25,000 × g, 10 min, 4 °C). Then, 200  $\mu$ L of the supernatant were taken as the cytosolic fraction and proteins were precipitated using methanol-chloroform. The pellet was washed with SEM buffer (250 mM sucrose, 80 mM KCl, 10 mM Mops, 2 mM PMSF, 1 mM EDTA, pH 7.2) and harvested again (25,000 × g, 10 min, 4 °C) to obtain the peroxisomes and mitochondria fraction. All fractions were dissolved in Laemmli buffer at a concentration of 2 mg/mL and heated for 10 min at 95 °C before analysis by SDS/PAGE and Western blotting using an anti-GFP antibody 1:2,000 (Torrey Pines), anti-Tom70 1:4,000 (Pineda, custom-made), anti-Pex14 1:2,500 (kindly provided by Ralf Erdmann), anti-Hxk1 1:4,000 (Biotrend), and anti-mCherry 1:10,000



(Abcam). Horseradish peroxidase-conjugates were used as secondary antibodies. Band intensities were quantified with AIDA software (Raytest).

**Chloroform/Methanol Protein Precipitation.** Chloroform/methanol precipitation was performed as follows: 4 vol of methanol were added to 200  $\mu$ L aqueous sample and the mixture was vortexed for 5 s. Then, 1 vol of chloroform was added to the sample, vortexed for 5 s, and 3 vol of water were added to the sample and vortexed 20 s. The mixture was centrifuged (16,000  $\times$  g, 1 min, room temperature), the upper layer was removed, and 3 vol of methanol were added and vortexed thoroughly for 20 s. The mixture was centrifuged again (16,000  $\times$  g, 1 min, room temperature), the supernatant was discarded, and the pellet containing the proteins was dried at 40 °C before analysis.

**Serial Dilutions on Oleate.** Serial 10-fold dilutions were created by growing cells overnight in 0.2% glucose and back dilution of  $\sim$ 6 h to start with OD<sub>600</sub> = 0.1 of all strains of interest in liquid media, and diluting them in 10-fold increments. Next, 2.5  $\mu$ L of each dilution were plated using Finn-pipette F1 Multichannel Pipettes (ThermoFisher Scientific) on oleate agar plates and imaged using Canon PC1591 digital camera after 2 to 8 d (as indicated) of growth at 30 °C.

**Protein Purification.** Full-length *S. cerevisiae* Pex5 was cloned in a petM30 vector. Pex5 was expressed in autoinduction medium (45) with 5 h at 37 °C and 26 h at 20 °C. Cells were harvested, resuspended in lysis buffer (50 mM Hepes pH 7.5, 150 mM NaCl, 20 mM imidazole, protease inhibitor [Roche], DNase [Sigma], and lysozyme [Sigma]), homogenized 1 h at 4 °C, and lysed by sonication. Lysate was then cleared by centrifugation and the supernatant loaded onto Ni-NTA resin (Qiagen). Bound protein was washed with buffer (50 mM Hepes pH 7.5, 750 mM NaCl, 20 mM imidazole) and the protein eluted with low salt buffer (50 mM Hepes pH 7.5, 150 mM NaCl, 250 mM imidazole). The eluate was then dialyzed against Hepes pH 7.5, 150 mM NaCl, 0.5 mM TCEP and simultaneously digested with 1 mg of tobacco etch virus (TEV)-protease. Undigested protein and TEV protease were removed by a second Ni-NTA step and flow-through containing Pex5 were concentrated for gel filtration (Hiload 16/60 Superdex 200 pg, GE Healthcare). Relevant fractions were pooled together and the protein was concentrated, flash-frozen in liquid nitrogen, and stored at  $-80$  °C.

**Fluorescence Anisotropy.** FITC-labeled peptides corresponding to the carboxyl-terminal (9 or 10) amino acids of Lys1, Cat2, Pcs60, and mCherry-SKL (Lys1: FITC-YARVKRSSRL, Cat2: FITC-YNENKRRKAKL, Pcs60: FITC-YKSSRNKSKL, mCherry-SKL: FITC-GMDELYKSKL; Genscript) were solubilized in water and used in the assay at a final concentration of 10 nM. A tyrosine was added at the N terminal of some peptides for concentration determination; in these cases only the last 9 aa of the PTS1 protein were used. Measurements of fluorescence anisotropy changes were performed in black 96-well plates (Greiner) with an Infinite M1000 plate reader (Tecan) with excitation/detection at 470/530 nm. The experiment was performed in 50 mM Hepes pH 7.5, 150 mM NaCl. A concentration range of 6.6  $\mu$ M to 1.5 nM (for Lys1, Cat2, and Pcs60) or 38  $\mu$ M to 160 nM for mCherry-SKL was obtained by serial dilution and each concentration measured in triplicate. Three independent experiments were performed and binding data were normalized and analyzed using Prism (GraphPad software). Kinetic information was obtained by least-square fitting of a Binding-Saturation model with one binding site.

**Data Availability.** All study data are included in the main text and *SI Appendix*.

**ACKNOWLEDGMENTS.** We thank Ralf Erdmann for kindly sharing the anti-Pex5 and anti-Pex14 antibodies; Bettina Warscheid, Silke Oeljeklaus, Miriam Eisenstein, Noa Dahan, and Yuri Bykov for critical reading of the manuscript and for helpful suggestions; and Bettina Warscheid and Silke Oeljeklaus for sharing the data shown in Fig. 5 and for kindly sharing plasmid pMS742. The work in the M.S. laboratory is supported by the European Research Council Consolidator Grant Peroxisystem 64660, a European Union International Training Network grant (PERICO 812968), and by the Minerva Foundation with funding from the Federal German Ministry for Education and Research (712935). The robotic set-up in the M.S. laboratory was purchased through kind support of the Blythe Brenden-Mann Foundation. The joint work of the M.S. and D.R. laboratories was supported by a collaborative grant from the German Israeli Foundation (GIF I-1458-412.13/2018). M.S. is an incumbent of the Dr. Gilbert Omenn and Martha Darling Professorial Chair in Molecular Genetics. J.B. is supported by the El3POD programme. E.Y. is supported by the Ariane de Rothschild women doctoral program. The work in the M.W. laboratory is supported by the Deutsche Forschungsgemeinschaft (WI 1058/9-2) via the Pertrans network.

- W.-K. Huh *et al.*, Global analysis of protein localization in budding yeast. *Nature* **425**, 686–691 (2003).
- G. Blobel, D. D. Sabatini, "Ribosome-membrane interaction in eukaryotic cells" in *Biomembranes*, L. A. Manson, Ed. (Springer US, 1971), pp. 193–195.
- M. Kunze, J. Berger, The similarity between N-terminal targeting signals for protein import into different organelles and its evolutionary relevance. *Front. Physiol.* **6**, 259 (2015).
- N. Aviram, M. Schuldiner, Targeting and translocation of proteins to the endoplasmic reticulum at a glance. *J. Cell Sci.* **130**, 4079–4085 (2017).
- M. L. Slawicki *et al.*, Identification of three distinct peroxisomal protein import defects in patients with peroxisome biogenesis disorders. *J. Cell Sci.* **108**, 1817–1829 (1995).
- R. Carapito *et al.*, Mutations in signal recognition particle SRP54 cause syndromic neutropenia with Shwachman-Diamond-like features. *J. Clin. Invest.* **127**, 4090–4103 (2017).
- T. V. Kurzchalia *et al.*, The signal sequence of nascent preprolactin interacts with the 54 K polypeptide of the signal recognition particle. *Nature* **320**, 634–636 (1986).
- G. Schatz, B. Dobberstein, Common principles of protein translocation across membranes. *Science* **271**, 1519–1526 (1996).
- D. Ghosh, J. M. Berg, A proteome-wide perspective on peroxisome targeting signal 1 (PTS1)-Pex5p affinities. *J. Am. Chem. Soc.* **132**, 3973–3979 (2010).
- E. Yifrach *et al.*, Characterization of proteome dynamics in oleate reveals a novel peroxisome targeting receptor. *J. Cell Sci.* **129**, 4067–4075 (2016).
- D. Effelsberg, L. D. Cruz-Zaragoza, W. Schliebs, R. Erdmann, Pex9p is a novel yeast peroxisomal import receptor for PTS1-proteins. *J. Cell Sci.* **129**, 4057–4066 (2016).
- T. Walter, R. Erdmann, Current advances in protein import into peroxisomes. *Protein J.* **38**, 351–362 (2019).
- C. Brocard, A. Hartig, Peroxisome targeting signal 1: Is it really a simple tripeptide? *Biochim. Biophys. Acta* **1763**, 1565–1573 (2006).
- S. J. Gould, G. A. Keller, N. Hosken, J. Wilkinson, S. Subramani, A conserved tripeptide sorts proteins to peroxisomes. *J. Cell Biol.* **108**, 1657–1664 (1989).
- C. Nötzel, T. Lingner, H. Klingenberg, S. Thoms, Identification of new fungal peroxisomal matrix proteins and revision of the PTS1 consensus. *Traffic* **17**, 1110–1124 (2016).
- R. Kintaka, K. Makanae, H. Moriya, Cellular growth defects triggered by an overload of protein localization processes OPEN. *Sci. Rep.* **6**, 31774 (2016).
- I. Yofe *et al.*, One library to make them all: Streamlining the creation of yeast libraries via a SWAp-tag strategy. *Nat. Methods* **13**, 371–378 (2016).
- N. Dahan, M. Schuldiner, E. Zalkvar, "Peroxisome mini-libraries: Systematic approaches to study peroxisomes made easy" in *Peroxisomes*, M. Schrader, Ed. (Methods Molecular Biology, vol. 1595, Humana Press, New York, 2017) pp. 305–331.
- U. Weill *et al.*, Genome-wide SWAp-tag yeast libraries for proteome exploration. *Nat. Methods* **15**, 617–622 (2018).
- M. Breker, M. Gymrek, M. Schuldiner, A novel single-cell screening platform reveals proteome plasticity during yeast stress responses. *Cell Biol.* **200**, 839–850 (2013).
- S. Grunau *et al.*, Peroxisomal targeting of PTS2 pre-import complexes in the yeast *Saccharomyces cerevisiae*. *Traffic* **10**, 451–460 (2009).
- K. Stein, A. Schell-Steven, R. Erdmann, H. Rottensteiner, Interactions of Pex7p and Pex18p/Pex21p with the peroxisomal docking machinery: Implications for the first steps in PTS2 protein import. *Mol. Cell. Biol.* **22**, 6056–6069 (2002).
- A. Schäfer, D. Kerssen, M. Veenhuis, W. H. Kunau, W. Schliebs, Functional similarity between the peroxisomal PTS2 receptor binding protein Pex18p and the N-terminal half of the PTS1 receptor Pex5p. *Mol. Cell. Biol.* **24**, 8895–8906 (2004).
- J. K. Hiltunen *et al.*, The biochemistry of peroxisomal  $\beta$ -oxidation in the yeast *Saccharomyces cerevisiae*. *FEMS Microbiol. Rev.* **27**, 35–64 (2003).
- Ł. Rymur, B. Kempirski, A. Chelstowska, M. Skoneczny, The budding yeast Pex5p receptor directs Fox2p and Cta1p into peroxisomes via its N-terminal part near the FxxxW domain. *J. Cell Sci.* **131**, jcs216986 (2018).
- J. K. Hiltunen *et al.*, Peroxisomal multifunctional beta-oxidation protein of *Saccharomyces cerevisiae*. Molecular analysis of the fox2 gene and gene product. *J. Biol. Chem.* **267**, 6646–6653 (1992).
- E. H. Hettema *et al.*, The ABC transporter proteins Pat1 and Pat2 are required for import of long-chain fatty acids into peroxisomes of *Saccharomyces cerevisiae*. *EMBO J.* **15**, 3813–3822 (1996).
- A. T. J. Klein, M. van den Berg, G. Bottger, H. F. Tabak, B. Distel, *Saccharomyces cerevisiae* acyl-CoA oxidase follows a novel, non-PTS1, import pathway into peroxisomes that is dependent on Pex5p. *J. Biol. Chem.* **277**, 25011–25019 (2002).
- D. M. Jameson, J. A. Ross, Fluorescence polarization/anisotropy in diagnostics and imaging. *Chem. Rev.* **110**, 2685–2708 (2010).
- W. C. DeLoache, Z. N. Russ, J. E. Dueber, Towards repurposing the yeast peroxisome for compartmentalizing heterologous metabolic pathways. *Nat. Commun.* **7**, 11152 (2016).
- M. Morgenstern *et al.*, Definition of a high-confidence mitochondrial proteome at quantitative scale. *Cell Rep.* **19**, 2836–2852 (2017).
- Y. Elgersma *et al.*, Analysis of the carboxyl-terminal peroxisomal targeting signal 1 in a homologous context in *Saccharomyces cerevisiae*. *J. Biol. Chem.* **271**, 26375–26382 (1996).

33. S. Hagen *et al.*, Structural insights into cargo recognition by the yeast PTS1 receptor. *J. Biol. Chem.* **290**, 26610–26626 (2015).
34. P. A. Walton, P. E. Hill, S. Subramani, Import of stably folded proteins into peroxisomes. *Mol. Biol. Cell* **6**, 675–683 (1995).
35. P. Minárik, N. Tomášková, M. Kollárová, M. Antalík, Malate dehydrogenases-structure and function. *Gen. Physiol. Biophys.* **21**, 257–265 (2002).
36. A. Schummer, S. Fischer, S. Oeljeklaus, B. Warscheid, Study of peroxisomal protein phosphorylation by functional proteomics. *Methods Mol. Biol.* **1595**, 267–289 (2017).
37. R. D. Gietz, R. A. Woods, Transformation of yeast by lithium acetate/single-stranded carrier DNA/polyethylene glycol method. *Methods Enzymol.* **350**, 87–96 (2002).
38. I. Yofe, M. Schuldiner, Primers-4-Yeast: A comprehensive web tool for planning primers for *Saccharomyces cerevisiae*. *Yeast* **31**, 77–80 (2014).
39. M. Kafri, E. Metzler-Raz, G. Jona, N. Barkai, The cost of protein production. *Cell Rep.* **14**, 22–31 (2016).
40. T. Unger, Y. Jacobovitch, A. Dantes, R. Bernheim, Y. Peleg, Applications of the restriction free (RF) cloning procedure for molecular manipulations and protein expression. *J. Struct. Biol.* **172**, 34–44 (2010).
41. D. K. Breslow *et al.*, A comprehensive strategy enabling high-resolution functional analysis of the yeast genome. *Nat. Methods* **5**, 711–718 (2008).
42. Y. Cohen, M. Schuldiner, Advanced methods for high-throughput microscopy screening of genetically modified yeast libraries. *Methods Mol. Biol.* **781**, 127–159 (2011).
43. A. H. Y. Tong, C. Boone, Synthetic genetic array analysis in *Saccharomyces cerevisiae*. *Methods Mol. Biol.* **313**, 171–192 (2006).
44. M. Albertini *et al.*, Pex14p, a peroxisomal membrane protein binding both receptors of the two PTS-dependent import pathways. *Cell* **89**, 83–92 (1997).
45. F. W. Studier, Protein production by auto-induction in high density shaking cultures. *Protein Expr. Purif.* **41**, 207–234 (2005).



ARTICLE

# Cnm1 mediates nucleus–mitochondria contact site formation in response to phospholipid levels

Michal Eisenberg-Bord<sup>1\*</sup>, Naama Zung<sup>1\*</sup>, Javier Collado<sup>2,3</sup>, Layla Drwesh<sup>4</sup>, Emma J. Fenech<sup>1</sup>, Amir Fadel<sup>1</sup>, Nili Dezarella<sup>5</sup>, Yury S. Bykov<sup>1</sup>, Doron Rapaport<sup>4</sup>, Ruben Fernandez-Busnadiego<sup>2,3</sup>, and Maya Schuldiner<sup>1</sup>

**Mitochondrial functions are tightly regulated by nuclear activity, requiring extensive communication between these organelles. One way by which organelles can communicate is through contact sites, areas of close apposition held together by tethering molecules. While many contacts have been characterized in yeast, the contact between the nucleus and mitochondria was not previously identified. Using fluorescence and electron microscopy in *S. cerevisiae*, we demonstrate specific areas of contact between the two organelles. Using a high-throughput screen, we uncover a role for the uncharacterized protein Ybr063c, which we have named Cnm1 (contact nucleus mitochondria 1), as a molecular tether on the nuclear membrane. We show that Cnm1 mediates contact by interacting with Tom70 on mitochondria. Moreover, Cnm1 abundance is regulated by phosphatidylcholine, enabling the coupling of phospholipid homeostasis with contact extent. The discovery of a molecular mechanism that allows mitochondrial crosstalk with the nucleus sets the ground for better understanding of mitochondrial functions in health and disease.**

## Introduction

During the evolution of eukaryotes, an  $\alpha$ -proteobacterium integrated into its archaeal host cell, giving rise to the mitochondrial organelle (Dyall et al., 2004). As mitochondrial genes transferred to the nuclear genome, the response to mitochondrial stress also became nuclear transcribed, and mitochondria number and function had to become coordinated with cellular needs and cell division. This increased dependence on the nucleus required that the two organelles evolve methods of communication. The importance of this communication is evident by how its breakdown contributes to a number of diseases, such as various forms of cancer (Mello et al., 2019; Xia et al., 2019; Yi, 2019), fatty liver disease (Yi, 2019), insulin resistance and obesity (Lee et al., 2015), and physiological conditions such as aging (Mohrin et al., 2015; Reynolds et al., 2020).

Over the years, many aspects of nucleus–mitochondria communication have been intensively studied. Signaling cascades between the organelles were found, dually targeted proteins described, and mitochondrial metabolites required for nuclear function characterized (Eisenberg-Bord and Schuldiner, 2017b; English et al., 2020). However, more direct forms of communication between the two organelles, such as through contact sites, were less explored.

Contact sites are areas where the membranes of two organelles are actively tethered by proteins. Contact sites house unique proteins and lipids and allow direct crosstalk between organelles. The short distance between organelles in these contacts (usually ranging between 10 and 80 nm; Scorrano et al., 2019), enables the rapid, efficient and directional transfer of ions, lipids and metabolites (Eisenberg-Bord et al., 2016; Eisenberg-Bord and Schuldiner, 2017a; Zung and Schuldiner, 2020). While contact sites between multiple pairs of organelles have been demonstrated and investigated in some depth (Shai et al., 2018), the contacts between mitochondria and the nucleus remain elusive. One reason for this gap in our knowledge is that the outer nuclear membrane is continuous with the membrane of the most abundant organelle in the cell, the ER. Since the ER forms extensive contacts with mitochondria, it was hence difficult to distinguish a contact that is unique to the nuclear envelope.

The ER–mitochondria contact site was the first to be described in the 1950s (Bernhard and Rouiller, 1956; Bernhard et al., 1952; Copeland and Dalton, 1959). However, it was not until 2009 that the tethering machinery mediating this contact

<sup>1</sup>Department of Molecular Genetics, Weizmann Institute of Science, Rehovot, Israel; <sup>2</sup>Institute for Neuropathology, Georg August Universität Göttingen, Göttingen, Germany; <sup>3</sup>Cluster of Excellence “Multiscale Bioimaging: from Molecular Machines to Networks of Excitable Cells,” University of Göttingen, Göttingen, Germany; <sup>4</sup>Interfaculty Institute of Biochemistry, University of Tuebingen, Tuebingen, Germany; <sup>5</sup>Electron Microscopy Unit, Chemical Research Support, Weizmann Institute of Science, Rehovot, Israel.

\*M. Eisenberg-Bord and N. Zung contributed equally to this paper; Correspondence to Maya Schuldiner: [maya.schuldiner@weizmann.ac.il](mailto:maya.schuldiner@weizmann.ac.il); Michal Eisenberg-Bord: [eisen.michal@gmail.com](mailto:eisen.michal@gmail.com).

© 2021 Eisenberg-Bord et al. This article is available under a Creative Commons License (Attribution 4.0 International, as described at <https://creativecommons.org/licenses/by/4.0/>).

in *Saccharomyces cerevisiae* (from here on termed yeast) was characterized and named the ER-mitochondria encounter structure (ERMES; Kornmann et al., 2009). This tethering complex is composed of one subunit spanning the mitochondrial membrane (Mdm10), one spanning the ER membrane (Mmm1), and two cytosolic subunits (Mdm34 and Mdm12; Kornmann et al., 2009). The ERMES complex was demonstrated to play a role in the transfer of phospholipids between the ER and mitochondria (Kawano et al., 2018; Kundu and Pasrija, 2020; Endo et al., 2018). In recent years, additional tethering machineries for the ER-mitochondria contact in yeast were discovered (Murley et al., 2015; Elbaz-Alon et al., 2015; Gatta et al., 2015; Lahiri et al., 2014), however whether any of these are required for communication between the nuclear envelope and mitochondria was not determined.

Recently, a contact site between the nucleus and mitochondria was described in human mammary cancer tissue and was then further studied in cell lines (Desai et al., 2020). This contact site was shown to have a role in the retrograde signaling response, occurring between the nucleus and mitochondria, and is facilitated by the cholesterol binding and translocator protein TSPO (Desai et al., 2020). The formation of this contact site was independent of two of the tethering machineries facilitating ER-mitochondria contacts in human cells (VAPB5 and mitofusin 2), suggesting that these contacts are distinct (Desai et al., 2020). However, a TSPO homolog is not found in the yeast proteome. In yeast, it has also recently been suggested that a dedicated contact site between mitochondria and the nucleus exists, since heme, created in mitochondria, bypasses cytosolic pools, and transfers directly into the nucleus (Martinez-Guzman et al., 2020). Hence, it became important to prove that such a contact site exists in yeast as well as uncover its molecular tethers.

Here, we describe a contact between mitochondria and the nuclear periphery (nuclear ER) in yeast that is ERMES independent. Using high-content screens, we find a dedicated tether formed by the previously unstudied nuclear envelope protein Ybr063c (which we name Cnm1 [contact nucleus mitochondria 1]) and uncover its interaction partner on mitochondria, the component of the TOM (translocase of outer membrane [OM]) complex, Tom70. We show that Cnm1 and Tom70 are sufficient for contact site formation and that Cnm1-mediated contact sites are regulated by phosphatidylcholine (PC) metabolism. Our studies pave the way for a more comprehensive understanding of nucleus-mitochondria communication.

## Results

### Mitochondria form ERMES-independent contact sites with the nuclear ER

EM images of yeast cells demonstrates three distinct types of contact sites between mitochondria and the ER: those with cortical ER, those with tubular ER, and some with the nuclear ER (which is continuous with the outer nuclear membrane; Fig. 1 A).

To corroborate the existence of mitochondria-nuclear ER (from here on called nucleus) contact sites and observe them at higher resolution, we used focused ion beam thinning of

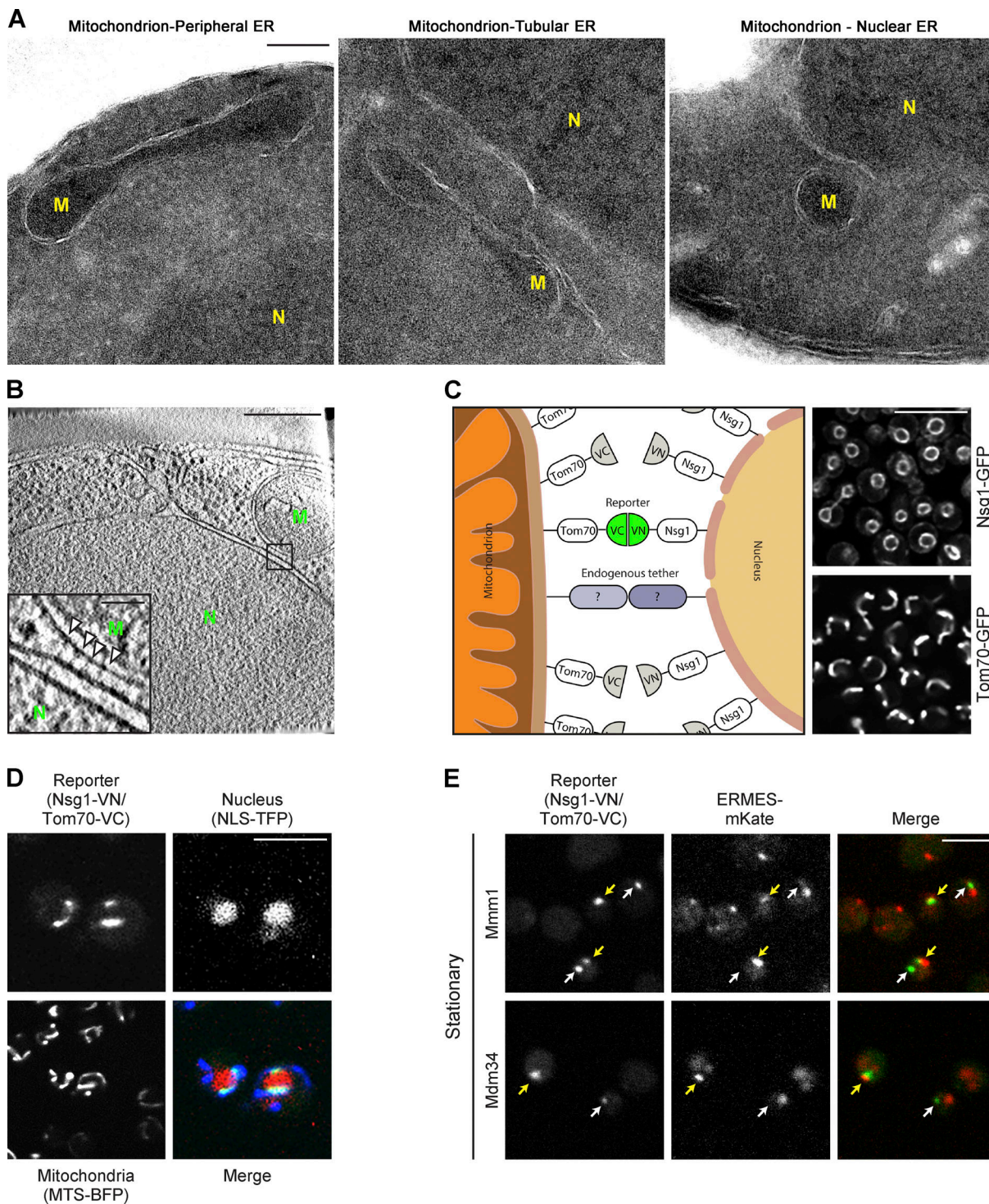
vitrified yeast and cryoelectron tomography (Collado and Fernández-Busnadiego, 2017; Collado et al., 2019). The enhanced resolution and sample preservation enabled us to not only measure (Salfer et al., 2020) the average distance between the nucleus and mitochondria in these areas to be ~20 nm, as would be expected from a bona fide contact site (Scorrano et al., 2019; Fig. S1 A), but also model the contact by 3D segmentation (Salfer et al., 2020; Fig. S1 B). Moreover, we could visualize native protein densities at the contact area that may represent specific tethering molecules underlying the formation of this contact site (Fig. 1 B).

To find potential tethers and resident proteins of the nucleus-mitochondria contact site, we first developed a method to visualize the contact using fluorescence microscopy. We used the split Venus approach for building a contact site reporter in the absence of prior knowledge as to the identity of the molecular tethers (Shai et al., 2018). In short, we attached one part of a split Venus molecule to Tom70, an outer mitochondrial membrane protein, and the second part to Nsg1, a nuclear periphery protein (see scheme in Fig. 1 C). The correct localization of fluorescently labeled variants of both proteins was confirmed by fluorescence microscopy (Fig. 1 C). Only at contact sites, where the two membranes are in proximity, the Venus fragments interact, the full Venus protein is formed, and the resulting fluorescence enables imaging by a fluorescent microscope. Indeed, we observed a clear fluorescent signal suggesting that the nucleus-mitochondria contact site can be imaged by this approach, and this was independent of the Venus fragment appended to either Nsg1 or Tom70 (Figs. 1 D and S1 C).

To verify that the reporters are specific, we imaged them relative to both mitochondria and the nucleus. Indeed, images of these cells verified that in all cases where a signal from the reporter was observed, it occurred at areas of apposition between the nucleus and mitochondria (Figs. 1 D and S1 C), meaning the reporters accurately identify proximity between the two organelles.

To test if our reporter is simply reflecting contact sites facilitated by the well-studied ER-mitochondria contact site machinery, we overexpressed one ERMES subunit, Mdm34, and analyzed its effect on our reporter and on an ER-mitochondria contact reporter as a control. It has been well documented that overexpressing a tether can expand contact extent (Shai et al., 2018). Indeed, we found that overexpression of Mdm34 caused the appearance of cells with increased extent of the ER-mitochondria contact site reporter. However, it did not extend the nucleus-mitochondria contact site reporter (Fig. S1, D and E), suggesting that the reporter is showing an ERMES-independent structure. We then visualized the nucleus-mitochondria contact reporter relative to two ERMES components, Mmm1 and Mdm34. The pattern of colocalization between Mmm1/Mdm34 and the reporter highlighted the existence of two distinct populations. Some reporter signals were in close proximity to Mmm1 (47%) or Mdm34 signals; however, some were only partially colocalized with Mmm1 (18%) or Mdm34, and others were completely distinct from ERMES subunits (35% for Mmm1 signals), demonstrating that nucleus-mitochondria proximity can be ERMES independent (Figs. 1 E and S1 F). These observations suggested that distinct





**Figure 1. Mitochondria form contact sites with the nuclear ER that are ERMES independent.** (A) EM images of yeast S288c background demonstrate different mitochondrial contact sites with the various subcompartments of the ER (peripheral, tubular, and nuclear). Each image was differentially adjusted for brightness. M, mitochondrion; N, nucleus. Scale bar, 200 nm. (B) Tomograms of yeast (SEY6210.1 background) show the contact sites between the two organelles. M, mitochondrion, N, nucleus, scale bar, 300 nm. Inset: High-density regions that may represent molecular tethers (arrowheads). Scale bar, 50 nm. (C) Schematic illustration of a nucleus-mitochondria contact site reporter. The C-terminal part of a Venus protein (VC) was attached to outer mitochondrial membrane protein, Tom70. The N-terminal part of the Venus protein (VN) was attached to the nuclear ER protein Nsg1. These proteins are homogeneously distributed on the OM of their respective organelles, as demonstrated by the images when tagged with GFP on their C terminus. Only in cases where the two organelles are in proximity, as in the case of contact sites, the full Venus protein forms and the fluorescent signal is detected. Scale bar, 5  $\mu$ m. (D) The nucleus-mitochondria reporter Nsg1-VN/Tom70-VC correctly identifies proximities between the two organelles. Nuclei are visualized by the red fluorophore (tdTomato) fused to a NLS (NLS-TFP). Mitochondria are visualized by a BFP fused to a mitochondrial targeting sequence (MTS-BFP). The fluorescent signal of the reporter is only localized to areas of proximity between mitochondria and the nucleus. Scale bar, 5  $\mu$ m. (E) Some nucleus-mitochondria contacts are

distinct from ERMES-mediated ER-mitochondria contacts. The ERMES subunits Mmm1 and Mdm34 were tagged with mKate and integrated into the nucleus-mitochondria reporter strain. Cells were imaged in stationary phase. Yellow arrows mark areas of colocalization between the ERMES-mKate signal and the reporter, while white arrows mark areas where only the reporter signal is detected (ERMES-independent contacts). Scale bar, 5  $\mu$ m.

tethering molecules facilitate the contact site between mitochondria and the nucleus.

### High-content screens reveal residents and effectors of the nucleus-mitochondria contact

The first step toward reaching a mechanistic understanding of a contact site is to uncover tethering molecules as well as resident proteins and regulators. To identify such proteins in an unbiased way, we performed a high-content screen using a collection of all yeast proteins tagged with mCherry at their N terminus and overexpressed from a *TEF2* promoter (Weill et al., 2018). Using automated approaches (Cohen and Schuldiner, 2011), we integrated into these strains the reporter of the nucleus-mitochondria contact site (*NSG1-VN/TOM70-VC*). We imaged the resulting ~6,000 yeast strains using a high-throughput microscopy setup and manually analyzed the images to find proteins that colocalize with the contact site signal (Fig. 2 A). The screen uncovered 48 proteins that partially colocalized with the reporter and 9 proteins that fully colocalized with it (Fig. 2 B; the full list of hits with their description is in Table S1).

To sift out potential tethers from this long list of resident proteins, we searched for those that extended the contact when overexpressed, since it is a known characteristic of a molecular tether (Eisenberg-Bord et al., 2016). We imaged both versions of the reporter on the background of all 57 hits from the primary screen. This secondary screen highlighted 12 hits that both colocalized with the reporter and increased its signal (Fig. 2 C), placing them as potential tethering molecules.

### Ybr063c (Cnm1) has the characteristics of a molecular tether

Out of the 12 candidate tethers uncovered by our screens, the protein that seemed most likely to be a direct tether was Ybr063c, an uncharacterized protein of unknown function. Ybr063c was fully colocalized with the reporter (Fig. 2 B), and its overexpression affected the extent of the reporter signal (Fig. 2 C). Moreover, it was predicted by several algorithms to be an integral membrane protein (Weill et al., 2019), a trait important for creating a tethering force. Finally, it was not previously studied or implicated in ER-mitochondria contacts. Hence, we decided to follow up on this protein.

To verify that Ybr063c is not simply a part of the ER-mitochondria contact site, we analyzed if its overexpression extends the ERMES-mediated contacts. We found that the extent of Mmm1-GFP or Mdm34-GFP patches is not affected by overexpressing or deleting Ybr063c (Fig. S2 A). Moreover, we could observe areas of Ybr063c expression that did not colocalize with ERMES components and vice versa (Fig. S2 B), supporting the idea that Ybr063c is not directly related to the ERMES complex. In support of Ybr063c acting in an ERMES-independent manner, we found that the combination of  $\Delta$ *mdm34* alongside repressed expression of Ybr063c (growth on glucose when expressed from a galactose-inducible promoter) exacerbated the growth defect

of the  $\Delta$ *mdm34* strain alone. In addition, it was shown that loss of both *vam6* (that reduces mitochondria-vacuole contacts) and ERMES is synthetic lethal (Elbaz-Alon et al., 2014). *Cnm1* repression on the background of the deletion in *vam6* not only did not result in lethality but rather completely rescued the growth defect of the  $\Delta$ *vam6* strain, pointing again to a different function (Fig. S2 C).

One of the main characteristics of a molecular tether is its enrichment at the contact site (Eisenberg-Bord et al., 2016). We therefore visualized Ybr063c N terminally tagged with mCherry relative to both the nucleus and mitochondria. Indeed, mCherry-Ybr063c was located at discrete regions on the nuclear envelope that were in contact with mitochondria (Fig. 3 A).

Protein tethers are often integral membrane proteins, enabling them to provide a direct link between the membranes. While some prediction algorithms predicted one or two membrane-spanning domains, others predicted Ybr063c to be a soluble protein (Weill et al., 2019). To test whether Ybr063c is an integral membrane protein, we performed carbonate extraction (CE) on Ybr063c tagged with a small tag (3HA) on its N terminus. CE dissociates peripheral proteins from membranes but cannot extract membrane-embedded polypeptides from the bilayer. Similarly to the mitochondrial OM protein Tom20 and in contrast to the mitochondrial matrix protein Hep1, 3HA-Ybr063c remained in the membrane fraction following this treatment, clearly indicating that it is embedded in the lipid bilayer (Fig. 3 B).

To assay if Ybr063c is sufficient for bringing together the two membranes, we imaged strains overexpressing untagged Ybr063c and monitored the association between mitochondria and the nucleus in the absence of the reporter. Overexpression of Ybr063c under the strong *TEF2* promoter had a striking effect on mitochondrial distribution in the cell, causing clustering of mitochondria around the perinuclear region (Fig. 3 C). Quantification of this proximity showed a nearly twofold increase in proximity between the two organelles (Fig. S2, D and E; and Fig. 3 D). Time-lapse analysis of Ybr063c induction (from a galactose inducible promoter) suggest that this increased proximity is caused by adherence of mitochondria to the nucleus after a random contact between the two organelles has occurred (Video 1).

Imaging the strains overexpressing Ybr063c by EM demonstrated that these proximities were indeed bona fide contact sites (Fig. 3 E). These results were corroborated by cryoelectron tomography, where 3D segmentation showed abundant nucleus-mitochondria contacts in the strain overexpressing Ybr063c (Fig. 3 F).

Since Ybr063c has the molecular characteristics of a tether affecting extensively the nucleus-mitochondria contact site, we named it Cnm1 for Contact Nucleus Mitochondria 1.

### Identifying factors involved in Cnm1-induced contact sites

To gain insight on the mechanism of Cnm1-mediated tethering, we set out to find proteins that are required for its ability to



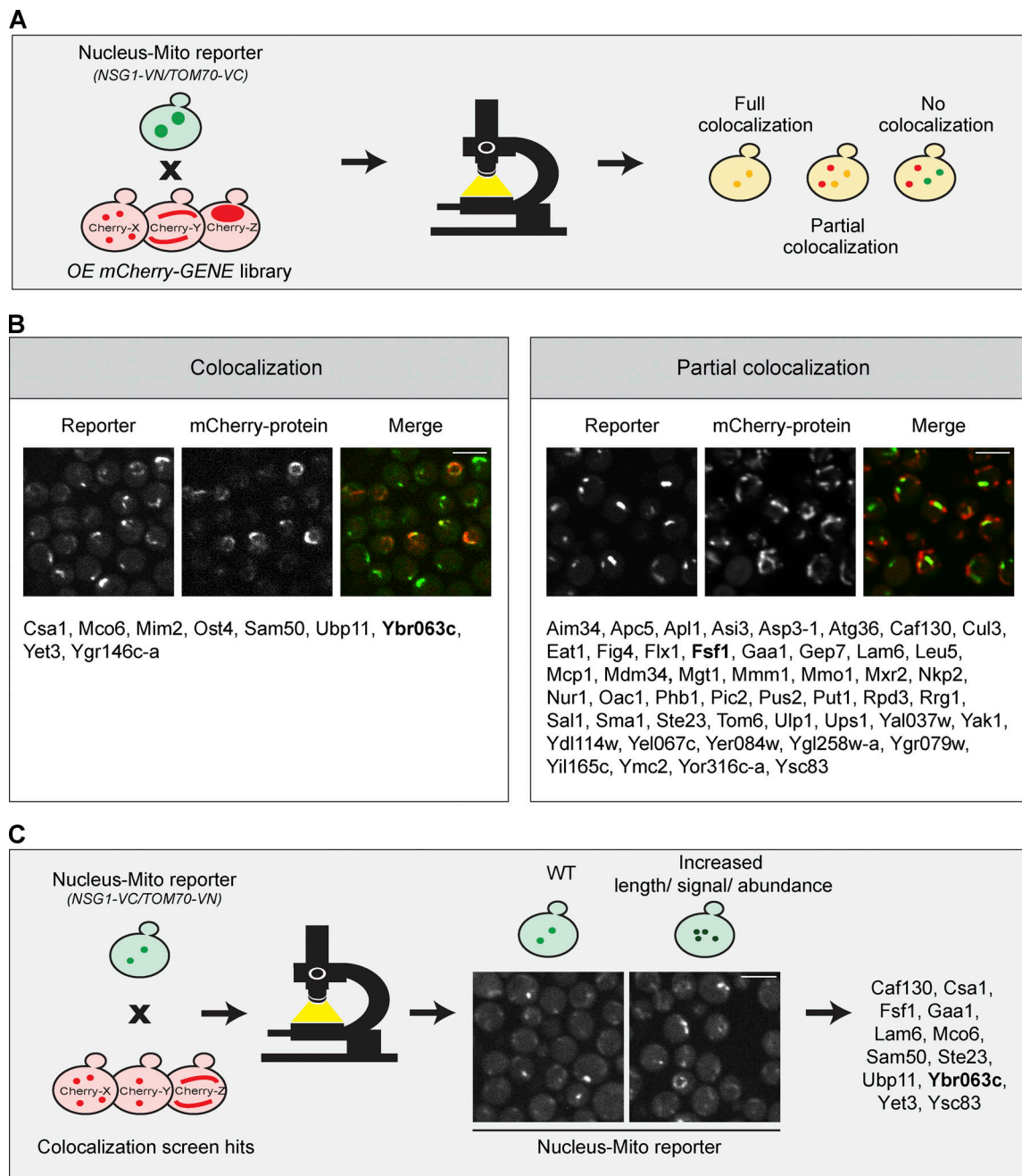


Figure 2. **High-content screens reveal residents and effectors of the nucleus-mitochondria contact.** (A) Illustration of the high-content screen directed at finding resident proteins of the nucleus-mitochondria contact site. The reporter (*NSG1-VN/TOM70-VC*) was integrated into a library of ~6,000 yeast strains, each harboring an overexpressed and mCherry-tagged version of a different yeast protein. Strains were imaged using automated microscopy, and images were manually examined to identify proteins that colocalize, either fully or partially, with the reporter. (B) List of all proteins that either fully (left) or partially (right) colocalized with the reporter, organized by alphabetical order. The proteins shown in the representative images are marked in bold. Scale bars, 5  $\mu$ m. For a complete list of all proteins and their descriptions, see Table S1. (C) Illustration of a screen aimed at identifying effectors of the nucleus-mitochondria contact site. The reporter (*NSG1-VC/TOM70-VN*) was integrated into all 57 hits from the primary screen (shown in B). The effect of their overexpression on the reporter was inspected and 12 hits were found. A representative image shows the protein marked in bold out of the full list of hits. Scale bar, 5  $\mu$ m.

promote clustering of mitochondria around the nucleus when overexpressed. We assumed that the deletion of such a gene, which is involved in the clustering of mitochondria around the nucleus, would result in the reversion of this phenotype and less clustering. To search for such a reversion, we integrated overexpressed *CNM1* and a nuclear marker into a collection of

mutants in every yeast gene (~5,000 knockouts of nonessential genes; Deletion library, Giaever et al., 2002; and ~1,000 hypomorphic alleles of essential ones; Decreased abundance by mRNA perturbation (DAmP) library, Breslow et al., 2008). Next, we performed a high-content microscopy screen on all strains and searched for those that showed less clustering of

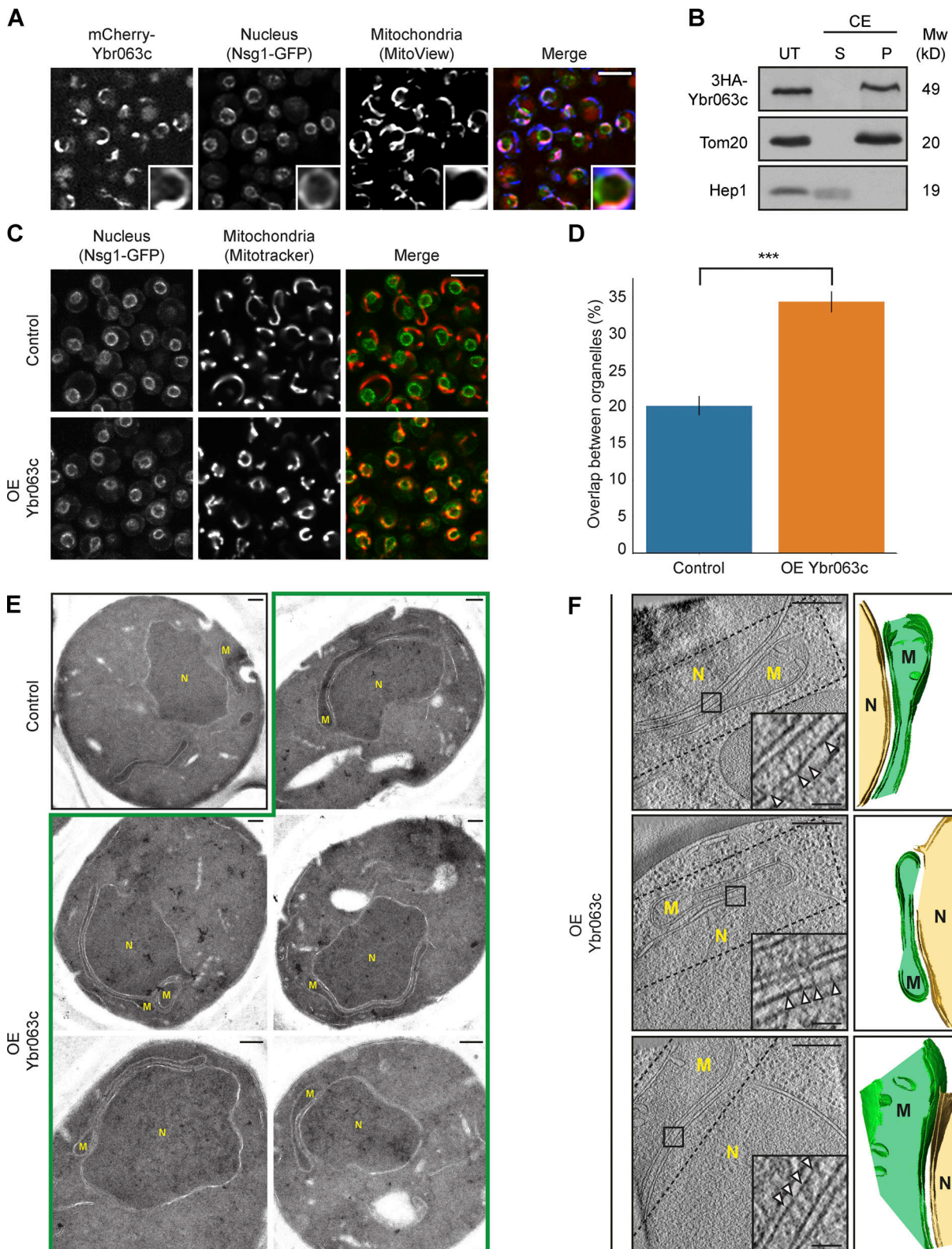


Figure 3. **Ybr063c (Cnm1) has the characteristics of a molecular tether.** (A) Overexpressed mCherry-Ybr063c is localized only to areas of proximity between the nuclear envelope and mitochondria. The nuclear envelope was visualized with Nsg1-GFP and mitochondria by the blue mitochondrial dye (MitoView 405). Insets show an enlarged region of a single nucleus and mitochondria interface with mCherry-Ybr063c signal present where the two organelles connect. Scale bar, 5  $\mu$ m. (B) Ybr063c is a membrane protein embedded in the lipid bilayer. Enriched mitochondrial fractions from cells overexpressing Ybr063c tagged with 3HA on its N terminus were either treated by CE or left untreated (UT). Following this, they were separated into membrane proteins in the pellet (P) or soluble proteins in the supernatant (S). (C) Overexpression (OE) of Ybr063c drives clustering of mitochondria around the nucleus. The nuclear membrane was visualized by Nsg1-GFP and mitochondria were stained using a red dye (MitoTracker Orange). Scale bar, 5  $\mu$ m. (D) Quantitation of the proximity between



mitochondria and nucleus from C is shown as the percentage of mitochondrial signal that overlaps with the nuclear envelope signal in both a strain that overexpresses Ybr063c (OE Ybr063c) and a control strain. Bars represent standard deviation.  $n = 500$ ;  $***, P = 7.24e^{-73}$ . **(E)** EM images of the extended contact sites between nucleus and the mitochondria that are formed by overexpressing Ybr063c (OE Ybr063c, highlighted by a green outline). Scale bars, 200 nm. **(F)** Tomograms of nucleus–mitochondria contacts in yeast overexpressing Ybr063c (OE Ybr063c, left). Scale bars, 300 nm. Insets show high densities that may indicate molecular tethers (arrowheads). Scale bars, 50 nm. 3D segmentations of the contact site area seen in the tomograms (right). The nucleus membrane is marked in yellow, and the mitochondrial membrane is marked in green. Dashed lines on tomograms indicate the area that is seen in the 3D segmentation. M, mitochondrion; N, nucleus.

mitochondria around the nucleus (Fig. 4 A). While 60 genes affected this phenotype to some extent (Table S2), only seven deletions (verified by both check-PCR and remaking the strains to confirm the phenotype; data not shown) completely abolished the effect of *CNMI* overexpression (Fig. 4 B). In support of *Cnm1* mediating ERMES-independent contacts, none of the ERMES mutants came up in the screen, and deletion of *mdm34* (verified by check-PCR; data not shown) did not alter the clustering phenotype of *CNMI* overexpression (Fig. S3).

### Cnm1-mediated contact sites are regulated by PC

Out of the seven hits that most affected the capacity of *Cnm1* to cause mitochondrial clustering around the nucleus, we found deletions in three genes (*CHO2*, *OPI3*, and *INO2*) whose protein products are all components of the PC biosynthesis pathway. To produce PC, phosphatidylserine (PS) is converted to phosphatidylethanolamine (PE) mainly in the inner membrane of mitochondria by *Psd1*, and then PE is transferred back to the ER membrane (Carman and Han, 2011). Both *Cho2* and *Opi3* are methyltransferases located on the ER membrane, where they convert PE to PC in two enzymatic steps (Fig. 5 A). The PC produced on ER membranes must then be transferred back to mitochondria, where it constitutes 44% of membrane lipids (Sperka-Gottlieb et al., 1988). *Ino2* is a transcriptional activator of *CHO2* and *OPI3* genes (Carman and Han, 2011). Identifying three genes of the PC pathway as modulators of *Cnm1* activity suggested a connection between PC and the nuclear–mitochondria contact.

Visualizing *Cnm1*-GFP under regulation of a constitutive promoter and on the background of a deletion of each of the three PC biosynthesis regulators showed a reduction in intensity compared with control. Moreover, we noticed that cells that retained *Cnm1* expression still had increased proximity between mitochondria and the nucleus, whereas cells with reduced *Cnm1* abundance displayed diminished clustering (Fig. 5 B). Thus, *Cho2*, *Opi3*, and *Ino2* might affect the capacity to extend the contact by regulating *Cnm1* levels.

*Cho2/Opi3/Ino2* might regulate *Cnm1* abundance directly or indirectly through their effect on PC levels. To discriminate between these possibilities, we took advantage of the fact that in yeast, there is a *Cho2/Opi3*-independent pathway to synthesize PC, the Kennedy pathway. The Kennedy pathway uses externally added choline to conjugate Cytidine 5'-diphosphocholine (CDP-choline) directly to the headgroup of diacylglycerol (Fig. 5 A; Atkinson et al., 1980). Indeed, it was shown that simply adding choline to yeast medium is enough to increase PC levels significantly (Atkinson et al., 1980). Therefore, we assayed whether addition of choline to the growth medium will rescue the levels of *Cnm1*-GFP in strains lacking *Cho2*, *Opi3*, or *Ino2*.

Imaging of these strains shows that this is indeed the case (Fig. S4 A), and this was verified by Western blot analysis (Fig. 5 C).

To support this phenotype being a result of PC levels, we assayed the effect of several additional members of this metabolic pathway. We deleted *INO4* encoding for a complex member of *Ino2* that is required for its activity as a transcription factor (Carman and Han, 2011; Fig. S4 B), and found that it too reduced *Cnm1* abundance and that this phenotype was reversed by addition of choline. Inversely, we deleted *OPII*, which encodes for a transcriptional repressor that binds the *Ino2*–*Ino4* complex and thus prevents expression of either *CHO2* or *OPI3* (Carman and Han, 2011). As expected, we could quantify more cells with higher intensity of the *Cnm1*-GFP signal compared with control (Fig. S5, C and D).

We could also rescue *Cnm1* levels by supplementation directly with PC, demonstrating that the effect of choline addition was through its integration into PC (Fig. S4 E). Importantly, choline-induced rescue of *Cnm1* levels on these backgrounds also restored the contacts between the nucleus and mitochondria (Fig. 5 D). Taken together, these results indicate that PC levels regulate *Cnm1* abundance, thus affecting mitochondrial clustering around the nucleus.

Having a tool in hand to pick apart the effect of *Cnm1* overexpression, contact site expansion, and PC levels, we turned to assay the effect of these factors on yeast growth. Growth assays demonstrated that inducing clustering of mitochondria around the nucleus by overexpressing *Cnm1* does not have an adverse effect on cell growth (Fig. 5 E). Deletion of *cho2*, *opi3*, and *ino2* (in the absence of exogenous choline) reduced growth rate, as would be expected from a diminished capacity to biosynthesize a central phospholipid. Surprisingly, overexpressed *Cnm1* exacerbated the adverse effect on growth rate displayed by the strains with reduced PC biosynthesis ( $\Delta cho2$ ,  $\Delta opi3$ , and  $\Delta ino2$ ; Fig. 5 E). The phenotype of overexpressed *Cnm1* upon deletions of the three PC biosynthetic genes was also rescued by the addition of choline (Fig. 5 F), suggesting that during conditions of low PC abundance, increasing nucleus–mitochondrial contact is deleterious to cells, potentially due to the shunting of too much PC into mitochondrial membranes.

### Cnm1-mediated contact sites require Tom70

Our results thus far show that *Cnm1* has the capacity to form contacts when overexpressed and that its reduced abundance caused reduced contact formation. Next, we wanted to explore the molecular mechanism of tethering between the nucleus and mitochondria. We first ascertained in which of the two organelles *Cnm1* resides. We imaged *Cnm1*-GFP relative to mitochondria and the nucleus during stationary phase. In this condition, there is reduced clustering of mitochondria around

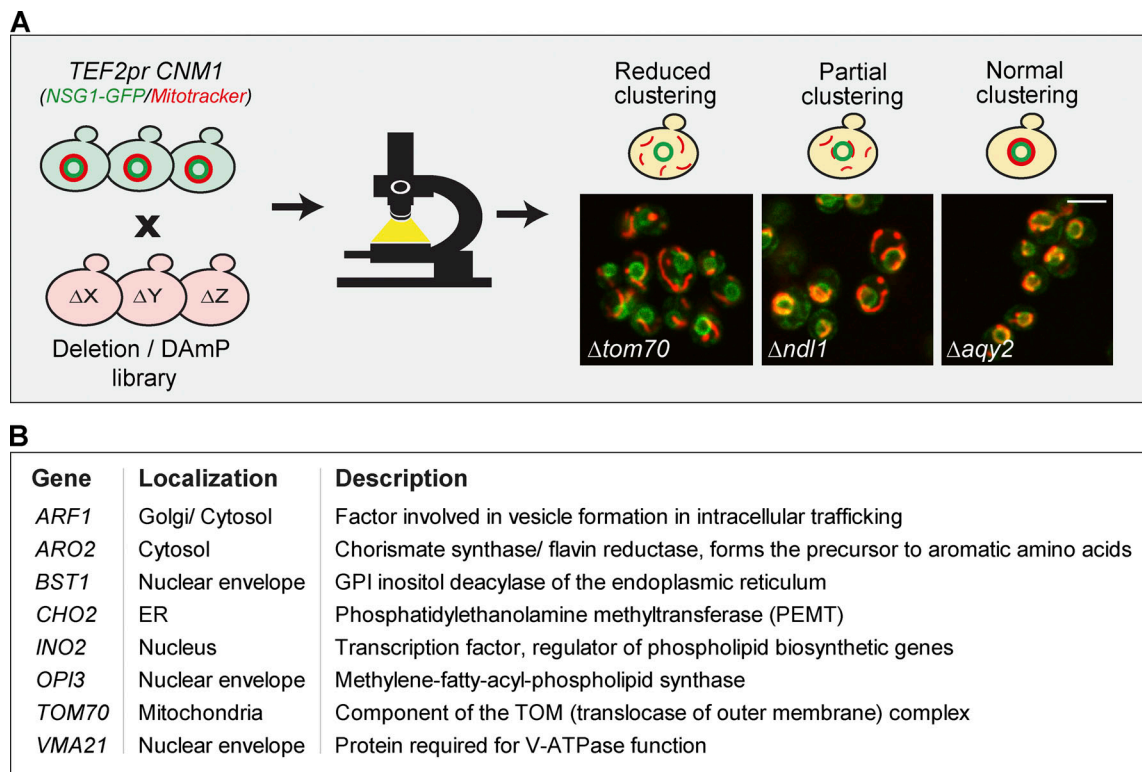


Figure 4. **Identifying factors that are involved in Cnm1-induced contact sites.** (A) A schematic representation of the systematic screen to find modulators of Cnm1 overexpression. Cnm1, overexpressed under the strong *TEF2* promoter, and the nuclear envelope protein Nsg1, tagged with GFP on its C terminus, were integrated into the deletion/hypomorphic allele library. In this library, each colony harbors a loss-of-function mutant in each of the ~6,000 yeast genes. Prior to imaging, cells were stained with a red mitochondrial dye (MitoTracker Orange). The genes that when mutated resulted in partial or reduced mitochondrial clustering around the nucleus were considered as hits. Representative images of the mutants labeled in white are shown. Scale bar, 5  $\mu$ m. (B) A table of all deleted genes that caused reduced mitochondrial clustering on the background of Cnm1 overexpression arranged by alphabetical order. GPI, glycosylphosphatidylinositol. Protein localization and description are presented in the middle and right columns, respectively. For a full list of the mutant genes that resulted in partial clustering, see Table S2.

the nucleus even when Cnm1 is overexpressed, and this enables better discrimination between the organelles. In this condition, Cnm1 was still highly enriched in the contact area but could also clearly be detected in areas of the nuclear ER that were not adjacent to mitochondria (Fig. 6 A). Since Cnm1 is an integral membrane protein (Fig. 3 B), this places it as a new nuclear membrane resident.

Finding that Cnm1 is a nuclear protein encouraged us to identify its mitochondrial tethering partner. Of the seven hits that dramatically alleviated Cnm1-mediated clustering (Fig. 4, A and B) only one was mitochondrial, Tom70. Moreover, Tom70 was previously shown to act as a tethering partner to Lam6 in the ER-mitochondria contact site (Elbaz-Alon et al., 2015; Murley et al., 2015). Interestingly, Lam6 also came up in our initial screen for proteins affecting the nucleus-mitochondria contact (Fig. 2 A).

To investigate whether Tom70 could be a tethering partner for Cnm1, we imaged cells which overexpressed Cnm1-GFP in a  $\Delta tom70$  background. Indeed, a dramatic effect on Cnm1 localization was observed and Cnm1-GFP could no longer be visualized on discrete areas of the nuclear membrane but rather was homogeneously distributed over the entire nuclear membrane (Fig. 6 B). A similar effect was previously seen for the ERMES

complex, where deleting one subunit resulted in the redistribution of other subunits to the entire organelle (Kornmann et al., 2009). Moreover, in this background, mitochondrial clustering was completely lost, supporting the notion that Tom70 could be a partner protein for Cnm1 on the outer mitochondrial membrane.

Tom70 is a mitochondrial protein import receptor loosely associated with the TOM complex (Dekker et al., 1998). Hence, Tom70 could be affecting Cnm1 indirectly by simply altering the abundance of another mitochondrial OM protein. To uncover if the effect was direct, we first assayed whether Tom70 and Cnm1 interact with one another by performing a coimmunoprecipitation experiment. Indeed, when we pulled down Cnm1, we found a twofold enrichment of Tom70 relative to another TOM component, Tom20 (Fig. 6 C).

To further back-up that the two proteins interact on the opposing membranes, we overexpressed a soluble GFP-Tom70 from its endogenous locus (no full length Tom70 was present in the cells) by deleting its membrane-spanning region (first 38 aa,  $\Delta tmd$ ; Wu and Sha, 2006; Brix et al., 2000). While  $\Delta tmd$  GFP-Tom70 is distributed homogeneously in the cytosol, overexpression of Cnm1 caused the redistribution of  $\Delta tmd$  GFP-Tom70 to surround the nuclear membrane (Fig. 6 D). High-resolution



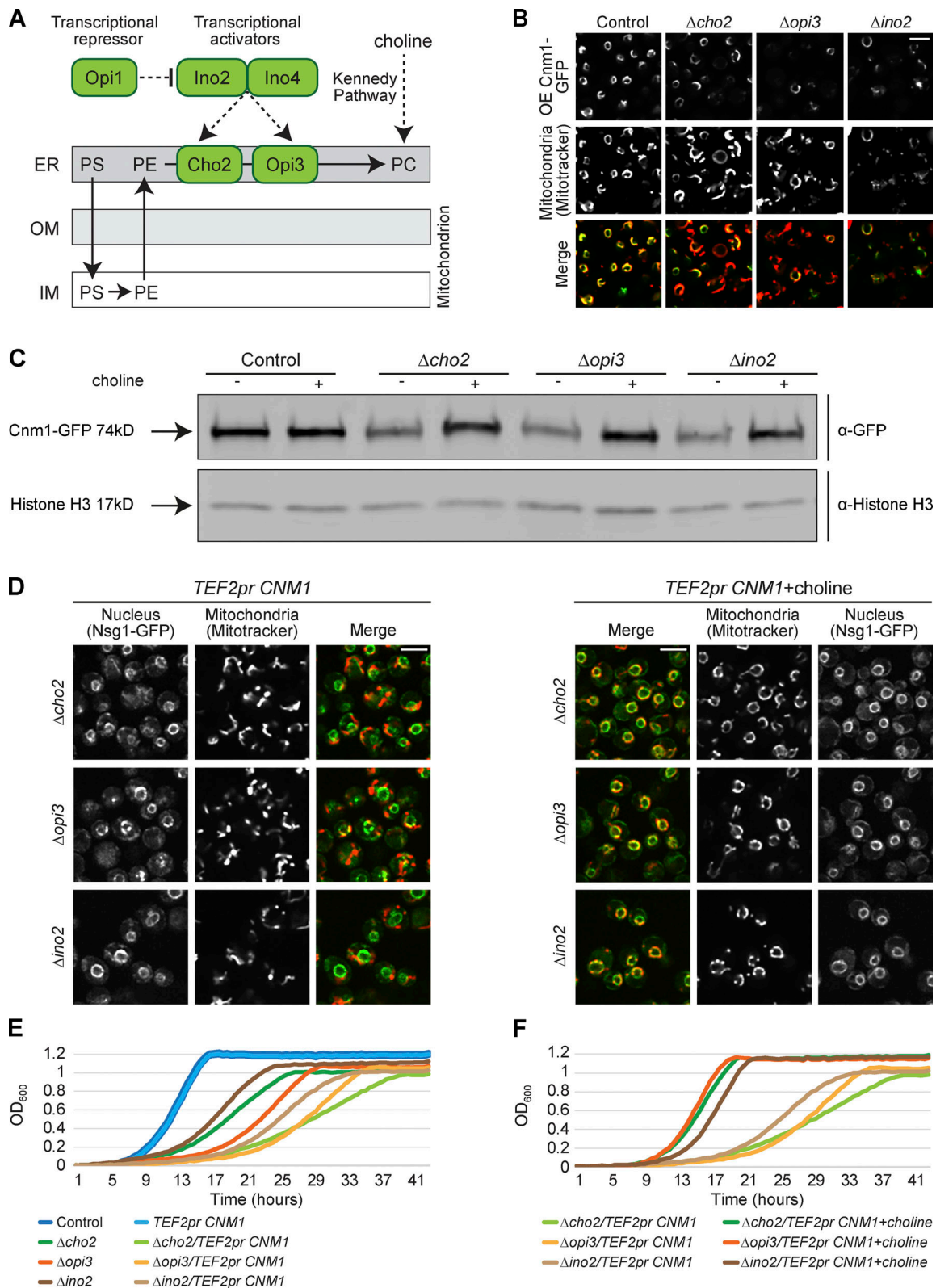


Figure 5. **Cnm1-mediated contact sites are affected by PC metabolism.** (A) Schematic illustration of the biosynthesis pathway of PC. PS formed in the ER is transferred to mitochondria to generate PE, which is then transferred back to the ER for the formation of PC by Cho2 and Opi3. Ino2 and Ino4 are the transcriptional activators of both Cho2 and Opi3. Opi1 is a negative regulator of the pathway. PC molecules can also be synthesized through the Kennedy pathway when exogenous choline is present. IM, inner membrane. (B) Deletion of PC biosynthesis-related genes reduced Cnm1 signal levels. Overexpressed (OE) Cnm1 was tagged with GFP on its C terminus and mitochondria were stained using MitoTracker Orange. Scale bar, 5  $\mu$ m. (C) Reduced levels of Cnm1-GFP (expressed from a strong constitutive promoter) in strains harboring a deletion of *cho2*, *opi3*, or *ino2* can be rescued by addition of choline. Western blot analysis

of four different strains without or with 5mM choline supplementation. Immunoblotting was performed with antibodies against GFP and Histone H3 as a loading control. **(D)** Cnm1 mediated mitochondrial clustering around the nucleus is dependent on choline levels. Cells overexpressing Cnm1 under the *TEF2* promoter and harboring deletion of *cho2*, *opi3*, or *ino2* were grown to mid-logarithmic phase in synthetic minimal medium without or with 5mM choline. The nucleus is visualized by Nsg1-GFP and mitochondria by MitoTracker Orange staining. Scale bar, 5  $\mu$ m. **(E)** Overexpression of Cnm1 using the *TEF2* promoter in strains deleted for proteins involved in PC biosynthesis resulted in a reduced growth rate. Strains were grown overnight in synthetic minimal medium, back diluted to  $OD_{600} \sim 0.05$  and monitored for growth over 48 h. **(F)** Choline buffered the growth defect of overexpressing Cnm1 in strains deleted for genes involved in PC biosynthesis. Strains were grown overnight in synthetic minimal medium, back diluted to  $OD_{600} \sim 0.05$  and monitored for growth over 48 h with or without 5mM choline supplementation.

images also demonstrate that the soluble GFP-Tom70 concentrated around the nuclear membrane in areas that were completely overlapping with the Cnm1-mCherry signal (Fig. 6 E). Moreover, despite the high expression of the cytosolic domain of Tom70 in these cells, there was a complete loss of mitochondrial clustering when Cnm1 was overexpressed (Fig. 6 D).

An additional support for Cnm1 directly binding Tom70 is the presence of an internal mitochondrial targeting signal-like (iMTS-L) sequence in the very C-terminal end of Cnm1 (Schneider et al., 2021; Fig. S5, A and B). Such iMTS-L signals have previously been shown to directly bind Tom70 (Backes et al., 2018). Indeed, a small deletion in this region abrogated the capacity of Cnm1 to increase contact extent (Fig. 6 F) and also resulted in loss of the discrete accumulations of Cnm1 on the nuclear membrane and its homogenous redistribution to the entire nuclear periphery (Fig. 6 F).

To assay the converse interaction, we deleted the predicted membrane-spanning region of Cnm1 (both transmembrane domains [TMDs] in the first 112 aa,  $\Delta$ tmd; Fig. S5 B) and followed its distribution in the cell when tagged with GFP. Indeed, we found that the soluble Cnm1 was no longer on the nuclear periphery but rather was cytosolic, with clear mitochondrial membrane accumulations. These accumulations became even stronger when Tom70 was overexpressed, supporting that recruitment to the mitochondrial OM occurs through Tom70 (Fig. 6 F). What was surprising, however, was that this manipulation of Cnm1 dramatically altered mitochondrial morphology, causing mitochondria to fragment (Fig. S5 C). Since deletion of Cnm1 did not cause this effect, we assume that this is due to buffering of Tom70 binding to its other clients and not loss of Cnm1 activity.

The above experiments highlight the need for Cnm1 to have a Tom70-binding site and for both Cnm1 and Tom70 to be integrated into their respective membranes to enable their tethering function.

## Discussion

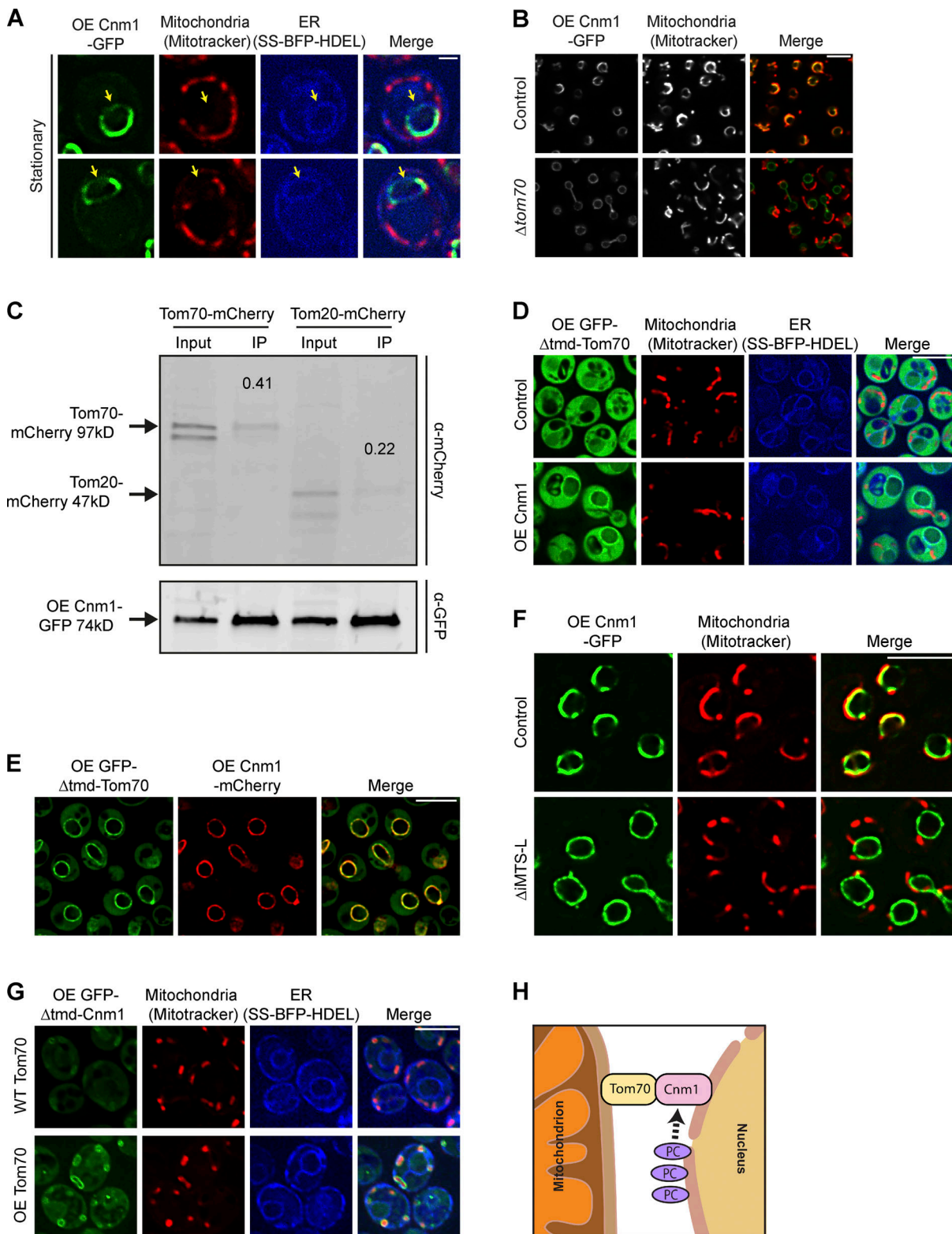
Nuclear-mitochondria communication is one of the hallmarks of eukaryotic cells, underlying the tight coordination between energy supply and cellular needs. While mitochondria were already shown to form close proximities with the nucleus in the late 1960s and early 1970s (Baker and Franchi, 1969; Kessel, 1968; Aikawa et al., 1970; Rowley et al., 1971; Franke et al., 1973), the nature and mechanism of these proximities remained unclear. Over the years, several functions were suggested for the interactions between these two organelles, including a role in fission-yeast mitosis (McCully and Robinow, 1971), ATP transfer in cardiac cells (Dzeja et al., 2002), and heme trafficking in

*S. cerevisiae* (Martinez-Guzman et al., 2020). However, the difficulties in differentiating the ER from the nuclear envelope have made it challenging to directly identify and study the molecular machinery of the contact.

Here, we present a methodology in yeast to clearly distinguish the contact site between the nucleus and mitochondria from the one formed with the ER. We identify the previously uncharacterized Ybr063c/Cnm1 as a new nuclear membrane protein that acts as a specific tether for mitochondria. Together with Tom70 on the mitochondrial membrane, Cnm1 can function to recruit mitochondria specifically to the nuclear ER. We show that Cnm1 levels are regulated by PC, coupling phospholipid biosynthesis with the extent of contact site formation (Fig. 6 H).

For years, it was assumed that every two organelles can form a singular type of contact between them. However, recent evidence suggests that between two organelles, several distinct contact sites can form, each with specific machinery and function. For example, it was recently shown that between mitochondria and the vacuole in yeast, there are two types of contacts: one mediated by Vam6-Tom40, which has a role in the cellular stress response, and the other mediated by Mcp1-Vps13 and has functions that can bypass the loss of the ERMES complex (González Montoro et al., 2018). The two types of vacuole and mitochondria patches are found adjacent to one another, suggesting that both functions are spatially restricted. Similarly, in mammalian cells, several types of ER-plasma membrane contacts have been identified (Besprozvannaya et al., 2018). Our work extends these findings to the contact between mitochondria and the ER. The discovery that Cnm1, a nuclear envelope protein, mediates nuclear ER-specific contacts that are distinct from ERMES-mediated contacts opens a new molecular window to exploring the intricate structure of nuclear envelope/ER and mitochondrial contact sites.

Why would the ER and mitochondria need to maintain two distinct contact sites? The ERMES-mediated ER-mitochondria contact site is known to have a role in metabolism of phospholipids. It was recently shown that Mmm1 and Mdm12 form a heterocomplex, which can mediate the transfer of phospholipids in vitro. Furthermore, mutations in Mmm1 or Mdm12 resulted in impaired phospholipid transfer in vivo (Kawano et al., 2018). Several observations support the idea that PE transport can occur through ERMES (Kundu and Pasrija, 2020); however, in vitro studies showed that PS to PE conversion rate was reduced in ERMES mutants, suggesting that ERMES mediates the transfer of PS from the ER to mitochondria (Kojima et al., 2016). All of these data suggest a role for the ERMES complex in the initial steps of PC production: the conversion of PS to PE to PC.



**Figure 6. Cnm1-mediated contact sites require Tom70.** (A) Cnm1 is an outer nuclear membrane protein. A strain overexpressing Cnm1-GFP (OE Cnm1-GFP) during stationary phase shows areas where Cnm1 is not localized to mitochondria (stained by MitoTracker Orange) but does colocalize with the outer nuclear membrane (nuclear ER) visualized using a BFP with a signal sequence and an ER retention signal (SS-BFP-HDEL). Arrows mark areas where Cnm1-GFP signals colocalize with the nuclear ER signal, but not with the mitochondrial signal. Scale bar, 1  $\mu$ m. (B) Loss of *tom70* results in Cnm1 redistributing uniformly around the nucleus. Shown are strains overexpressing (OE) Cnm1-GFP on the background of  $\Delta tom70$  or control cells, imaged in mid-logarithmic phase using MitoTracker Orange for mitochondrial staining. Scale bar, 5  $\mu$ m. (C) Tom70 physically interacts with Cnm1. Pull-down of overexpressed Cnm1 tagged with GFP on its C terminus in strains expressing either Tom70 or Tom20 tagged with mCherry on their C termini. Coimmunoprecipitation (co-IP) samples were analyzed by



Western blotting and probed with antibodies against GFP and mCherry. Input (10% of total immunoprecipitates) is shown. The number above each immunoprecipitation band represents the enrichment of the protein. **(D)** Overexpression (OE) of Cnm1 results in the accumulation of soluble GFP-Tom70 around the nuclear membrane. Overexpressed Tom70 whose TMD (1–38 aa) has been truncated and is tagged with GFP on its N terminus (OE GFP- $\Delta$ tmd-Tom70) shows cytosolic distribution in control cells. Overexpression of Cnm1 concentrates the soluble Tom70 around the nuclear membrane marked by a BFP with a signal sequence and an ER retention signal (SS-BFP-HDEL). Mitochondria were dyed with MitoTracker Orange. Control and overexpressed Cnm1 strains are adjusted to different intensities. Scale bar, 5  $\mu$ m. **(E)** Overexpressed (OE) GFP- $\Delta$ tmd-Tom70 is fully colocalized with overexpressed Cnm1-mCherry on the nuclear periphery. Scale bar, 5  $\mu$ m. **(F)** Deletion of the predicted iMTS-L sequence of Cnm1 (350–404 aa) abrogates mitochondrial clustering around the nucleus and results in redistribution of Cnm1 over the entire nuclear membrane. Cnm1-GFP (full length or mutant) were expressed under a *TEF2* promoter. Mitochondria are dyed with MitoTracker Orange. Scale bar, 5  $\mu$ m. **(G)** Soluble Cnm1 decorates the mitochondrial OM. Overexpressed Cnm1 truncated at its N terminus by fusion of a GFP molecule to remove its predicted TMD (1–112 aa; OE GFP- $\Delta$ tmd-Cnm1) was expressed in either WT Tom70 cells or cells overexpressing Tom70 (OE Tom70) under the *NOPI* promoter. The nuclear envelope is visualized by a BFP with a signal sequence and an ER retention signal (SS-BFP-HDEL; SS-BFP-HDEL in WT Tom70 and OE Tom70 strains is adjusted to different intensities). Mitochondria are marked by MitoTracker Orange. In control cells, GFP- $\Delta$ tmd-Cnm1 shows cytosolic distribution as well as enrichment around the mitochondrial periphery and no nuclear periphery staining. Overexpression of Tom70 causes an even brighter signal to accumulate around mitochondria, suggesting that its levels are restrictive to Cnm1 recruitment to mitochondrial surfaces. Scale bar, 5  $\mu$ m. **(H)** Schematic working model on Cnm1 activity in mediating nucleus–mitochondria contacts. PC levels regulate Cnm1 abundance in the cell. Cnm1 on the nuclear ER membrane interacts with Tom70 on the mitochondrial membrane.

However, once PC is formed in the nuclear envelope/ER membrane, how does it return to mitochondria, where it makes up more than 40% of its membranes (Sperka-Gottlieb et al., 1988)? We have shown that Cnm1 is regulated by PC levels. In strains deleted for enzymes required for the biosynthesis of PC, levels of Cnm1 are reduced; however, upon the addition of choline, which allows that rescue of PC levels (Carman and Han, 2011), Cnm1 levels are restored. This extends the nucleus–mitochondria contact. It is highly appealing to hypothesize that regulation of Cnm1 levels by PC reflects a role of the nucleus–mitochondrial contact in the transfer of PC from the nuclear envelope/ER, where it is formed, to mitochondria, where it is highly abundant. Interestingly, several PC biosynthesis-related proteins, including the rate-limiting enzyme of the Kennedy pathway Pct1 and the transcriptional regulator Opi1, are enriched in the nuclear ER (Breker et al., 2014; Dubreuil et al., 2019). This suggests that high PC levels may be found specifically in the perinuclear area or that nuclear PC has a regulatory role. However, whether nucleus–mitochondria contacts have indeed a role in the PC transfer to mitochondria remains to be studied. Having the molecular machinery at hand should now make this feasible.

How PC abundance affects Cnm1 levels is still unclear. In our study, Cnm1 was expressed from a constitutive promoter, suggesting that the difference in the levels of Cnm1, observed upon deletion of PC enzymes, is a result of a posttranslational regulatory event. Indeed, other pathways constituents, such as the choline transporter Hnm1, are posttranslationally regulated through phosphorylation and ubiquitination (Fernández-Murray et al., 2013).

An interesting feature of Cnm1 function is that it pairs with Tom70 on the mitochondrial membrane to form the nucleus–mitochondria contact. Tom70 has a well-known role in protein translocation (Dekker et al., 1998) as well as a role in the tubular ER–mitochondria contact site through interactions with Lam6 (Elbaz-Alon et al., 2015; Murley et al., 2015). What would be the cellular benefits of pairing Cnm1 with Tom70, a protein that is already involved in many other interactions? In recent years, several proteins that have roles in protein translocation across organelle membranes were shown to have an additional function as contact site tethers. The ERMES subunit Mdm10 (Kornmann et al., 2009) is also part of the mitochondrial sorting and assembly machinery (SAM; Ellenrieder et al., 2016). The

ER–mitochondria contact site proteins Lam6 and ER membrane protein complex (EMC) were shown to interact with two subunits of the TOM translocon, Tom70 and Tom5, respectively (Murley et al., 2015; Elbaz-Alon et al., 2015; Lahiri et al., 2014). Finally, the vacuole–mitochondria tether Vam6 was shown to interact with Tom40 (González Montoro et al., 2018). Having a limiting amount of proteins that can be used either for translocation or for contact site formation might therefore be a general mechanism to balance between lipid and protein abundance in an organelle.

More broadly, our work opens up a new molecular window into an underexplored contact site in yeast. Cnm1, Tom70, as well as the many other proteins that were highlighted by our screen, can serve as tools to now manipulate the extent of the contact and study its various potential functions. A better understanding of how two information hubs, the nucleus and mitochondria, communicate in healthy cells, should provide us with insights into communication failures in disease.

## Materials and methods

### Yeast strains and plasmids

*S. cerevisiae* strains were based on the laboratory strain BY4741 (Brachmann et al., 1998) or SEY6210.1 (Robinson et al., 1988). Genetic manipulations were performed using the lithium acetate, polyethylene glycol, single-stranded DNA method (Gietz and Woods, 2006). Plasmids for PCR-mediated homologous recombination were previously described (Janke et al., 2004; Longtine et al., 1998), and primers were designed using Primers-4-Yeast (Yofe and Schuldiner, 2014). Table S3 and Table S4 list the plasmids and strains used in this study, respectively. Plasmid pRs316-PGK-CFP-HDEL-URA3 (a blue fluorescent protein [BFP] fused to an ER retrieval sequence) was kindly provided by Prof. J. Goodman (University of Texas Southwestern Medical Center, Dallas, TX). The pESC-NLS-TFP plasmid expressing the nuclear marker (tdTomato conjugated to a nuclear localization signal [NLS]) was kindly provided by Prof. D. Kaganovich (Göttingen University, Göttingen, Germany). The plasmid of pADHpr mtBFP426 (BFP fused to a mitochondrial targeting sequence) was kindly provided by Prof. C. Ungermann (Osnabrück University, Osnabrück, Germany). pBS35 mCherry-HygroR plasmid

(PCR-mediated homologous recombination for C-terminal tagging with mCherry and hygromycin resistance) was kindly provided by Prof. N. Barkai (Weizmann Institute of Science, Rehovot, Israel). pFA6a-His3MX6-GAL1pr plasmid (PCR-mediated homologous recombination for changing a promoter sequence of a gene using the galactose [GAL] promoter with Nourseothricin [NAT] resistance) was kindly provided by Prof. J. Gerst (Weizmann Institute of Science, Rehovot, Israel).

### Culturing of yeast

Yeast cells were cultured overnight at 30°C in synthetic minimal medium (0.67% wt/vol yeast nitrogen base with ammonium sulfate and amino acid supplements) with glucose (2%; SD) or galactose (2%; SGal). The next day, cells were either diluted and grown until reaching mid-logarithmic phase (0.4–0.9 OD<sub>600</sub>) or kept undiluted for experiments performed in stationary phase (1 < OD<sub>600</sub>).

### Manual fluorescence microscopy and organelle staining

Glass-bottom, 384-well microscopy plates (Matrical Bioscience) coated with Concanavalin A (Sigma-Aldrich) were used for imaging. Cells in stationary or mid-logarithmic phase were adhered to the plates by incubating at RT for 15 min and were then washed and imaged in synthetic minimal medium.

For red mitochondrial staining, upon adherence to the plate, media was replaced with media containing 50 nM MitoTracker (MitoTracker Orange CMTMRos; Invitrogen), and cells were incubated at RT for 10 min, washed once, and imaged. For blue mitochondrial staining, upon adherence to the plate, media was replaced with media containing 500 nM MitoView 405 (MitoView 405; Biotium), and cells were incubated at RT for 10 min, washed three times, and imaged in synthetic minimal medium.

Imaging was performed at RT using a VisiScope Confocal Cell Explorer system composed of a Zeiss Yokogawa spinning disk scanning unit (CSU-W1) coupled with an inverted IX83 microscope (Olympus). Single-focal-plane and Z-stack images were acquired with a 60× oil lens (NA 1.4) and were captured using a PCO-Edge sCMOS camera, controlled by VisiView software (GFP [488 nm], RFP [561 nm], or BFP [405 nm]). Manual inspection and brightness adjustment were performed using ImageJ (Schindelin et al., 2012). Overlap analysis for quantification in Fig. 3 was done by the Artificial Intelligence feature of the ScanR Olympus soft imaging solutions version 3.2.

High-resolution imaging was performed at RT using automated inverted fluorescence microscope system (Olympus) harboring a spinning disk high-resolution module (Yokogawa CSU-W1 SoRa confocal scanner with double micro lenses and 50-μm pinholes). Images of cells in the 384-well plates were using a 60× oil lens (NA 1.42) and with a Hamamatsu ORCA-Flash 4.0 camera. Fluorophores were excited by a laser and images were captured in three channels: GFP (excitation wavelength 488 nm, emission filter 525/50 nm), mCherry (excitation wavelength 561 nm, emission filter 617/73 nm) and DAPI (excitation wavelength 405 nm, emission filter 447/60). All images were taken in a Z-stack, and using cellSens software. Best focal plane for presentation, images were deconvoluted using cellSens software.

### Library preparation and high-throughput screening

The synthetic genetic array method was used for integrating the desired genomic manipulations into yeast libraries (Tong and Boone, 2006; Cohen and Schuldiner, 2011). Query strains for screens were constructed on an synthetic genetic array-ready strain (YMS721; Breslow et al., 2008), and libraries were handled using a RoToR bench-top colony array instrument (Singer Instruments). Briefly, query strains were mated with strains from the library on rich medium plates to generate diploid cells. Cells were then transferred to nitrogen starvation media for 7 d to induce sporulation. Haploid cells were selected using canavanine and thialysine (Sigma-Aldrich) lacking leucine to select for MATalpha. The final library was generated by selecting for the combination of manipulations desired. Representative strains from the final library were validated by both microscopy and check-PCR.

For screens described in Fig. 2, screening was performed using an automated, inverted fluorescence microscopic ScanR Olympus soft imaging solutions system (Breker et al., 2013). Images were acquired using a 60× air lens (NA 0.9, GFP [490 nm], and RFP [572 nm]). For the screen described in Fig. 4, libraries were imaged using a Hamamatsu flash orca 4.0 camera and a CSU-W1 Confocal Scanner Unit of Yokogawa with a 50 μm pinhole disk. The software used was ScanR Olympus soft imaging solutions acquisition 3.2, and images were acquired using a 60× air lens (NA 0.9, GFP [488 nm], and RFP [561 nm]). For all screens, libraries were imaged at RT, during mid-logarithmic growth. Images were manually inspected using ImageJ software (Schindelin et al., 2012).

### EM

The Tokuyasu method was used for imaging (Tokuyasu, 1973). In brief, samples were fixed in 0.1% glutaraldehyde (EMS) and 4% paraformaldehyde (EMS) in 0.1 M cacodylate buffer (prepared from dimethylarsinic acid sodium salt trihydrate; Sigma-Aldrich) containing 5 mM CaCl<sub>2</sub> (pH 7.4; Sigma-Aldrich) for 2 h and then washed and embedded in 10% gelatin (EMS) and further fixed for 24 h at 4°C. The samples were then cryoprotected by infiltration with 2.3 M sucrose (J.T. Baker) for 48 h at RT and frozen by plunging into liquid nitrogen. Ultrathin (70–90 nm) frozen sections were obtained with a Leica EM UC7 cryoultramicrotome and then transferred to formvar-coated 200-mesh nickel transmission EM grids (EMS). Grids were washed and embedded in 2% methyl cellulose (Sigma-Aldrich) and 0.4% uranyl acetate (EMS). Images were acquired using a Thermo Fisher Scientific Tecnai T12 transmission electron microscope equipped with a bottom mounted TVIPS TemCam-XF416 4k × 4k CMOS camera.

### Cryoelectron tomography

For cell vitrification, cryo-EM grids (R1.2/1.3, Cu 200 mesh grid; Quantifoil MicroTools) were glow-discharged in a plasma cleaner (PDC-3XG; Harrick) to charge the surface of the carbon film. The grids were then mounted onto a Vitrobot Mark IV (FEI), and 3.5 μl cell culture (0.8 OD<sub>600</sub> in YPD) was deposited on the carbon side of each grid before blotting. Blotting was performed from the back of the grid with filter paper (Whatman

Filter Paper 597; Sigma-Aldrich) at a strength setting of 10 for 10 s. The grids were plunged immediately after into liquid ethane cooled by liquid nitrogen and quickly transferred to a storage Cryo-box. Cryo-boxes were stored in liquid nitrogen until needed.

For cryo-focused ion beam milling, the frozen grids were mounted into Autogrid carriers (FEI) and secured to them with a copper clip ring. The grids were then inserted in a Scios 2 - DualBeam microscope (FEI) under high vacuum and kept at  $-180^{\circ}\text{C}$ . The sample was coated with a thin layer of organometallic platinum using a gas injection system to protect it from unnecessary damage from the focused ion beam.

As many as six clusters of  $<10$  cells were selected as milling positions in each grid. The milling process was done with the  $\text{Ga}^{2+}$  ion beam at an inclination of  $20^{\circ}$  and in sequential steps, from 30 kV and 500 pA for the elimination of most of the material above and below the plane of interest to 30 kV and 30 pA for the final thinning down. The milling progress was monitored by scanning EM imaging at 3 kV and 8.9 pA, and the resulting lamellas were  $\sim 14\ \mu\text{m}$  wide and 150–200 nm thick. The grids were afterwards stored in Cryo-boxes submerged in liquid nitrogen.

For cryoelectron tomography, the grids were loaded into a Polara cryoelectron microscope (FEI) and kept under high vacuum at  $-180^{\circ}\text{C}$ . The microscope was equipped with a 300-kV field emission gun, energy filter (Gatan), and K2 summit direct electron detector (Gatan). Overview pictures of the lamellas were taken at low magnification ( $4,500\times$ ,  $27\ \text{\AA}/\text{pixel}$ , and  $-105\ \mu\text{m}$  defocus) to identify the location of nucleus-mitochondria contact sites. Tilt series were taken at these regions of interest with a unidirectional scheme from  $-54^{\circ}$  to  $45^{\circ}$  in  $3^{\circ}$  steps at high magnification ( $34,000\times$ ,  $3.509\ \text{\AA}/\text{pixel}$ , and  $-5\ \mu\text{m}$  defocus) using SerialEM software (<https://bio3d.colorado.edu/SerialEM/>; RRID SCR\_017293; Mastronarde, 2005). The tilt series images were taken in dose-fractionation mode and constant exposure to obtain a final electron dose of  $\sim 120\text{e}^{-}/\text{\AA}^2$  per tilt series.

For tomogram reconstruction, the different frames that compose each tilt were aligned using TOMOMAN software (<https://github.com/williamnwan/TOMOMAN>; Nickell et al., 2005), and the resulting aligned images were used to create new tilt series. These new tilt series were aligned in IMOD software (<https://bio3d.colorado.edu/imod/>; RRID SCR\_003297; Kremer et al., 1996) using patch tracking, and the tomograms were reconstructed using back-projection. The tomograms were binned to a voxel size of  $14.036\ \text{\AA}$  for better visualization.

For postprocessing, a deconvolution filter ([https://github.com/dtegunov/tom\\_deconv](https://github.com/dtegunov/tom_deconv)) was used to improve contrast in the tomograms.

Computational measurements of contact site extent and 3D segmentation analysis of the tomograms were performed as previously described (Salfer et al., 2020).

### Western blot

Four  $\text{OD}_{600}$  of cells expressing Cnm1 tagged with GFP on a control strain or on the background of  $\Delta\text{cho2}$ ,  $\Delta\text{opi3}$ , or  $\Delta\text{ino2}$ , with or without 5 mM choline supplementation, were grown in SD complete media until reaching mid-logarithmic phase. Cells

were then collected by centrifugation at  $3,000g$  for 3 min, subsequently transferred to a fresh 1.5-ml microcentrifuge tube, and washed with 1 ml nuclease-free water. Cells were resuspended in  $200\ \mu\text{l}$  lysis buffer (8 M urea, 50 mM Tris, pH 7.5, and protease inhibitors; Merck) and subsequently lysed by vortexing at high speed with glass beads (Scientific Industries) at  $4^{\circ}\text{C}$  for 10 min.  $25\ \mu\text{l}$  of 20% SDS was added to each sample before incubation at  $45^{\circ}\text{C}$  for 15 min. The bottom of the microcentrifuge tubes was then pierced, loaded into 5-ml tubes, and centrifuged at  $4,000g$  for 10 min to separate the lysate from the glass beads. The flow-through collected in the 5-ml tubes was transferred to a fresh 1.5-ml microcentrifuge tube and centrifuged at  $20,000g$  for 5 min. The supernatant was collected and 4x SDS-free sample buffer (0.25 M Tris, pH 6.8, 15% glycerol, and 16% Orange G containing 100 mM DTT) was added to the lysates, which were incubated at  $45^{\circ}\text{C}$  for 15 min.

Protein samples were separated by SDS-PAGE using a 4–20% gradient gel (Bio-Rad) and then transferred onto  $0.45\text{-}\mu\text{m}$  nitrocellulose membrane (Pall Corporation) using the Trans-Blot Turbo transfer system (Bio-Rad). Membranes were blocked in SEA BLOCK buffer (Thermo Scientific; diluted 1:5 in PBS) for 1 h at RT and subsequently incubated overnight at  $4^{\circ}\text{C}$  with primary antibodies diluted in a 2% wt/vol BSA/PBS solution containing 0.01%  $\text{NaN}_3$ . Primary antibodies used were rabbit anti-GFP (ab290, 1:3,000; Abcam) and rabbit anti-Histone H3 (ab1791, 1:5,000; Abcam). After washing, membranes were then probed with secondary antibody (800CW Goat anti-Rabbit IgG, ab216773; Abcam) diluted 1:10,000 in 5% wt/vol nonfat milk/Tris-buffered saline with 0.05% Tween 20 (TBST) for 1 h at RT. Blots were washed and imaged on the LI-COR Odyssey Infrared Scanner.

### Coimmunoprecipitation

Yeast overexpressing Cnm1-GFP with either Tom20-mCherry or Tom70-mCherry were grown to mid-logarithmic phase, and a total of five  $\text{OD}_{600}$  were collected by centrifugation and washed once in water. The cell pellets were subsequently resuspended in  $500\ \mu\text{l}$  ice-cold lysis buffer (1% digitonin, 150 mM NaCl, 50 mM Tris-HCl, pH 8.0, 5% glycerol, 1 mM  $\text{MgCl}_2$ , and protease inhibitors; Merck) and transferred to FastPrep tubes containing 1-mm silica spheres (lysing matrix C; MP Biomedicals). The tubes were loaded into a FastPrep24 instrument (MP Biomedicals), and the cells were lysed by six cycles of 1 min beating at maximum speed, followed by 5 min on ice. Lysates were then centrifuged at  $16,000g$  for 10 min at  $4^{\circ}\text{C}$ , and of the  $400\ \mu\text{l}$  cleared lysate, 10% was removed as “input,” which was reduced and denatured by incubation at  $45^{\circ}\text{C}$  for 15 min with Laemmli buffer containing 12.5 mM DTT. The rest of the cleared lysate was used for immunoprecipitation by rotation with  $30\ \mu\text{l}$  washed GFP-Trap (Chromotek) slurry for 1 h at  $4^{\circ}\text{C}$ . The GFP-Trap beads were subsequently washed three times in  $500\ \mu\text{l}$  wash buffer (150 mM NaCl and 50 mM Tris-HCl, pH 8.0), resuspended in  $100\ \mu\text{l}$  2x Laemmli buffer (containing 25 mM DTT), and incubated at  $45^{\circ}\text{C}$  for 15 min before separation by SDS-PAGE. 10% input was loaded relative to the immunoprecipitation samples. Densitometry was performed on Image Studio Lite (LI-COR) software and used to calculate enrichment values.



### Procedures for carbonate extraction (CE)

Isolation of mitochondria from yeast cells was performed by differential centrifugation, as previously described (Daum et al., 1982). On these purified mitochondria, CE was performed. 100  $\mu$ g mitochondria was purified from a strain overexpressing 3HA-Ybr063c from its genomic locus and resuspended in 100  $\mu$ l of 200 mM sodium carbonate ( $\text{Na}_2\text{CO}_3$ ), followed by 30 min incubation at 4°C. Supernatant and pellet fractions representing soluble and membrane-embedded proteins, respectively, were obtained by centrifugation (80,000g, 30 min, 4°C). Proteins from the supernatant were extracted by TCA precipitation. TCA was added to final concentration of 12% (wt/vol), and the mixture was incubated for 30 min at 4°C followed by centrifugation (36,800g, 15 min, 2°C). The pellet was washed with 100  $\mu$ l 90% acetone. The mixture was centrifuged again (36,700g, 5 min, 2°C), and the pellet containing the proteins was dried at 40°C before analysis. For analysis, both fractions were resuspended in 40  $\mu$ l of 2x Laemmli buffer, heated for 10 min at 95°C, and analyzed by SDS-PAGE and immunoblotting. Protein samples for immune decoration were analyzed on 12.5% SDS-PAGE and subsequently transferred onto nitrocellulose membranes by semi-dry Western blotting. Proteins were detected by blocking the membrane with 5% milk and subsequently incubating them with primary antibodies (either polyclonal rat anti-HA diluted 1:1,000, polyclonal rabbit anti-Tom20 diluted 1:5,000, or polyclonal rabbit anti-Hep1 diluted 1:3,000) and then with horseradish peroxidase conjugates of goat anti-rabbit secondary antibody.

### Spot assay

Serial dilutions were grown on synthetic minimal medium with either glucose or galactose supplementation. Cells were grown overnight in 2% galactose media containing their respective selections. They were back diluted to an  $\text{OD}_{600} = 0.2$  in 2% galactose media and incubated for ~6 h at 30°C. After at least one cell division or after reaching mid-logarithmic phase, strains were back diluted again to  $\text{OD}_{600} = 0.1$  and then diluted in 10-fold increments. Next, 2.5  $\mu$ l of each dilution was plated using a multichannel pipette (Gilson) on SD and SGal agar plates, both containing all amino acids. Plates were imaged using Canon PC1591 digital camera after 3 d of growth at 30°C.

### Growth assay

The growth assays were performed using a Spark (Tecan) plate reader. Transparent 96-well plates (Greiner) were used. Cells were grown in an incubator (Liconic) at 30°C and shaking at 500 rpm. Samples were measured every 30 min following a strong resuspension on a plate shaker (bioshake 3000) at 1,200 rpm. OD was measured at 600 nm wavelength.

### PC supplementation

PC supplementation was performed as previously described (Grant et al., 2001), with some modifications. Cells were grown to a logarithmic phase in synthetic minimal medium at 30°C and then transferred to 4°C for 15 min. 1 mM of 1-myristoyl-2-{6-[(7-nitro-2-1,3-benzoxadiazol-4-yl)amino]hexanoyl}-sn-glycero-3-phosphocholine (NBD-PC; Sigma-Aldrich) diluted in DMSO was added to the cells while the plate was on ice, and after 15 min, cells were imaged as described above.

### Statistical analysis

Statistical analysis was done using two-tailed Student's *t* tests. Bars represent standard deviation. Data distribution was assumed to be normal, but this was not formally tested.

### Online supplemental material

Fig. S1 shows overexpression of the ERMES complex subunit Mdm34 does not extend the nucleus-mitochondria contact. Fig. S2 shows that Ybr063c (Cnm1) does not affect the ERMES complex and is only partially colocalized with its subunits. Fig. S3 shows that mitochondrial clustering around the nucleus mediated by overexpressing Cnm1 is ERMES independent. Fig. S4 shows that choline addition rescues Cnm1 levels in cells harboring mutation in PC biosynthesis-related genes. Fig. S5 shows that domain architecture of Cnm1 and the effect of losing its TMD on mitochondrial morphology. Table S1 lists all mCherry-tagged proteins that fully or partially colocalized with the nucleus-mitochondria contact site reporter from Fig. 2. Table S2 lists all genes whose deletions altered Cnm1-mediated clustering of mitochondria around the nucleus from Fig. 4. Table S3 lists the plasmids used in this study. Table S4 lists the yeast strains used in this study. Video 1 shows time-lapse imaging of the effect of activating Ybr063c expression from a GAL promoter.

### Acknowledgments

EM studies were conducted at the Irving and Cherna Moskowitz Center for Nano and Bio-Nano Imaging at the Weizmann Institute of Science. Cryoelectron tomography was carried out at the Max Planck Institute of Biochemistry, Germany. We thank Wolfgang Baumeister and Jürgen Plitzko for providing access to cryoelectron tomography infrastructure, as well as Philipp Erdmann and Miroslava Schaffer for cryoelectron tomography support. We are grateful to Profs. Christian Ungermann (Osnabrück University, Osnabrück, Germany), Daniel Kaganovich (Göttingen University, Göttingen, Germany), Joel Goodman (University of Texas Southwestern Medical Center, Dallas, TX), Naama Barkai (Weizmann Institute of Science, Rehovot, Israel), and Jeffrey Gerst (Weizmann Institute of Science, Rehovot, Israel) for kindly sharing plasmids. We are grateful to Prof. Tim Levine and Dr. Gat Krieger for helpful discussions. We thank Dr. Einat Zalckvar for critical reading of the manuscript.

M. Eisenberg-Bord was funded by an Azrieli Foundation PhD fellowship. L. Drwesh was supported by a Minerva Foundation long-term fellowship. E.J. Fenech was supported by a Weizmann Institute of Science Dean of Faculty Fellowship. Y. Bykov was supported by an EMBO long-term postdoctoral fellowship. This work was supported by several collaborative grants, including Deutsche Forschungsgemeinschaft (SFB1190 to R. Fernandez Busnadiego and M. Schuldiner), the Deutsch-Israelische Projektkooperation (collaborative grant 2585/1-1 to D. Rapaport and M. Schuldiner), and the German Israeli Foundation (collaborative grant I-1458-412.13/2018 to D. Rapaport and M. Schuldiner). J. Collado and R. Fernandez Busnadiego acknowledge funding from Germany's Excellence Strategy (EXC 2067/1- 390729940). Research in the Rapaport laboratory is supported by the Deutsche Forschungsgemeinschaft (grant RA 1028/7-2). The Schuldiner

laboratory is kindly supported by the Hadar Impact Fund and the Edmond de Rothschild Foundations. The high-throughput microscopy system of the Schuldiner laboratory was purchased through kind support of the Blythe Brenden-Mann Foundation. M. Schuldiner is an Incumbent of the Dr. Gilbert Omenn and Martha Darling Professorial Chair in Molecular Genetics.

The authors declare no competing financial interests.

Author contributions: M. Eisenberg-Bord, N. Zung, J. Collado, L. Drwesh, E.J. Fenech, A. Fadel, N. Dezorella, and Y. Bykov performed the experiments; M. Eisenberg-Bord, N. Zung, and M. Schuldiner wrote the manuscript; all authors read the manuscript and provided feedback; and D. Rapaport, R. Fernandez Busnadiego, and M. Schuldiner supervised the work.

Submitted: 22 April 2021

Revised: 12 August 2021

Accepted: 21 September 2021

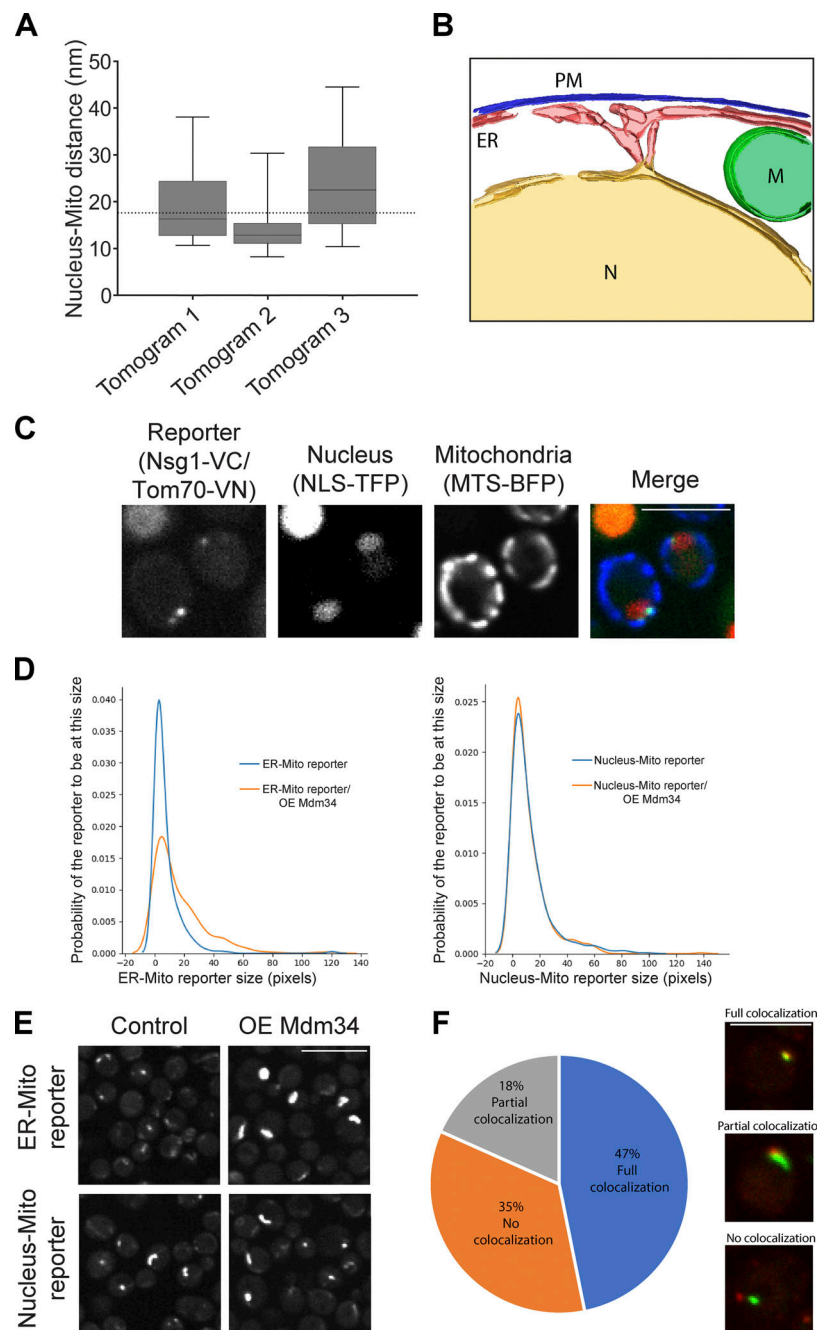
## References

- Aikawa, M., C.G. Huff, and C.P.A. Strome. 1970. Morphological study of microgametogenesis of *Leucocytozoon simondi*. *J. Ultrastruct. Res.* 32: 43–68. [https://doi.org/10.1016/S0022-5320\(70\)80037-5](https://doi.org/10.1016/S0022-5320(70)80037-5)
- Atkinson, K., S. Fogel, and S.A. Henry. 1980. Yeast mutant defective in phosphatidylserine synthesis. *J. Biol. Chem.* 255:6653–6661. [https://doi.org/10.1016/S0021-9258\(18\)43619-8](https://doi.org/10.1016/S0021-9258(18)43619-8)
- Backes, S., S. Hess, F. Boos, M.W. Woellhaf, S. Gödel, M. Jung, T. Mühlhaus, and J.M. Herrmann. 2018. Tom70 enhances mitochondrial preprotein import efficiency by binding to internal targeting sequences. *J. Cell Biol.* 217:1369–1382. <https://doi.org/10.1083/jcb.201708044>
- Baker, T.G., and L.L. Franchi. 1969. The origin of cytoplasmic inclusions from the nuclear envelope of mammalian oocytes. *Z. Zellforsch. Mikrosk. Anat.* 93:45–55. <https://doi.org/10.1007/BF00325022>
- Bernhard, W., and C. Rouiller. 1956. Close topographical relationship between mitochondria and ergastoplasm of liver cells in a definite phase of cellular activity. *J. Biophys. Biochem. Cytol.* 2(4, Suppl):73–78. <https://doi.org/10.1083/jcb.2.4.73>
- Bernhard, W., F. Haguenu, A. Gautier, and C. Oberling. 1952. [Submicroscopical structure of cytoplasmic basophils in the liver, pancreas and salivary gland; study of ultrafine slices by electron microscope]. *Z. Zellforsch. Mikrosk. Anat.* 37:281–300. <https://doi.org/10.1007/BF00343816>
- Besprozvannaya, M., E. Dickson, H. Li, K.S. Ginburg, D.M. Bers, J. Auwerx, and J. Nunnari. 2018. GRAM domain proteins specialize functionally distinct ER-PM contact sites in human cells. *eLife.* 7:e31019. <https://doi.org/10.7554/eLife.31019>
- Boos, F., L. Krämer, C. Groh, F. Jung, P. Haberkant, F. Stein, F. Wollweber, A. Gackstatter, E. Zöller, M. van der Laan, et al. 2019. Mitochondrial protein-induced stress triggers a global adaptive transcriptional programme. *Nat. Cell Biol.* 21:442–451. <https://doi.org/10.1038/s41556-019-0294-5>
- Brachmann, C.B., A. Davies, G.J. Cost, E. Caputo, J. Li, P. Hieter, J.D. Boeke, C.B. Brachmann, A. Davies, et al. 1998. Designer deletion strains derived from *Saccharomyces cerevisiae* S288C: a useful set of strains and plasmids for PCR-mediated gene disruption and other applications. *Yeast.* 14:115–132. [https://doi.org/10.1002/\(SICI\)1097-0061\(19980130\)14:2<115::AID-YEA204>3.0.CO;2-2](https://doi.org/10.1002/(SICI)1097-0061(19980130)14:2<115::AID-YEA204>3.0.CO;2-2)
- Breker, M., M. Gymrek, and M. Schuldiner. 2013. A novel single-cell screening platform reveals proteome plasticity during yeast stress responses. *J. Cell Biol.* 200:839–850. <https://doi.org/10.1083/jcb.201301120>
- Breker, M., M. Gymrek, O. Moldavski, and M. Schuldiner. 2014. LoQATE--Localization and Quantitation Atlas of the yeast proteome. A new tool for multiparametric dissection of single-protein behavior in response to biological perturbations in yeast. *Nucleic Acids Res.* 42(D1):D726–D730. <https://doi.org/10.1093/nar/gkt933>
- Breslow, D.K., D.M. Cameron, S.R. Collins, M. Schuldiner, J. Stewart-Ornstein, H.W. Newman, S. Braun, H.D. Madhani, N.J. Krogan, and J.S. Weissman. 2008. A comprehensive strategy enabling high-resolution functional analysis of the yeast genome. *Nat. Methods.* 5:711–718. <https://doi.org/10.1038/nmeth.1234>
- Brix, J., G.A. Ziegler, K. Dietmeier, J. Schneider-Mergener, G.E. Schulz, and N. Pfanner. 2000. The mitochondrial import receptor Tom70: identification of a 25 kDa core domain with a specific binding site for preproteins. *J. Mol. Biol.* 303:479–488. <https://doi.org/10.1006/jmbi.2000.4120>
- Carman, G.M., and G.S. Han. 2011. Regulation of phospholipid synthesis in the yeast *Saccharomyces cerevisiae*. *Annu. Rev. Biochem.* 80:859–883. <https://doi.org/10.1146/annurev-biochem-060409-092229>
- Cohen, Y., and M. Schuldiner. 2011. Advanced methods for high-throughput microscopy screening of genetically modified yeast libraries. *Methods Mol. Biol.* 781:127–159. [https://doi.org/10.1007/978-1-61779-276-2\\_8](https://doi.org/10.1007/978-1-61779-276-2_8)
- Collado, J., and R. Fernández-Busnadiego. 2017. Deciphering the molecular architecture of membrane contact sites by cryo-electron tomography. *Biochim. Biophys. Acta Mol. Cell Res.* 1864:1507–1512. <https://doi.org/10.1016/j.bbamcr.2017.03.009>
- Collado, J., M. Kalemánov, F. Campelo, C. Bourgoing, F. Thomas, R. Loewith, A. Martínez-Sánchez, W. Baumeister, C.J. Stefan, and R. Fernández-Busnadiego. 2019. Tricalbin-Mediated Contact Sites Control ER Curvature to Maintain Plasma Membrane Integrity. *Dev. Cell.* 51:476–487.e7. <https://doi.org/10.1016/j.devcel.2019.10.018>
- Copeland, D.E., and A.J. Dalton. 1959. An association between mitochondria and the endoplasmic reticulum in cells of the pseudobranch gland of a teleost. *J. Biophys. Biochem. Cytol.* 5:393–396. <https://doi.org/10.1083/jcb.5.3.393>
- Daum, G., P.C. Böhni, and G. Schatz. 1982. Import of proteins into mitochondria. Cytochrome b2 and cytochrome c peroxidase are located in the intermembrane space of yeast mitochondria. *J. Biol. Chem.* 257: 13028–13033. [https://doi.org/10.1016/S0021-9258\(18\)33617-2](https://doi.org/10.1016/S0021-9258(18)33617-2)
- Dekker, P.J.T., M.T. Ryan, J. Brix, H. Müller, A. Hönlinger, and N. Pfanner. 1998. Preprotein translocase of the outer mitochondrial membrane: molecular dissection and assembly of the general import pore complex. *Mol. Cell Biol.* 18:6515–6524. <https://doi.org/10.1128/MCB.18.11.6515>
- Desai, R., D.A. East, L. Hardy, D. Faccenda, M. Rigon, J. Crosby, M.S. Alvarez, A. Singh, M. Maimenti, L.K. Hussey, et al. 2020. Mitochondria form contact sites with the nucleus to couple prosurvival retrograde response. *Sci. Adv.* 6:eabc9955. <https://doi.org/10.1126/sciadv.abc9955>
- Dubreuil, B., E. Sass, Y. Nadav, M. Heidenreich, J.M. Georgeson, U. Weill, Y. Duan, M. Meurer, M. Schuldiner, M. Knop, and E.D. Levy. 2019. YeastRGB: comparing the abundance and localization of yeast proteins across cells and libraries. *Nucleic Acids Res.* 47(D1):D1245–D1249. <https://doi.org/10.1093/nar/gky941>
- Dyall, S.D., M.T. Brown, and P.J. Johnson. 2004. Ancient invasions: from endosymbionts to organelles. *Science.* 304:253–257. <https://doi.org/10.1126/science.1094884>
- Dzeja, P.P., R. Bortolon, C. Perez-Terzic, E.L. Holmuhamedov, and A. Terzic. 2002. Energetic communication between mitochondria and nucleus directed by catalyzed phosphotransfer. *Proc. Natl. Acad. Sci. USA.* 99: 10156–10161. <https://doi.org/10.1073/pnas.152259999>
- Eisenberg-Bord, M., and M. Schuldiner. 2017a. Mitochondria - If only we could be a fly on the cell wall. *Biochim. Biophys. Acta Mol. Cell Res.* 1864: 1469–1480. <https://doi.org/10.1016/j.bbamcr.2017.04.012>
- Eisenberg-Bord, M., and M. Schuldiner. 2017b. Ground control to major TOM: mitochondria-nucleus communication. *FEBS J.* 284:196–210. <https://doi.org/10.1111/febs.13778>
- Eisenberg-Bord, M., N. Shai, M. Schuldiner, and M. Bohnert. 2016. A Tether Is a Tether: Tethering at Membrane Contact Sites. *Dev. Cell.* 39:395–409. <https://doi.org/10.1016/j.devcel.2016.10.022>
- Elbaz-Alon, Y., E. Rosenfeld-Gur, V. Shinder, A.H. Futerman, T. Geiger, and M. Schuldiner. 2014. A dynamic interface between vacuoles and mitochondria in yeast. *Dev. Cell.* 30:95–102. <https://doi.org/10.1016/j.devcel.2014.06.007>
- Elbaz-Alon, Y., M. Eisenberg-Bord, V. Shinder, S.B. Stiller, E. Shimoni, N. Wiedemann, T. Geiger, and M. Schuldiner. 2015. Lam6 Regulates the Extent of Contacts between Organelles. *Cell Rep.* 12:7–14. <https://doi.org/10.1016/j.celrep.2015.06.022>
- Ellenrieder, L., Ł. Opaliński, L. Becker, V. Krüger, O. Mirus, S.P. Straub, K. Ebell, N. Flinner, S.B. Stiller, B. Guiard, et al. 2016. Separating mitochondrial protein assembly and endoplasmic reticulum tethering by selective coupling of Mdm10. *Nat. Commun.* 7:13021. <https://doi.org/10.1038/ncomms13021>
- Endo, T., Y. Tamura, and S. Kawano. 2018. Phospholipid transfer by ERMES components. *Aging (Albany NY).* 10:528–529. <https://doi.org/10.18632/aging.101434>
- English, J., J.M. Son, M.D. Cardamone, C. Lee, and V. Perissi. 2020. Decoding the rosetta stone of mitonuclear communication. *Pharmacol. Res.* 161: 105161. <https://doi.org/10.1016/j.phrs.2020.105161>
- Fernández-Murray, J.P., M.H. Ngo, and C.R. McMaster. 2013. Choline transport activity regulates phosphatidylcholine synthesis through choline transporter Hnml stability. *J. Biol. Chem.* 288:36106–36115. <https://doi.org/10.1074/jbc.M113.499855>



- Franke, W.W., H. Zentgraf, and U. Scheer. 1973. Membrane linkages at the nuclear envelope. *Cytobiologie*. 7:89–100.
- Gatta, A.T., L.H. Wong, Y.Y. Sere, D.M. Calderón-Noreña, S. Cockcroft, A.K. Menon, and T.P. Levine. 2015. A new family of StART domain proteins at membrane contact sites has a role in ER-PM sterol transport. *eLife*. 4: e07253. <https://doi.org/10.7554/eLife.07253>
- Giaever, G., A.M. Chu, L. Ni, C. Connelly, L. Riles, S. Véronneau, S. Dow, A. Lucau-Danila, K. Anderson, B. André, et al. 2002. Functional profiling of the *Saccharomyces cerevisiae* genome. *Nature*. 418:387–391. <https://doi.org/10.1038/nature00935>
- Gietz, R.D., and R.A. Woods. 2006. Yeast transformation by the LiAc/SS Carrier DNA/PEG method. *Methods Mol. Biol.* 313:107–120. <https://doi.org/10.1385/1-59259-958-3:107>
- González Montoro, A., K. Auffarth, C. Hönscher, M. Bohnert, T. Becker, B. Warscheid, F. Reggiori, M. van der Laan, F. Fröhlich, and C. Ungermann. 2018. Vps39 Interacts with Tom40 to Establish One of Two Functionally Distinct Vacuole-Mitochondria Contact Sites. *Dev. Cell*. 45: 621–636.e7. <https://doi.org/10.1016/j.devcel.2018.05.011>
- Grant, A.M., P.K. Hanson, L. Malone, and J.W. Nichols. 2001. NBD-labeled phosphatidylcholine and phosphatidylethanolamine are internalized by transbilayer transport across the yeast plasma membrane. *Traffic*. 2: 37–50. <https://doi.org/10.1034/j.1600-0854.2001.020106.x>
- Janke, C., M.M. Magiera, N. Rathfelder, C. Taxis, S. Reber, H. Maekawa, A. Moreno-Borchart, G. Doenges, E. Schwob, E. Schiebel, and M. Knop. 2004. A versatile toolbox for PCR-based tagging of yeast genes: new fluorescent proteins, more markers and promoter substitution cassettes. *Yeast*. 21:947–962. <https://doi.org/10.1002/yea.1142>
- Kawano, S., Y. Tamura, R. Kojima, S. Bala, E. Asai, A.H. Michel, B. Kornmann, I. Riezman, H. Riezman, Y. Sakae, et al. 2018. Structure-function insights into direct lipid transfer between membranes by Mmm1-Mdm12 of ERMES. *J. Cell Biol.* 217:959–974. <https://doi.org/10.1083/jcb.201704119>
- Kessel, R.G. 1968. An electron microscope study of differentiation and growth in oocytes of *Ophioderma panamensis*. *J. Ultrastruct. Res.* 22:63–89. [https://doi.org/10.1016/S0022-5320\(68\)90050-6](https://doi.org/10.1016/S0022-5320(68)90050-6)
- Kojima, R., T. Endo, and Y. Tamura. 2016. A phospholipid transfer function of ER-mitochondria encounter structure revealed in vitro. *Sci. Rep.* 6: 30777. <https://doi.org/10.1038/srep30777>
- Kornmann, B., E. Currie, S.R. Collins, M. Schuldiner, J. Nunnari, J.S. Weissman, and P. Walter. 2009. An ER-mitochondria tethering complex revealed by a synthetic biology screen. *Science*. 325:477–481. <https://doi.org/10.1126/science.1175088>
- Kremer, J.R., D.N. Mastronarde, and J.R. McIntosh. 1996. Computer visualization of three-dimensional image data using IMOD. *J. Struct. Biol.* 116: 71–76. <https://doi.org/10.1006/jjsbi.1996.0013>
- Kundu, D., and R. Pasirja. 2020. The ERMES (Endoplasmic Reticulum and Mitochondria Encounter Structures) mediated functions in fungi. *Mitochondrion*. 52:89–99. <https://doi.org/10.1016/j.mito.2020.02.010>
- Lahiri, S., J.T. Chao, S. Tavassoli, A.K.O. Wong, V. Choudhary, B.P. Young, C.J.R. Loewen, and W.A. Prinz. 2014. A conserved endoplasmic reticulum membrane protein complex (EMC) facilitates phospholipid transfer from the ER to mitochondria. *PLoS Biol.* 12:e1001969. <https://doi.org/10.1371/journal.pbio.1001969>
- Lee, C., J. Zeng, B.G. Drew, T. Sallam, A. Martin-Montalvo, J. Wan, S.J. Kim, H. Mehta, A.L. Hevener, R. de Cabo, and P. Cohen. 2015. The mitochondrial-derived peptide MOTS-c promotes metabolic homeostasis and reduces obesity and insulin resistance. *Cell Metab.* 21:443–454. <https://doi.org/10.1016/j.cmet.2015.02.009>
- Longtine, M.S., A. McKenzie III, D.J. Demarini, N.G. Shah, A. Wach, A. Brachat, P. Philippsen, and J.R. Pringle. 1998. Additional modules for versatile and economical PCR-based gene deletion and modification in *Saccharomyces cerevisiae*. *Yeast*. 14:953–961. [https://doi.org/10.1002/\(SICI\)1097-0061\(199807\)14:10<953::AID-YEA293>3.0.CO;2-U](https://doi.org/10.1002/(SICI)1097-0061(199807)14:10<953::AID-YEA293>3.0.CO;2-U)
- Martínez-Guzmán, O., M.M. Willoughby, A. Saini, J.V. Dietz, I. Bohovych, A.E. Medlock, O. Khalimonchuk, and A.R. Reddi. 2020. Mitochondrial-nuclear heme trafficking in budding yeast is regulated by GTPases that control mitochondrial dynamics and ER contact sites. *J. Cell Sci.* 133: jcs237917. <https://doi.org/10.1242/jcs.237917>
- Mastronarde, D.N. 2005. Automated electron microscope tomography using robust prediction of specimen movements. *J. Struct. Biol.* 152:36–51. <https://doi.org/10.1016/j.jsb.2005.07.007>
- McCully, E.K., and C.F. Robinow. 1971. Mitosis in the fission yeast *Schizosaccharomyces pombe*: a comparative study with light and electron microscopy. *J. Cell Sci.* 9:475–507. <https://doi.org/10.1242/jcs.9.2.475>
- Mello, T., I. Simeone, and A. Galli. 2019. Mito-Nuclear Communication in Hepatocellular Carcinoma Metabolic Rewiring. *Cells*. 8:417. <https://doi.org/10.3390/cells8050417>
- Mohrin, M., J. Shin, Y. Liu, K. Brown, H. Luo, Y. Xi, C.M. Haynes, and D. Chen. 2015. A mitochondrial UPR-mediated metabolic checkpoint regulates hematopoietic stem cell aging. *Science*. 347:1374–1377.
- Murley, A., R.D. Sarsam, A. Toulmay, J. Yamada, W.A. Prinz, and J. Nunnari. 2015. Tlcl1 is an ER-localized sterol transporter and a component of ER-mitochondria and ER-vacuole contacts. *J. Cell Biol.* 209:539–548. <https://doi.org/10.1083/jcb.201502033>
- Nickell, S., F. Förster, A. Linaroudis, W.D. Net, F. Beck, R. Hegerl, W. Baumeister, and J.M. Plitzko. 2005. TOM software toolbox: acquisition and analysis for electron tomography. *J. Struct. Biol.* 149:227–234. <https://doi.org/10.1016/j.jsb.2004.10.006>
- Reynolds, J.C., C.P. Bwiza, and C. Lee. 2020. Mitonuclear genomics and aging. *Hum. Genet.* 139:381–399. <https://doi.org/10.1007/s00439-020-02119-5>
- Robinson, J.S., D.J. Klionsky, L.M. Banta, and S.D. Emr. 1988. Protein sorting in *Saccharomyces cerevisiae*: isolation of mutants defective in the delivery and processing of multiple vacuolar hydrolases. *Mol. Cell. Biol.* 8: 4936–4948. <https://doi.org/10.1128/MCB.8.11.4936>
- Rowley, M.J., J.D. Berlin, and C.G. Heller. 1971. The ultrastructure of four types of human spermatogonia. *Z. Zellforsch. Mikrosk. Anat.* 112:139–157. <https://doi.org/10.1007/BF00331837>
- Salfer, M., J.F. Collado, W. Baumeister, R. Fernández-Busnadiego, and A. Martínez-Sánchez. 2020. Reliable estimation of membrane curvature for cryo-electron tomography. *PLOS Comput. Biol.* 16:e1007962. <https://doi.org/10.1371/journal.pcbi.1007962>
- Schindelin, J., I. Arganda-Carreras, E. Frise, V. Kaynig, M. Longair, T. Pietzsch, S. Preibisch, C. Rueden, S. Saalfeld, B. Schmid, et al. 2012. Fiji: an open-source platform for biological-image analysis. *Nat. Methods*. 9: 676–682. <https://doi.org/10.1038/nmeth.2019>
- Schneider, Kevin, David Zimmer, Henrik Nielsen, Johannes M Herrmann, and Timo Mühlhaus. 2021. iMLP, a predictor for internal matrix targeting-like sequences in mitochondrial proteins. *Biol. Chem.* 402(8): 937–943. <https://doi.org/10.1515/hsz-2021-0185>
- Scorrano, L., M.A. De Matteis, S. Emr, F. Giordano, G. Hajnóczky, B. Kornmann, L.L. Lackner, T.P. Levine, L. Pellegrini, K. Reinisch, et al. 2019. Coming together to define membrane contact sites. *Nat. Commun.* 10: 1287. <https://doi.org/10.1038/s41467-019-09253-3>
- Shai, N., E. Yifrach, C.W.T. van Roermund, N. Cohen, C. Bibi, L. IJlst, L. Cavellini, J. Meuris, R. Schuster, L. Zada, et al. 2018. Systematic mapping of contact sites reveals tethers and a function for the peroxisome-mitochondria contact. *Nat. Commun.* 9:1761. <https://doi.org/10.1038/s41467-018-03957-8>
- Sperka-Gottlieb, C.D.M., A. Hermetter, F. Paltauf, and G. Daum. 1988. Lipid topology and physical properties of the outer mitochondrial membrane of the yeast, *Saccharomyces cerevisiae*. *Biochim. Biophys. Acta.* 946:227–234.
- Tokuyasu, K.T. 1973. A technique for ultracytometry of cell suspensions and tissues. *J. Cell Biol.* 57:551–565. <https://doi.org/10.1083/jcb.57.2.551>
- Tong, A.H.Y., and C. Boone. 2006. Synthetic genetic array analysis in *Saccharomyces cerevisiae*. *Methods Mol. Biol.* 313:171–192.
- Weill, U., I. Yofe, E. Sass, B. Stynen, D. Davidi, J. Natarajan, R. Ben-Menachem, Z. Avihou, O. Goldman, N. Harpaz, et al. 2018. Genome-wide SWAp-Tag yeast libraries for proteome exploration. *Nat. Methods*. 15: 617–622. <https://doi.org/10.1038/s41592-018-0044-9>
- Weill, U., N. Cohen, A. Fadel, S. Ben-Dor, and M. Schuldiner. 2019. Protein Topology Prediction Algorithms Systematically Investigated in the Yeast *Saccharomyces cerevisiae*. *BioEssays*. 41:e1800252. <https://doi.org/10.1002/bies.201800252>
- Wu, Y., and B. Sha. 2006. Crystal structure of yeast mitochondrial outer membrane translocon member Tom70p. *Nat. Struct. Mol. Biol.* 13: 589–593. <https://doi.org/10.1038/nsmb1106>
- Xia, M., Y. Zhang, K. Jin, Z. Lu, Z. Zeng, and W. Xiong. 2019. Communication between mitochondria and other organelles: a brand-new perspective on mitochondria in cancer. *Cell Biosci.* 9:27. <https://doi.org/10.1186/s13578-019-0289-8>
- Yi, H.S. 2019. Implications of mitochondrial unfolded protein response and mitokines: A perspective on fatty liver diseases. *Endocrinol. Metab. (Seoul)*. 34:39–46. <https://doi.org/10.3803/EnM.2019.34.1.39>
- Yofe, I., and M. Schuldiner. 2014. Primers-4-Yeast: a comprehensive web tool for planning primers for *Saccharomyces cerevisiae*. *Yeast*. 31:77–80. <https://doi.org/10.1002/yea.2998>
- Zung, N., and M. Schuldiner. 2020. New horizons in mitochondrial contact site research. *Biol. Chem.* 401:793–809. <https://doi.org/10.1515/hsz-2020-0133>

## Supplemental material



**Figure S1. Overexpression of the ERMES complex does not extend nucleus-mitochondria contacts.** **(A)** Quantitation of the distances (nanometers) between the nuclear and mitochondrial membranes in a SEY6210.1 strain as determined by three different tomograms. The boxes represent the interquartile range of distance measurements per tomogram (tomogram 1:  $n = 27,743$ ; tomogram 2:  $n = 40,401$ ; tomogram 3:  $n = 9,509$ ); bars mark 0.95 and 0.05 percentiles. The line at the center of the box represents the median. The dotted line represents the mean distance of all three samples. **(B)** 3D segmentation of the nucleus-mitochondria contact in yeast based on the tomogram in Fig. 1 B. M, mitochondrion; N, nucleus; PM, plasma membrane. **(C)** The nucleus-mitochondria reporter Nsg1-VC/Tom70-VN correctly identifies proximities between the two organelles. Nuclei are visualized by the red fluorophore (tdTomato) fused to a nuclear localization signal (NLS-TFP). Mitochondria are visualized by a BFP fused to a mitochondrial targeting sequence (MTS-BFP). The fluorescent signal of the reporter is only localized to areas of proximity between mitochondria and the nucleus. Scale bar, 5  $\mu\text{m}$ . **(D)** Quantitation of either the nucleus-mitochondria reporter (Nsg1-VN/Tom70-VC) or the ER-mitochondria reporter (Tom70-VN/Pho88-VC) sizes in control strains or those overexpressing Mdm34 (OE Mdm34) N terminally tagged with mCherry. The reporter sizes were determined by the number of pixels of the reporter signal using ScanR Olympus soft imaging solutions version 3.2. While Mdm34 overexpression affects the ER-mitochondria reporter, it does not alter the nucleus-mitochondria one. **(E)** An example of the effect of overexpressing Mdm34 N terminally tagged with mCherry on the background of the two reporters in D. Scale bar, 5  $\mu\text{m}$ . **(F)** Statistical analysis of colocalization between the nucleus-mitochondria contact reporter and the ERMES subunit Mmm1 tagged with mKate on its C terminus. Cells were imaged in stationary phase, and colocalization events were counted manually using a cell counter plugin in ImageJ (Schindelin et al., 2012). Full colocalization was denoted in cases where both punctate signals were completely overlapping (see top image), partial colocalization was designated if the Mmm1 signal only colocalized with a small fraction of the reporter signal (see middle image), whereas no colocalization was scored when the reporter did not overlap any Mmm1 signal whatsoever (see bottom image). Scale bar, 5  $\mu\text{m}$ ;  $n = 400$ .

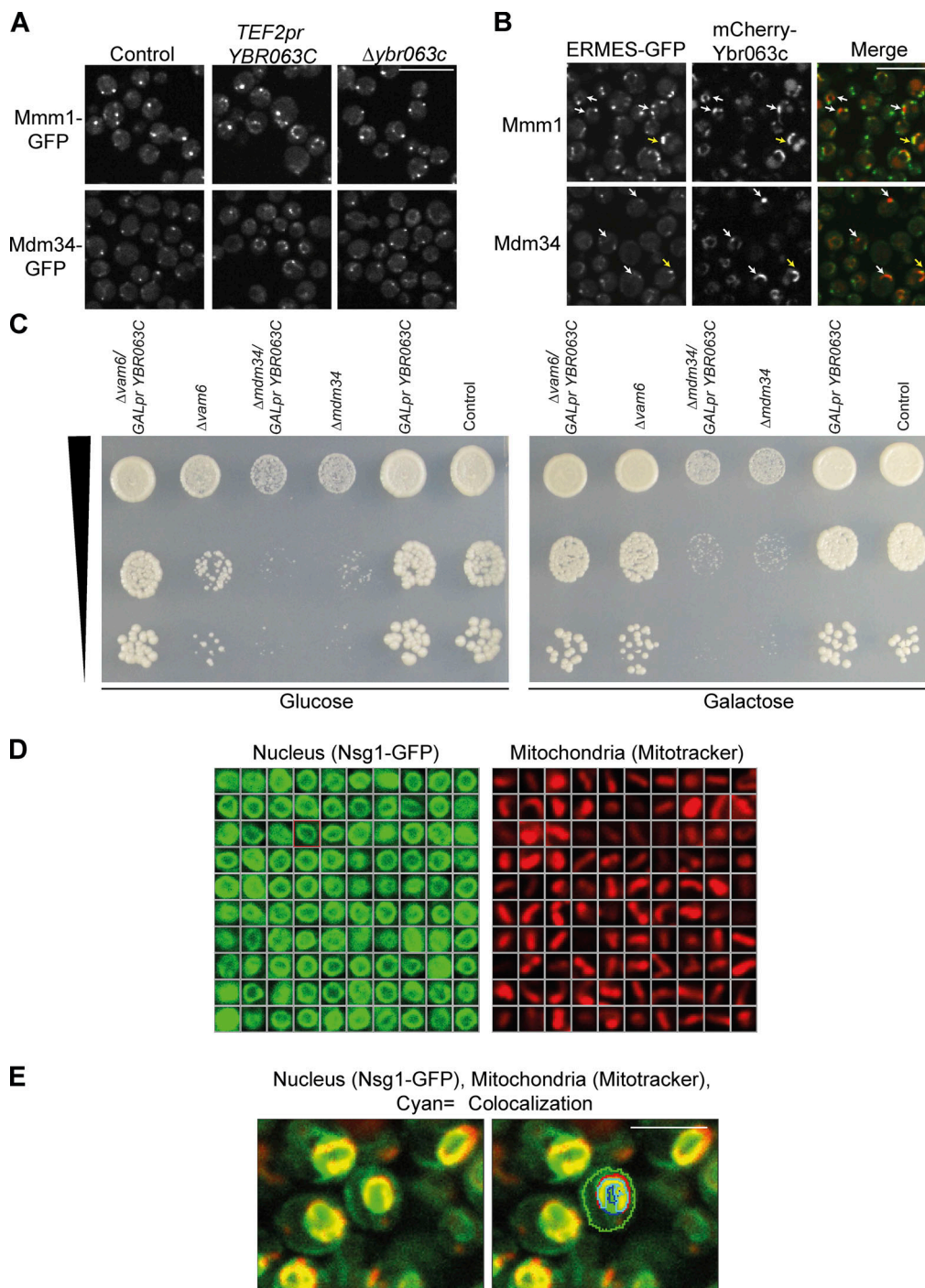


Figure S2. **Ybr063c (Cnm1) does not affect the extent of ERMES-mediated contacts.** (A) ERMES components Mmm1 or Mdm34 were C terminally tagged with GFP on the background of a control strain or strains overexpressing *YBR063C* (*TEF2pr-YBR063C*) or deleted for it (*Δybr063c*). Overexpression of Ybr063c resulted in clustering of ERMES signal to the nuclear ER area but did not change the number or intensity of ERMES puncta. Deleting *ybr063c* had no effect on these proteins. Scale bar, 5 μm. (B) Ybr063c can be found in distinct areas from ERMES subunits. Overexpressed Ybr063c was N terminally tagged with mCherry on the background of Mdm34 or Mmm1 C terminally tagged with GFP. The yellow arrows represent areas of proximity between the Ybr063c signal and the ERMES proteins, while the white arrows represent areas of Ybr063c signal that does not colocalize with ERMES. Scale bar, 5 μm. (C) A spot dilution assay of strains expressing *ybr063c* under a *GAL* promoter in control strains and strains that harbor deletions in *mdm34* or *vam6*. Repressed expression of *ybr063c* when controlled under the *GALpr* and grown in glucose caused a complete rescue of the growth defect of *Δvam6* in glucose. In contrast, repressing *ybr063c* on the background of *Δmdm34* aggravated the severe growth phenotype of this strain. All strains were grown on both synthetic media with glucose (no expression of Ybr063c) or galactose (Ybr063c is expressed) as a control. (D) 100 representative samples of either the nucleus (on the left) or mitochondria (on the right) that were considered in the quantification analysis of Fig. 3 D. The nuclei were marked by Nsg1-GFP, while the mitochondria were dyed using MitoTracker Orange. (E) Representation of the overlap analysis between the nucleus and mitochondria by artificial intelligence algorithms (ScanR Olympus soft imaging solutions, version 3.2). Mitochondria segmented in the RFP channel (561 nm) are recognized and marked in red, the nucleus segmented in the GFP channel (488 nm) is recognized and marked in blue, and the overlap between them is recognized and marked with cyan. Scale bar, 5 μm.



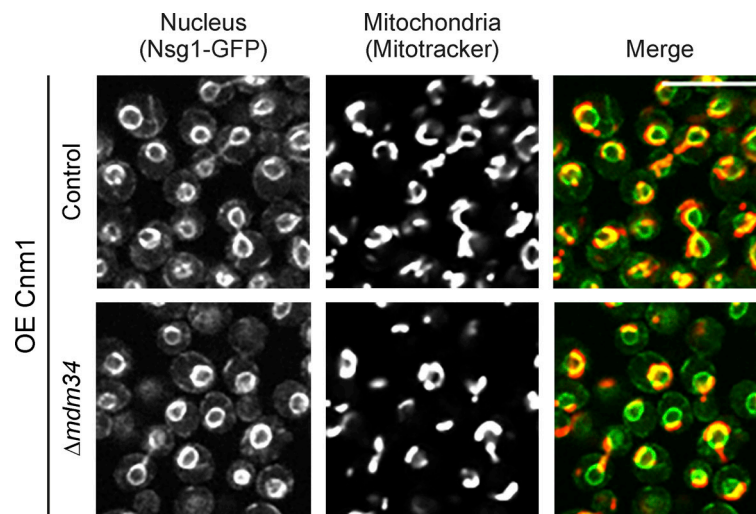


Figure S3. **Cnm1-mediated clustering of mitochondria around the nucleus is ERMES independent.** A strain overexpressing Cnm1 (OE Cnm1) and deleted for the ERMES subunit *mdm34* shows no difference in mitochondrial clustering around the nucleus. The nucleus was visualized with Nsg1-GFP and mitochondria with MitoTracker Orange. Scale bar, 5  $\mu$ m.

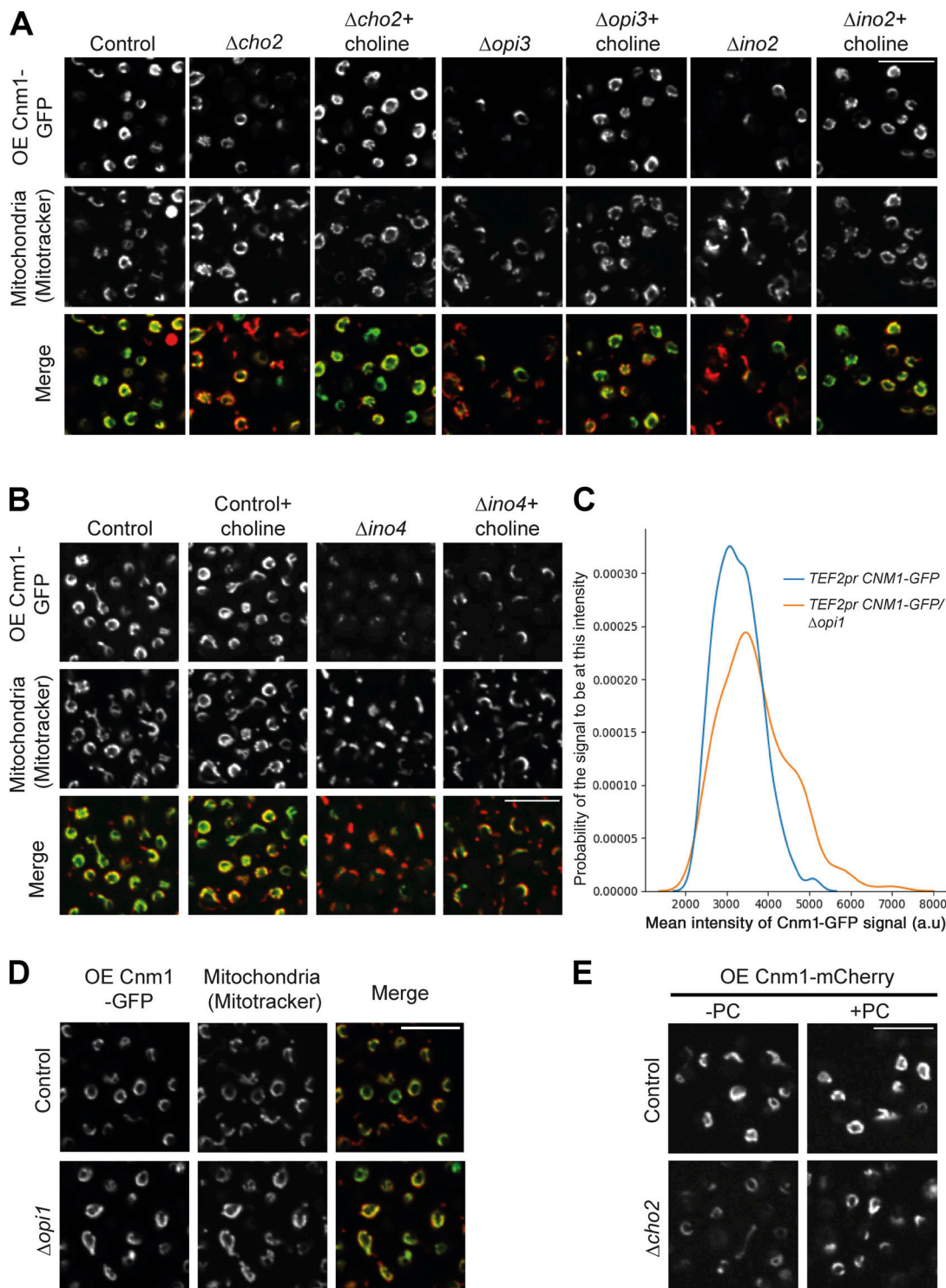


Figure S4. **Choline supplementation rescues reduced Cnm1-GFP levels in strains lacking genes related to PC biosynthesis.** (A) Cells overexpressing Cnm1-GFP (OE Cnm1-GFP) on the background of deletions in *cho2*, *opi3*, and *ino2* were grown to mid-logarithmic phase in synthetic minimal medium and imaged with or without 5 mM choline. Mitochondria were dyed using MitoTracker Orange. Scale bar, 5  $\mu$ m. (B) Cells lacking *ino4* and overexpressing (OE) Cnm1-GFP were grown to mid-logarithmic phase in synthetic minimal medium and imaged with or without 5 mM choline supplementation. Mitochondria were stained using MitoTracker Orange. Scale bar, 5  $\mu$ m. (C) Quantitation of the overexpressed (by *TEF2pr*) Cnm1-GFP signal brightness in either control or  $\Delta opi1$  strains, determined by the mean intensity level of the 488-nm excitation wavelength using ScanR Olympus soft imaging solutions, version 3.2. While the mean intensity was maintained in most control cells, deletion of *opi1* resulted in a higher probability of having cells with stronger Cnm1-GFP signal. a.u., arbitrary units. (D) An example of the strains quantified in C. Overexpression of Cnm1 tagged with GFP (OE Cnm1-GFP) on its C terminus on the background of *opi1* deletion showed enhanced GFP signal intensity in some of the cells compared with control. Mitochondria were dyed using MitoTracker Orange. Scale bar, 5  $\mu$ m. (E) Cells overexpressing (OE) Cnm1 and C terminally tagged with mCherry on the background of  $\Delta cho2$  strain were grown to mid-logarithmic phase in synthetic minimal medium and imaged with or without supplementation of 1 mM PC. Scale bar, 5  $\mu$ m.

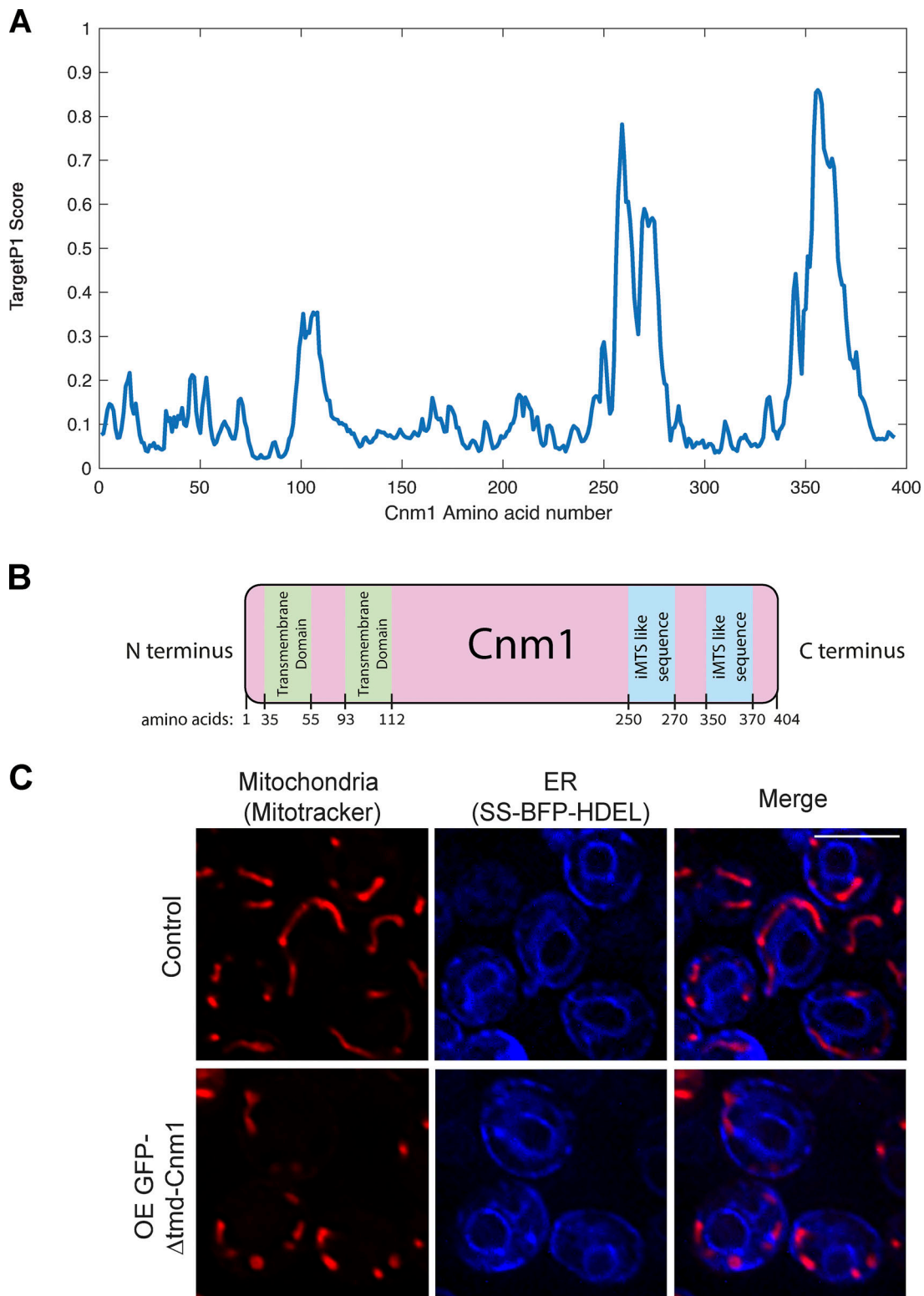


Figure S5. **Domain architecture of Cnm1 and the effect of losing its TMD on mitochondrial morphology.** (A) Prediction of an internal mitochondrial targeting signal-like (iMTS-L) sequence in Cnm1 calculated as described before (Boos et al., 2019). A peak with the highest TargetP1 scores can be found around amino acids 350–370 of the nuclear protein Cnm1, suggesting the presence of an iMTS-L sequence in this region. Since iMTS-Ls have been shown to directly bind Tom70, this highlights this region as a potential binding interface of Cnm1 with Tom70 on the mitochondrial membrane. (B) An illustrated model of Cnm1 protein containing the localization of its two predicted transmembrane domains and the predicted iMTS-like signals. (C) Overexpression of the soluble Cnm1 ( $\Delta$ 1–112 aa) tagged with GFP on its N terminus (OE GFP- $\Delta$ tmd-Cnm1) has a dramatic effect on mitochondrial morphology. The ER is marked by a BFP with a signal sequence and an ER retention signal (SS-BFP-HDEL). Mitochondria were dyed with MitoTracker Orange. Scale bar, 5  $\mu$ m.

Video 1. **Activating Ybr063c expression from a GAL promoter results in mitochondrial adherence to the nucleus when the two organelles come into proximity.** The nucleus is marked by Nsg1-GFP and mitochondria were marked in red using MitoTracker Orange.

Table S1, Table S2, Table S3, and Table S4 are provided online as separate Excel files. Table S1 lists all mCherry-tagged proteins that fully or partially colocalized with the nucleus-mitochondria contact site reporter from Fig. 2. Table S2 lists all genes whose deletions altered Cnm1-mediated clustering of mitochondria around the nucleus from Fig. 4. Table S3 lists the plasmids used in this study. Table S4 lists the yeast strains used in this study.



**b) Manuscripts in revision**

5. **Drwesh, L.**, Heim, B., Graf, M., Kher, L., Hansen-Palmus L., Franz-Wachtel M., Macek, B., Kalbacher, H., Buchner, J., and Rapaport, D. (2022). eLife, *in revision*

1 **A network of cytosolic (co)chaperones promotes the biogenesis of**  
2 **mitochondrial signal-anchored outer membrane proteins**

3

4 Layla Drwesh<sup>1</sup>, Benjamin Heim<sup>2</sup>, Max Graf<sup>1</sup>, Linda Kehr<sup>1</sup>, Lea Hansen-Palmus<sup>1</sup>, Mirita Franz-  
5 Wachtel<sup>3</sup>, Boris Macek<sup>3</sup>, Hubert Kalbacher<sup>1</sup>, Johannes Buchner<sup>2</sup>, and Doron Rapaport<sup>1,\*</sup>

6

7 <sup>1</sup> Interfaculty Institute of Biochemistry, University of Tübingen, 72076 Tübingen, Germany

8 <sup>2</sup> Center for Integrated Protein Science, Department Chemie, Technische Universität München,  
9 85748 Garching, Germany

10 <sup>3</sup> Proteome Center Tübingen, Interfaculty Institute for Cell Biology, University of Tübingen,  
11 72076 Tübingen, Germany

12

13

14 \* To whom correspondence should be addressed:

15 Interfaculty Institute of Biochemistry, University of Tübingen, Auf der Morgenstelle 34, 72076  
16 Tübingen, Germany.

17 Tel: +49-7071-2974184; E-mail: [doron.rapaport@uni-tuebingen.de](mailto:doron.rapaport@uni-tuebingen.de).

18 ORCID: 0000-0003-3136-1207

19

20 **Running title:**

21 Biogenesis of mitochondrial outer membrane proteins

22

## 23 **Abstract**

24 Signal-anchored (SA) proteins are anchored into the mitochondrial outer membrane (OM) via  
25 a single transmembrane segment at their N-terminus while the bulk of the proteins is facing the  
26 cytosol. These proteins are encoded by nuclear DNA, translated on cytosolic ribosomes, and  
27 are then targeted to the organelle and inserted into its OM by import factors. Recently, research  
28 on the insertion mechanisms of these proteins into the mitochondrial OM have gained a lot of  
29 attention. In contrast, the early cytosolic steps of their biogenesis are unresolved. Using various  
30 proteins from this category and a broad set of *in vivo*, *in organello*, and *in vitro* assays, we  
31 reconstituted the early steps of their biogenesis. We identified a subset of molecular  
32 (co)chaperones that interact with newly synthesized SA proteins, namely, Hsp70 and Hsp90  
33 chaperones and co-chaperones from the Hsp40 family like Ydj1 and Sis1. These interactions  
34 were mediated by the hydrophobic transmembrane segments of the SA proteins. We further  
35 demonstrate that interfering with these interactions inhibits the biogenesis of SA proteins to  
36 varying extents. Finally, we could demonstrate direct interaction of peptides corresponding to  
37 the transmembrane segments of SA proteins with the (co)chaperones and reconstitute *in vitro*  
38 the transfer of such peptides from the Hsp70 chaperone to the mitochondrial Tom70 receptor.  
39 Collectively, this study unravels an array of cytosolic chaperones and mitochondrial import  
40 factors that facilitates the targeting and membrane integration of mitochondrial SA proteins.

## 41 **Introduction**

42 Even though mitochondria have their own genome, the vast majority of their proteins are  
43 encoded by the nuclear genome, synthesized on cytosolic ribosomes, and then imported into  
44 the organelle. The early stages of these pathways are believed to be mediated by cytosolic  
45 factors and chaperones, whereas the later ones are facilitated by protein import machineries  
46 that have evolved in the different mitochondrial compartments (Neupert and Herrmann, 2007;  
47 Wiedemann and Pfanner, 2017).

48 The mitochondrial outer membrane harbors proteins with variable topologies that can span the  
49 membrane once, twice, or as multi-span proteins. Proteins that span the membrane once can  
50 have their single transmembrane segment (TMS) in the center of the protein or at the N- or C-  
51 terminus (Drwesh and Rapaport, 2020; Gupta& Becker, 2021). The latter group is called the  
52 tail-anchored proteins whereas those anchored via an N-terminal segment are known as signal-  
53 anchored (SA) proteins. Some known members of SA proteins are the TOM receptors Tom70  
54 and Tom20, the quality control protein Msp1 (Okreglak and Walter, 2014; Chen et al., 2014),  
55 and the mitochondrial outer membrane isoform of Mcr1 (Mcr1mom) (Lamb et al., 1999).

56 Despite sharing similar protein topology, SA proteins do not appear to follow the same  
57 insertion route. While insertion of Tom70 and Tom20 was previously reported to be dependent  
58 on the MIM complex and elements of the TOM complex (Ahting et al., 2005; Becker et al.,  
59 2008; Popov-Čeleketić et al., 2008), Msp1 mitochondrial insertion was shown to require only  
60 the MIM complex. The biogenesis of another member of the group Mcr1mom, has been  
61 proposed to be independent of the TOM complex, although it is yet unclear whether the MIM  
62 complex is involved (Meineke et al., 2008; Vitali et al., 2020; Doan et al., 2020).

63 Like the rest of the mitochondrial OM proteins, SA proteins are initially synthesized in the  
64 cytosol before being targeted to mitochondria. Such proteins contain an exposed hydrophobic  
65 transmembrane segment, which makes them vulnerable to aberrant folding and aggregation.  
66 This situation can potentially result in cytotoxic protein species, which might contribute to the  
67 pathomechanism of various neurodegenerative and other diseases (Bohush et al., 2019; Chaari,  
68 2019). Hence, it is widely thought that cytosolic factors bind such newly synthesized proteins,  
69 thereby maintaining their import-competent conformation by counteracting aggregation,  
70 degradation, and misfolding (Neupert and Pfanner, 1993).

71 In the yeast *Saccharomyces cerevisiae*, a large repertoire of molecular chaperones was  
72 identified that regulate protein quality control. These elements are classified into different  
73 families according to their molecular masses and the way they interact with their substrate  
74 (Mokry et al., 2015). Chaperones from the Hsp100 family have high binding affinity to  
75 aggregated proteins and function as disaggregases by both reactivating and resolubilizing them  
76 (Zolkiewski et al., 2012). Chaperones from the Hsp70 family (like Ssa1-4 in yeast) function in  
77 a wide range of biological processes, such as modulating folding and preventing aggregation.  
78 Chaperones from this family associate with a broad spectrum of client proteins in an ATP-  
79 regulated cycle. Client protein recognition is regulated mainly by J-proteins (co-chaperones  
80 like Ydj1 and Sis1 in yeast) from the Hsp40 family that stimulate ATP hydrolysis, thereby  
81 facilitating client capture by Hsp70 (Cry, 1995; Kampinga and Craig, 2010; Wyszowski et  
82 al., 2021). Beside their crucial role in modulating the ATPase cycle of Hsp70 through their J-  
83 domain, Hsp40 chaperones can also bind unfolded protein substrates (Johnson and Craig, 2001;  
84 Li et al., 2009). In addition, cells harbour small heat shock proteins (sHSPs) that bind non-  
85 native proteins and are crucial for preventing irreversible aggregation processes. Such sHSPs  
86 were recently found to be involved also in protecting proteins from mechanical stress (Haslbeck  
87 et al., 2019; Collier and Benesch, 2020). In yeast, Hsp26 is a chaperone from this family that  
88 has been reported to associate with cytosolic aggregates allowing the Ssa1-Hsp104 chaperone  
89 system to efficiently disassemble and refold them (Haslbeck et al., 2005; Cashikar et al., 2005).  
90 Chaperones of the Hsp70 family as well as some of their co-chaperones were implicated in the  
91 import of mitochondrial presequence-containing substrates (Hoseini et al., 2016; Xie et al.,  
92 2017; Endo et al., 1996; Deshaies et al., 1988; Caplan et al., 1992) and carrier proteins of the  
93 inner membrane (Young et al., 2003; Bhangoo et al., 2007). For example, the co-chaperone  
94 Djp1 plays a key role in the ER-SURF pathway which involves a de-tour of mitochondrial  
95 substrates to the ER (Hansen et al., 2018). Such (co)chaperones were also reported to facilitate  
96 the import of mitochondrial OM proteins like Mim1 or Tom22 (Papić et al., 2013; Opaliński  
97 et al., 2018). Furthermore, we previously reported that cytosolic Hsp70 and Hsp40 chaperones  
98 enable the biogenesis of mitochondrial  $\beta$ -barrel proteins (Jores et al., 2018). Pex19, which is a  
99 cytosolic chaperone associated with the peroxisomal import of membrane proteins, has also  
100 been found, along with Ssa1 and its co-chaperone Sti1, to assist the biogenesis of mitochondrial  
101 tail-anchored proteins namely, Fis1 and Gem1 (Cichocki et al., 2018) (Jansen and van der Klei,  
102 2019).

103 Despite this progress in our understanding of the contribution of cytosolic chaperones to  
104 mitochondrial biogenesis, no cytosolic factors have been reported so far as mediators of the  
105 biogenesis of mitochondrial SA proteins. Currently, there is scarce information regarding the  
106 early cytosolic events that assure their safe passage through the cytosol. To fill this gap, we  
107 have employed a combined experimental strategy consisting of assays with yeast cells extract,  
108 isolated organelles, and in vitro experiments with purified proteins. We could identify a subset  
109 of Hsp70 and Hsp40 (co)chaperones that interacts with SA proteins. These (co)chaperones  
110 were further shown to be crucial for the mitochondrial import of SA proteins. Furthermore, we  
111 suggest a novel role of the import receptors Tom70 in promoting the insertion of SA proteins  
112 by serving as a docking site for the Hsp70 chaperone.

113

## 114 **Results**

### 115 **Cytosolic chaperones interact with newly synthesized signal-anchored proteins**

116 Signal-anchored proteins are, due to their hydrophobic segments, at a high risk of aggregation  
117 and misfolding following their translation in the cytosol. We aimed to search for factors that  
118 can prevent such a scenario and maintain the SA substrates in an import-competent  
119 conformation. We chose four SA model proteins to study the potential involvement of such  
120 cytosolic components: the two receptor subunits of the TOM complex, Tom20 and Tom70, and  
121 two additional proteins namely, Msp1 and the OM isoform of Mcr1 (Mcr1<sup>om</sup>). Initially, we  
122 wanted to determine which factors can interact with newly synthesized SA proteins. To this  
123 end, we used yeast extract to translate in vitro signal-anchored proteins with a C-terminally  
124 HA-tag. Since the yeast extract does not contain organelles to where the freshly translated  
125 proteins can be targeted, we anticipated that such SA proteins should associate in the  
126 hydrophilic environment of the extract with factors, which will maintain them in an import-  
127 competent conformation. The tail-anchored protein Fis1 and the  $\beta$ -barrel protein Porin were  
128 included for comparison and the unrelated protein dihydrofolate reductase (DHFR) was used  
129 as a control. After their synthesis, all proteins were pulled down with anti-HA beads and co-  
130 purified proteins in the elution fraction were analyzed by western blot followed by  
131 immunodecoration with antibodies against different cytosolic elements (Fig. 1A, B).

132 All four signal-anchored proteins co-eluted with the Hsp70 chaperones Ssa1/2, and the Hsp40  
133 co-chaperones Ydj1, Sis1 and Djp1. Weaker interactions were observed with the Hsp90

134 chaperones Hsc82/Hsp82 and their co-chaperones Aha1 and Sti1. The eluates contained also  
135 Hsp104 chaperone and minor amounts of Hsp42 chaperone, suggesting that minor portion of  
136 the newly synthesized proteins got aggregated. The co-chaperone Hch1 and the cytosolic  
137 protein Bmh1 were not co-eluted with any of the tested proteins (Fig. 1A, B). Control elution  
138 fraction containing newly synthesized DHFR had neglectable amounts of co-purified  
139 (co)chaperones, indicating the binding specificity of chaperone-substrate. As we observed  
140 previously (Jores et al., 2018), the  $\beta$ -barrel protein Porin also associated with the various  
141 (co)chaperones.

142 To validate the western blot results and to search for additional (co)chaperones co-purified with  
143 the newly translated SA proteins, the elution fractions from such pull-down assays were  
144 analyzed also by mass spectrometry. The mass spectrometry analysis of the eluates from pull-  
145 downs with Msp1, Mcr1, or (as a control) with mock pull-down where no mRNA was added  
146 to the lysate are shown in Table S1. Several chaperones, which are not included in the western  
147 blot due to lack of antibodies, were additionally detected in the eluate of both proteins Msp1  
148 and Mcr1. The detected proteins are presented in two groups. The first contained those proteins  
149 that were not found at all in the mock eluate, hence their enrichment ratio in Msp1 and Mcr1  
150 eluates could not be calculated (Table S1A). Among these were chaperones from the Hsp70  
151 family namely, Ssa4, Snl1 and Lhs1. The second group is the set of proteins that were found  
152 in minor amounts also in the mock elution, and thus their relative enrichment as compared to  
153 the mock pull-down could be determined (Table S1B). Amongst them, the Hsp70 chaperones  
154 Ssc1, Sse1 and Ssb1/2, in addition to the ribosome associated complex (RAC) chaperone Zuo1  
155 were detected. Taken together, the combined analysis of the pull-down assays shows  
156 multifaceted interactions between newly synthesized SA proteins and cytosolic chaperones and  
157 co-chaperones.

### 158 **The hydrophobic transmembrane domain of SA proteins mediates their interactions with** 159 **cytosolic (co)chaperones**

160 The detected interactions of a subset of cytosolic (co)chaperones with SA proteins led us to ask  
161 which part of these latter proteins mediate such association. A likely candidate for this task is  
162 the proteins' hydrophobic TMS. To test this assumption, we constructed two additional C-  
163 terminally HA-tagged versions of each SA protein – one construct encodes the cytosolic part  
164 of the protein (indicated by protein name-C, Fig. 2) and the second encodes only the  
165 hydrophobic TMS (indicated by protein name-T, Fig. 2). These two constructs together with



166 the full-length (FL) version were used for in vitro translation in yeast extract followed by pull-  
167 down assay. As expected for small proteins, all three constructs encoding the hydrophobic  
168 TMSs were synthesized to a lower extent as compared to the constructs representing the  
169 cytosolic moieties or the full-length proteins (Fig. 2, input panels). Yet, similar levels of bound  
170 (co)chaperones were observed in the eluates of the hydrophobic TMSs and the full-length  
171 versions (Fig. 2A-C). In contrast, only marginal binding of (co)chaperones to the soluble  
172 cytosolic parts of the SA proteins or to the control protein DHFR was detected (Fig. 2A-C).  
173 Taken together, our findings suggest that the interactions between SA proteins and molecular  
174 chaperones are mainly governed by the TMSs of the mitochondrial proteins.

### 175 **Signal-anchored proteins show variable dependence on Hsp40 co-chaperones**

176 After demonstrating that Hsp40 co-chaperones like Ydj1 and Sis1 can physically interact with  
177 newly synthesized SA proteins, we wanted to test if these interactions are relevant to the  
178 biogenesis of the latter group. These two co-chaperones were previously reported to be  
179 involved in the biogenesis of the  $\beta$ -barrel protein Porin (Jores et al., 2018). Moreover, Ydj1 has  
180 been implicated in the mitochondrial import of presequence-containing proteins (Caplan et al.,  
181 1992; Xie et al., 2017). To gain insight into the physiological relevance of these co-chaperones  
182 for the biogenesis of signal-anchored proteins, we created strains expressing YDJ1, SIS1 or  
183 both genes under the control of a tetracycline-repressible promoter. To accelerate the depletion  
184 process, ubiquitin was fused N-terminally to the down-regulated protein. To monitor the effect  
185 of depleted chaperones over time, cells were grown for two hours in the absence of  
186 doxycycline. Then, down-regulation was induced by supplementing doxycycline (Dox) to the  
187 medium, cells were harvested immediately (time=0) or after 1, 2 or 4 hours, and cytosolic and  
188 mitochondrial fractions were obtained. For comparison, cells were grown in the absence of  
189 doxycycline and harvested as well.

190 As anticipated, cytosolic levels of Ydj1 and Sis1 were gradually decreased over time after  
191 addition of doxycycline, whereas levels of other chaperones like Hsp104 and Hsp26 were not  
192 changed, demonstrating doxycycline's selectivity in suppressing the expression of only the  
193 genes regulated by the tetracycline promoter (Fig. 3A, C). Inspecting the mitochondrial  
194 fractions revealed that none of the inspected mitochondrial proteins was altered in Ydj1  
195 depleted cells. In contrast, mitochondrial levels of Tom20 and Tom70 in Sis1 depleted cells  
196 were moderately reduced after 4 hours, while no change was detected in the levels of the other  
197 signal-anchored proteins Msp1 and Mcr1, or other outer membrane proteins like Porin or Fis1

198 (Fig. 3A-B). These findings might be explained by previous observations that the J-domain of  
199 Sis1 can compensate for the loss of Ydj1 J-domain but not the other way around (Yan and  
200 Craig, 1999).

201 To avoid such cross compensation of the two co-chaperones, we wanted next to check the effect  
202 of the parallel depletion of both on the biogenesis of SA proteins. Interestingly, the levels of  
203 Tom20 and Tom70 were gradually reduced over time down to 40-50% of their levels in control  
204 conditions while levels of Msp1 and Mcr1 were not altered. As expected from our previous  
205 study (Jores et al., 2018), Porin also showed a decrease to 40% (Fig. 3C-D). Altogether, these  
206 results suggest that biogenesis of various SA proteins rely to a different degree on Hsp40 co-  
207 chaperones.

208 The highly reduced steady-state levels of Tom20 and Tom70 upon depletion of both co-  
209 chaperones led us to conduct in vitro import assays. In these experiments we translated  
210 radiolabeled variants of Tom20 and Tom70 in yeast extract from either control or Ydj1 and  
211 Sis1 depleted cells and incubated the newly synthesized proteins with isolated mitochondria.  
212 We found that extract depleted of both co-chaperones can support to a lower extent the import  
213 of Tom20 but to a normal level that of Tom70 (Fig. 4A, B). Thus, it seems that the import of  
214 Tom70 under these in vitro conditions can be compensated by other, yet unknown, factors.

### 215 **Depletion of Ydj1 and Sis1 can increase the risk for aggregation of newly synthesized** 216 **proteins**

217 To better understand the involvement of Ydj1 and Sis1 in the cytosolic maintenance of signal-  
218 anchored proteins, we aimed to analyze the interaction pattern between the other chaperones  
219 and the newly synthesized SA proteins in yeast cells depleted of Ydj1 and Sis1. We chose to  
220 utilize a strain that is depleted of both co-chaperones since their mutual function allows them  
221 to compensate for each other's loss. To this end, we translated HA-tagged variants of the four  
222 signal-anchored proteins in extract of either WT or Ydj1 and Sis1 depleted cells (YS↓) and  
223 then performed pull down with anti-HA beads. Interestingly, we found that the interaction  
224 between the newly synthesized proteins and some of the chaperones was altered in cells  
225 depleted for both co-chaperones while other chaperones did not show any significant change.  
226 The co-purified levels of Hsp104 and Hsp26 chaperones were increased in the eluates of all  
227 SA proteins translated in the extract of the depletion strain (Fig. 5A, B). Both Hsp104 and  
228 Hsp26 are involved in disaggregation of substrate proteins. Hence the co-purification, in the  
229 absence of Sis1 and Ydj1, of these chaperones with newly synthesized SA proteins suggests

230 that the cytosol of cells with highly reduced levels of these co-chaperones can offer less  
231 stabilization for the newly synthesized substrates and hence these substrates are more prone to  
232 aggregation under these conditions. These findings indicate a role of the Hsp40 co-chaperones  
233 in keeping the signal-anchored proteins stable in the cytosol.

### 234 **The binding affinity of substrate to Hsp70 chaperone Ssa1 is higher than the affinity to** 235 **the co-chaperone Sis1**

236 To better understand the dynamics of chaperone-substrate interactions, we next aimed to  
237 investigate their binding kinetics and affinity using fluorescence anisotropy. Since we have  
238 shown that the interaction between chaperones and signal-anchored proteins is mediated by  
239 their transmembrane domain (Fig. 2), we synthesized peptides corresponding to residues 1-34  
240 of Mcr1 and Tom70, which contain the TMS, and modified the peptides with the fluorescent  
241 dye Tetramethylrhodamine (TAMRA). Then, we monitored the anisotropy changes of these  
242 fluorescently labeled peptides upon their interaction with recombinantly expressed purified  
243 (co)chaperones. The fluorescence anisotropy of the TAMRA-labeled Tom70 and Mcr1  
244 peptides increased upon addition of recombinant Ssa1 indicating the formation of a peptide-  
245 Ssa1 complex. As a control, such an increase was not observed when BSA was added,  
246 underlining the specificity of the chaperone-substrate interaction (Fig. 6A, B). These  
247 observations demonstrate that transmembrane segments of SA proteins can bind directly to  
248 Ssa1.

249 Next, we implemented a titration assay in which increasing concentrations of Ssa1 (Fig. 6 C,  
250 D) or Sis1 (Fig. 6 E, F) were sequentially added to either Tom70 or Mcr1 peptides. This  
251 approach enabled us to monitor the binding parameters and compare the binding affinity  
252 between substrate and different (co)chaperones. Based on these experiments, dissociation  
253 constants (Kd) were determined according to hyperbolic regression curves fitted to the data.  
254 These Kds were calculated to be 2.42  $\mu\text{M}$  for Ssa1-Tom70(TMS) complex and 3.27  $\mu\text{M}$  for  
255 Ssa1-Mcr1(TMS) complex (Fig. 6C, D). Interestingly, dissociation constants (Kd) of 18.3  $\mu\text{M}$   
256 and 25.75  $\mu\text{M}$  were measured for Sis1-Tom70(TMS) complex and Sis1-Mcr1(TMS) complex,  
257 respectively (Fig. 6E, F). Collectively, these results show that the affinity between the  
258 substrates and the Hsp70 chaperone Ssa1 is several folds higher than their affinity to the co-  
259 chaperone, Sis1. This observation supports the notion that the co-chaperone facilitates the  
260 initial low-affinity interaction with the substrate before transferring it to the main chaperone  
261 that has a higher affinity to the substrate.

## 262 **Hsp70 chaperones are required for optimal biogenesis of SA proteins**

263 Hsp70 chaperones cooperate with different cofactors and are known to be regulated mainly by  
264 J-protein co-chaperones like Ydj1 and Sis1. Our results so far have shown that these chaperones  
265 play an important role in the biogenesis of SA proteins. To substantiate this assumption, we  
266 wished to examine whether inhibiting this chaperone can interfere with the import of SA  
267 proteins. Thus, we performed in vitro import assays in which the yeast extract used for protein  
268 translation was supplemented with the Hsp70 inhibitor, CBag (C-terminal Bag domain of  
269 human Bag-1M) prior to import into mitochondria (Jores et al., 2018). As a result, the import  
270 efficiency of both, Msp1 and Mcr1 decreased to 50% and 20% respectively, as compared to  
271 control BSA-supplemented yeast extract (Fig. 7 A, B). We previously observed that this  
272 inhibitor does not cause a general damage to the import capacity of mitochondria as it did not  
273 affect the import of the matrix-destined protein pSu9-DHFR (Jores et al., 2018). Altogether,  
274 these experiments suggest a crucial role for Hsp70 in facilitating proper insertion of SA  
275 proteins into the mitochondrial OM.

276 Considering the physiological relevance of both Hsp70 and Hsp40 (co)chaperones for the  
277 biogenesis of SA proteins, we aimed to understand the dynamics of the complex formation  
278 between the SA substrate, the Hsp40 co-chaperones (Sis1), and the Hsp70 chaperones (Ssa1).  
279 To this end, we performed additional set of fluorescence anisotropy experiments in which Ssa1,  
280 ATP and Sis1, each a few minutes apart and in a different order, were added to the Mcr1-  
281 TAMRA-labeled peptide (Fig. 7 C-E). Since Ssa1 has ATPase activity that is modulated by  
282 Hsp40 co-chaperones, we tested whether the binding of Hsp40 or Hsp70 to the substrate is  
283 ATP-dependent. Higher anisotropy values were observed when Ssa1 was supplemented first,  
284 indicating complex formation between Ssa1-Mcr1 peptide. After adding ATP, the anisotropy  
285 was reduced indicating that the complex started to disassociate as a result of ADP exchange  
286 for ATP, which promotes chaperone-substrate release. However, addition of Sis1 increased the  
287 anisotropy again suggesting either a complex formation between Sis1 and the substrate or that  
288 Sis1 restored the complex formation between Ssa1 to Mcr1 peptide by tuning the ATPase-  
289 driven chaperone cycle of Ssa1 (Fig. 7C).

290 In another experiment we first added Sis1 to the Mcr1 peptide and, as expected, complex  
291 formation was observed (Fig. 7D). Only a slight decrease in the anisotropy was detected once  
292 Ssa1 was added to the mixture. This behaviour could be attributed to a transfer of the substrate  
293 from Sis1 to Ssa1 due to higher affinity of the substrate of the latter protein. Interestingly, when

294 ATP was supplied to the mixture at last, no further decrease in the anisotropy was measured  
295 (Fig. 7D). This lack of effect could be explained by one of the two possibilities – (i) since there  
296 is still Sis1 in the mixture, following the Ssa1-substrate disassociation due to ATP, the substrate  
297 re-associated with Sis1, or (ii) due to the presence of Sis1, the ATP hydrolysis is accelerated  
298 which retains Hsp70 chaperone conformation in favor of substrate binding, making the Ssa1-  
299 substrate complex no longer sensitive to ATP.

300 In the last experiment, Sis1 was supplemented after Ssa1 and an additional increase in  
301 anisotropy was observed (Fig. 7E). Since the total change in anisotropy is even larger than the  
302 increase observed in the presence of either Ssa1 or Sis1 alone, this observation might suggest  
303 the formation of a ternary complex composed of Ssa1-Sis1-substrate. Importantly, this rise was  
304 not long-lasting, and the complex appears to dissociate over time (Fig. 7E). As before, the  
305 addition of ATP at this stage did not change the levels of anisotropy. Overall, these findings  
306 support a complex formation between Hsp70 and its SA substrate. In addition, they suggest a  
307 regulatory effect of ATP on this complex, which is no longer observed when Sis1 is in the  
308 mixture, suggesting a role of Sis1 in stabilizing this complex.

### 309 **Tom20 and Tom70 receptors might play an offsetting role in the biogenesis of the SA** 310 **proteins Msp1 and Mcr1**

311 Next, we wanted to decipher the late cytosolic events involving the recognition of newly  
312 synthesized proteins at the mitochondrial surface. To that goal we investigated, using different  
313 approaches, the potential involvement of the canonical import receptors Tom20 and Tom70 in  
314 the biogenesis of Mcr1 or Msp1. First, we performed in vitro pull-down assays using the  
315 cytosolic domains of either Tom20 or Tom70 N-terminally fused to a GST moiety. GST alone  
316 was included as a negative control. These GST-fusion proteins were incubated with freshly  
317 translated HA-tagged variants of Msp1, Mcr1 or DHFR (as a control). Following two hours of  
318 incubation in the presence of ATP to allow the release of potentially bound chaperones, the  
319 elution fraction was collected, and bound proteins were detected using anti-HA antibody. Msp1  
320 and Mcr1 displayed variable degrees of interaction with both receptors. After normalizing for  
321 the background binding to GST, Mcr1 exhibited four times higher binding to the cytosolic  
322 domain of Tom20 compared to that of Tom70, while Msp1 interacted with both almost equally.  
323 Of note, no binding was detected when DHFR was incubated with the receptors, demonstrating  
324 the specificity of the assay (Fig. 8A).

325 Since prior to their incubation with the receptors, the SA proteins were translated in yeast  
326 extract containing the repertoire of molecular chaperones, we asked whether chaperones can  
327 be involved in the recognition process of the newly synthesized proteins by the receptors.  
328 Hence, we aimed to examine the potential interaction between the TOM receptors and different  
329 chaperones using the same approach namely, pull-down from yeast extract. Notably, Ydj1  
330 showed similar binding levels to both receptors while Ssa1/2, Sti1 and Hsp104 exhibited  
331 stronger binding to the cytosolic domain of Tom70. On the other hand, Aha1 displayed a very  
332 strong interaction with the Tom20 receptor. Other chaperones, like Hsp26 and Hch1 did not  
333 bind to either receptor (Fig. S1A).

334 Since the cooperation between the Hsp70 chaperone and Tom70/Tom20 receptors in  
335 facilitating productive delivery of a subset of preproteins to the receptor for subsequent  
336 membrane translocation has been reported in multiple publications (Mills et al., 2009; Fan et  
337 al., 2010; Fan et al., 2011; Komiya et al., 1997; Young et al., 2003, Wegele et al., 2006), we  
338 decided to further investigate the implications of such interactions for the biogenesis of SA  
339 proteins. Given that Tom70 contains a docking site for Hsp70s and Hsp90 chaperones, along  
340 with our observation that Ssa1/2 is probably involved in the insertion process of Msp1 and  
341 Mcr1, we asked whether the Tom70 receptor recognizes the polypeptide substrate while in  
342 complex with Ssa1 and whether Hsp70 docking is required for the formation of a productive  
343 substrate/Tom70 complex. For this purpose, we analyzed Mcr1 peptide binding to the GST-  
344 Tom70 receptor in the presence of Ssa1, Sis1 and ATP supplemented in different orders and  
345 monitored the change in the anisotropy. As in other experiments (Fig. 7C), we observed  
346 complex formation after adding Ssa1 to Mcr1-peptide, which was detached upon ATP addition  
347 (Fig. 8B). However, once GST-Tom70 was added, a complex that caused an even higher  
348 anisotropy shift was formed (Fig. 8B), suggesting that Mcr1 peptide, after being released from  
349 Ssa1, formed a complex with Tom70 with higher affinity. Interestingly, a complex between  
350 Mcr1-peptide and Tom70, as indicated by a large increase in the measured anisotropy, was also  
351 formed when GST-Tom70 was supplemented first while Ssa1 was absent (Fig. 8C). Once Ssa1  
352 and ATP were supplemented to this Tom70-Mcr1(TMS) complex, only a slight reduction shift  
353 was observed (Fig. 8 C), suggesting that the complex between Mcr1 substrate and Tom70  
354 receptor remained mostly stable. This observation supports the assumption that the substrate  
355 interacts with the receptor with higher binding affinity than with the chaperone. Such an  
356 increased affinity can promote transfer of the substrate from the chaperone to the receptor.



357 To test if the substrate-receptor interaction can occur even when the substrate is compounded  
358 with the Ssa1 chaperone, we enabled substrate-chaperone complex formation by  
359 supplementing Ssa1 first, followed by the addition of GST-Tom70. Surprisingly, a higher  
360 anisotropy shift was detected right after addition of GST-Tom70, indicating that the Tom70  
361 receptor can bind the substrate while the latter is in complex with the chaperone. Addition of  
362 ATP, which aids the release of the substrate from the chaperone, resulted in an even higher  
363 increase in anisotropy (Fig. 8D), suggesting that the Tom70 receptor may bind the substrate  
364 with enhanced efficiency upon its release from the chaperone. To ensure that the receptor can  
365 indeed bind the substrate-chaperone complex, we stabilized the complex formed by Ssa1-  
366 Mcr1(TMS) by co-addition of Sis1 to the mixture. Even in this case, the receptor Tom70 still  
367 interacted with the substrate (Fig. 8E). Overall, these findings suggest that SA substrate has a  
368 higher affinity for the receptor than for the chaperone. Furthermore, Tom70 is capable of  
369 binding substrates irrespective of the presence or absence of the Hsp70 chaperone Ssa1.

370 Having demonstrated that Tom20 and Tom70 can bind newly translated SA proteins to a  
371 different degree (Fig. S1), we aimed to assess whether these interactions are required for their  
372 mitochondrial insertion. Previous studies have shown that the absence of either one of the TOM  
373 receptors does not cause a reduction in the mitochondrial steady state levels of Msp1 or Mcr1  
374 (Vitali et al., 2020; Meineke et al., 2008). Nevertheless, since both receptors, Tom20 and  
375 Tom70 can interact with Msp1 and Mcr1, we assume that when one receptor is deleted, the  
376 other one can compensate due to their partial overlapping function (Young et al., 2003). To test  
377 this hypothesis, we wanted to examine the direct effect of the loss of both receptors on the  
378 mitochondrial insertion of Msp1 and Mcr1. To this end, we conducted in vitro import assays  
379 of radiolabeled proteins (Msp1 and Mcr1) using two approaches. The first approach included  
380 mitochondria that had been trypsin-treated before import, and the second involved using  
381 mitochondria lacking the Tom20 receptor (tom20 $\Delta$  strain) and treated with the C-terminal  
382 domain of human Hsp90 (C90) which is known to block the chaperone binding site on the  
383 mitochondrial import receptor Tom70, thus inhibiting its activity. Both Tom20 and Tom70 had  
384 their cytosolic domains degraded following trypsin treatment, and as a result, the import  
385 efficiency of Msp1 was decreased by 25% (Fig. 9A). In line with a previous report (Meineke  
386 et al., 2008), the import efficiency of Mcr1 was not affected (Fig. 9B).

387 When WT mitochondria were treated with C90, which results in non-functional Tom70, import  
388 of Msp1 was reduced by 23%. This seemingly contradicts a former study in which  
389 mitochondrial levels of Msp1 were not decreased in a Tom70 deleted strain (Vitali et al., 2020).



390 However, this difference can be explained by the fact that in the previous study, the cells  
391 lacking Tom70 could adopt for the loss of Tom70, while the effect of inhibition by C90, on the  
392 other hand, is immediate and not reversible. Interestingly, insertion efficiency of Msp1 into  
393 mitochondria lacking Tom20 was around 25% higher as compared to control WT mitochondria  
394 (Fig. 9C, D), maybe because of the slightly elevated levels of Tom70 in these cells (Fig. S1B).  
395 Supporting this assumption, when the samples lacking Tom20 were treated with C90, the  
396 membrane integration of Msp1 was reduced by 32% (Fig. 9C). Similar results were obtained  
397 with Mcr (Fig. 9D). These findings substantiate the importance of Tom70 as a docking site for  
398 substrate SA proteins associated with (co)chaperones.

399

## 400 **Discussion**

401 The early cytosolic events in the biogenesis of mitochondrial outer membrane proteins are  
402 believed to involve cytosolic factors and chaperones to keep the newly synthesized proteins in  
403 an import-competent conformation, which is crucial for their effective membranal insertion.  
404 Such factors have been identified for some of the mitochondrial outer membrane proteins, such  
405 as the  $\beta$ -barrel proteins (Jores et al., 2018), and some single-span proteins (Cichocki et al.,  
406 2018; Papić et al., 2013; Opaliński et al., 2018). In this study, we employed four different model  
407 proteins from the SA family and identified several cytosolic chaperones that can interact with  
408 such newly synthesized proteins through their hydrophobic transmembrane domain. Of note,  
409 the cytosolic domains of these SA proteins were not associated with chaperones indicating that  
410 they are less prone to forming aggregates or to misfold in the cytosol. These observations are  
411 in line with the widely accepted concept that chaperones recognize mainly hydrophobic patches  
412 to bind their substrates (Li et al., 2009; Saio et al., 2014; Clerico et al., 2015).

413 We identify chaperones from the Hsp90, Hsp70, and Hsp40 families to interact with SA  
414 proteins. When we tested the role of the Hsp40 co-chaperones, Ydj1 and Sis1, which are two  
415 major J-domain proteins in the yeast cytosol, we observed that mitochondrial steady state levels  
416 of Tom20 and Tom70 were largely reduced upon depletion of both chaperones and this effect  
417 was less pronounced when only one of the co-chaperones was depleted. This observation  
418 indicates, in agreement with an earlier study (Johnson and Craig, 2001), that Ydj1 and Sis1  
419 share overlapping functions. In contrast, the steady-state levels of Msp1 and Mcr1, although  
420 they also interact with Ydj1 and Sis1, were unaffected by the co-depletion of the co-

421 chaperones. This suggests that other Hsp40 co-chaperones most likely play a more central role  
422 in the biogenesis of these SA proteins. Furthermore, we could demonstrate that upon co-  
423 depletion of both Ydj1 and Sis1, the newly synthesized SA proteins exhibited enhanced binding  
424 to Hsp26 and Hsp104 chaperones that are implicated in binding aggregated proteins  
425 (Zolkiewski et al., 2012; Zhou et al., 2011; Franzmann et al., 2005). These findings emphasize  
426 the involvement of Ydj1 and Sis1 in preventing cytotoxic protein aggregation and are in  
427 agreement with other proposed functions of both co-chaperones (Cry, 1995; Klaips et al.,  
428 2020).

429 Additionally, we have shown that both the in vitro import efficiency and the steady-state levels  
430 of Tom20 are reduced upon depletion of Ydj1 and Sis1. In the case of Tom70, in vitro insertion  
431 was unaffected despite reduced mitochondrial steady state levels. These combined  
432 observations suggest that Ydj1 and Sis1 are involved in the biogenesis of SA proteins to  
433 varying degrees. The cis characteristics of the substrate proteins that dictate the variable  
434 dependency will be the topic of future studies.

435 We also validated via fluorescence anisotropy the interactions between a peptide corresponding  
436 to the transmembrane segment of Mcr1 and the two (co)chaperones Ssa1 and Sis1.  
437 Interestingly, the binding affinity of the substrate to the co-chaperone (Sis1) was 10-fold lower  
438 than the binding to the Hsp70 chaperone (Ssa1). These observations support the hypothesis that  
439 the substrate transfer from the co-chaperone to the main Hsp70 chaperones is driven by  
440 increased affinity to the latter. Similar results were also previously observed for a peptide  
441 representing the mitochondrial targeting element of the  $\beta$ -barrel protein Porin (Jores et al.,  
442 2018). According to our findings, the complex formed by Ssa1/substrate is regulated by the J-  
443 protein Sis1. Although we could show that a potential substrate is able to bind Hsp70 chaperone  
444 also in the absence of Sis1, this interaction was susceptible to ATP. In contrast, in the presence  
445 of Sis1 the complex was no longer responsive to ATP, pointing out the regulatory function of  
446 Sis1 on the Hsp70 ATPase activity. In agreement with our findings, previous studies have  
447 shown that both Sis1 and Ydj1 facilitate binding between substrate and Hsp70 chaperone  
448 (Kampinga and Craig, 2010).

449 Our current findings show that inhibiting Ssa1 activity significantly reduces the integration of  
450 Msp1 and Mcr1 into the OM. This implies that in addition to its well-known function in  
451 facilitating protein folding, Ssa1 also directly supports the mitochondrial insertion of Msp1 and  
452 Mcr1. Of note, we could show that SA proteins can interact with the TOM receptor Tom70,

453 suggesting that TOM receptors may play a role in recognizing newly synthesized SA proteins  
454 on the mitochondrial surface. At least for Mcr1, such a recognition by the import receptors  
455 might be related to the presence of an MTS-like stretch at residues 1-10 of the protein (Hahne  
456 et al., 1994). Furthermore, in accordance with previous observations (Backes et al., 2021;  
457 Kreimendahl and Rassow, 2020; Young et al., 2003), this recognition may involve an interplay  
458 between the Hsp70 chaperone and the Tom70 receptor. Based on our findings, we propose that  
459 the Ssa1/substrate complex is initially identified by Tom70 receptor, most likely using the  
460 docking site in Tom70, which may be crucial for correct targeting. The substrate is then  
461 released from the complex and relayed to Tom70 to which it has a higher affinity. These  
462 findings support the previously published study which proposed that the monomeric form of  
463 Tom70 is responsible for mediating initial chaperone docking and precursor recognition via its  
464 clamp domain followed by substrate release. This recognition is assumed to be facilitated by  
465 the exchange of ATP for ADP at the chaperone ATPase domain and results in the dimerization  
466 of Tom70 which favors interactions solely with the substrate (Mills et al., 2009).

467 When we analyzed the direct involvement of the TOM receptors in the biogenesis of Msp1 and  
468 Mcr1, we found that their insertion was reduced upon inhibition of Tom70 by C90. Surprisingly  
469 however, their insertion was enhanced upon Tom20 deletion. This finding is in line with a  
470 previous study showing higher steady state levels of Msp1 in mitochondria devoid of Tom20  
471 (Vitali et al., 2020). This enhancement could be attributed to higher expression of Tom70 to  
472 compensate for the deletion of Tom20. Moreover, inhibition of Tom70 in a deletion strain of  
473 Tom20 led to further reduction of the insertion of SA proteins, supporting the assumption that  
474 each receptor can compensate for the absence of the other one. Hence, it seems that both  
475 receptors might be involved in the biogenesis of the SA proteins Msp1 and Mcr1.

476 Altogether, our current findings, when combined with prior information, provide new insights  
477 into the cytosolic chain of events from the synthesis of SA proteins until their recognition at  
478 the mitochondrial surface. We propose that interactions between newly synthesized SA  
479 proteins and molecular chaperones are mediated by their hydrophobic patches. Such  
480 interactions are not only crucial for keeping the substrate protein in an import-competent  
481 conformation, but also for their proper mitochondrial targeting which involves the TOM  
482 complex receptors Tom20 and Tom70. Although both receptors may not be vividly crucial for  
483 the actual membrane integration process, we propose that they are required for facilitating  
484 efficient delivery in the crowded environment of the cell.

## 485 **Materials and Methods**

### 486 **Yeast strains and growth methods**

487 The parental strain YMK120 was used to create strains with genes under the control of a  
488 tetracycline-repressible promoter (Gnanasundram and Koš, 2015). The tetracycline operator  
489 was inserted into the genome by homologous recombination using an insertion cassette  
490 amplified from the plasmids pMK632Kan and pMK632His (Gnanasundram and Koš, 2015).  
491 Strains with two genes under the control of the tetracycline operator were obtained by mating  
492 of strains with a single tet-regulated gene followed by tetrad dissection. Yeast strains  
493 expressing Ydj1 and Sis1 under tetracycline promoter were grown in YP-Sucrose medium (for  
494 mitochondria isolation) or in YPD medium (for isolation of cell extract). For mitochondria  
495 isolation, cells were grown for 2 h on medium lacking doxycycline before adding 2 µg/ml of  
496 doxycycline to the culture. Then, cells were cultured for different time periods before their  
497 harvest. All strains used in this study are listed in Table S2.

### 498 **Recombinant DNA techniques**

499 The plasmids pRS426-TPI-Tom20 and pRS426-TPI-Tom70 were used as templates for the  
500 PCR-amplification of the TOM20 and TOM70 genes, respectively. The amplification product  
501 was inserted into the plasmid pGEM4polyA-3HA using KpnI and BamHI restriction sites. The  
502 MSP1 gene was amplified by PCR from yeast genomic DNA with specific primers containing  
503 BamHI and HindIII restriction sites. The PCR product was cloned into the plasmid pGEM4 to  
504 obtain pGEM4-yk-Msp1 which was used as a template for cloning yk-Msp1 into  
505 pGEM4polyA-3HA plasmid using SacI and BamHI restriction sites. MCR1 gene was  
506 amplified by PCR using pGEM4-yk-Mcr1 plasmid as template. The amplification product was  
507 inserted into pGEM4polyA-3HA using EcoRI and SmaI restriction sites.

508 The sequences encoding either the cytosolic domain (a.a 33-363) or the transmembrane domain  
509 (a.a 1-32) of Msp1 were amplified by PCR using the pGEM4-YK-Msp1-3HA plasmid as a  
510 template. The sequence encoding either the cytosolic domain (a.a 35-302) or the  
511 transmembrane domain (a.a 1-39) of Mcr1 were amplified by PCR using pGEM4-YK-Mcr1-  
512 3HA plasmid as a template. The sequences encoding either the cytosolic domain (a.a 33-183)  
513 or the transmembrane domain (a.a 1-30) of Tom20 were amplified by PCR using the pGEM4-  
514 YK-Tom20-3HA plasmid as a template. The sequences encoding either the cytosolic domain  
515 (a.a 33-617) or the transmembrane domain (a.a 1-32) of Tom70 were amplified by PCR using  
516 the pGEM4-YK-Tom70-3HA plasmid as a template. All these PCR products were inserted

517 with suitable restriction sites into the pGEM4polyA-3HA plasmid for their translation in yeast  
518 extract. In all the constructs mentioned above the yeast Kozak (YK) sequence was introduced  
519 via a primer directly upstream of the start codon. All primers and plasmids used in this study  
520 are listed in Tables S3 and S4, respectively.

### 521 **Protein purification**

522 Recombinant cBag and C90 were expressed in BL21 cells from the plasmid pPROEX-HTa-  
523 cBag or pPROEX-HTa-C90, respectively (Young et al., 2003). Expression was induced for 4  
524 h with 1 mM IPTG at 37 °C. The cells were harvested, resuspended in French Press buffer (40  
525 mM HEPES, 100 mM KCl, 20 mM imidazole, 2 mM PMSF, EDTA-free cOmplete protease  
526 inhibitor [Roche], pH 7.5) for 1 hour followed by homogenization using tight douncer. Cells  
527 were then lysed with an EmulsiFlex-C5 French Press. The cell lysate was subjected to a  
528 clarifying spin (15000 x g, 15 min, 4 °C) and the supernatants were incubated overnight with  
529 2 mL Ni-NTA Agarose beads (Cube Biotech). The bound proteins were washed with 20 mL  
530 wash buffer (40 mM HEPES, 100 mM KCl, 50 mM imidazole, pH 7.5) and eluted with elution  
531 buffer (40 mM HEPES, 100 mM KCl, 300 mM imidazole, pH 7.5).

532 GST, GST-Tom70 and GST-Tom20 were expressed and purified as described earlier (Papić et  
533 al., 2013).

### 534 **Biochemical procedures**

535 Protein samples for immunodecoration were analyzed on 8, 10, 12, or 15% SDS-PAGE and  
536 subsequently transferred onto nitrocellulose membranes by semi-dry Western blotting. Proteins  
537 were detected by incubating the membranes first with primary antibodies and then with  
538 horseradish peroxidase-conjugates of either goat anti-rabbit or goat anti-rat secondary  
539 antibodies. A list of antibodies used in this study is included in Table S5.

540 Mitochondria were isolated from WT yeast cells for in vitro imports by differential  
541 centrifugation as described. Pull-down assays with in vitro translated proteins were performed  
542 using cell-free yeast extract as described before (Jores et al., 2018).

### 543 **In vitro translation and GST Pull-down**

544 Purified GST and GST-recombinant proteins (GST-Tom20 and GST-Tom70) were incubated  
545 with glutathione sepharose beads for 1 hour followed by 1 hour blocking with 5% BSA in GST  
546 basic buffer (20 mM Hepes, 100 mM NaCl, 1 mM MgCl<sub>2</sub>, protease inhibitor mix, pH 7.25).  
547 The beads with the bound GST-proteins were centrifuged (500xg, 1 min, 2 °C). In-vitro

548 translated HA-tagged proteins were centrifuged (100000xg, 60 min, 2 °C) to remove ribosomes  
549 and aggregated proteins and were then mixed with the beads for 1 hour. An aliquot of 2% of  
550 the translated material was taken as input. The reaction was supplemented with ATP every 30  
551 minutes. The beads were then washed three times with GST basic buffer and the bound material  
552 was eluted by incubating the beads for 10 min at 95 °C in 4x sample buffer supplemented with  
553 0.05%  $\beta$ -ME. Eluted material was analysed by SDS-PAGE followed by Ponceau staining and  
554 western blotting using antibody against either the indicated proteins or the HA tag.

### 555 **In vitro translation and import of radiolabeled proteins**

556 Yeast extracts for in vitro translation were prepared as described (Wu and Sachs, 2014). For  
557 the preparation of yeast extracts from Ydj1- and Sis1-depleted cells, cells were grown for 8 h  
558 in the presence of 2  $\mu$ g/mL doxycycline prior to extract preparation.

559 Proteins were synthesized in yeast extract lysate after in vitro transcription by SP6 polymerase  
560 from pGEM4 vectors. Radiolabeled proteins were synthesized for 30 minutes in the presence  
561 of 35S-labeled Methionine and Cysteine. After translation, the reactions were supplemented  
562 with 58 mM “cold” Methionine-Cysteine mix and 1.5 M Sucrose followed by centrifugation  
563 (100000xg, 60 min, 2 °C) to remove ribosomes and aggregated proteins. The supernatant was  
564 diluted with import buffer (250 mM sucrose, 0.25 mg/ml BSA, 80 mM KCl, 5 mM MgCl<sub>2</sub>, 10  
565 mM MOPS, 2 mM NADH, 2 mM ATP, pH 7.2). Where indicated, the supernatant was  
566 supplemented with 20  $\mu$ M cBag or, as a control, with an equivalent amount of BSA. Isolated  
567 mitochondria were diluted in import buffer and supplemented with 4 mM ATP and 2 mM  
568 NADH and, where indicated, with 20  $\mu$ M of C90. Some samples were treated with 40  $\mu$ g/ml  
569 of trypsin. The import reactions were started by addition of the radiolabeled proteins to the  
570 samples containing the isolated organelles and further incubation at 25°C for the indicated  
571 times. The import reactions were stopped by diluting the samples with SEM-K80 buffer (250  
572 mM sucrose, 80 mM KCl, 10 mM MOPS, 1 mM EDTA, pH 7.2) and re-isolation of  
573 mitochondria (13200xg, 2 min, 2 °C). The import of the proteins was analyzed by carbonate  
574 extraction. To that aim, the re-isolated mitochondria were resuspended in 0.1 M Na<sub>2</sub>CO<sub>3</sub>,  
575 incubated on ice for 30 min, and re-isolated by centrifugation (100000xg, 30 min, 2 °C). The  
576 pellets were resuspended in 2x sample buffer, incubated for 10 min at 95°C and subjected to  
577 SDS-PAGE followed by western blotting and/or autoradiography. Quantifications of bands  
578 intensities were obtained using the software *AIDA Image Analyzer*. Values obtained by AIDA  
579 were analysed and formatted into graphs using Excel software.



## 580 **Fluorescence anisotropy**

581 Peptides corresponding to the transmembrane domains of either Mcr1 or Tom70 were  
582 synthesized as described previously (Jores et al., 2016). Next, the peptides were coupled to  
583 TAMRA and used for the determination of binding interactions and affinities of  
584 peptide/(co)chaperone complexes by fluorescence anisotropy. Measurements were performed  
585 at 30°C in a Jasco FP-8500 Fluorospectrometer equipped with polarizers. Excitation and  
586 emission wavelength were set to 554 nm and 579 nm, respectively. Samples containing 2 µM  
587 TAMRA-labeled peptide were equilibrated for 15 min before 10 µM Ssa1, 30 µM Sis1, 10 µM  
588 GST-Tom70, 10 µM BSA or 1 mM ATP in the indicated order or alone were added. For  
589 affinity measurements, 2 µM TAMRA-labeled peptides were supplemented with the indicated  
590 concentrations of Ssa1 or Sis1 and the difference in anisotropy of bound and free peptide were  
591 plotted against the (co)chaperone concentration.

592 For the sequential anisotropy measurements: Each experiment was performed in triplicates  
593 including biological duplicates (two independent protein purifications). For kD measurements  
594 the experiments were performed in triplicates, including biological duplicates (two  
595 independent protein purifications). The data analysis was performed using the OriginLab  
596 software. The mean value of each triplicate was calculated, and the delta anisotropy values  
597 plotted against the concentration the stated protein. A Hill fit was performed to calculate the  
598 kD value.

599

## 600 **NanoLC-MS/MS analysis and data processing**

601 Coomassie-stained gel pieces were digested in gel with trypsin, and desalted peptide mixtures  
602 (Rappsilber et al., 2007) were separated on an Easy-nLC 1200 coupled to a Q Exactive HF  
603 mass spectrometer (both Thermo Fisher Scientific) as described elsewhere (Kliza et al., 2017)  
604 with slight modifications: peptide mixtures were separated using a 57 minute segmented  
605 gradient of 10-33-50-90% of HPLC solvent B (80% acetonitrile in 0.1% formic acid) in HPLC  
606 solvent A (0.1% formic acid) at a flow rate of 200 nl/min. In each scan cycle, the seven most  
607 intense precursor ions were sequentially fragmented using higher energy collisional  
608 dissociation (HCD) fragmentation. In all measurements, sequenced precursor masses were  
609 excluded from further selection for 30 sec. The target values for MS/MS fragmentation were  
610 105 charges, and for the MS scan 3x10<sup>6</sup> charges.



611 Acquired MS spectra were processed with MaxQuant software package version 1.6.7.0 (Cox  
612 and Mann, 2008) with integrated Andromeda search engine (Cox et al., 2011). Database search  
613 was performed against a target-decoy *Saccharomyces cerevisiae* database obtained from  
614 Uniprot containing 6078 protein entries, and 286 commonly observed contaminants. In  
615 database search, full trypsin digestion specificity was required and up to two missed cleavages  
616 were allowed. Carbamidomethylation of cysteine was set as fixed modification; protein N-  
617 terminal acetylation, and oxidation of methionine were set as variable modifications. Initial  
618 precursor mass tolerance was set to 4.5 ppm and 20 ppm at the MS/MS level. A false discovery  
619 rate of 1% was applied at the peptide and protein level. The mass spectrometry proteomics data  
620 have been deposited to the ProteomeXchange Consortium via the PRIDE partner repository  
621 with the dataset identifier PXD031610.

622

### 623 **Acknowledgments**

624 We thank E. Kracker for excellent technical assistance and T. Becker for antibodies. This work  
625 was supported by the Deutsche Forschungsgemeinschaft (RA 1028/10-2 to D.R.). L.D. was  
626 supported by a long-term fellowship from the Minerva Foundation.

627

### 628 **Competing financial interests**

629 The authors declare no competing financial interests.

## 630 **References**

- 631 Ahting, U., T. Waizenegger, W. Neupert, and D. Rapaport. 2005. Signal-anchored proteins  
632 follow a unique insertion pathway into the outer membrane of mitochondria. *The Journal of*  
633 *biological chemistry*. 280:48–53. doi:10.1074/JBC.M410905200.
- 634 Backes, S., Y.S. Bykov, T. Flohr, M. Räschele, J. Zhou, S. Lenhard, L. Krämer, T. Mühlhaus,  
635 C. Bibi, C. Jann, J.D. Smith, L.M. Steinmetz, D. Rapaport, Z. Storchová, M. Schuldiner, F.  
636 Boos, and J.M. Herrmann. 2021. The chaperone-binding activity of the mitochondrial  
637 surface receptor Tom70 protects the cytosol against mitoprotein-induced stress. *Cell reports*.  
638 35. doi:10.1016/J.CELREP.2021.108936.
- 639 Becker, T., S. Pfannschmidt, B. Guiard, D. Stojanovski, D. Milenkovic, S. Kutik, N. Pfanner,  
640 C. Meisinger, and N. Wiedemann. 2008. Biogenesis of the mitochondrial TOM complex:  
641 Mim1 promotes insertion and assembly of signal-anchored receptors. *The Journal of*  
642 *biological chemistry*. 283:120–127. doi:10.1074/JBC.M706997200.
- 643 Bhangoo, M.K., S. Tzankov, A.C.Y. Fan, K. Dejgaard, D.Y. Thomas, and J.C. Young. 2007.  
644 Multiple 40-kDa heat-shock protein chaperones function in Tom70-dependent  
645 mitochondrial import. *Molecular biology of the cell*. 18:3414–3428.  
646 doi:10.1091/MBC.E07-01-0088.
- 647 Bohush, A., P. Bieganowski, and A. Filipek. 2019. Hsp90 and Its Co-Chaperones in  
648 Neurodegenerative Diseases. *International journal of molecular sciences*. 20.  
649 doi:10.3390/IJMS20204976.
- 650 Caplan, A.J., D.M. Cyr, and M.G. Douglas. 1992. YDJ1p facilitates polypeptide translocation  
651 across different intracellular membranes by a conserved mechanism. *Cell*. 71:1143–1155.  
652 doi:10.1016/S0092-8674(05)80063-7.
- 653 Cashikar, A.G., M. Duennwald, and S.L. Lindquist. 2005. A chaperone pathway in protein  
654 disaggregation. Hsp26 alters the nature of protein aggregates to facilitate reactivation by  
655 Hsp104. *The Journal of biological chemistry*. 280:23869–23875.  
656 doi:10.1074/JBC.M502854200.
- 657 Chaari, A. 2019. Molecular chaperones biochemistry and role in neurodegenerative diseases.  
658 *International journal of biological macromolecules*. 131:396–411.  
659 doi:10.1016/J.IJBIOMAC.2019.02.148.
- 660 Chen, Y., G.K.E. Umanah, N. Dephoure, S.A. Andrabi, S.P. Gygi, T.M. Dawson, V.L.  
661 Dawson, and J. Rutter. 2014. Msp1/ATAD1 maintains mitochondrial function by  
662 facilitating the degradation of mislocalized tail-anchored proteins. *The EMBO journal*.  
663 33:1548–1564. doi:10.15252/EMBJ.201487943.
- 664 Cichocki, B.A., K. Krumpe, D.G. Vitali, and D. Rapaport. 2018. Pex19 is involved in importing  
665 dually targeted tail-anchored proteins to both mitochondria and peroxisomes. *Traffic*.  
666 19:770–785. doi:10.1111/TRA.12604.

- 667 Clerico, E.M., J.M. Tilitsky, W. Meng, and L.M. Gierasch. 2015. How hsp70 molecular  
668 machines interact with their substrates to mediate diverse physiological functions. *Journal*  
669 *of molecular biology*. 427:1575–1588. doi:10.1016/J.JMB.2015.02.004.
- 670 Collier, M.P., and J.L.P. Benesch. 2020. Small heat-shock proteins and their role in mechanical  
671 stress. *Cell stress & chaperones*. 25:601–613. doi:10.1007/S12192-020-01095-Z.
- 672 Cox, J., and M. Mann. 2008. MaxQuant enables high peptide identification rates,  
673 individualized p.p.b.-range mass accuracies and proteome-wide protein quantification.  
674 *Nature biotechnology*. 26:1367–1372. doi:10.1038/NBT.1511.
- 675 Cox, J., N. Neuhauser, A. Michalski, R.A. Scheltema, J. v. Olsen, and M. Mann. 2011.  
676 Andromeda: a peptide search engine integrated into the MaxQuant environment. *Journal of*  
677 *proteome research*. 10:1794–1805. doi:10.1021/PR101065J.
- 678 Cry, D.M. 1995. Cooperation of the molecular chaperone Ydj1 with specific Hsp70 homologs  
679 to suppress protein aggregation. *FEBS letters*. 359:129–132. doi:10.1016/0014-  
680 5793(95)00024-4.
- 681 Deshaies, R.J., B.D. Koch, M. Werner-Washburne, E.A. Craig, and R. Schekman. 1988. A  
682 subfamily of stress proteins facilitates translocation of secretory and mitochondrial  
683 precursor polypeptides. *Nature*. 332:800–805. doi:10.1038/332800A0.
- 684 Doan, K.N., A. Grevel, C.U. Mårtensson, L. Ellenrieder, N. Thornton, L.S. Wenz, Ł. Opaliński,  
685 B. Guiard, N. Pfanner, and T. Becker. 2020. The Mitochondrial Import Complex MIM  
686 Functions as Main Translocase for  $\alpha$ -Helical Outer Membrane Proteins. *Cell reports*. 31.  
687 doi:10.1016/J.CELREP.2020.107567.
- 688 Drwesh, L., and D. Rapaport. 2020. Biogenesis pathways of  $\alpha$ -helical mitochondrial outer  
689 membrane proteins. *Biological Chemistry*. 401:677–686. doi:10.1515/HSZ-2019-0440.
- 690 Endo, T., S. Mitsui, M. Nakai, and D. Roise. 1996. Binding of mitochondrial presequences to  
691 yeast cytosolic heat shock protein 70 depends on the amphiphilicity of the presequence. *The*  
692 *Journal of biological chemistry*. 271:4161–4167. doi:10.1074/JBC.271.8.4161.
- 693 Fan, A.C.Y., L.M. Gava, C.H.I. Ramos, and J.C. Young. 2010. Human mitochondrial import  
694 receptor Tom70 functions as a monomer. *The Biochemical journal*. 429:553–563.  
695 doi:10.1042/BJ20091855.
- 696 Fan, A.C.Y., G. Kozlov, A. Hoegl, R.C. Marcellus, M.J.H. Wong, K. Gehring, and J.C. Young.  
697 2011. Interaction between the human mitochondrial import receptors Tom20 and Tom70 in  
698 vitro suggests a chaperone displacement mechanism. *The Journal of biological chemistry*.  
699 286:32208–32219. doi:10.1074/JBC.M111.280446.
- 700 Franzmann, T.M., M. Wühr, K. Richter, S. Walter, and J. Buchner. 2005. The Activation  
701 Mechanism of Hsp26 does not Require Dissociation of the Oligomer. *Journal of Molecular*  
702 *Biology*. 350:1083–1093. doi:10.1016/J.JMB.2005.05.034.
- 703 Gnanasundram, S.V., and M. Koš. 2015. Fast protein-depletion system utilizing tetracycline  
704 repressible promoter and N-end rule in yeast. *Molecular biology of the cell*. 26:762–768.  
705 doi:10.1091/MBC.E14-07-1186.

- 706 Hahne, K., V. Haucke, L. Ramage, and G. Schatz. 1994. Incomplete arrest in the outer  
707 membrane sorts NADH-cytochrome b5 reductase to two different submitochondrial  
708 compartments. *Cell*. 79:829–839. doi:10.1016/0092-8674(94)90072-8.
- 709 Haslbeck, M., A. Miess, T. Stromer, S. Walter, and J. Buchner. 2005. Disassembling protein  
710 aggregates in the yeast cytosol. The cooperation of Hsp26 with Ssa1 and Hsp104. *The*  
711 *Journal of biological chemistry*. 280:23861–23868. doi:10.1074/JBC.M502697200.
- 712 Haslbeck, M., S. Weinkauff, and J. Buchner. 2019. Small heat shock proteins: Simplicity meets  
713 complexity. *The Journal of Biological Chemistry*. 294:2121.  
714 doi:10.1074/JBC.REV118.002809.
- 715 Hettema, E.H., C.C.M. Ruigrok, M.G. Koerkamp, M. van den Berg, H.F. Tabak, B. Distel, and  
716 I. Braakman. 1998a. The cytosolic DnaJ-like protein djp1p is involved specifically in  
717 peroxisomal protein import. *The Journal of cell biology*. 142:421–434.  
718 doi:10.1083/JCB.142.2.421.
- 719 Hettema, E.H., C.C.M. Ruigrok, M.G. Koerkamp, M. van den Berg, H.F. Tabak, B. Distel, and  
720 I. Braakman. 1998b. The cytosolic DnaJ-like protein djp1p is involved specifically in  
721 peroxisomal protein import. *The Journal of cell biology*. 142:421–434.  
722 doi:10.1083/JCB.142.2.421.
- 723 Hoseini, H., S. Pandey, T. Jores, A. Schmitt, M. Franz-Wachtel, B. Macek, J. Buchner, K.S.  
724 Dimmer, and D. Rapaport. 2016. The cytosolic cochaperone Stil is relevant for  
725 mitochondrial biogenesis and morphology. *The FEBS journal*. 283:3338–3352.  
726 doi:10.1111/FEBS.13813.
- 727 Jansen, R.L.M., and I.J. van der Klei. 2019. The peroxisome biogenesis factors Pex3 and  
728 Pex19: multitasking proteins with disputed functions. *FEBS letters*. 593:457–474.  
729 doi:10.1002/1873-3468.13340.
- 730 Johnson, J.L., and E.A. Craig. 2001. An essential role for the substrate-binding region of  
731 Hsp40s in *Saccharomyces cerevisiae*. *The Journal of cell biology*. 152:851–856.  
732 doi:10.1083/JCB.152.4.851.
- 733 Jores, T., A. Klinger, L.E. Groß, S. Kawano, N. Flinner, E. Duchardt-Ferner, J. Wöhnert, H.  
734 Kalbacher, T. Endo, E. Schleiff, and D. Rapaport. 2016. Characterization of the targeting  
735 signal in mitochondrial  $\beta$ -barrel proteins. *Nature communications*. 7.  
736 doi:10.1038/NCOMMS12036.
- 737 Jores, T., J. Lawatscheck, V. Beke, M. Franz-Wachtel, K. Yunoki, J.C. Fitzgerald, B. Macek,  
738 T. Endo, H. Kalbacher, J. Buchner, and D. Rapaport. 2018. Cytosolic Hsp70 and Hsp40  
739 chaperones enable the biogenesis of mitochondrial  $\beta$ -barrel proteins. *Journal of Cell*  
740 *Biology*. 217:3091–3108. doi:10.1083/JCB.201712029.
- 741 Kampinga, H.H., and E.A. Craig. 2010. The HSP70 chaperone machinery: J proteins as drivers  
742 of functional specificity. *Nature reviews. Molecular cell biology*. 11:579–592.  
743 doi:10.1038/NRM2941.

- 744 Klaips, C.L., M.H.M. Gropp, M.S. Hipp, and F.U. Hartl. 2020. Sis1 potentiates the stress  
745 response to protein aggregation and elevated temperature. *Nature Communications* 2020  
746 11:1. 11:1–16. doi:10.1038/s41467-020-20000-x.
- 747 Kliza, K., C. Taumer, I. Pinzuti, M. Franz-Wachtel, S. Kunzelmann, B. Stieglitz, B. MacEk,  
748 and K. Husnjak. 2017. Internally tagged ubiquitin: a tool to identify linear polyubiquitin-  
749 modified proteins by mass spectrometry. *Nature methods*. 14:504–512.  
750 doi:10.1038/NMETH.4228.
- 751 Komiya, T., S. Rospert, G. Schatz, and K. Mihara. 1997. Binding of mitochondrial precursor  
752 proteins to the cytoplasmic domains of the import receptors Tom70 and Tom20 is  
753 determined by cytoplasmic chaperones. *The EMBO journal*. 16:4267–4275.  
754 doi:10.1093/EMBOJ/16.14.4267.
- 755 Kreimendahl, S., and J. Rassow. 2020. The Mitochondrial Outer Membrane Protein Tom70-  
756 Mediator in Protein Traffic, Membrane Contact Sites and Innate Immunity. *International*  
757 *journal of molecular sciences*. 21:1–32. doi:10.3390/IJMS21197262.
- 758 Lamb, D.C., D.E. Kelly, N.J. Manning, M.A. Kaderbhai, and S.L. Kelly. 1999. Biodiversity of  
759 the P450 catalytic cycle: yeast cytochrome b5/NADH cytochrome b5 reductase complex  
760 efficiently drives the entire sterol 14-demethylation (CYP51) reaction. *FEBS letters*.  
761 462:283–288. doi:10.1016/S0014-5793(99)01548-3.
- 762 Li, J., X. Qian, and B. Sha. 2009. Heat shock protein 40: structural studies and their functional  
763 implications. *Protein and peptide letters*. 16:606–612. doi:10.2174/092986609788490159.
- 764 Meineke, B., G. Engl, C. Kemper, A. Vasiljev-Neumeyer, H. Paulitschke, and D. Rapaport.  
765 2008. The outer membrane form of the mitochondrial protein Mcr1 follows a TOM-  
766 independent membrane insertion pathway. *FEBS letters*. 582:855–860.  
767 doi:10.1016/J.FEBSLET.2008.02.009.
- 768 Mills, R.D., J. Trehwella, T.W. Qiu, T. Welte, T.M. Ryan, T. Hanley, R.B. Knott, T. Lithgow,  
769 and T.D. Mulhern. 2009. Domain organization of the monomeric form of the Tom70  
770 mitochondrial import receptor. *Journal of molecular biology*. 388:1043–1058.  
771 doi:10.1016/J.JMB.2009.03.070.
- 772 Mokry, D.Z., J. Abrahão, and C.H.I. Ramos. 2015. Disaggregases, molecular chaperones that  
773 resolubilize protein aggregates. *Anais da Academia Brasileira de Ciências*. 87:1273–1292.  
774 doi:10.1590/0001-3765201520140671.
- 775 Neupert, W., and J.M. Herrmann. 2007. Translocation of proteins into mitochondria. *Annual*  
776 *review of biochemistry*. 76:723–749. doi: 10.1146/ANNUREV.BIOCHEM.  
777 76.052705.163409.
- 778 Neupert, W., and N. Pfanner. 1993. Roles of molecular chaperones in protein targeting to  
779 mitochondria. *Philosophical transactions of the Royal Society of London. Series B,*  
780 *Biological sciences*. 339. doi:10.1098/RSTB.1993.0034.

- 781 Okreglak, V., and P. Walter. 2014. The conserved AAA-ATPase Msp1 confers organelle  
782 specificity to tail-anchored proteins. *Proceedings of the National Academy of Sciences of*  
783 *the United States of America*. 111:8019–8024. doi:10.1073/PNAS.1405755111.
- 784 Opaliński, Ł., J. Song, C. Priesnitz, L.S. Wenz, S. Oeljeklaus, B. Warscheid, N. Pfanner, and  
785 T. Becker. 2018. Recruitment of Cytosolic J-Proteins by TOM Receptors Promotes  
786 Mitochondrial Protein Biogenesis. *Cell reports*. 25:2036-2043.e5.  
787 doi:10.1016/J.CELREP.2018.10.083.
- 788 Papić, D., Y. Elbaz-Alon, S.N. Koerdts, K. Leopold, D. Worm, M. Jung, M. Schuldiner, and D.  
789 Rapaport. 2013. The role of Djpl in import of the mitochondrial protein Mim1 demonstrates  
790 specificity between a cochaperone and its substrate protein. *Molecular and cellular biology*.  
791 33:4083–4094. doi:10.1128/MCB.00227-13.
- 792 Popov-Čeleketić, J., T. Waizenegger, and D. Rapaport. 2008. Mim1 functions in an oligomeric  
793 form to facilitate the integration of Tom20 into the mitochondrial outer membrane. *Journal*  
794 *of molecular biology*. 376:671–680. doi:10.1016/J.JMB.2007.12.006.
- 795 Rappsilber, J., M. Mann, and Y. Ishihama. 2007. Protocol for micro-purification, enrichment,  
796 pre-fractionation and storage of peptides for proteomics using StageTips. *Nature protocols*.  
797 2:1896–1906. doi:10.1038/NPROT.2007.261.
- 798 Saio, T., X. Guan, P. Rossi, A. Economou, and C.G. Kalodimos. 2014. Structural basis for  
799 protein antiaggregation activity of the trigger factor chaperone. *Science (New York, N.Y.)*.  
800 344. doi:10.1126/SCIENCE.1250494.
- 801 Vitali, D.G., L. Drwesh, B.A. Cichocki, A. Kolb, and D. Rapaport. 2020. The Biogenesis of  
802 Mitochondrial Outer Membrane Proteins Show Variable Dependence on Import Factors.  
803 *iScience*. 23. doi:10.1016/J.ISCI.2019.100779.
- 804 Wegele, H., S.K. Wandinger, A.B. Schmid, J. Reinstein, and J. Buchner. 2006. Substrate  
805 Transfer from the Chaperone Hsp70 to Hsp90. *Journal of Molecular Biology*. 356:802–811.  
806 doi:10.1016/J.JMB.2005.12.008.
- 807 Wiedemann, N., and N. Pfanner. 2017. Mitochondrial Machineries for Protein Import and  
808 Assembly. *Annual review of biochemistry*. 86:685–714. doi:10.1146/ANNUREV-  
809 BIOCHEM-060815-014352.
- 810 Wu, C., and M.S. Sachs. 2014. Preparation of a *Saccharomyces cerevisiae* cell-free extract for  
811 in vitro translation. *Methods in enzymology*. 539:17–28. doi:10.1016/B978-0-12-420120-  
812 0.00002-5.
- 813 Wyzkowski, H., A. Janta, W. Sztangierska, I. Obuchowski, T. Chamera, A. Kłosowska, and  
814 K. Liberek. 2021. Class-specific interactions between Sis1 J-domain protein and Hsp70  
815 chaperone potentiate disaggregation of misfolded proteins. *Proceedings of the National*  
816 *Academy of Sciences*. 118:e2108163118. doi:10.1073/PNAS.2108163118.
- 817 Xie, J.L., I. Bohovych, E.O.Y. Wong, J.P. Lambert, A.C. Gingras, O. Khalimonchuk, L.E.  
818 Cowen, and M.D. Leach. 2017. Ydj1 governs fungal morphogenesis and stress response,



- 819 and facilitates mitochondrial protein import via Mas1 and Mas2. *Microbial cell (Graz,*  
820 *Austria)*. 4:342–361. doi:10.15698/MIC2017.10.594.
- 821 Yan, W., and E.A. Craig. 1999. The glycine-phenylalanine-rich region determines the  
822 specificity of the yeast Hsp40 Sis1. *Molecular and cellular biology*. 19:7751–7758.  
823 doi:10.1128/MCB.19.11.7751.
- 824 Young, J.C., N.J. Hoogenraad, and F.U. Hartl. 2003. Molecular chaperones Hsp90 and Hsp70  
825 deliver preproteins to the mitochondrial import receptor Tom70. *Cell*. 112:41–50.  
826 doi:10.1016/S0092-8674(02)01250-3.
- 827 Zhou, C., B.D. Slaughter, J.R. Unruh, A. Eldakak, B. Rubinstein, and R. Li. 2011. Motility and  
828 segregation of Hsp104-associated protein aggregates in budding yeast. *Cell*. 147:1186–  
829 1196. doi:10.1016/J.CELL.2011.11.002.
- 830 Zolkiewski, M., T. Zhang, and M. Nagy. 2012. Aggregate reactivation mediated by the Hsp100  
831 chaperones. *Archives of biochemistry and biophysics*. 520:1–6.  
832 doi:10.1016/J.ABB.2012.01.012.



## 833 **Figure legends**

834 **Figure 1:** Cytosolic chaperones interact with newly synthesized signal-anchored proteins. (A  
835 and B) In-vitro translation reactions using yeast extracts without mRNA ( $\emptyset$ ) or programmed  
836 with mRNA encoding HA-tagged variants of signal-anchored proteins (Msp1, Mcr1, Tom20  
837 and Tom70), the tail-anchored protein Fis1, the  $\beta$ -barrel protein Porin, or, as a control,  
838 dihydrofolate reductase (DHFR). The reactions were subjected to a pull-down with anti-HA  
839 beads. Samples from the input and the eluates were analyzed by SDS-PAGE and  
840 immunodecoration with the indicated antibodies. Each experiment was done as three  
841 independent repeats. Two different yeast extracts were employed. Each repeat was done with  
842 new preparation of mRNA.

843 **Figure 2:** Cytosolic chaperones interact with newly synthesized signal-anchored proteins  
844 through their transmembrane domain. (A-C) In-vitro translation reactions using yeast extracts  
845 without mRNA ( $\emptyset$ ) or programmed with mRNA encoding HA-tagged versions of DHFR or  
846 the full length (FL), cytosolic domain (C) or transmembrane domain (T) of the SA proteins.  
847 Mcr1 (A), Msp1 (B) and Tom70 (C). The reactions were subjected to a pull-down with anti-  
848 HA beads. Samples from the input and the eluates were analyzed by SDS-PAGE and  
849 immunodecoration with the indicated antibodies. Each experiment was done as three  
850 independent repeats. The same yeast extract was used with different mRNAs in each repeat.

851 **Figure 3:** Depletion of both co-chaperones Ydj1 and Sis1 results in decreased steady-state  
852 levels of Tom20 and Tom70 proteins. (A and C) Mitochondrial and cytosolic fractions were  
853 isolated from WT, depleted for Ydj1 (Ydj1 $\downarrow$ ), depleted for Sis1 (Sis1 $\downarrow$ ), and double depleted  
854 for both co-chaperones (Ydj1 $\downarrow$ Sis1 $\downarrow$ ) yeast cells, after being grown without doxycycline  
855 (time=0) or in the presence of Dox. for 1, 2 or 4 hours. Samples were analyzed by SDS-PAGE  
856 followed by immunodecoration with the indicated antibodies. (B and D). Intensities of the  
857 bands corresponding to the depicted proteins in the mitochondrial fractions from three  
858 independent experiments were quantified and normalized to Ponceau levels. The levels of the  
859 proteins in each depletion strain in the absence of doxycycline (time=0) was set to 100%. Error  
860 bars represent  $\pm$  SD.

861 **Figure 4:** Signal-anchored proteins show variable dependence on Ydj1 and Sis1. (A and B) *In*  
862 *vitro* import of radiolabeled Tom20 (C) or Tom70 (D) that were translated in either WT or in  
863 Ydj1 and Sis1 depleted yeast extract (YS $\downarrow$ ). The radiolabeled proteins were incubated with WT  
864 mitochondria for the indicated time points (1, 5, 10 and 20 minutes). After import,

865 mitochondria were subjected to alkaline extraction and the pellet was analyzed by SDS-PAGE  
866 and autoradiography. Intensities of the bands corresponding to Tom20 and Tom70 were  
867 quantified. The intensities of the bands corresponding to import from WT yeast extract after  
868 20 min were set to 100%. The graph represents the mean values  $\pm$  SD of three independent  
869 experiments.

870 **Figure 5:** Depletion of Ydj1 and Sis1 can increase the risk for aggregation of newly synthesized  
871 proteins. (A and B) In-vitro translation reactions using yeast extracts from either WT cells or  
872 from cells depleted for both Ydj1 and Sis1 (YS $\downarrow$ ) were programmed with mRNA encoding  
873 HA-tagged versions of the indicated proteins. The reactions were subjected to a pull-down with  
874 anti-HA beads. Samples from the input and the eluates were analyzed by SDS-PAGE and  
875 immunodecoration with the indicated antibodies.

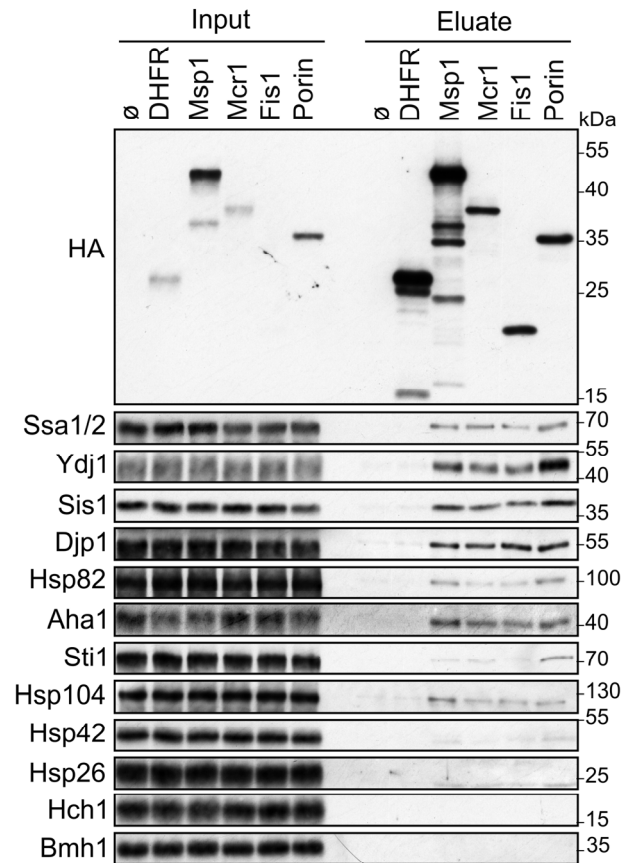
876 **Figure 6:** The hydrophobic segment of signal-anchored proteins interacts with the Hsp70  
877 chaperone and its co-chaperone Sis1. (A and B) The fluorescence anisotropy of TAMRA-  
878 labeled peptides corresponding to the TMDs of either Tom70 (A) or Mcr1 (B) was measured  
879 in the presence of 10  $\mu$ M Ssa1 (black circles) or 30  $\mu$ M BSA, as a control (red circles). (C-F)  
880 For affinity determinations, the TMD-labelled peptides of either Tom70 (C and E) or Mcr1 (D  
881 and F) were mixed with the indicated concentrations of either Ssa1 (C and D) or Sis1 (E and  
882 F), and the difference in anisotropy ( $\Delta$  anisotropy) of the bound and free peptide was plotted  
883 against the co-chaperone concentration.

884 **Figure 7:** The Hsp70 chaperone Ssa1 is required for proper insertion of signal-anchored  
885 proteins. (A and B) Left panels: Radiolabeled Msp1 (A) and Mcr1 (B) were translated in WT  
886 yeast extract and subjected to in-vitro import assay using isolated mitochondria. Prior to the  
887 import, the yeast extract translation reaction was incubated with either CBag (Hsp70 inhibitor)  
888 or with BSA, as a control. After import for the indicated time points, the samples were  
889 subjected to carbonate extraction and the pellets fraction were analyzed by SDS-PAGE  
890 followed by autoradiography. Right panels: The bands corresponding to Msp1 and Mcr1 were  
891 quantified and the results of three independent experiments are presented as mean values  $\pm$  SD.  
892 The intensities of the bands corresponding to import for 10 min in the presence of BSA were  
893 set to 100%. (C-E) The fluorescence anisotropy of TAMRA-labelled Mcr1-TMD peptide was  
894 measured while supplementing 10  $\mu$ M Ssa1, 30  $\mu$ M Sis1 and 1 mM ATP in the order indicated  
895 in the various panels.

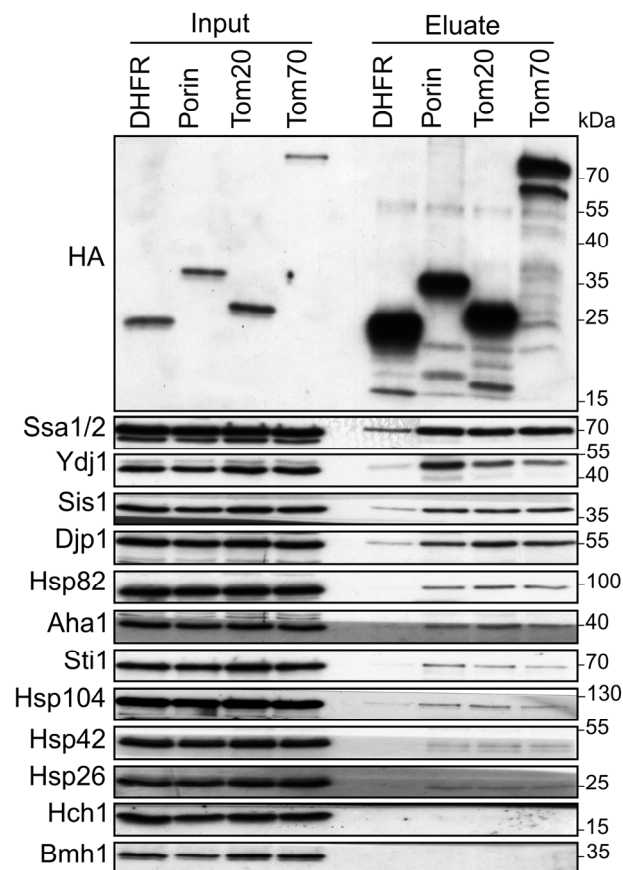
896 **Figure 8:** Newly synthesized signal-anchored proteins can be recognized by the cytosolic  
897 domains of the TOM receptors. (A) HA-tagged versions of the signal-anchored proteins, Mcr1  
898 and Msp1 or of the control protein DHFR, were freshly translated in yeast extract. Next, they  
899 were mixed with GST alone or GST fused to the cytosolic domain of either Tom20 (GST-  
900 Tom20) or Tom70 (GST-Tom70) bound to glutathione beads. Input (2%) and eluate (100%)  
901 samples were subjected to SDS-PAGE. GST fusion proteins were detected by Ponceau staining  
902 whereas SA proteins via immunodecoration with antibodies against the HA-tag. Lower panels:  
903 Bands corresponding to Msp1-3HA and Mcr1-3HA from three independent experiments were  
904 quantified and the level of binding to GST alone was set as 1. Error bars represent  $\pm$  SD. (B-  
905 E) Fluorescence anisotropy of TAMRA-labeled Mcr1 peptide was monitored after  
906 supplementing 10  $\mu$ M Ssa1, 1 mM ATP, or 10  $\mu$ M GST-Tom70 in the indicated order. (E) The  
907 first addition was of 10  $\mu$ M Ssa1 together with 30  $\mu$ M Sis1, followed by addition of 1 mM ATP  
908 and then finally 10  $\mu$ M GST-Tom70.

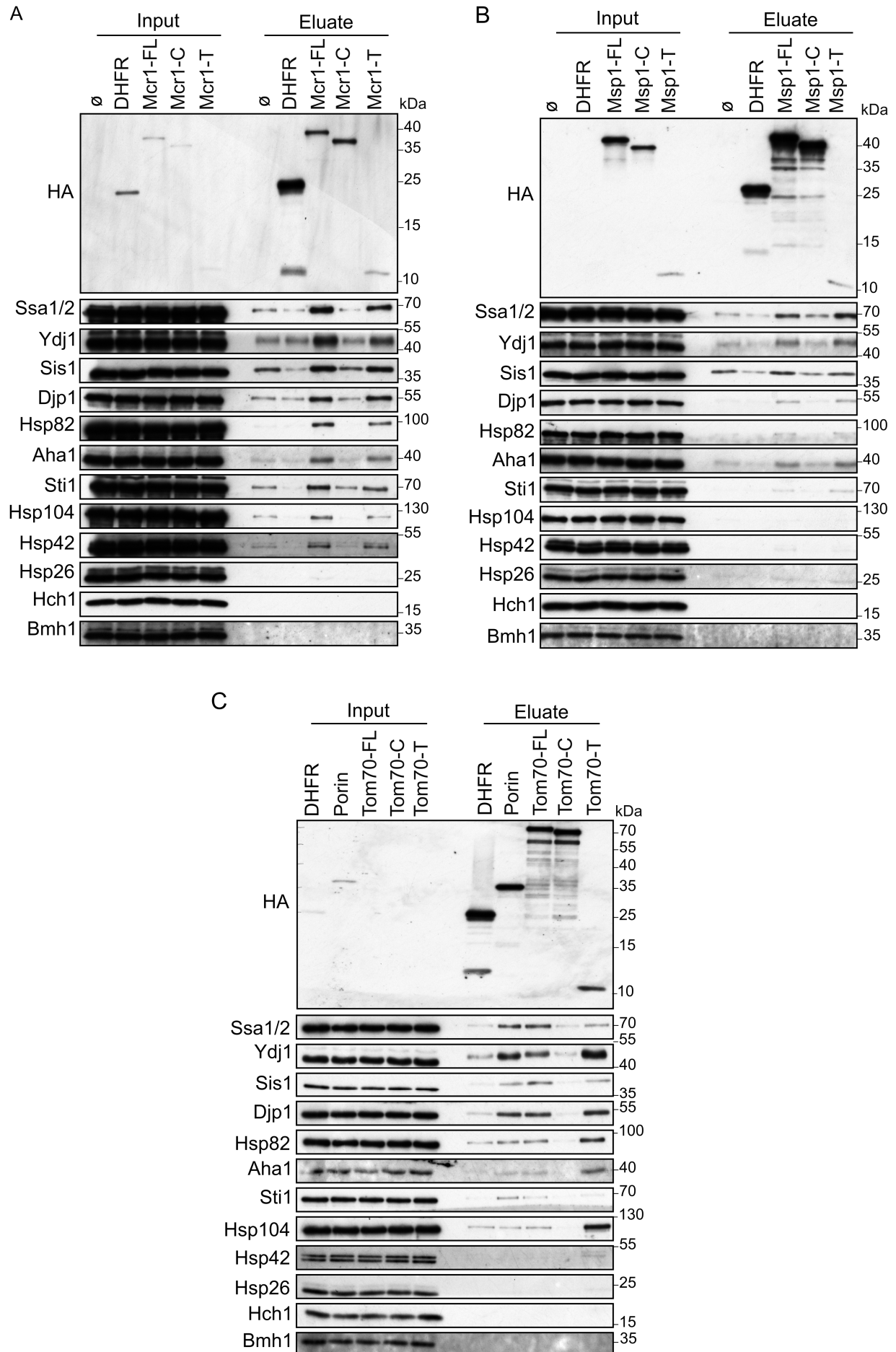
909 **Figure 9:** Tom70 and Tom20 may have offsetting function in mediating the biogenesis of Msp1  
910 and Mcr1. (A and B) Left panels: Radiolabeled Msp1 (A) and Mcr1 (B) were translated in WT  
911 yeast extract and subjected to in-vitro import assay using isolated mitochondria. Prior to the  
912 import, mitochondria were incubated for 30 minutes in the presence or absence of trypsin. After  
913 import for the indicated time points, the samples were subjected to carbonate extraction and  
914 the pellet fractions were subjected to SDS-PAGE followed by autoradiography. To verify the  
915 activity of the protease, the same membranes were immunodecorated with antibodies against  
916 the indicated proteins. Right panels: The bands corresponding to Msp1 and Mcr1 were  
917 quantified and the results of three independent experiments are presented as mean values  $\pm$  SD.  
918 The intensities of the bands corresponding to import for 15 min in the absence of Trypsin were  
919 set to 100%. (C and D) Left panels: Radiolabeled Msp1 (C) and Mcr1 (D) were translated in  
920 WT yeast extract and subjected to in-vitro import assay using mitochondria isolated from either  
921 WT or tom20 $\Delta$  strain. Prior to the import reactions, mitochondria were incubated in the  
922 presence or absence of 20  $\mu$ M C90 (blocker of Tom70). After import for the indicated time  
923 points, the samples were subjected to carbonate extraction and the pellet fractions were  
924 subjected to SDS-PAGE followed by autoradiography. Right panels: The bands corresponding  
925 to Msp1 and Mcr1 were quantified and the results of three independent experiments are  
926 presented as mean values  $\pm$  SD. The intensities of the bands corresponding to import for 15  
927 min in the absence of C90 were set to 100%.

A



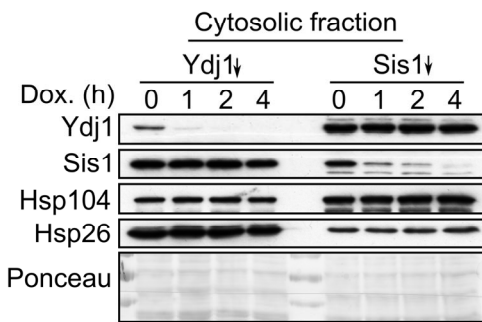
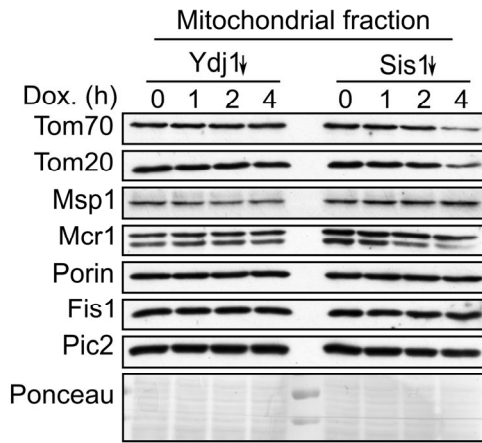
B



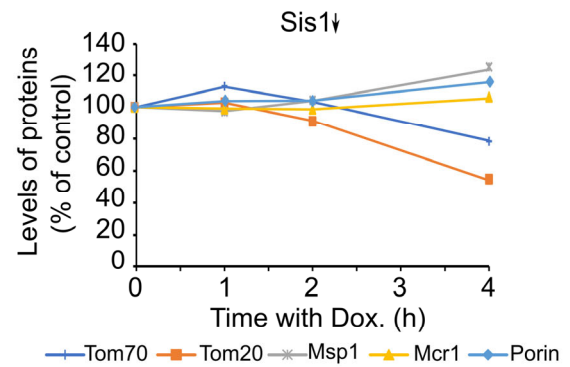
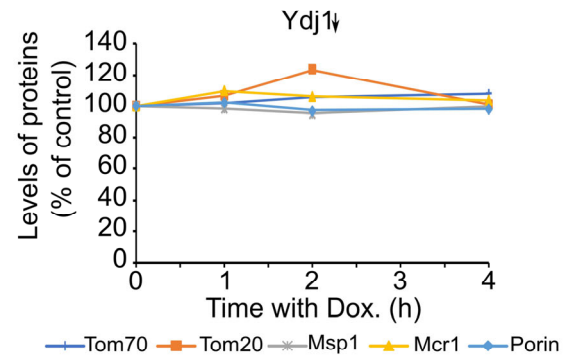




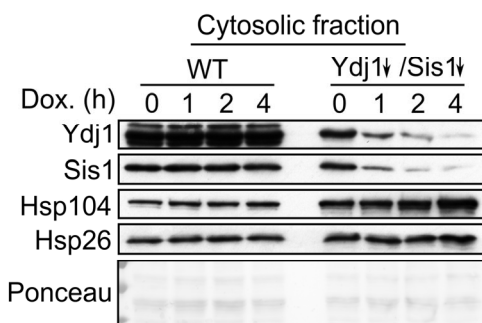
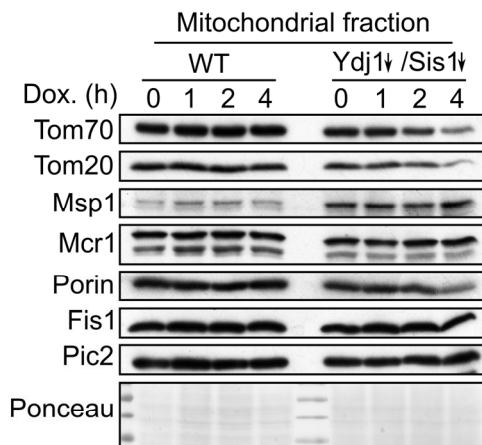
A



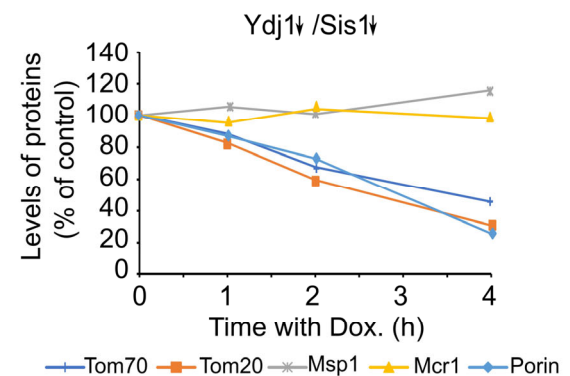
B



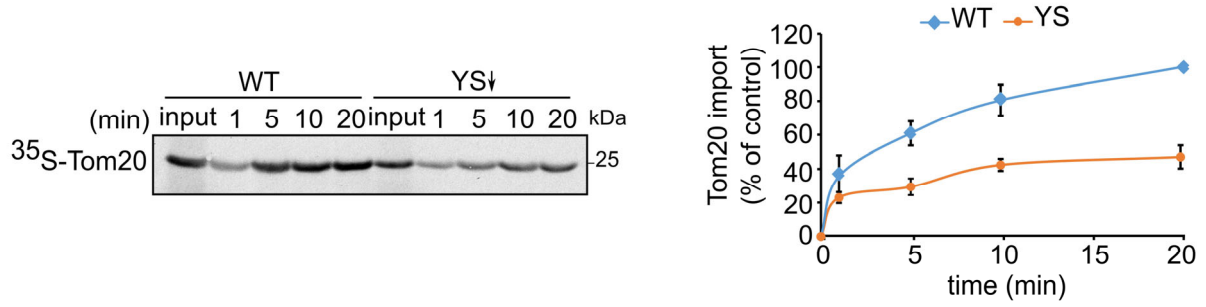
C



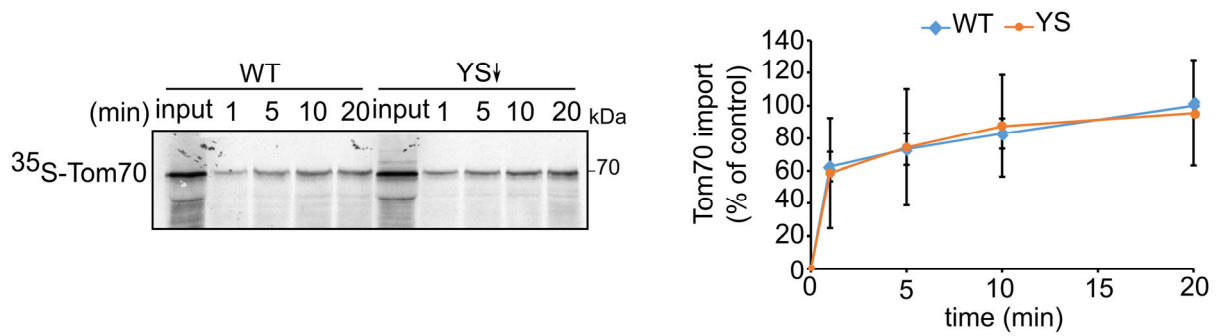
D



A

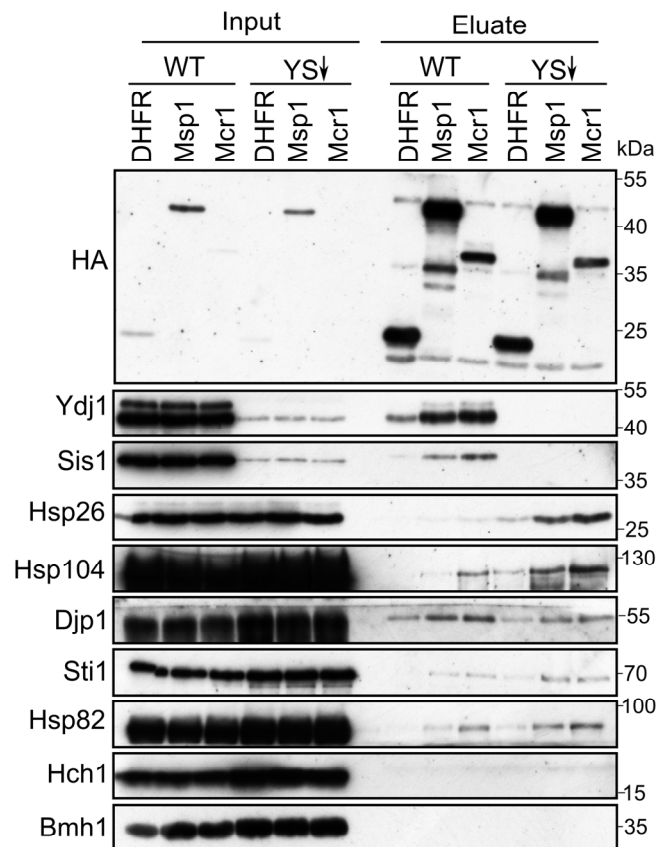


B

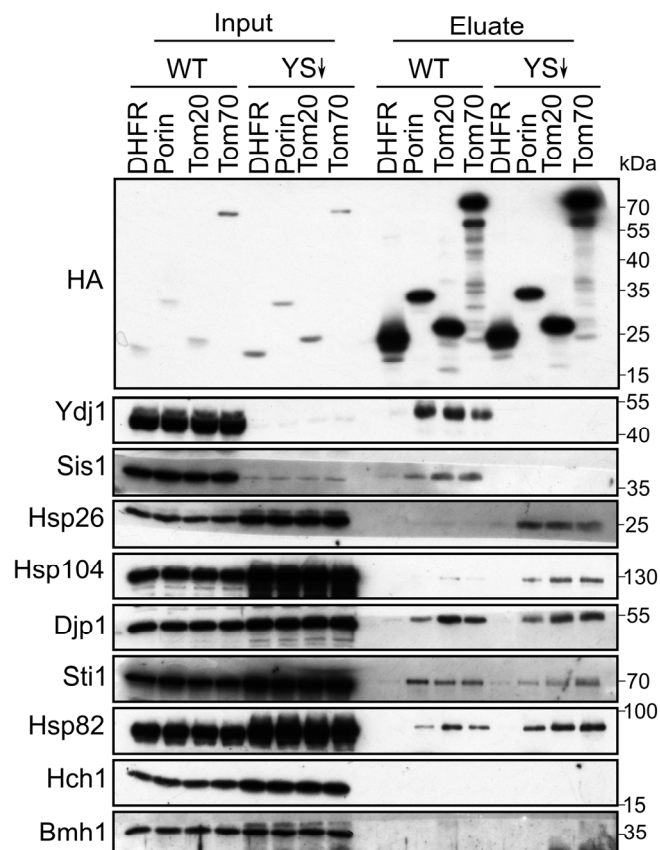


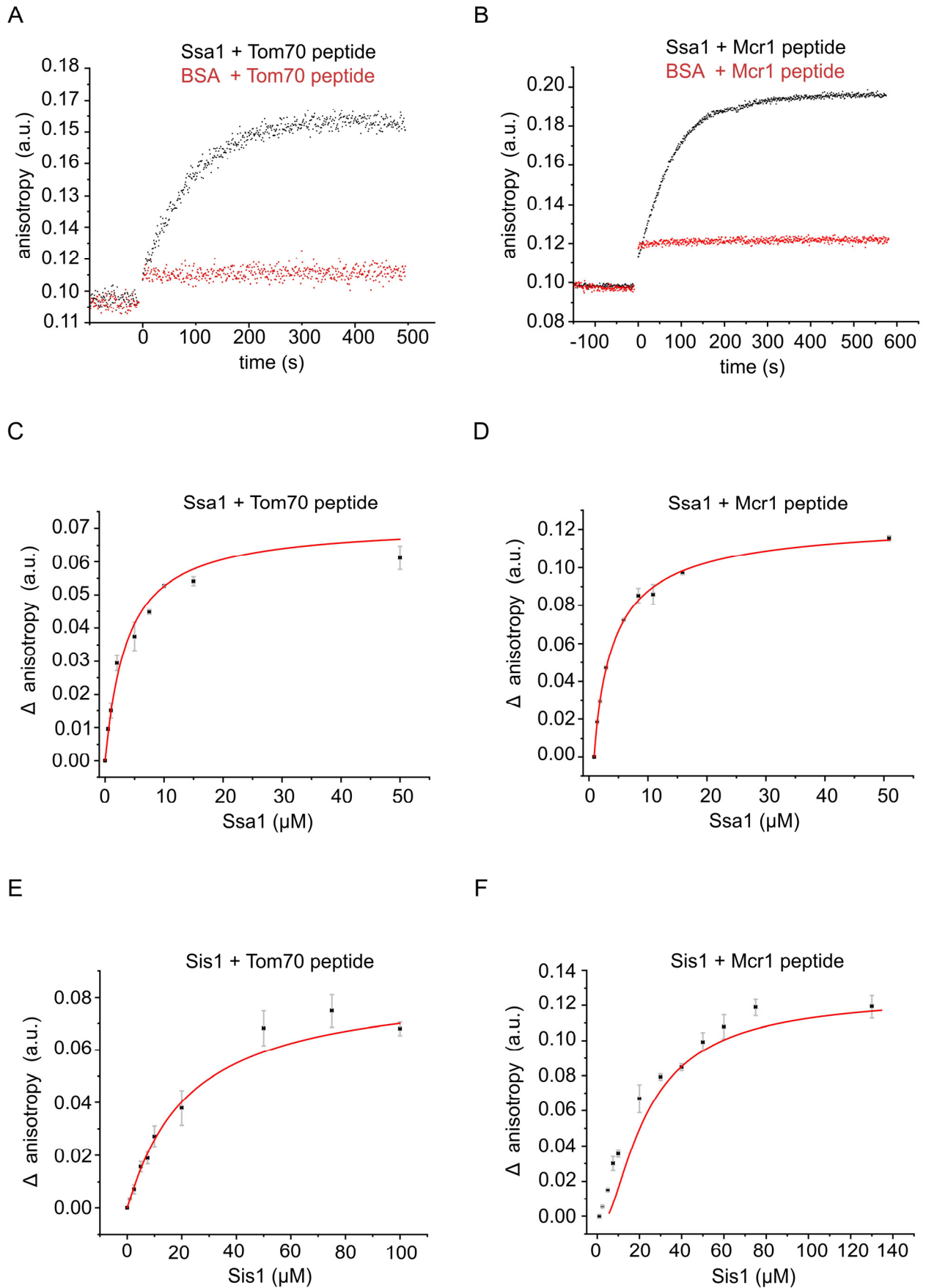


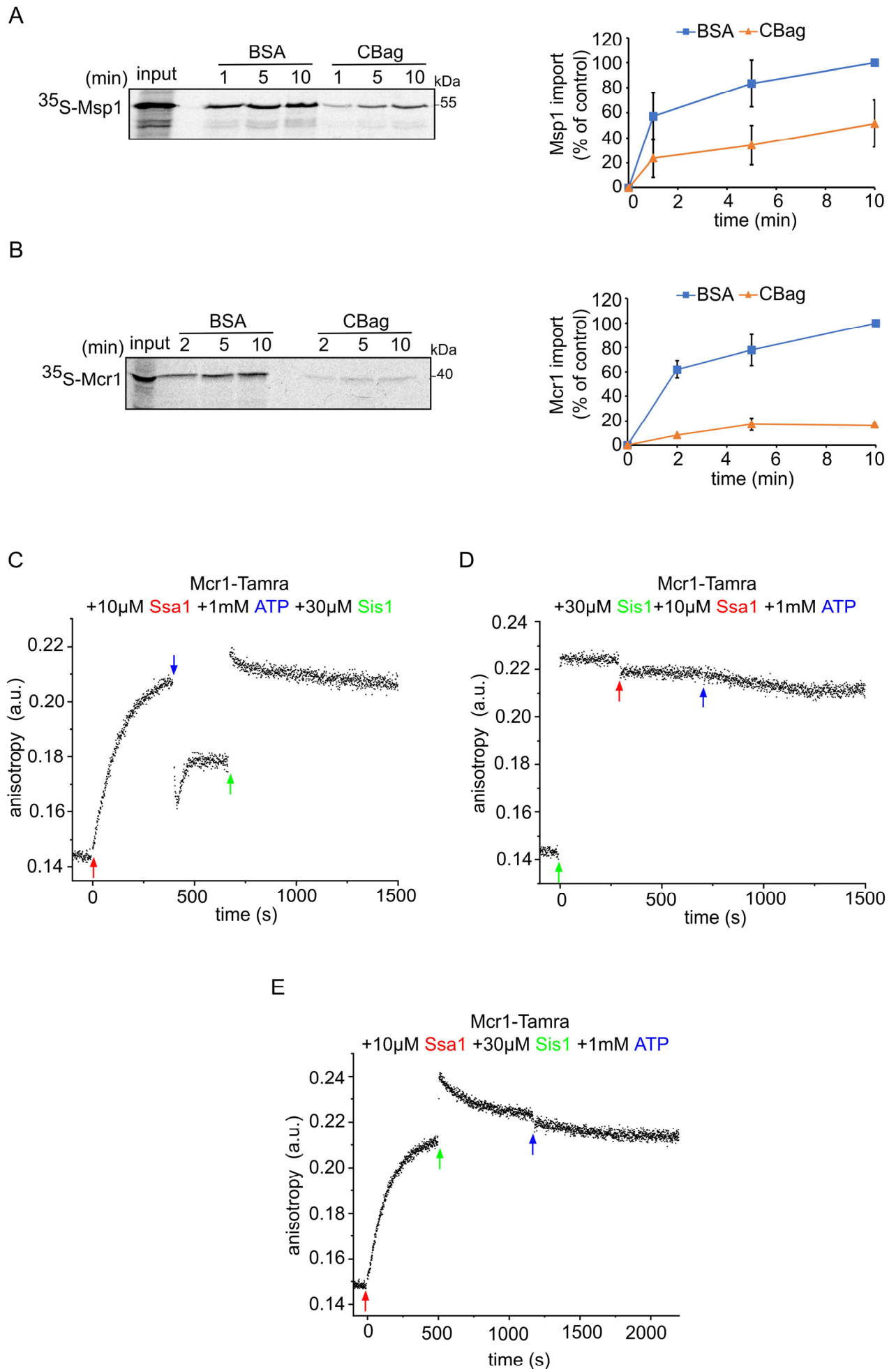
A

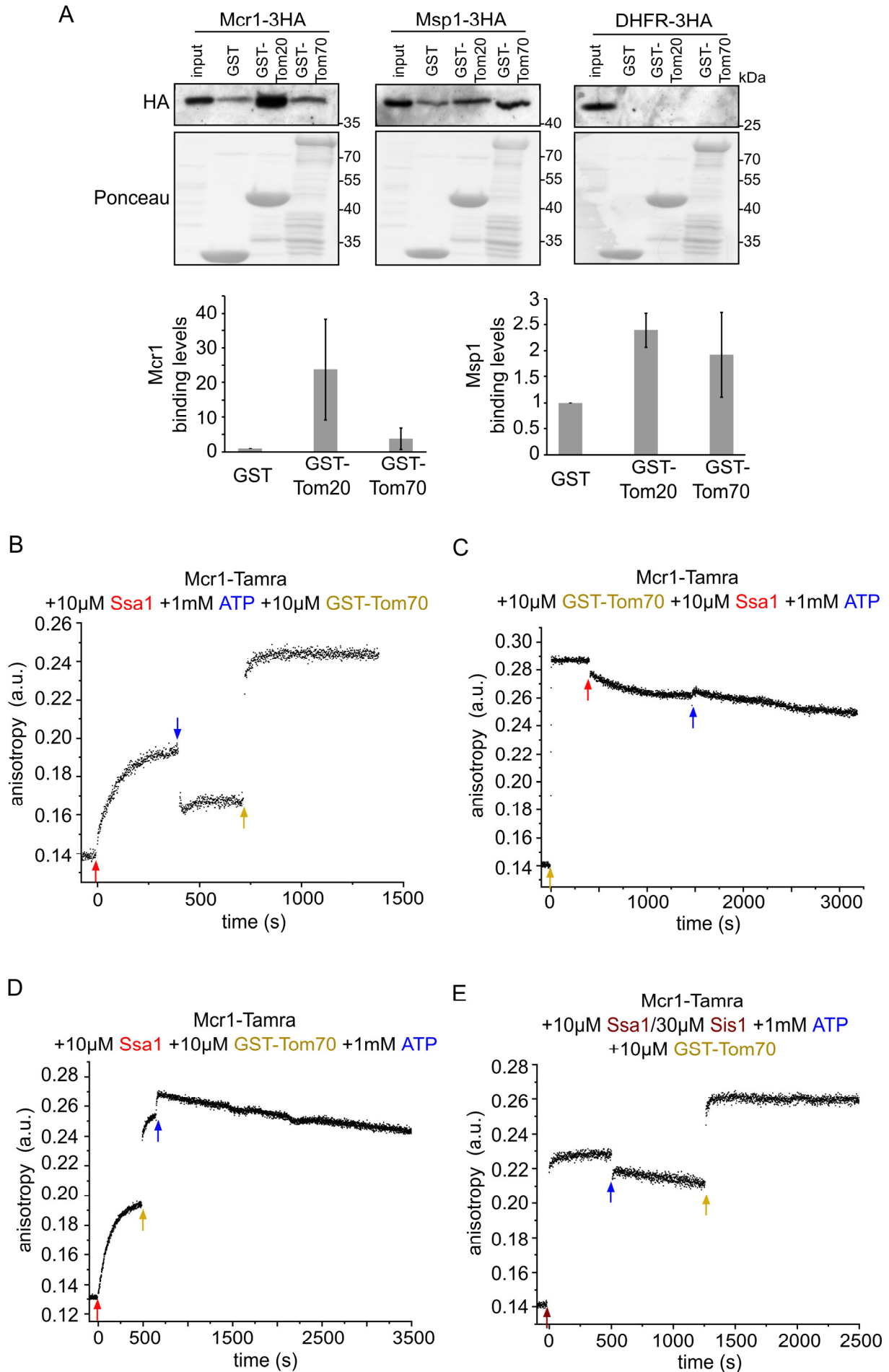


B

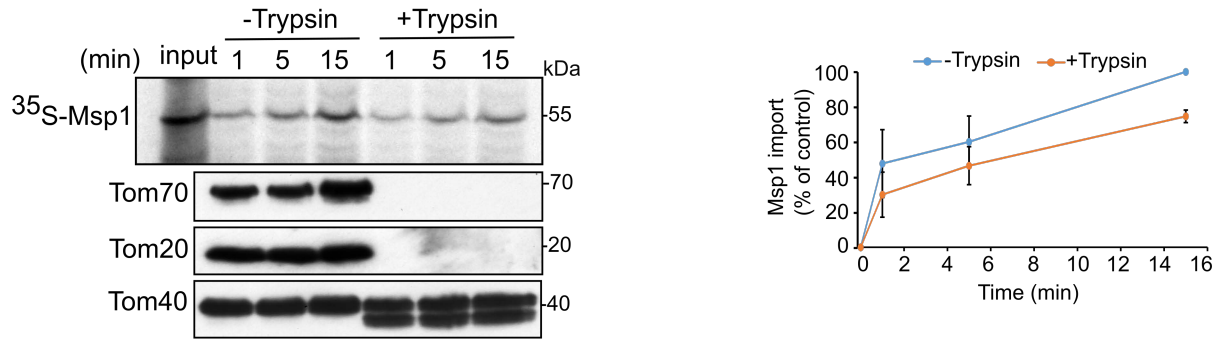




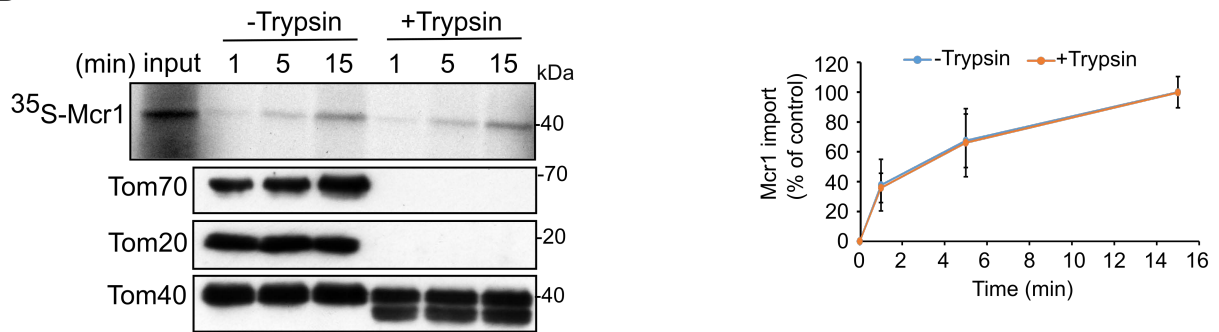




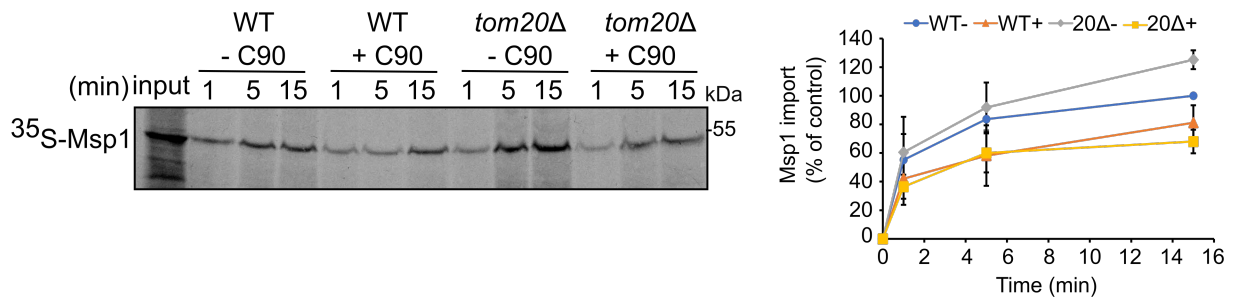
A



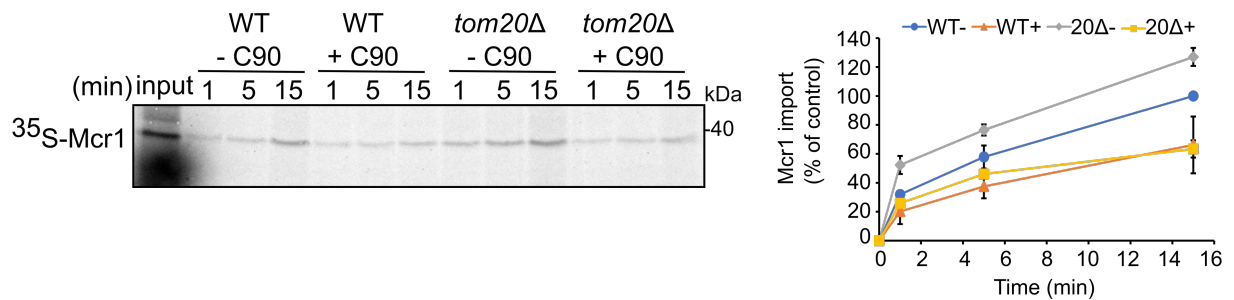
B

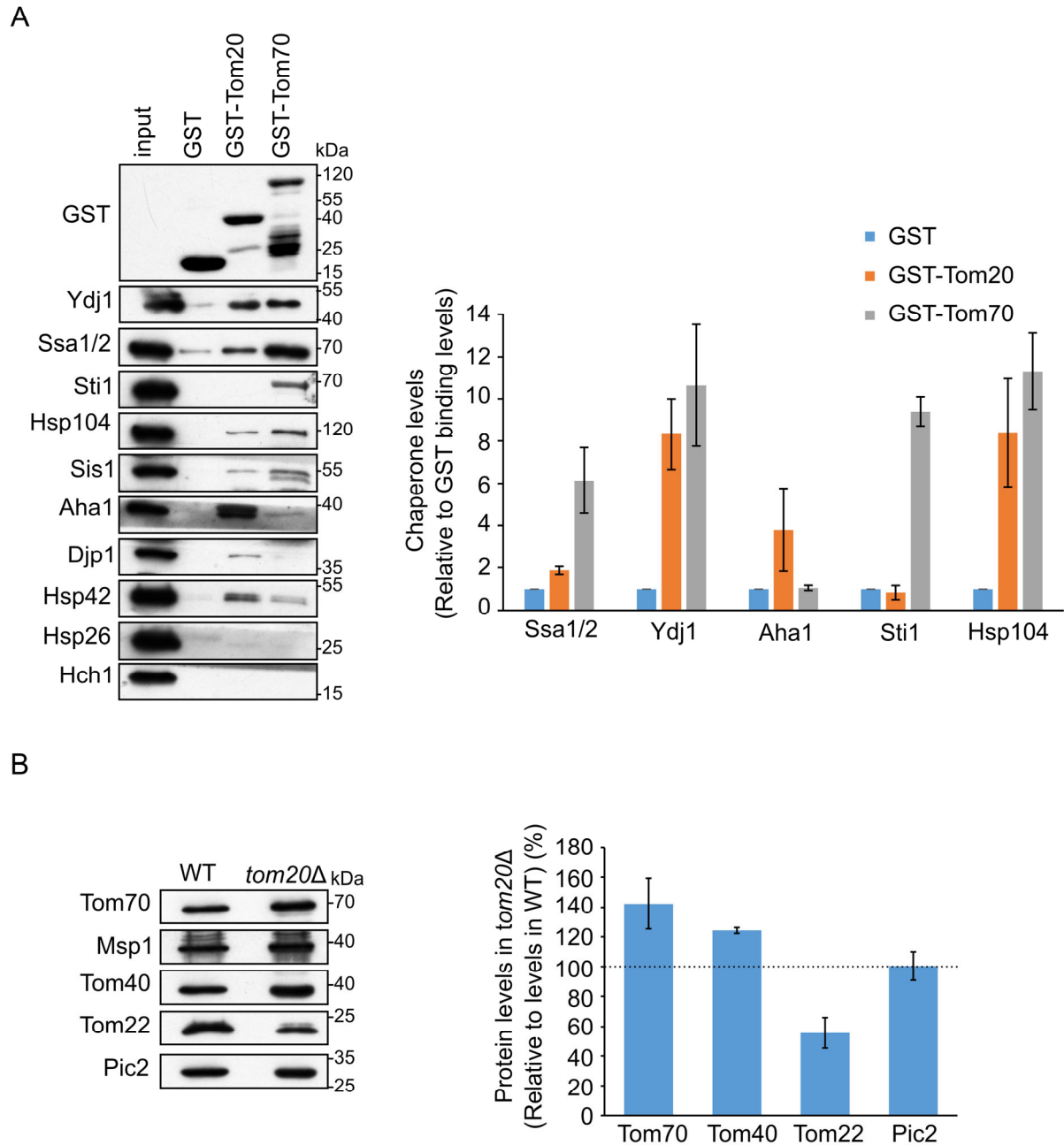


C



D





**Figure S1:** The cytosolic domains of the Tom receptors can associate with cytosolic (co)chaperones. **(A)** Left panel: Yeast extract was incubated with GST alone or with GST fused to the cytosolic domain of either Tom20 (GST-Tom20) or Tom70 (GST-Tom70). Samples of the input (1%) and the eluate (100%) were subjected to SDS-PAGE followed by immunodecoration with the indicated antibodies. Right panel: Bands representing the different (co)chaperones were quantified and the protein levels in the elution fraction by using GST alone was set to 1. The results of three independent experiments are presented as mean values  $\pm$  SD of. **(B)** Left panel: Mitochondria isolated from either *tom20* $\Delta$ , or its corresponding WT strain were analyzed by SDS-PAGE and immunodecoration with antibodies against the indicated proteins. Pic2, an inner membrane protein that was used as a loading control. Right panel: Protein levels were quantified and the values of the bands corresponding to control organelles were set to 100%. Results of three independent experiments are presented as mean values  $\pm$  SD



**Table S1: (co)chaperones that co-purified with *in vitro* translated proteins**

**A**

Protein name	Gene name	Mock	Msp1 (iBAQ)	Mcr1 (iBAQ)
Heat shock protein STI1	STI1	0	1383200	6860600
Vacuolar transporter chaperone 4	VTC4	0	1575800	3677300
Vacuolar transporter chaperone 2	VTC2	0	270840	2372800
Mitochondrial clpX-like chaperone MCX1	MCX1	0	719400	2178900
ATP-dependent molecular chaperone HSP82	HSP82	0	180250	1771700
HSP70 co-chaperone SNL1	SNL1	0	171400	1531500
Heat shock protein SSA4	SSA4	0	0	828380
Heat shock protein 70 homolog LHS1	LHS1	0	178030	384110
SEC14 cytosolic factor	SEC14	0	356900	0

**B**

Protein name	Gene name	Mock	Msp1 (relative iBAQ)	Mcr1 (relative iBAQ)
Hsp90 co-chaperone AHA1	AHA1	1	59.2	70.1
Heat shock protein SSB2	SSB2	1	6.6	17.6
ATP-dependent molecular chaperone HSC82	HSC82	1	8.6	16.1
Heat shock protein SSA2	SSA2	1	3.5	11.0
Heat shock protein SSC1, mitochondrial	SSC1	1	4.9	9.7
Heat shock protein 104	HSP104	1	4.7	9.4
Heat shock protein SSA1	SSA1	1	3.3	8.7
Heat shock protein 60, mitochondrial	HSP60	1	14.9	8.0
Heat shock protein homolog SSE1	SSE1	1	3.0	7.6
Heat shock protein SSB1	SSB1	1	1.8	4.7
Mitochondrial protein import protein MAS5	YDJ1	1	4.0	2.8
Protein SIS1	SIS1	1	1.4	2.0
Zuotin	ZUO1	1	1.50	1.87

**Table S1:** (A) List of chaperones that were found in the elution fraction of Msp1 and Mcr1 but not in the elution of mock pull-down. The iBAQ values of the specified proteins are indicated. (B) List of chaperones that were enriched in the elution fraction of Msp1 and Mcr1 as compared to their levels in the elution from mock pull-down assay are indicated. The iBAQ value of each protein in the eluate of the mock pull-down was set to 1 and the relative values in the pull-down assays with either Msp1 or Mcr1 as compared to the value in the mock sample are indicated.



## Key Resource Tables

**Table S2. Yeast strains used in this study**

Strain	Genotype	Reference
WT	W303 $\alpha$	Lab stock
tetO7-Ubi-L-Ydj1	YMK120 $\alpha$ , ydj1::tetO7-Ubiquitin-Leu-YDJ1 KanMX4	This Study
tetO7-Ubi-L-Sis1	YMK120 $\alpha$ , sis1::tetO7-Ubiquitin-Leu-SIS1 His3MX	This Study
tetO7-Ubi-L-Ydj1/Sis1	YMK120 $\alpha$ , tetO7-Ubi-Leu-SIS1:HisMX3a; tetO7-Ubi-Leu-YDJ1:KanMX4	This Study
<i>Tom20A</i>	W303 $\alpha$ , tom20::HIS3	Lab stock

**Table S3. Primers used in this study**

Construct	Primer name	Sequence 5' - 3'	Note
Msp1	LDFWD07	GGG- <i>GGATCC</i> -ATGTCTCGC AAATTTGATTTAAAAACGAT TACTGATCTTT	Amplification of <i>MSP1</i> , BamHI restriction site at 5'
	LDREV08	GGG- <i>AAGCTT</i> -ATCAAGAGG TTGAGATGACAACGTA CTTG	Amplification of <i>MSP1</i> , HindIII restriction site at 5'
yk Msp1	LDFWD09	GGG- <i>GGATCC</i> -AAAAAATG TCTCGCAAATTTGATTTAAA AACGATTACTGATCTTT	Amplification of yk- <i>MSP1</i> , BamHI restriction site at 5'
	LDREV08	GGG- <i>AAGCTT</i> -TTAATCAAGA GGTTGAGATGACAAC	Amplification of <i>MSP1</i> , HindIII restriction site at 5'
yk Msp1-3HA	LDRFWD028	CACAC- <i>GAGCTC</i> -AAAAAA- ATGTCTCGCAAATTTGATTT AAAAACG	Amplification of yk- <i>MSP1</i> , SacI restriction site at 5'
	LDRREV029	CACAC-GGATCC-CCATCAA GAGGTTGAGATGACAACGT AC	Amplification of <i>MSP1</i> , BamHI restriction site at 5'
yk Mcr1-3HA	LDFWD038	GGG- <i>GAATTC</i> -AAAAAA- ATGTTTTCCAGATTATCCAG ATCTCACTCAA AAGC	Amplification of yk- <i>MCRI</i> , EcoRI restriction site at 5'

	LDREV039	GGG- <i>CCCGGG</i> -AAATTTGA AAACTTGGTCCTTGGAGTAG CCC	Amplification of <i>MCRI</i> , SmaI restriction site at 5'
<b>yk Tom20-3HA</b>	LDFWD0102	GGG- <i>GGTACC</i> -AAAAAA- ATGTCCCAGTCGAACCCTAT CTTAC	Amplification of yk- <i>TOM20</i> , KpnI restriction site at 5'
	LDREV0103	GGG- <i>GGATCC</i> -GG- GTCATCGATATCGTTAGCTT CAGC	Amplification of <i>TOM20</i> , BamHI restriction site at 5'
<b>yk Tom70-3HA</b>	LDFWD0106	GGG- <i>GGTACC</i> -AAAAAA- ATGAAGAGCTTCATTACAAG GAACAAGAC	Amplification of yk- <i>TOM70</i> , KpnI restriction site at 5'
	LDREV0107	GGG- <i>GGATCC</i> -GGCATTAAAC CCTGTTCGCGTAATTTAGC	Amplification of <i>TOM70</i> , BamHI restriction site at 5'
<b>yk Msp1-TMD-3HA</b>	LDFWD040	GGG- <i>GAATTC</i> -AAAAAA- ATGTCTCGCAAATTTGATTT AAAAACG	Amplification of yk-TMD (1-32) of <i>MSP1</i> , EcoRI restriction site at 5'
	LDREV041	GGG- <i>GGATCC</i> -CCGTTGAGT AGCCGACTGACCA	Amplification of TMD (1- 32) of <i>MSP1</i> , BamHI restriction site at 5'
<b>yk Msp1-CD--3HA</b>	LDRFWD05 2	CACAC- <i>GAGCTC</i> -AAAAAA- ATGGATGTTGAATCAGGACC GTTATCAGG	Amplification of yk-CD (33-363) of <i>MSP1</i> , SacI restriction site at 5'
	LDREV053	CACAC- <i>GGATCC</i> -CCATCA AGAGGTTGAGATGACAACG TACTTGTAGC	Amplification of CD (33- 363) of <i>MSP1</i> , BamHI restriction site at 5'
<b>yk Mcr1-TMD-3HA</b>	LDFWD060	CACAC- <i>GAATTC</i> -AAAAAA- ATGTTTTCCAGATTATCCAG ATCTC	Amplification of yk-TMD (1-39) of <i>MCRI</i> , EcoRI restriction site at 5'
	LDREV061	CACAC- <i>CCCGGG</i> -GAC AAA GGA ATG TTG GTT ACG GTT T	Amplification of TMD (1- 39) of <i>MCRI</i> , XmaI restriction site at 5'
<b>yk Mcr1-CD-3HA</b>	LDRFWD05 4	CACAC- <i>GAATTC</i> -AAAAAA- ATGCATTCTTTGTCTTCAA TGAATC	Amplification of yk-CD (35-302) of <i>MCRI</i> , EcoRI restriction site at 5'
	LDREV055	CACAC- <i>CCCGGG</i> -AAATTTGA AAACTTGGTCCTTGGAGTAG	Amplification of CD (35- 302) of <i>MCRI</i> , XmaI restriction site at 5'

<b>yk Tom20-TMD-3HA</b>	LDFWD0102	GGG-GGTACC-AAAAAA-ATGTCCCAGTCGAACCCTATCTTAC	Amplification of yk-TMD (1-30) of <i>TOM20</i> , KpnI restriction site at 5'
	LDREV0113	GGG- <i>GGATCC</i> -GGGTCAAAGTAGATAGCATAACCGGTG	Amplification of TMD (1-30) of <i>TOM20</i> , BamHI restriction site at 5'
<b>yk Tom20-CD-3HA</b>	LDFWD0112	GGG- <i>GGTACC</i> -AAAAAA-ATGAGAAATAGCCCGCAATTCAGGAA	Amplification of yk-CD (33-183) of <i>TOM20</i> , KpnI restriction site at 5'
	LDREV0103	GGG- <i>GGATCC</i> -GGGTTCATCGATATCGTTAGCTTCAGC	Amplification of CD (33-183) of <i>TOM20</i> , BamHI restriction site at 5'
<b>yk Tom70-TMD-3HA</b>	LDFWD0106	GGG- <i>GGTACC</i> -AAAAAA-ATGAAGAGCTTCATTACAAGGAACAAGAC	Amplification of yk-TMD (1-32) of <i>TOM70</i> , KpnI restriction site at 5'
	LDREV0111	GGG- <i>GGATCC</i> -GGCAATTGGTTGTAATAATAGTAGGCACC	Amplification of TMD (1-32) of <i>TOM70</i> , BamHI restriction site at 5'
<b>yk Tom70-CD-3HA</b>	LDFWD0110	GGG- <i>GGTACC</i> -AAAAAA-ATGCAACAACAACAACGAGGAAAAAGAACAC	Amplification of yk-CD (33-617) of <i>TOM70</i> , KpnI restriction site at 5'
	LDREV0107	GGG- <i>GGATCC</i> -GGCATTAAACCCTGTTCGCGTAATTTAGC	Amplification of CD (33-617) of <i>TOM70</i> , BamHI restriction site at 5'
<b>tetO<sub>7</sub>-Ubi-L-Ydj1</b>	TJ192	CATATCTTTTGATAGAACATAATTAATAATTATCCAACTGAATTCTACACAGTATAGCGACCAGCATTACATACG	Amplification of a cassette containing tetO <sub>7</sub> promotor-Ubiquitin-Leu, to genomically fuse to <i>YDJ1</i>
	TJ193	GTGGCAGTTACTGGAACACCTAGAATATCGTAAAACCTTAGTTTCTTTAACCAAACCACTCTCAATCTCAAGACCAAG	Amplification of a cassette containing tetO <sub>7</sub> promotor-Ubiquitin-Leu, to genomically fuse to <i>YDJ1</i>
<b>tetO<sub>7</sub>-Ubi-L-Sis1</b>	TJ196	GGATAAGTTGTTTGCATTTTAAGATTTTTTTTTTAATACATTCACATCAACAGTATAGCGACCAGCATTACATACG	Amplification of a cassette containing tetO <sub>7</sub> promotor-Ubiquitin-Leu, to genomically fuse to <i>SIS1</i>
	TJ197	TTAGCACTTGGAGATACTCCAAGTAAATCATAAAGTTTTGTCTCCTTGACCAAACCACTCTCAATCTCAAGACCAAG	Amplification of a cassette containing tetO <sub>7</sub> promotor-Ubiquitin-Leu, to genomically fuse to <i>SIS1</i>

**Table S4: Plasmids used in this study**

<b>Plasmid</b>	<b>Insert</b>	<b>Marker</b>	<b>Reference</b>
<b>pGEM4polyA-3HA</b>	C-terminal 3 x HA-tag	Amp <sup>R</sup>	Jores et al. 2018
<b>pGEM4polyA-yk-DHFR-3HA</b>	Yeast kozak sequence (AAAAAAATG) DHFR-3 × HA-tag	Amp <sup>R</sup>	Jores et al. 2018
<b>pGEM4polyA-yk-Porin-3HA</b>	Yeast kozak sequence (AAAAAAATG) Porin-3 × HA-tag	Amp <sup>R</sup>	Jores at al. 2018
<b>pGEM4polyA-yk-Fis1-3HA</b>	Yeast kozak sequence (AAAAAAATG) Fis1-3 × HA-tag	Amp <sup>R</sup>	
<b>pGEM4polyA-yk-Msp1-3HA</b>	Yeast kozak sequence (AAAAAAATG) Msp1-3 × HA-tag	Amp <sup>R</sup>	This study
<b>pGEM4polyA-yk-Mcr1-3HA</b>	Yeast kozak sequence (AAAAAAATG) Mcr1-3 × HA-tag	Amp <sup>R</sup>	This study
<b>pGEM4polyA-yk-Tom20-3HA</b>	Yeast kozak sequence (AAAAAAATG) Tom20-3 × HA-tag	Amp <sup>R</sup>	This study
<b>pGEM4polyA-yk-Tom70-3HA</b>	Yeast kozak sequence (AAAAAAATG) Tom70-3 × HA-tag	Amp <sup>R</sup>	This study
<b>pGEM4polyA-yk-Msp1(33-363)-3HA</b>	Yeast kozak sequence (AAAAAAATG) Msp1(1-363)-3 × HA-tag	Amp <sup>R</sup>	This study
<b>pGEM4polyA-yk-Msp1(1-32)-3HA</b>	Yeast kozak sequence (AAAAAAATG) Msp1(1-32)-3 × HA-tag	Amp <sup>R</sup>	This study
<b>pGEM4polyA-yk-Mcr1(35-302)-3HA</b>	Yeast kozak sequence (AAAAAAATG) Mcr1(35-302)-3 × HA-tag	Amp <sup>R</sup>	This study
<b>pGEM4polyA-yk-Mcr1(1-39)-3HA</b>	Yeast kozak sequence (AAAAAAATG) Mcr1(1-39)-3 × HA-tag	Amp <sup>R</sup>	This study
<b>pGEM4polyA-yk-Tom20(33-183)-3HA</b>	Yeast kozak sequence (AAAAAAATG) Tom20(33-183)-3 × HA-tag	Amp <sup>R</sup>	This study

<b>pGEM4polyA-yk-Tom20(1-30)-3HA</b>	Yeast kozak sequence (AAAAAAATG) Tom20(1-30)-3× HA-tag	Amp <sup>R</sup>	This study
<b>pGEM4polyA-yk-Tom70(33-617)-3HA</b>	Yeast kozak sequence (AAAAAAATG) Tom70(33-617)-3 × HA-tag	Amp <sup>R</sup>	This study
<b>pGEM4polyA-yk-Tom70(1-32)-3HA</b>	Yeast kozak sequence (AAAAAAATG) Tom70(1-32)-3 × HA-tag	Amp <sup>R</sup>	This study
<b>pMK632His</b>	HIS3MX cassette tetO7-CYC1 promoter-Ubiquitin-Leucin-HA-tag	Amp <sup>R</sup>	Jores et al. 2018
<b>pMK632Kan</b>	KanMX cassette tetO7-CYC1 promoter-Ubiquitin-Leucin-HA-tag	Amp <sup>R</sup>	Jores et al. 2018
<b>pGEX4T1-GST</b>	GST	Amp <sup>R</sup>	
<b>pGEX4T1-GST-Tom20(35-183)</b>	Tom20(35-183)	Amp <sup>R</sup>	
<b>pGEX4T1-GST-Tom70(46-617)</b>	Tom70(46-617)	Amp <sup>R</sup>	
<b>pPROEX-HTa-cBag</b>	His6-tag-TEV-human Bag-1M(151-263)	Amp <sup>R</sup>	Young et al. 2003
<b>pPROEX-HTa-(C90)</b>	His6-tag-TEV-human Hsp90a(566-732)	Amp <sup>R</sup>	Young et al. 2003

**Table S5. Antibodies used in this study**

<b>Antibody raised against</b>	<b>Species</b>	<b>Dilution</b>	<b>Source</b>
Ssa1/2	Rabbit	1:20000	Lab stocks
Ydj1	Rabbit	1:10000	Lab stocks
Sis1	Rabbit	1:20000	Lab stocks
Hsp26	Rabbit	1:4000	Lab stocks
Hsp104	Rabbit	1:25000	Lab stocks
Hsp42	Rabbit	1:4000	Lab stocks
Hsp82	Rabbit	1:20000	Lab stocks
Hch1	Rabbit	1:4000	Lab stocks
Bmh1	Rabbit	1:1000	Lab stocks
Djp1	Rabbit	1:2000	Lab of Ineke Braakman
Sti1	Rabbit	1:10000	Lab stocks
Aha1	Rabbit	1:2000	Lab stocks
Msp1	Rabbit	1:2000	Lab of Toshiya Endo
Mcr1	Rabbit	1:2000	Lab stocks
Fis1	Rabbit	1:1000	Lab stocks
Tom20	Rabbit	1:4000	Lab stocks
Tom70	Rabbit	1:5000	Lab stocks
Porin	Rabbit	1:6000	Lab stocks
Pic2	Rabbit	1:2000	Lab stocks
HA	Rat	1:1000	11867423001, Roche
Rabbit IgG HRP conjugate	Goat	1:10000	1721019, Bio-Rad
Rat IgG HRP conjugate	Goat	1:2000	ab6845, Abcam